MINISTÉRIO DA EDUCAÇÃO
UNIVERSIDADE FEDERAL DO RIO GRANDE DO SUL
PROGRAMA DE PÓS-GRADUAÇÃO EM ENGENHARIA MECÂNICA

COMPARAÇÃO DA REATIVIDADE DE CARVÕES EM REATORES CICLÔNICOS

por

Adriano Roberto da Silva Carotenuto

Tese para obtenção do Título de
Doutor em Engenharia

Porto Alegre, maio de 2013

COMPARAÇÃO DA REATIVIDADE DE CARVÕES EM REATORES CICLÔNICOS

por

Adriano Roberto da Silva Carotenuto

Engenheiro Mecânico

Tese submetida ao Programa de Pós-Graduação em Engenharia Mecânica, da Escola de Engenharia da Universidade Federal do Rio Grande do Sul, como parte dos requisitos necessários para a obtenção do Título de

Doutor em Engenharia

Área de Concentração: Fenômenos de Transporte

Orientador: Prof. Dr. Paulo Smith Schneider
Co-orientador: Prof. Dr. Nilson Romeu Marcílio

Aprovada por:

Prof. Dr. Pedro Teixeira Lacava, ITA

Prof. Dr. Eduardo Osório, UFRGS/PPGEM

Prof. Dr. Fernando Marcelo Pereira, UFRGS/PROMEC

Prof[a]. Dra. Thamy Cristina Hayashi, UFRGS/PROMEC

Prof. Dr. Rogério Marczak
Coordenador do PROMEC

Porto Alegre, 13, maio 2013

AGRADECIMENTOS

Primeiramente, agradeço a Deus, por me dar saúde plena para a realização da tese. Agradeço à família, em especial a minha mãe, Cleci Carotenuto, aos meus irmãos, Thiago e Simone Carotenuto, a minha vó, Eva R. da Silva, a minha sobrinha, Amanda L. Carotenuto, que tanto apoio me deram, quando eu estava também na Alemanha. Agradeço ao meu pai, Paulo Carotenuto, por estar sempre comigo em pensamento e me protegendo. Agradeço a minha noiva, Andréa Brites, por estar sempre ao meu lado, acompanhando-me nos momentos de grandes desafios, dando-me força e boas energias para vencer as etapas necessárias para a conclusão da tese, suportando a distância durante o período que eu estive na Alemanha. Aos meus sogros Noeli e Marcírio Brites, a minha cunhada, Ângela Brites, pela força e atenção que me deram ao longo do Doutorado. Agradeço ao meu anjo da guarda pela proteção.

Agradeço aos professores orientadores Paulo S. Schneider e Romeu N. Marcílio por me proporcionarem a oportunidade do tema, orientação e desenvolvimento da pesquisa. Agradeço à Universidade Técnica de Cottbus (BTU), Alemanha, por ter me proporcionado a realização dos trabalhos experimentais da tese no doutorado sanduíche, ao excelente acolhimento e ao saudável ambiente de trabalho. Agradeço ao professor Hans Joachim Krautz por ter-me co-orientado no trabalho de pesquisa em BTU. Agradeço aos colegas Rodrigo Corrêa da Silva e Sunil Ramachandra pelo auxílio nos experimentos, os quais foram incansáveis no busca dos melhores resultados experimentais com a bancada ALVA 20, entrando noites e madrugadas de trabalhos comigo no rigoroso inverno alemão. Agradeço também aos colegas Matthias Schreiber, Tanin Kangwanpongpan e Teklay W. Asegehgn pela oportunidade da discussão dos resultados experimentais. Agradeço aos técnicos Torsten Sänger, Heinz Schallmea e Doris Seifart pelo auxílio na preparação das atividades do laboratório. Aos engenheiros Raimo Kauffmann e Jörg Waske na investigação e eliminação de panes na bancada experimental. Especial agradecimento à colega engenheira Stephanie Tappe por ter projetado a bancada experimental ALVA 20 e ter-nos proporcionando e nos incentivado a continuidade da pesquisa dos trabalhos experimentais em BTU com a bancada. Agradeço aos colegas do GESTE e aos funcionários do PROMEC pelo excelente convívio nestes anos e ao técnico João Batista pelo apoio nas atividades experimentais no LETA. Agradeço ao prof. René Lúcio Rech pelas horas de estudo em BTU e na UFRGS. Agradeço as valiosas informações dos professores da Banca Examinadora na revisão da tese. Agradeço à CAPES/DAAD e ao PROBRAL (projeto N^{o} 348/10) pelo financiamento da pesquisa.

RESUMO

Um novo laboratório experimental desenvolvido para investigar a combustão de carvão em atmosferas de oxicombustão é descrito em detalhes na tese. Um reator ciclônico é utilizado para a combustão de carvões de baixo *rank* em condições de escoamento turbulento e com *swirl*, e operando em temperaturas similares às encontradas em câmaras de combustão industriais. Um sensor potenciométrico de oxigênio, instalado dentro do reator ciclônico, é utilizado para medir o consumo de oxigênio durante a combustão das amostras de carvão. Amostras de carvão com alto teor de cinzas, das minas do Leão e Bonito localizadas no sul do Brasil, e amostras de carvão linhito pré-seco (LTBK), da região da Lusácia, na Alemanha, foram submetidos à combustão em atmosferas de ar e de oxicombustão ($O_2/CO_2/H_2O$). Os experimentos foram realizados em três temperaturas médias do gás de combustão: 1073, 1173 e 1273 K. Para as amostras do carvão LTBK, a oxicombustão foi composta com duas atmosferas de O_2/CO_2 sem vapor d'água (21/79 e 30/70) e três atmosferas de $O_2/CO_2/H_2O$ (30/60/10, 30/50/20 e 30/40/30) em base molar, enquanto para as amostras dos carvões Leão e Bonito, a oxicombustão foi composta com duas atmosferas de O_2/CO_2 (21/79 e 30/70). As amostras de carvão foram peneiradas para uma faixa de tamanho de partículas de 1250 a 2000 µm e 125 a 500 µm, e com massas de 1g e 3g. Em adição aos testes, amostras de char dos carvões Leão e LTBK foram preparadas para investigar o comportamento da combustão de suas matrizes carbonosas com diferentes níveis de matéria volátil. Primeiramente, a investigação da combustão do carvão é feita diretamente a partir das curvas de concentração de oxigênio medidas para a combustão das amostras de carvão LTBK submetidos às atmosferas de ar e oxicombustão com vapor d'água, conforme explicado no Capítulo 2 desta tese. Entretanto, devido ao grande número de experimentos realizados e a necessidade de entender a influência dos fatores, como temperatura e as composições das atmosferas oxidantes, e as interações entre esses fatores na combustão do carvão, a análise pela metodologia do Projeto de Experimentos (DoE) é aplicada nos experimentos, conforme detalhado no Capítulo 3. A reatividade dos carvões de baixo *rank* é investigada por meio do cálculo dos parâmetros cinéticos globais e dos coeficientes da taxa de reação de combustão do char, considerando a hipótese de um reator bem misturado, a ser verificada ao longo da investigação, conforme descrito no Capítulo 4. A partir da análise das curvas de concentração de oxigênio (Capítulos 2 e 3), os resultados mostram que a atmosfera de oxicombustão com 79% de CO_2 (21/79, O_2/CO_2) aumenta o consumo de oxigênio para os carvões de alto teor de

cinzas, Bonito e Leão, e para o carvão linhito com alto teor de voláteis (LTBK), devido à influência da reação de gaseificação do CO_2 a partir de temperaturas acima de 1073 K. A partir da análise dos parâmetros cinéticos globais calculados para avaliar a reatividade dos carvões, os resultados mostram que a hipótese do reator bem misturado não é o suficiente para capturar a cinética da combustão do carvão por batelada no interior do reator ciclônico. A reatividade dos carvões investigados, através das constantes efetivas da taxa de reação, variando-se a composição da atmosfera oxidante, temperatura do gás de combustão, tamanho de partículas, massa da amostra e posição do sensor de oxigênio, têm influência do escoamento com *swirl* e seus termos advectivos e difusivos.

Palavras-chave: oxicombustão, reator de combustão ciclônico, sensor potenciométrico de oxigênio, parâmetros cinéticos globais, carvão de baixo *rank*

ABSTRACT

A novel laboratory facility designed to investigate coal oxy-fuel combustion is described in the present work. A cyclone chamber allows for the combustion of low-rank coal under turbulent conditions and swirling flows, covering a temperature range similar to those found on practical furnaces. A potentiometric oxygen sensor with oxide-ion conducting solid electrolytes, as stabilized zirconia, installed within the cyclone reactor, is used to measure the oxygen consumption during the combustion of coal samples. High ash coals samples, from Leão and Bonito mining sites located in South Brazil, and pre-dried lignite coal samples (LTBK), from the Lusatian region, in Germany, were burned under air and oxy-fuel ($O_2/CO_2/H_2O$) atmospheres. Experiments were carried out at three average gas combustion temperatures: 1073, 1173 and 1273 K. For LTBK coal, oxy-fuel combustion was composed with two O_2/CO_2 atmospheres (21/79 and 30/70) and three $O_2/CO_2/H_2O$ atmospheres (30/60/10, 30/50/20 and 30/40/30) in molar basis, whereas for Leão and Bonito coals, the oxy-fuel combustion was composed with two O_2/CO_2 atmospheres (21/79 and 30/70). Coal samples were sieved to a size range of 1250 to 2000 µm and 125 to 500 µm and with 1g and 3g. In addition, char samples from Leão and lignite coals were prepared in order to investigate the combustion behavior of its carbon matrix for different levels of volatile matter. The investigation of coal combustion behavior is made firstly directly on the oxygen concentration curves measured for LTBK coal samples burned under air and oxy-fuel atmospheres with water vapor, as detailed in Chapter 2 of this thesis. However, due to the great number of experiments performed and the need to understand the influence of the factors, as temperature and atmosphere compositions, and the interactions between them on the coal combustion, the Design of Experiments (DoE) analysis is applied in the laboratory test facility, as developed in Chapter 3. The reactivity of low rank coals is assessed by means of global kinetic parameters and of char combustion reaction coefficients, under assumption of a well stirred reactor to be tested along the investigation, as described in Chapter 4. From the analysis of oxygen concentration curves (Chapter 2 and 3), results show that oxidizer oxy-fuel atmosphere with 79% CO_2 (21/79, O_2/CO_2) increases the oxygen consumption for high ash coals, Bonito and Leão, and for pre-dried lignite coal, LTBK, due to the influence of CO_2 gasification reaction on their coal combustion reactions from gas combustion temperatures higher than 1073 K. From the analysis of global kinetic parameters calculated to assess the coal reactivity, the results show that the hypothesis of a well stirred reactor is not enough to capture the kinetic involved in coal combustion burned in batch mode within the cyclone

reactor. The coal reactivity investigated with the effective reaction rate constants for different oxidizer atmospheres, gas combustion temperatures, particle diameters, sample masses and oxygen sensor position, is influenced by the swirling flow with its advective and diffusive terms.

Keywords: oxy-fuel combustion, cyclone reactor, potentiometric oxygen sensor, global kinetic parameters, low-rank coals

SUMÁRIO

LISTA DE FIGURAS

LISTA DE TABELAS

LISTA DE SIGLAS E ABREVIATURAS

ALVA 20	Laboratório com câmara de combustão ciclônica de 20 kW de potência térmica, operando em condições atmosféricas.
ANOVA	Análise de variância
BTU	Universidade de Tecnologia de Brandemburgo, Cottbus, Alemanha
CCS	Captura e armazenamento de carbono
CDS	Ciclone separador de cinzas
CFD	Dinâmica de fluidos computacional
CLC	Combustão em reatores de leito fluidizado circulante de combustível e de ar
CR	Reator de combustão ciclônico
CRZ	Zona central de recirculação
CTRZ	Zona central de recirculação toroidal
daf	Seco, sem cinzas
DoE	Projeto de experimentos
DTF	Reator para combustão de partículas de carvão em queda livre
EFR	Reator para combustão de partículas de carvão por arrasto
IEA	Agência Internacional de Energia
IGCC	Ciclos combinados de gaseificação integrada
FBC	Reator de combustão em leito fluidizado
LTBK	Carvão Linhito pré-seco da região da Lusácia na Alemanha
LETA	Laboratório de Estudos Térmicos e Aerodinâmicos, UFRGS
Max	Máximo
Min	Mínimo
OECD	Organização para Cooperação Econômica e Desenvolvimento
PCC	Pós-câmara de combustão
PROBRAL	Projeto de Cooperação entre Brasil e Alemanha
PSA	Adsorção do gás por ciclagem de pressão
TGA	Balança termogravimétrica
TPB	Fronteira de tripla fase das reações de dissociação de O_2 no sensor de oxigênio.
vol.	Volume
VPSA	Adsorção do gás por ciclagem de pressão à vácuo
YSZ	Composto de zircônia-ítrio estabilizado

LISTA DE SÍMBOLOS

A	Área tangencial dos injetores da corrente do oxidante do reator de combustão ciclônico, m^{-2}
A	Fator controlável no planejamento fatorial do DoE
B	Fator controlável no planejamento fatorial do DoE
Bi	Número de Biot, -
c	Constante, utilizada no número de Sherwood
$c_{p,g}$	Calor específico do gás à pressão constante, J kg^{-1} K^{-1}
C	Concentração, gmol O_2 m^{-3} or % vol
C_g	Concentração do oxigênio no ambiente, gO_2 cm^{-3}
C_s	Concentração do oxigênio na superfície externa da partícula, gO_2 cm^{-3}
d	Diâmetro do reator ciclônico antes da expansão, m
d_p	Diâmetro da partícula de char, cm
D	Diâmetro do reator ciclônico depois da expansão, m
D_{O2}	Coeficiente binário de difusão mássica do oxigênio, cm^2 s^{-1}
e	Carga elementar do elétron, $1.60217733 \pm 0{,}00000059 \times 10^{-19}$ C
e	Distância do centro dos injetores em relação ao eixo longitudinal central do reator de combustão ciclônico, m
E	Energia global de ativação, kJ mol^{-1}
E	Expectância
f	Fração molar, -
F	Constante de Faraday, 9.648×10^4 C mol^{-1}
F	Função de distribuição de probabilidade
g	Energia livre de gibbs específica, J mol^{-1}
G_x	Fluxo axial da quantidade de movimento axial, (kg m s^{-1}) s^{-1}
G_ϕ	Fluxo axial da quantidade de movimento angular, (kg m s^{-1}) s^{-1} m
h	Coefficiente da taxa de transferência de massa (fluxo de CO), cm s^{-1}
H	Altura do reator de combustão ciclônico, m
H	Hipótese
H	Entalpia da reação, cal g^{-1}, J g^{-1}
I	Corrente elétrica devido à vazão molar de elétrons do combustível utilizado, A
k	Constante da taxa de reação, (gmol O_2 m^{-3})$^{n-1}$ s^{-1}
k_g	Condutividade térmica do gás, W m^{-1} K^{-1}
k_p	Condutividade térmica do carvão, W m^{-1} K^{-1}
L_c	Comprimento característico da partícula, m
$\dot{m}$	Vazão mássica, kg s^{-1}
M	Massa molecular, g $gmol^{-1}$
n	Total de elementos da amostra, tamanho da amostra, número de réplicas
$\dot{n}$	Vazão molar, mol s^{-1}
N	Constante de Avogadro, $6.02214179 \times 10^{23}$ mol^{-1}

N	Total de elementos da população
p	Pressão, atm
p	Nível de significância do teste estatístico, calculado pelo software Minitab
P	Potência elétrica reversível da célula de combustível, W
$\overline{p}$	Pressão média no tempo, atm
Pr	Número de Prandtl, -
r	Direção radial, -
r_p	Raio da partícula de char ou de carvão, m
$\dot{r}_{a,c}$	Taxa global ou observada da reação de combustão, gC cm^{-2} s^{-1}
$\dot{r}_m$	Máxima taxa de reação ou de transferência de massa, gC cm^{-2} s^{-1}
$\dot{r}_{O_2}$	Taxa de reação pelo Método Integral, gmol O_2 m^{-3} s^{-1}
$\dot{r}_p$	Taxa de reação de combustão do char, gC cm^{-2} s^{-1}
R	Constante do gás ideal, 8.314 J K^{-1} mol^{-1}
R	Raio do reator de combustão ciclônico, m
Re	Número de Reynolds
R_a	Taxa global da reação de combustão por área externa da partícula em termos da pressão parcial do oxigênio no meio, gC [cm^{-2} s^{-1} $(atmO_2)^{-1}$]
$R_{a,c}$	Coeficiente da taxa de combustão (por área externa da partícula) por reação química, gC [cm^{-2} s^{-1} $(atmO_2)^{-n}$]
$R_{a,d}$	Coeficiente da taxa de combustão (por área externa da partícula) por difusão de massa, gC [cm^{-2} s^{-1} $(atmO_2)^{-1}$]
S	Desvio padrão da amostra
S^2	Variância da amostra
Sc	Número de Schmidt, -
Sh	Número de Scherwood, -
SS	Soma dos quadrados
t	Tempo, s
T	Temperatura, K or ºC
u_g	Velocidade superficial do gás na partícula de carvão, m s^{-1}
$\overline{u}$	Velocidade axial média no tempo, m s^{-1}
u'	Flutuação turbulenta da velocidade axial, m s^{-1}
U	Potencial elétrico da célula, mV
$\dot{V}$	Vazão volumétrica, m^3 h^{-1}
$\overline{v}$	Velocidade radial média no tempo, m s^{-1}
v'	Flutuação turbulenta da velocidade radial, m s^{-1}
W	Trabalho reversível da célula de combustível, W
w	Trabalho reversível específico, kJ mol^{-1}
$\overline{w}$	Velocidade tangencial média no tempo, m s^{-1}
w'	Flutuação turbulenta da velocidade tangencial, m s^{-1}
x	Direção axial, -
X_{O2}	Conversão do oxigênio, -
y	Variável aleatória normal

$\bar{y}$	Média da amostra

SÍMBOLOS GREGOS

α	Nível de significância do teste estatístico
ß	Efeito ou influência dos níveis referentes ao fator do experimento colocado na coluna da tabela fatorial dos experimentos do DoE
Δ	Incremento, variação
ε	Emissividade da partícula, porosidade do leito,-
Λ	Coeficiente estequiométrico gravimétrico, gC $(gO_2)^{-1}$
μ	Viscosidade dinâmica, kg $m^{-}1$ s^{-1}
μ	Potencial químico, kJ mol^{-1}
μ	Média da população
ν	Viscosidade cinemática, cm^2 s^{-1};
ν	Coeficiente estequiométrico
ρ	Densidade, g cm^{-3}, kg m^{-3}
σ	Desvio padrão da população
σ	Constante de Stefan-Boltzmann, 5.67E-8 W m^{-2} $(K^4)^{-1}$
τ	Efeito ou influência dos níveis referentes ao fator do experimento colocado na linha da tabela de planejamento fatorial dos experimentos do DoE
ϕ_s	Fator de forma da partícula de carvão, -
ϕ	Direção azimuthal, -
χ	Razão entre taxa de combustão por reação química e a taxa de combustão máxima, -

SUBÍNDICES

0	Inicial, no estado de referência
1	Gerador de *swirl* do reator de combustão ciclônico, antes da expansão
2	Gerador de *swirl* do reator de combustão ciclônico, depois da expansão
∞	Infinito, na corrente não perturbada
a	Nível do fator *A* da tabela fatorial do DoE
a	Área, superfície externa da partícula de char
A	Aparente
A	Avogadro
ads	Adsorvido
an	Anodo da célula de medição do sensor potenciométrico de oxigênio
ap	Aparente
atm	Atmosférico
b	Nível do fator *B* da tabela fatorial do DoE
c	Reação química, char, carbono, característico
cons	Consumido
CO	Gás monóxido de carbono
CO_2	Gás dióxido de carbono
d	Difusão de massa

eff	Efetiva
el	Elétrons de oxigênio
g	Gás
i	Níveis do fator *A*
in	Entrada do reator de combustão ciclônico
j	Níveis do fator *B*
k	Níveis de réplicas ou número de repetições do teste
m	Massa
m	Ordem real da reação, devido ao controle cinético
n	Ordem da reação, ordem aparente da reação
N_2	Gás nitrogênio
out	Saída do reator de combustão ciclônico
O_2	Gás oxigênio
p	Partícula
ref	Referência
s	Superfície
th	Térmico
tot	Total
T	Total
w	Parede do reator de combustão ciclônico

SUPERÍNDICES

m	Ordem real da reação
n	Ordem aparente da reação química, ordem da reação química
X	Posição de ocupação dos íons de oxigênio na matrix do eletrólito de zircônia
0	No estado de referência
2^-	Íons de oxigênio

1. INTRODUÇÃO

A geração de energia elétrica a partir do carvão é uma tecnologia bem conhecida e largamente usada no mundo e, provavelmente, manter-se-á por um bom tempo. As economias emergentes, tais como Brasil, China e Índia estão enfrentando um crescimento na demanda de energia elétrica, motivando novas e continuadas pesquisas na área de geração de energia, visando manter um desenvolvimento sustentável na utilização dos recursos naturais e nos projetos de novas plantas industriais.

Demandas por todos os tipos de energias lideradas pelos combustíveis como carvão, óleo e gás têm aumentado nos países que não são participantes *OECD-Organization for Economic Cooperation and Development*, enquanto que nos 34 países membros da *OECD*, as demandas de energias à base de carvão e óleo têm diminuído, sendo substituídos por fontes de energias renováveis [*IEA-International Energy Agency*, 2012].

O carvão é o combustível mais barato e abundante do que qualquer outro combustível fóssil e, ao mesmo tempo, tem comprovada estabilidade no custo e no fornecimento. Portanto, tem grandes chances de continuar com uma importante posição entre as fontes energéticas por um longo tempo [Buhre et al., 2005].

Entretanto, a combustão do carvão em atmosferas de ar lança produtos que são nocivos ao meio ambiente, devido às emissões dos óxidos de nitrogênio (N_xO_x), óxidos de enxofre (S_xO_x), monóxido de carbono (CO), cinzas e elementos químicos, tais como arsênio (As), chumbo (Pb), cádmio (Cd), selênio (Se) e mercúrio [Croiset et al., 2000; Furimsky, E., 2000]. Visando manter estas concentrações dentro dos limites legais de emissões, de acordo com as legislações ambientais, as plantas de geração de energia elétrica utilizam processos mecânicos e químicos para limpar os gases de exaustão antes de lançá-los na atmosfera.

Substâncias químicas como o dióxido de carbono (CO_2), metano (CH_4) e óxido nitroso (N_2O) são lançados pela combustão do carvão, e são importantes gases causadores do efeito estufa. Suas concentrações têm aumentado consideravelmente desde os meados de 1750 [Toftegaard et al., 2010]. Devido à tendência no aumento da concentração dos gases do efeito estufa, estes números têm chamado atenção nas questões referentes ao aquecimento global, levando a maioria das nações a discuti-los em iniciativas internacionais como o Protocolo de Quioto em 1997 e a Conferência de Doha em 2012, que estendeu as diretrizes do Protocolo de Quioto até 2020.

Como as plantas de geração de energia elétrica constituem fontes intensivas de emissão de CO_2, várias tecnologias possíveis estão sendo investigadas para viabilizar o processo de captura de carbono e armazenamento (*CCS-Carbon Capture and Storage*) das plantas de geração de energia. A eliminação das emissões de CO_2 inclui duas operações consecutivas: captura do CO_2 a partir das correntes dos gases de exaustão do forno e posterior armazenamento do CO_2, que inclui transporte até a armazenagem. Os processos de captura são agrupados em quatro categorias [Wall et al., 2009]: captura na pós-combustão, captura na pré-combustão, tecnologias emergentes, tais como separação por membranas e *chemical looping combustion* (*CLC*) e combustão com a substituição do N_2 do ar pelo CO_2 na corrente do oxidante (*oxy-fuel combustion*).

Em processos de captura na pós-combustão, o CO_2 da corrente dos gases de exaustão é separado por processos químicos de absorção com solventes ou materiais minerais, empregando membranas.

Os processos de captura na pré-combustão são encontrados nos ciclos combinados de gaseificação integrada (*IGCC-Integrated Gasification Combined Cycles*). No *IGCC*, a gaseificação do carvão é aplicada para obter o gás de síntese, contendo CO, CO_2 e H_2O. O CO é convertido em CO_2 em reatores pela reação $CO_{(g)} + H_2O_{(v)} \rightarrow CO_{2(g)} + H_{2(g)}$, seguido de processos de captura do CO_2, utilizando membranas.

A separação de gases com membranas tem motivado vários pesquisadores em todo o mundo a investir elevados recursos no desenvolvimento de membranas para a separação de gases CO_2 e H_2 ao longo do ciclo *IGCC*, principalmente em etapas com temperaturas superiores a 200 ^oC, visando a diminuir o uso de energia para resfriar esses gases, penalizando menos o ciclo. A separação de gases em elevadas temperaturas pode ser obtida pelo emprego de membranas inorgânicas de material cerâmico, sílica e ligas metálicas. Membranas densas metálicas constituídas de ligas de paládio (Pd) são caras, embora em muitos aspectos sejam as ideais para separação do H_2 com elevado grau de pureza a partir de uma mistura de gases. No entanto, estas membranas são susceptíveis ao ataque de CO e de contaminantes (enxofre), embora as ligas de Pd com cobre (Cu) têm melhorado as propriedades das membranas para lidar com concentrações de ácido sulfídrico [Morreale et al., 2007].

O processo de combustão denominado *chemical-looping combustion* (*CLC*) é uma das tecnologias emergentes, que utiliza dois reatores de leito fluidizado circulante, no qual o oxigênio, carregado por substâncias químicas em estado sólido (óxido de metal, como óxido de níquel 2NiO(s)) que formam o leito, reage com o combustível (C(s)) para produzir elevada

concentração de CO_2 e vapor d´água na corrente dos gases de exaustão (reator de combustível), que é dada pela reação $C(s) + 2NiO(s) \rightarrow CO_2(g) + 2Ni(s)$. Os óxidos de metal reduzidos são transportados para o segundo reator (reator de ar), onde reagem com ar, liberando N_2 e retornando ao primeiro reator (de combustível), onde a reação $2Ni(s) + O_2(g) \rightarrow 2NiO(s)$ ocorre, conforme Hossain e Lasa, 2008.

A oxicombustão é um processo que combina a um corrente de oxigênio com concentração alta (tipicamente maior do que 95% de pureza em vol.) com a corrente reciclada dos gases de exaustão. Eliminado o nitrogênio da corrente do oxidante, o gás de exaustão se torna uma corrente rica em CO_2 com pequena quantidade em vapor d´água (depende também do teor de umidade dos combustíveis fósseis), permitindo o seqüestro do CO_2. A corrente reciclada dos gases de exaustão ajuda a controlar a temperatura de chama adiabática dentro dos limites aceitáveis de funcionamento dos fornos [Wall et al., 2009].

A tecnologia da oxicombustão é uma alternativa para países que querem continuar usando o carvão como combustível fóssil para geração de energia elétrica por um longo tempo e diminuir as suas emissões de poluentes, visando respeitar os acordos de cooperação internacional sobre as questões referentes ao aquecimento global.

A oxicombustão dispõe de grande vantagem em comparação às plantas convencionais de geração energia elétrica (i.e. em atmosfera oxidante de ar), porque aumenta a eficiência de captura e armazenagem do CO_2, com redução das concentrações de emissões de espécies químicas nocivas ao meio ambiente, tais como os óxidos de nitrogênio (NO_x).

Em plantas de oxicombustão de geração de energia elétrica, a corrente do oxidante formada pelo ar atmosférico é substituída pelas correntes de O_2 e CO_2. As correntes de alimentação de O_2 e CO_2 precisam proporcionar condições operacionais semelhantes às obtidas na combustão em ar atmosférico, com temperaturas de chama adiabática e transferência de calor similares as da combustão convencional [Wall et al., 2009].

A substituição do N_2 pelo CO_2 afeta a ignição e as características da combustão pulverizada, estabilidade do queimador, propagação da chama, temperatura dos gases, combustão do char do carvão, propriedades radiantes da chama, eficiência da caldeira e a geração dos poluentes [Bejarano e Levendis, 2008]. Muito desses efeitos são explicados pela diferença entre as propriedades dos gases CO_2 e N_2, tais como densidade, calor específico, e difusividades térmica e mássica. Se a tecnologia de oxicombustão for utilizada para transformar plantas de energia elétrica convencionais ou projetar novas instalações, estes efeitos precisam ser solucionados.

Entretanto, há algumas penalidades no processo de oxicombustão, devido à captura e o armazenamento do CO_2, e à produção do oxigênio, impondo uma penalidade de 7 a 10% na eficiência do processo de geração de energia elétrica [Wall et al., 2009]. Os maiores contribuintes pela penalidade na eficiência são a compressão do CO_2 e produção de oxigênio. Isto ocorre devido à necessidade de obter elevada concentração de O_2 na corrente do oxidante (aproximadamente 95% em vol.) A tecnologia em larga escala disponível para os processos de separação de ar é baseada em destilação criogênica, que impõe enorme penalidade na eficiência do processo das plantas de geração de energia à base de carvão.

Dentro das tecnologias existentes para separação de ar, as plantas criogênicas são desenvolvidas para atender elevadas vazões de concentração de oxigênio com alta pureza (entre 95 e 97% em vol.), conforme McCauley et al., 2009. Processos de separação de ar baseados em membranas, adsorção por pressão (*PSA-Pressure Swing Adsorption*), adsorção a vácuo (*VPSA-Vacuum Pressure Swing Adsorption*), e outros métodos químicos ainda precisam de pesquisa continuada para competir em larga escala com a produção das plantas criogênicas e serem usadas no processo de oxicombustão [Toftegaard et al., 2010].

Diante desse cenário, no presente trabalho, as atividades experimentais são realizadas com o carvão linhito pré-seco da região da Lusácia na Alemanha e dois carvões brasileiros com alto teor de cinzas das reservas carboníferas das Minas do Leão (RS) e da Camada Bonito (SC), utilizando um laboratório com uma câmara de combustão de 20 kW de capacidade térmica, denominada ALVA 20.

Esta bancada experimental utiliza um reator de combustão ciclônico em regime de escoamento turbulento com *swirl* para combustão de diversos tipos de carvão. Um sensor potenciométrico de oxigênio, à base de zircônia, instalado no interior do reator, é utilizado para medir a variação da concentração de oxigênio durante a combustão das amostras de carvão. Os resultados obtidos são utilizados para calcular os parâmetros cinéticos globais da combustão do carvão, assumindo um reator bem misturado e aplicando o balanço de massa de oxigênio em todo o reator [Tappe e Krautz, 2011, 2009; Krüger, 2010].

1.1 Motivação

Entender como é o comportamento da combustão de carvões de baixo *rank* em atmosferas de oxicombustão e em condições de escoamento turbulento e com *swirl* no reator ciclônico, tendo em vista que os reatores convencionais *DTF* (*Drop Tube Furnace*) e *EFR*

(*Entrained Flow Reactor*) operam em condições de escoamento laminar, conforme revisão bibliográfica [Brix et al., 2010; Rathnam et al., 2009; Bejarano e Levendis, 2008; Borrego e Alvarez, 2007; Murphy e Shaddix, 2006].

Acordo de cooperação de pesquisa através do projeto PROBRAL entre o laboratório de combustão e novas tecnologias na conversão de energia a partir do carvão da Universidade de Tecnologia de Cottbus, em Brandemburgo, Alemanha, com o laboratório LETA, da Universidade Federal do Rio Grande do Sul, para o estudo da reatividade de carvões com alto teor de cinzas.

1.2 Objetivos

Investigar a influência da concentração de vapor d´água em atmosferas de oxicombustão na reatividade do carvão linhito (LTBK), através da curvas de concentração de oxigênio medidas pelo sensor potenciométrico de oxigênio na combustão das amostras do carvão. A descrição da bancada experimental e como os experimentos são realizados para a investigação da combustão do carvão são apresentados em detalhes, porque são utilizados na seqüência de experimentos realizados com a bancada experimental (Capítulo 2).

Investigar através do Planejamento de Experimentos (DoE) quais os fatores, como temperatura, atmosfera oxidante, diâmetro de partícula, carvão, posição do sensor de oxigênio no interior do reator, são mais influentes na reatividade dos carvões LTBK, Leão e Bonito e dos chars obtidos dos carvões Leão e LTBK, analisando as curvas de concentração de oxigênio com a ferramenta estatística ANOVA (Capítulo 3).

Investigar a reatividade dos carvões e chars estudados no Capítulo 3 através da determinação dos parâmetros cinéticos globais e dos coeficientes das taxas de reação do char em atmosferas de oxicombustão e de ar (Capítulo 4).

1.3 Revisão Bibliográfica

A revisão bibliográfica está dividida nas seguintes seções: fundamentos, i.e, a Teoria das Três Zonas, a qual é necessária para a apresentação da terminologia e comentários utilizados na revisão; principais resultados da literatura e dos trabalhos realizados com a bancada experimental ALVA 20 e as conclusões, identificando as oportunidades de trabalho a serem investigadas na presente tese.

1.3.1 Teoria das Três Zonas

Smoot e Smith, 1985, descrevem a Teoria dos Três Regimes ou Zonas de combustão do char do carvão em atmosfera de ar, conforme mostrado na Fig. 1.1. O "char" é a massa residual enriquecida em carbono, sem a presença do oxigênio e hidrogênio, mas, que ainda contém grande parte da matéria mineral e com pequena quantidade de nitrogênio e enxofre, após o carvão ter passado pelo processo de desvolatilização.

Os regimes de controle da taxa de reação da partícula de char $\dot{r}_p$ levam em conta os seguintes parâmetros:

- d_p, diâmetro da partícula de char;
- E_{ap}, energia de ativação "aparente";
- m, ordem real da reação;
- n, ordem "aparente" da reação;
- ρ_{ap}, densidade "aparente" da partícula de char;
- C_g, concentração do oxigênio na atmosfera oxidante.

A denominação do termo "aparente" se refere aos parâmetros obtidos nos Regimes II e III da taxa de reação de combustão do char, onde o controle da combustão não é mais exclusivamente cinético. A densidade "aparente" ou "bulk" do char é resultante da reação química do oxidante na superfície dos poros da partícula, alterando o volume dos poros, sendo necessária a medição da densidade "bulk" ao longo da conversão para o cálculo da taxa de reação de combustão. A energia de ativação "aparente" ou global é resultante do controle cinético das reações químicas do oxidante com o carbono da partícula e do controle difusivo do oxidante pelos poros da partícula ou pela camada limite do filme de oxidante que se forma na partícula, é obtida através da manipulação da Equação de Arrhenius em base logarítmica, determinada pelo coeficiente angular da Eq. 1.1, depois de determinados os parâmetros cinéticos globais da reação de combustão (k_{eff}, n).

$$\ln k_{eff} = \ln k_o - E_{ap} \big/ RT_p \tag{1.1}$$

onde

k_{eff} é a constante global da taxa de reação de combustão ou velocidade de reação, que incorpora o controle cinético das reações químicas, controle difusivo do oxidante pelos poros e o controle difusivo do oxidante pela camada limite na partícula de char e dos voláteis.

k_o é o fator de freqüência ou pré-exponencial, que é proporcional ao número de colisões de moléculas.

R é a constante universal do gás ideal.

Na presente tese, os parâmetros globais da combustão do carvão (k_{eff}, n) em atmosferas de ar e de oxicombustão serão determinados experimentalmente.

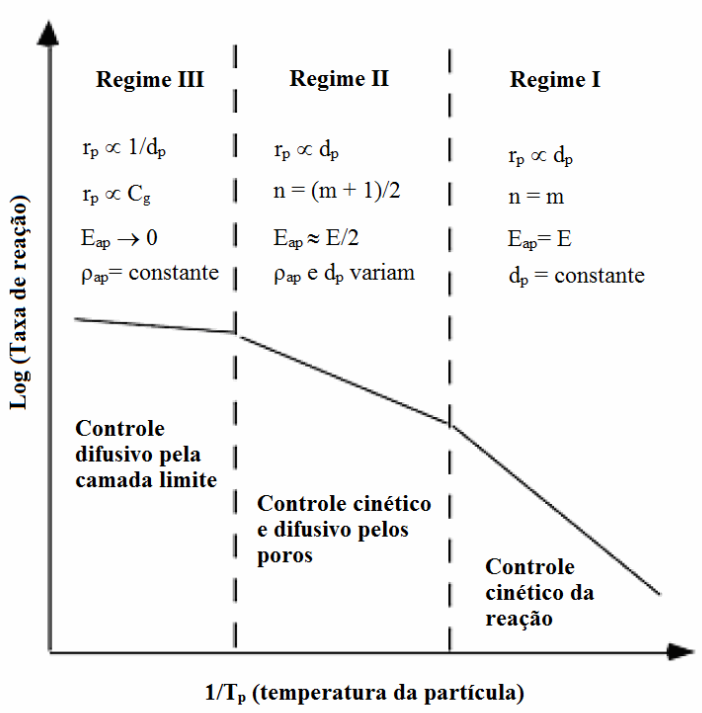

Figura 1.1 - Investigação sobre os regimes de controle em atmosfera de ar na combustão heterogênea do char [adaptado de Smoot e Smith, 1985].

No Regime I, o controle da taxa de reação de combustão do char $\dot{r}_p$ é cinético, logo, a energia de ativação E e ordem de reação m obtidas são exclusivamente devidas às reações químicas do oxidante com o carbono da partícula [Smith, 1982; Smith, 1977]. Neste regime, o oxidante difunde completamente no interior da partícula sem resistência da difusão do oxigênio pelos poros da partícula. A taxa de reação de combustão é diretamente proporcional ao diâmetro da partícula de char. Como o oxigênio é consumido totalmente na superfície dos poros da partícula, o diâmetro da partícula permanece constante e a densidade do char varia.

A taxa de reação de combustão é influenciada pela temperatura, porque o controle da taxa é cinético.

No Regime II, o controle da taxa de reação de combustão do char $\dot{r}_p$ é cinético devido às reações químicas do oxidante com o carbono da partícula, e difusivo devido à resistência do oxidante se difundir no interior da partícula de char. Neste caso, a energia de ativação e a ordem da reação obtida não estão somente sob o controle cinético, mas, agora, com a participação do controle difusivo pelos poros da partícula também. Logo, a energia de ativação e a ordem de reação são denominadas aparentes. Sendo assim, energia de ativação aparente E_{ap} é aproximadamente metade da energia de ativação obtida no controle cinético, enquanto que a ordem reação aparente n é dada pela relação $n=(m+1)/2$. Neste regime, a taxa de reação de combustão é diretamente proporcional ao diâmetro da partícula de char. Como o oxigênio é consumido parcialmente na superfície dos poros da partícula, o diâmetro e a densidade do char variam. A temperatura ainda tem influência na taxa de reação de combustão do char influenciando o controle cinético das reações químicas do oxidante com o carbono da superfície dos poros da partícula.

No Regime III, o controle da taxa de reação de combustão do char $\dot{r}_p$ é dada pela difusão do oxidante pela camada limite que se forma na partícula. Neste caso, as reações químicas do oxidante com o carbono da partícula ocorrem na superfície da partícula do char, sem a difusão do oxigênio no interior dos poros da partícula, e são mais rápidas do que taxa de difusão do oxigênio pela camada limite. Como o controle da taxa de reação de combustão é difusivo pela camada limite, a energia de ativação aparente será próxima de zero e a variação da temperatura não tem influência sobre a taxa de reação química. Neste regime, a taxa de reação de combustão é inversamente proporcional ao diâmetro da partícula de char e proporcional à concentração de oxigênio na atmosfera do oxidante C_g. Como o oxigênio é consumido totalmente na superfície da partícula, há uma redução proporcional do volume e da densidade da partícula. Conforme observados pelos autores Smoot e Smith, 1985, os parâmetros cinéticos obtidos em qualquer investigação devem ser interpretados à luz das condições nos quais foram obtidos.

A densidade aparente, a área da superfície específica dos poros e o tamanho final das partículas de char vão depender, portanto, do regime de controle de combustão no qual a partícula faz parte.

Wall et al., 2009, fizeram uma análise dos regimes da taxa de reação de combustão do char em atmosferas de oxicombustão (O_2/CO_2) comparando-os com os resultados obtidos em atmosfera de ar (O_2/N_2) para experimentos realizados em fornos *DTF* e balança termogravimétrica (*TGA*) com quatro tipos de carvões pulverizados [Rathnam et al., 2009], conforme mostrado na Fig. 1.2.

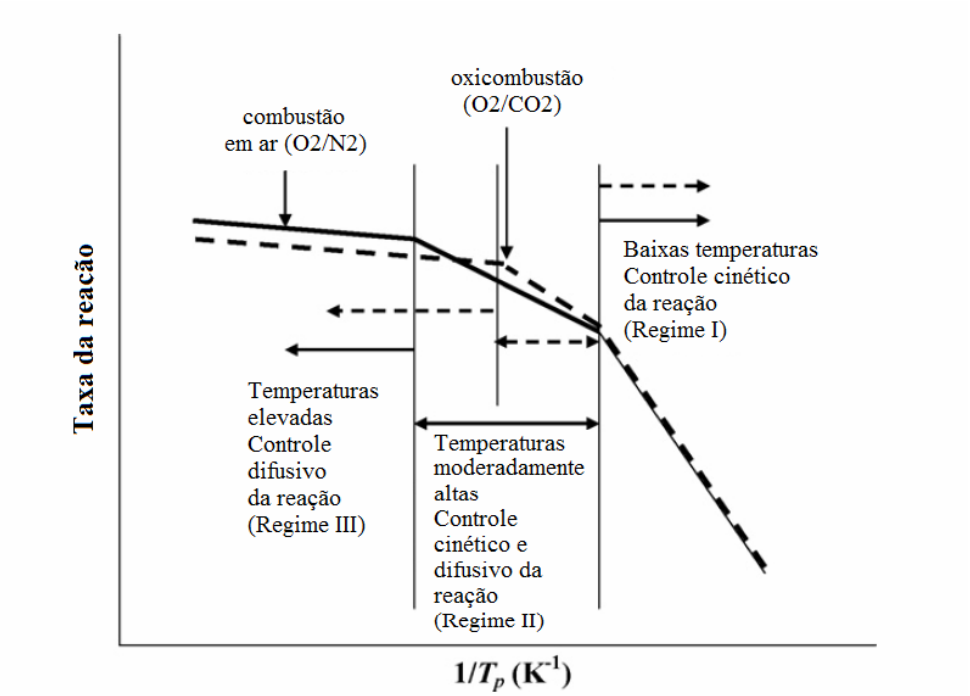

Figura 1.2 - Investigação sobre os regimes de controle em atmosfera de ar e de oxicombustão para o mesmo carvão: as linhas pontilhadas se referem à atmosfera de oxicombustão e as linhas cheias se referem à atmosfera de ar [adaptado de Wall et al., 2009].

Os autores concluíram que no Regime I, controlado pela cinética das reações químicas, a taxa da reação de combustão é similar entre as atmosferas de ar e oxicombustão. No Regime II, controlado pela cinética e pela difusão do oxidante pelos poros da partícula, ocorre a reação de gaseificação do CO_2 com o carbono do char ($C + CO_2 \rightarrow 2CO$), a partir de 1073 K, que aumenta a reatividade do carvão nas condições de oxicombustão [Rathnam et al., 2009]. No Regime III, em temperaturas mais elevadas, como a taxa de reação de combustão é controlada pela difusão do oxigênio pelo filme da partícula, e o coeficiente de difusividade binário do O_2 no CO_2 é mais baixo do que o do O_2 no N_2, taxas de combustão mais baixas são observadas nas atmosferas de oxicombustão em relação às obtidas em atmosferas de ar. As transições e as taxas de reação de combustão nos Regimes II e III dependem do tamanho de partícula, já que deste depende a espessura do filme e do tamanho dos poros para a difusão do

oxidante. Como o tamanho de partícula tem menor importância em relação à temperatura para determinar os regimes de controle na escala de plantas piloto para carvão pulverizado, a análise dos regimes pelos autores foi baseada somente na temperatura [Wall et al., 2009].

É importante ressaltar que os regimes de controle da taxa de reação de combustão observados para as atmosferas de oxicombustão são específicos para determinados tipos de carvão e equipamentos, e resultados diferentes podem ser obtidos para outros tipos de carvão, condições de teste e equipamentos [Brix et al., 2010].

1.3.2 Resumo dos principais resultados da literatura e conclusões

O trabalho dos autores Lorentz e Rau, 1998, tem destaque especial na presente tese, porque deles vem a medição do consumo de oxigênio pelo sensor potenciométrico no estudo dos parâmetros cinéticos globais da combustão de combustíveis sólidos em leito fluidizado, cuja medição foi utilizada, posteriormente, no reator de combustão ciclônico do projeto da bancada experimental ALVA 20 [Tappe, 2011, 2009], sobre a qual a presente tese é desenvolvida.

Lorentz e Rau, 1998 e 2004, desenvolveram uma bancada experimental para obtenção dos parâmetros cinéticos globais da combustão de diversos tipos de combustíveis sólidos em atmosfera de ar, através da medição do consumo de oxigênio da amostra por batelada no reator de leito fluidizado com sensor potenciométrico de oxigênio (à base de zirconia), conforme mostrado na Fig. 1.3.

Vários tipos de combustíveis sólidos foram testados, desde carvões de baixo *rank* até carvões com alto teor de carbono, como os antracitos, além de materiais como resíduos de madeiras, biomassa e entre outros. As amostras de combustíveis investigados têm massas de 0,05 g, 0,1 g e 0,15 g e diâmetros de partículas entre 0,2 a 0,4 mm (200 a 400 μm). O material do leito é constituído de areia de quartzo com diâmetro de partícula entre 0,25-0,315 mm e altura do leito de 50 mm. As temperaturas de combustão são de 750, 850 e 950 ^{o}C, sendo que a vazão volumétrica do ar oxidante é de 400 l/h em 20 ^{o}C. Os sensores estão posicionados 30 mm acima do leito fixo.

O sensor potenciométrico de oxigênio para a utilização no leito fluidizado foi desenvolvido em parceria com o fabricante Zirox, porque o elemento sensor de medição da concentração de oxigênio, localizado na extremidade da sonda, precisa de uma proteção

especial contra a abrasividade do leito e das partículas [Lorentz, H., 2004] entre os quais estava imerso.

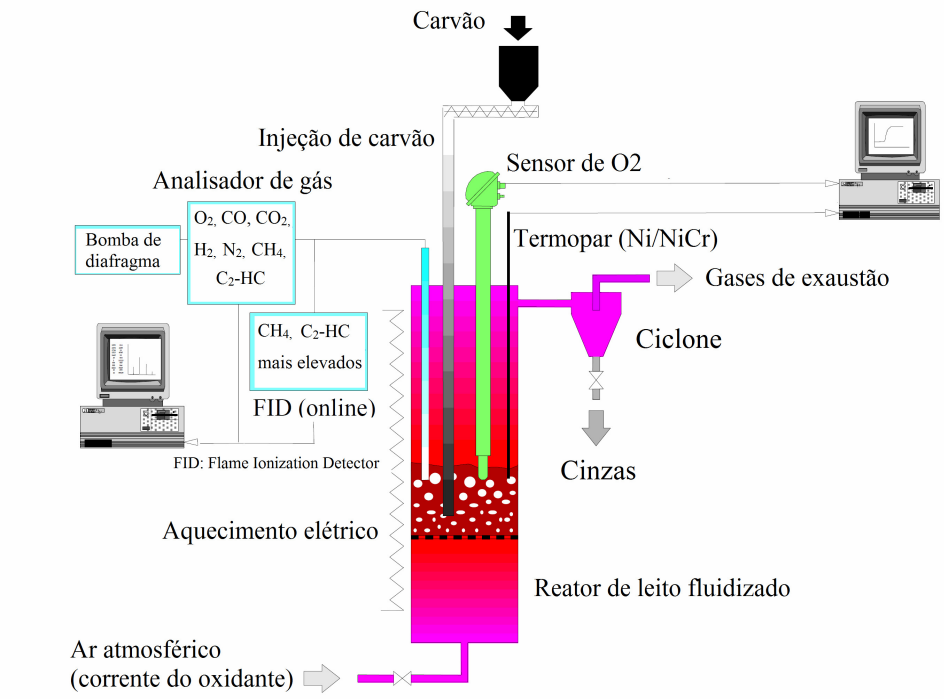

Figura 1.3 - Diagrama esquemático da bancada com reator de leito fluidizado com o sensor potenciométrico de oxigênio [adaptado de Lorentz, H., 2004].

O método do balanço de oxigênio é empregado para calcular os parâmetros cinéticos globais dos combustíveis investigados, considerando que toda a variação da concentração de oxigênio medida ao longo da combustão da amostra é exclusivamente devido ao consumo de oxigênio pela amostra. Os parâmetros cinéticos globais são analisados por meio da constante efetiva (global) da taxa de reação k_{eff} e da energia de ativação global E_{ap}, para ordem de reação aparente n igual 1 calculada pelo método integral de determinação dos parâmetros cinéticos globais, considerando uma reação unimolecular e irreversível de ordem 1 [Levenspiel, 1999].

Os resultados obtidos mostram que a maioria dos combustíveis sólidos analisados tem as suas taxas de reação controladas pelos regimes cinético e difusivo do oxigênio pelos poros das partículas, com energia de ativação entre 28 e 64 kJ/mol, incluindo o carvão linhito. O char do carvão betuminoso tem uma energia de ativação de 105 kJ/mol, o que indica controle cinético da reação de combustão, devido à influência do aumento da temperatura no controle da taxa de reação de combustão.

Bejarano e Levendis, 2008, investigaram a combustão de partículas de carvão pulverizadas (betuminoso e linhito com tamanho de partículas entre 45-180 μm e 45-90 μm, respectivamente) em um forno *DTF* usando dois tipos de atmosferas oxidantes: O_2/N_2 e O_2/CO_2, e com concentrações de O_2 entre 20 a 100% (em vol.).

Os principais resultados e conclusões são:

- Os tempos de "burnout" das partículas de linhito foram menores do que os obtidos para as partículas de char do carvão betuminoso; isto é atribuído parcialmente à reatividade mais elevada do linhito em relação ao carvão betuminoso.
- A combustão do carvão resultou em taxas de reação e temperaturas de partículas mais elevadas em atmosferas de O_2/N_2 em relação às obtidas em O_2/CO_2 para toda a variação molar de oxigênio e tamanho de partícula. Esse resultado indica que a taxa de reação de combustão é controlada pela difusão do oxigênio pelo filme da partícula (Regime III), e como o coeficiente de difusividade binário do O_2 no CO_2 é mais baixo do que o do O_2 no N_2, taxas de combustão mais baixas são observadas nas atmosferas de oxicombustão em relação às obtidas nas atmosferas de O_2/N_2.

Rathnam et al., 2009, investigaram a reatividade da combustão do carvão pulverizado em atmosferas de ar (O_2/N_2) e de oxicombustão (O_2/CO_2) usando o forno *DTF* e a balança termogravimétrica (*TGA*). Quatro tipos de carvão foram testados com o diâmetro das partículas variando de 63 a 90 μm. Os experimentos com *DTF* foram utilizados para preparar as quatro amostras de char a fim de analisar suas reatividades nos experimentos com *TGA*.

Os principais resultados e conclusões são:

- As amostras de char apresentaram maior formação de voláteis em atmosferas de O_2/CO_2 em relação às obtidas em O_2/N_2 nos experimentos com *DTF*, e isto é atribuído à reação de gaseificação do CO_2 com o char. As amostras apresentaram um aumento da área da superfície específica do char de aproximadamente 10-43% em atmosfera de CO_2 em comparação com as obtidas em atmosfera de N_2; esta constatação é, também, resultado de uma maior exposição da área da superfície interna do char criada pela reação de gaseificação do CO_2, que é influenciada pela temperatura e pelo tipo de carvão, o qual oferece menor ou maior resistência à difusão do oxigênio pelos poros da partícula (Regime II).
- As diferenças dos *burnouts* dos carvões testados entre as atmosferas de O_2/CO_2 e O_2/N_2 são explicadas pela reatividade do char mais elevada na atmosfera de oxicombustão devida à reação de gaseificação do CO_2-char, a qual depende também do tipo de carvão e

da temperatura do experimento. Testes realizados com um tipo de carvão nos experimentos com *TGA* em atmosferas de 100% de N_2 e 100% de CO_2 mostraram a presença da maior taxa de perda de massa do char em temperaturas maiores do que 1030 K em atmosfera de CO_2.

- Em atmosferas de O_2/CO_2 com concentração de 2% O_2 (em vol.) e temperaturas acima 1030 K nos experimentos com *TGA*, a reação de gaseificação do CO_2 com char influencia a reatividade do carvão, mostrando que a reação de gaseificação do CO_2 com o char está presente em baixas concentrações de O_2 e temperaturas acima de 1073 K.

1.3.3 Trabalhos realizados com a bancada experimental ALVA 20

Tappe e Krautz, 2011, 2009a, 2009b, investigaram o comportamento da combustão do carvão em atmosferas de ar e de oxicombustão (O_2/CO_2) usando um laboratório experimental denominado ALVA 20, monitorando o consumo de oxigênio por um sensor potenciométrico (de zircônia) no interior de uma câmara de combustão ciclônica. Os principais estágios da combustão do carvão (voláteis e char) foram analisados pela medição da curva de concentração de oxigênio ao longo do tempo de combustão da amostra de carvão. Diferentes amostras de carvão (linhito pré-seco e antracito) e tamanhos de partículas são investigados em atmosferas de oxicombustão e de ar nos resultados dos parâmetros cinéticos globais.

Os principais resultados e conclusões são:

- Os tempos de combustão diminuem de 10 a 15% na atmosfera de O_2/CO_2 (21/79 vol. %) em comparação aos resultados obtidos na atmosfera de ar para os carvões de baixo *rank* (no caso do linhito) influenciados pelo aumento da temperatura do gás do reator a partir de 1223 K. Estes resultados são explicados pela influência da reação de gaseificação do CO_2 com a partícula de carvão a partir de temperaturas superiores a 1073 K. Tempos maiores de combustão e pouco efeito da temperatura da atmosfera oxidante na taxa de reação de combustão são obtidos para carvões de alto *rank* como o caso do antracito. A diferença dos resultados obtidos entre os carvões de baixo e alto *rank* nas mesmas condições de testes está relacionada principalmente à porosidade do carvão, à quantidade de matéria volátil e de carbono na sua estrutura. Carvões de alto *rank* demoram mais tempo para queimar, porque o oxigênio não penetra completamente no interior dos poros da partícula, ocorrendo um controle cinético e difusivo pelos poros (Regime II), ou um controle completamente difusivo pelo filme na partícula (Regime III). Para estes carvões, a reação de gaseificação do CO_2 no char tem pouco efeito com o aumento da temperatura. Carvões

de baixo *rank* demoram menos tempo para queimar, devido à quantidade de matéria volátil existente na sua matriz, e devido a sua porosidade formada depois da pirólise e combustão dos voláteis, favorecendo a difusão do oxigênio no interior da partícula de char, propiciando um ambiente favorável à reação de gaseificação do CO_2 com o char, e o controle cinético e difusivo do oxigênio através dos poros da partícula (Regime II). Há casos, que a taxa de reação na superfície da partícula de char é tão rápida que a taxa de reação de combustão é controlada pela difusão do oxigênio pelo filme da partícula, onde não há mais o efeito do aumento da temperatura na taxa de reação global de combustão e o que influencia é o diâmetro da partícula (Regime III), conforme observado para partículas na faixa da granulometria pulverizada.

- Amostras de carvão linhito pré-seco com tamanho médio de partículas de 312 μm têm tempos de combustão menores em comparação aos tempos obtidos para partículas de 1625 μm, testados em atmosferas de ar e de oxicombustão (O_2/CO_2) com 21% O_2, com pouca influência da temperatura do gás a partir de 1173 K na atmosfera de ar em partículas de 312 μm de diâmetro médio. Nestes resultados, o efeito do tamanho de partícula prepondera sobre os efeitos das composições das atmosferas oxidantes e da temperatura do gás na taxa de reação de combustão. É uma evidência de que a taxa de combustão é controlada pela difusão do oxigênio através do filme formado entorno das partículas de 312 μm (Regime III) nestas condições [Smoot e Smith, 1985].
- Os parâmetros cinéticos globais determinados para diversos tipos de carvão e atmosferas oxidantes mostram que a taxa de reação de combustão está sob o controle dos Regimes II e III, com valor de energia global de ativação menor do que 50 kJ/mol [Tappe, 2011], o que evidencia um controle cinético e difusivo pelos poros e camada limite da partícula.

Diante deste cenário, abrem-se as seguintes oportunidades de trabalho com a bancada experimental ALVA 20 identificadas na revisão bibliográfica da presente tese:

- Investigar a reatividade de carvões com alto teor de cinzas em atmosferas de ar e de oxicombustão através da determinação dos parâmetros cinéticos globais do carvão.
- Investigar qual é o regime de controle da taxa de reação de combustão nestes tipos de carvões, isto é, cinético, difusivo pelos poros, difusivo pela camada limite.
- Investigar qual é a reatividade dos chars preparados a partir dos carvões com alto teor de cinzas (Leão) e com alto teor de voláteis (linhito pré-seco) quando submetidos à combustão em atmosferas de ar e de oxicombustão no reator ciclônico.

REFERÊNCIAS BIBLIOGRÁFICAS

Bejarano, P.A., Levendis, Y.A., 2008**.** "Single-coal-particle combustion in O_2/N_2 and O_2/CO_2 environments", Combustion and Flame, v. 153, p. 270-287.

Borrego, A.G., Alvarez, D., 2007. "Comparison of chars obtained under oxy-fuel and conventional pulverized coal combustion atmospheres", Energy & Fuels, v. 21, p. 3171-3179.

Brix, J., Jensen, P.A., Jensen, A.D., 2010. "Coal devolatilization and char conversion under suspension fired conditions in O_2/N_2 and O_2/CO_2 atmospheres", Fuel, v. 89, p. 3373-3380.

Buhre, B.J.P., Elliott, L.K., Sheng, C.D., Gupta, R.P., Wall, T., 2005. "Oxy-fuel combustion technology for coal-fired power generation", Progress in Energy and Combustion Science, v. 31, p. 283-307.

Croiset, E.; Thambimuthu, K.; Palmer, A., 2000. "Coal combustion in O_2/CO_2 mixtures compared with air", The Canadian Journal of Chemical Engineering, v. 78, p. 402-407.

Furimsky, E., 2000. "Characterization of trace element emissions from coal combustion by equilibrium calculation", Fuel Processing Technology, v. 63, p. 29-44.

Hossain, M., Lasa, H., 2008. "Chemical-looping combustion (CLC) for inherent CO_2 separations - a review", Chemical Engineering Science, v. 63, p. 4433-4451.

International Energy Agency (IEA), 2012. "World energy outlook", IEA Publications 2012, http://www.worldenergyoutlook.org/docs

Krüger, P., 2010. "Inbetriebnahme einer 20 kWth-atmosphärischen Laborverbrennungsanlage und Durchführung erster experimenteller Arbeiten zum Abbrandverhalten von Lausitzer Trockenbraunkohle", Dissertation, Brandenburg University of Technology, Cottbus, Alemanha, 93 p.

Levenspiel, O., 1999. “Chemical Reaction Engineering”, 3rd Edition, John Wiley & Sons, New York, USA, p. 668.

Lorentz, H., 2004. “Heterogene Prozesse am Beispiel der Verbrennung fester Stoffe und der Kristallisation aus Lösungen”, Tese, Faculdade de Processos e Sistemas de Engenharia, Universidade Otto von Guericke de Magdeburg, Alemanha, p. 99.

Lorentz, H., Rau, H., 1998. “A new method for investigating the combustion behavior of solid fuel in FBC”, Fuel, v. 77, p. 127-134.

McCauley, K.J.; Farzan, H.; Alexander, K.C.; McDonald, D.K.; Varagani, R.; Prabhakar, J.P.; Tranier, J.P.; Perrin, N., 2009. “Commercialization of oxy-coal combustion: Applying results of a large 30MWth pilot project”, Energy Procedia, v. 1, p. 439-446.

Morreale, B., Killmeyer, R., Iyoha, O., Howard, B., Enick, R., Ciocco, M., 2007a. “Wall-catalyzed water-gas shift reaction in multi-tubular Pd and 80 wt%Pd–20 wt%Cu membrane reactors at 1173K”, Journal of Membrane Science, v. 298, p. 14–23.

Morreale, B., Killmeyer, R., Iyoha, B., Enick, R., 2007b. “The influence of hydrogen sulfide-to-hydrogen partial pressure ratio on the sulfidization of Pd and 70mol% Pd-Cu membranes”, Journal of Membrane Science, v. 305, p. 77–92.

Murphy, J.J, Shaddix, C.R., 2006. “Combustion kinetics of coals chars in oxygen-enriched environments”, Combustion and Flame, v. 144, p. 710-729.

Rathnam, R.K., Elliot, L.K., Wall, T., Liu, Y., Moghtaderi, B., 2009. “Differences in reactivity of pulverized coal in air (O_2/N_2) and oxy-fuel (O_2/CO_2) conditions”, Fuel Processing Technology, v. 90, p. 797-802.

Smith, I.W., 1982. “The combustion rates of coal chars: a review”, 19th Symposium (International) on Combustion/ The Combustion Institute, 1045-1065.

Smith, I.W., 1977. “The intrinsic reactivity of carbons to oxygen”, Fuel, v. 57, p. 409-414.

Smoot, L.D., Smith, P.J., 1985. “Coal Combustion and Gasification”, Plenum Press, New York, USA, p. 443.

Tappe,S., 2011. “Gaspotentiometrische und thermogravimetrische Abbranduntersuchungen von Braun und Steinkohlen in Luft und O_2/CO_2-Atmosphären”, Thesis, Brandenburg University of Technology, Cottbus, Germany, p. 145.

Tappe, S., Krautz, H.J., 2009a. “ALVA 20: A 20 kWth Atmospheric Laboratory Test Facility to Investigate the Combustion Behavior under Close-to-Reality Conditions”, Proceedings of the European Combustion Meeting, p. 6.

Tappe, S.; Krautz, H.J., 2009b. “Influence of various O_2/CO_2 concentrations on the burning behavior of different coals”, 34th International Technical Conference on Coal Utilization & Fuel Systems, Clearwater, USA**,** p. 7.

Toftegaard, M. B., Brix, J., Jensen, P.A., Glarborg, P., Jensen, A.D., 2010. “Oxy-fuel combustion of solids fuels”, Progress in Energy and Combustion Science, v. 36, p. 585-625.

Wall, T., Liu, Y., Spero, C., Elliot, L., Khare, S., Rathman, R., Zeenathal, F., Moghtaderi, B., Buhre, B., Sheng, C., Gupta, R., Yamada, T., Makino, K., Yu, J., 2009. “An overview on oxy-fuel coal combustion - State of the art research and technology development”, Chemical Engineering Research and Design, v. 87, p. 1003-1016.

2. Assessment of lignite coal combustion under air and oxy-fuel atmospheres on a laboratory cyclone reactor

Abstract

A novel laboratory facility designed to investigate coal oxy-fuel combustion is described in the present work. A cyclone chamber allows for the combustion of low-rank coal under turbulent conditions and swirling flows, covering a temperature range similar to those found on actual furnaces. Lignite coal samples were sieved to a size range of 1250 to 2000 μm and burned under both air and oxy-fuel conditions. Oxy-fuel combustion is performed under two O_2/CO_2 atmospheres (21/79 and 30/70) and three $O_2/CO_2/H_2O$ atmospheres (30/60/10, 30/50/20 and 30/40/30) in molar basis. A potentiometric oxygen sensor with oxide-ion conducting electrolytes is installed within the cyclone reactor to investigate the oxygen consumption during the combustion of coal samples. Experiments were carried out at three average gas combustion temperature: 1073, 1173 and 1273 K. Results show that higher values of oxygen concentration variation are attained under oxy-fuel (21/79) at 1173 and 1273 K than that under air conditions, due to the influence of CO_2 gasification reaction on coal combustion from temperature values higher than 1073 K, and higher total elapsed times under oxy-fuel (21/79) than that in air conditions at high values of temperature (1173 and 1273 K) evidence that the oxy-fuel atmosphere properties influence on the coal sample combustion.

Keywords: Oxy-fuel combustion, low-rank coal, swirling flow, cyclone combustion reactor, potentiometric oxygen sensor.

LIST OF ABREVIATIONS AND SYMBOLS

Abbreviations

ALVA20	20 kW_{th} - Atmosphärische Laborverbrennungsanlage Laboratory test facility with cyclone reactor rated capacity of 20 kW_{th} operating under 1 atm.
BTU	Brandenburg University of Technology
CDS	Cyclone dust separator
CFD	Computational fluid dynamics
CR	Cyclone reactor
CRZ	Central recirculation zone
CTRZ	Central toroidal recirculation zone
daf	Dry, ash free
FBC	Fluidized bed combustion
LTBK	Lausitzer Trockenbraunkohle, Lusatian pre-dried brown coal
Max	Maximum
Min	Minimum
PCC	Post-combustion chamber
TPB	Triple phase boundary
vol.	Volume
YSZ	Yttria stabilized zirconia

Symbols

A	Tangential inlet area of cyclone reactor nozzles, m^{-2}
C	Concentration, gmol O_2 m^{-3} or % vol
d	Cyclone reactor diameter before the expansion, m
D	Cyclone reactor diameter after the expansion, m
e	Elementary charge, $1.60217733 \pm 0{,}00000059 \times 10^{-19}$ C
e	Distance of the centre of nozzles in relation to cyclone reactor longitudinal axis, m
f	Molar fraction, -
F	Faraday constant, 9.648×10^{4} C mol^{-1}
g	Specific gibbs free energy, J mol^{-1}
G_x	Axial flux of axial momentum, (kg m s^{-1}) s^{-1}
G_ϕ	Axial flux of swirl momentum, (kg m s^{-1}) s^{-1} m
H	Cyclone reactor height, m
I	Electrical current given by the molar flow of the electrons of the spent fuel, A
$\dot{m}$	Mass flow rate, kg s^{-1}
$\dot{n}$	Molar flow, mol s^{-1}
N	Avogadro constant number, $6.02214179 \times 10^{23}$ mol^{-1}
p	Pressure, atm
P	Reversible electrical power of the fuel cell, W
$\overline{p}$	Time mean pressure, atm
r	Radial direction, -

R	Ideal gas law constant, 8.314 J K^{-1} mol^{-1}
R	Cyclone reactor radius, m
t	Time, s
T	Temperature, K or ºC
$\overline{u}$	Time mean axial velocity, m s^{-1}
u'	Turbulent fluctuating axial velocity, m s^{-1}
U	Cell potential, mV
$\dot{V}$	Volumetric flow, m^3 h^{-1}
$\overline{v}$	Time mean radial velocity, m s^{-1}
v'	Turbulent fluctuating radial velocity, m s^{-1}
W	Reversible work of the fuel cell, W
w	Specific reversible work, kJ mol^{-1}
$\overline{w}$	Time mean tangential velocity, m s^{-1}
w'	Turbulent fluctuating radial velocity, m s^{-1}
x	Axial direction,-

Greek symbols

Δ	Increment, change
μ	Chemical potential, kJ mol^{-1}
ρ	Density, kg m^{-3}
σ	Standard deviation, s, % vol.
ϕ	Azimuthal direction, -

Subscripts

0	Initial, at reference state
1	Cyclone reactor swirler, before the expansion
2	Cyclone reactor swirler, after the expansion
∞	Infinite, at reference stream
A	Avogadro
ads	Adsorbed
an	Oxygen sensor anode
atm	Atmospheric
el	Electrons of oxygen
gas	Gas
ref	Reference
th	Thermal
T	Total

Superscripts

X	Oxygen ions vacancy
0	At reference state
2^-	Ions of oxygen

2.1 Introduction

Many works have been carried out in the last years in order to understand the influence of the presence of CO_2 on devolatilization and ignition [Toftegaard et al., 2010], and volatile and char burnout [Brix et al., 2010; Zhang et al., 2010]. Literature reveals a significant number of works on the impacts of oxy-fuel atmospheres on low-rank coals combustion [Corrêa, 2013; Tappe and Krautz, 2011, 2009; Zhang et al., 2010b]. Additionally, most of these studies were carried out applying standard techniques of analysis, such as thermogravimetric tests [Liu, 2009] and entrained-flow reactors [Rathnam et al., 2009]. It is well-known that thermogravimetric tests operate under conditions that are far from those in real furnaces, whereas entrained flow reactors are the unique equipments that can simulate more closely actual combustion environments. Consequently, there is a need of quantitative information obtained out of reactors operating under conditions encountered in existing furnaces. Successful results have been obtained with fluidized bed reactors to understand the combustion behavior of solid fuels under air-fired conditions with the aid of solid electrolyte oxygen sensor as stabilized zirconia to calculate the global kinetic parameters [Lorentz and Rau, 1998].

The experiment described in the present work was performed in a laboratory test facility developed at the Chair of Power Plant Technology of the Brandenburg University of Technology - BTU at Cottbus, Germany, to study the coal combustion behavior under oxy-fuel atmospheres as well as regular air conditions. This test facility aims to approximate coal combustion to the environment conditions found in existing furnaces. Results allow for the calculation of the coal global kinetic parameters by measuring the variation on oxygen concentration with the aid of a potentiometric oxygen sensor installed within the reactor. The test methodology for obtaining the global kinetic parameters from this test facility was extensively studied by Tappe, 2011 and 2009.

The present chapter describes the laboratory test facility and its main features, the experimental methodology, the most relevant results obtained out of 1g samples of pre-dried lignite coal from the Lusatian German region (LTBK) under air and oxy-fuel atmospheres with water vapor based on the oxygen concentration curves analysis.

2.2 Description of the laboratory facility

A schematic diagram of the experimental setup is shown in Fig. 2.1. The combustion takes place in a cyclone reactor with a thermal rated capacity of 20 kW. Basically, crushed and pre-dried coal is previously transported into a storage silo which feeds a metering system. The size of the coal particles for continuously operation should not be smaller than 50 µm and should not exceed 2000 µm. The coal can be also inserted into the reactor discontinuously by means of an independent system for investigation of rates of the combustion process of single samples.

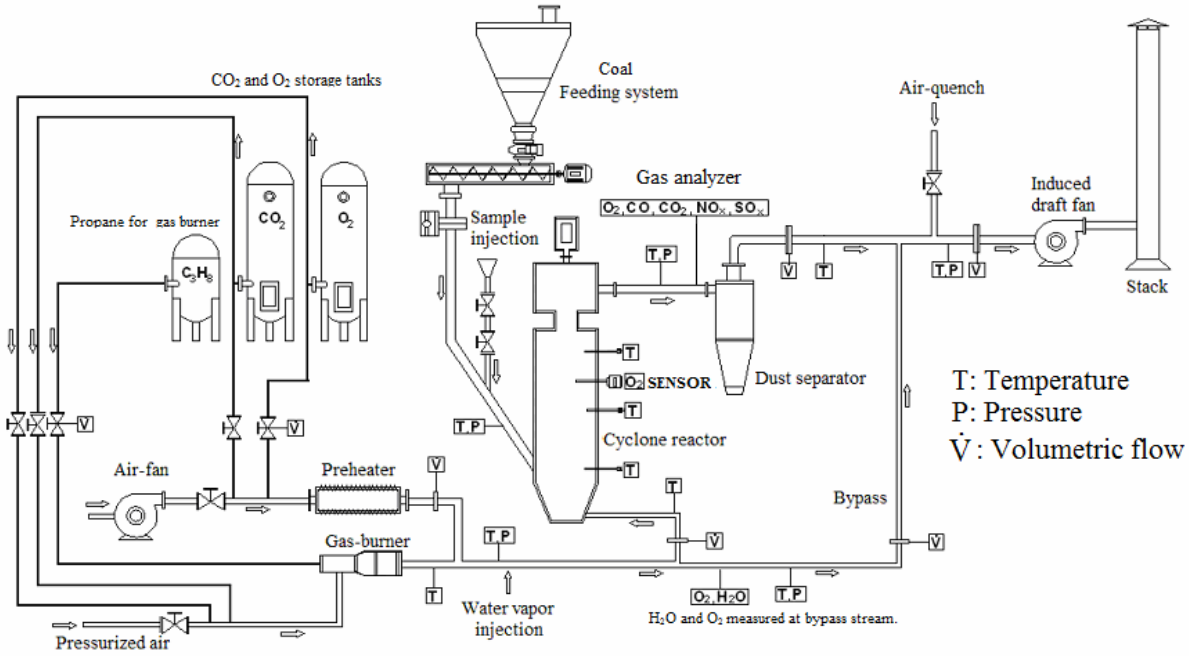

Figure 2.1 - Schematic of ALVA 20 test facility [adapted from Carotenuto and Corrêa, 2011].

Air stream is supplied by a variable speed fan, whereas in the case of oxy-fuel combustion, O_2 and CO_2 are supplied by storage tanks. In this case, the gas flow is controlled with pressure regulators and valves and the flow rate measured by calibrated rotameters. Flow rate upstream of the furnace are also measured by an orifice plate for all operating conditions. Temperature of the oxidant stream before entering into the furnace is increased by means of a pre-heater and a propane burner. Water vapor is injected into the oxidizer stream with the aid of steam generator, which operates at range of 435-445 K and of 4-5 atm. After the reactor, the flue gas is passed through a cyclone dust separator to remove fly ashes and other particulates before being cooled down by an air quench and vent out by a stack. Furnace chamber is kept in depression by an induced draft fan.

2.2.1 Equipments and instrumentation

Table 2.1 shows the equipments and its main specifications used in the experimental setup [Krüger, 2010; Tappe, 2007], depicted in Fig. 2.1.

Table 2.1 - List of the equipments and its main specifications

Equipments	Specifications
Air fan (radial)	Max. flow rate: 65 m^3/h @ 1 atm Min. flow rate: 30 m^3/h @ Δp:15000 Pa (150 mbar)
Induced draft fan (radial)	Max. flow rate: 1500 m^3/h @ 1 atm Min. flow rate: 360 m^3/h @ Δp:4500 Pa (45 mbar)
Pre-heater	Power consumption: 11 kW Max. air outlet temperature: 900 ^oC Min. air flow rate: 38.1 m^3/h
Gas burner	Thermal power: 4 kW Propane flow rate: 0.17 m^3/h @ 20 mbar
Coal feeding system	Mass flow rate: 1 to 4.0 kg/h
Steam generator	Steam flow rate: 16 kg/h Pressure range: 1 to 10 bar Temperature range: 0 to 300 ^oC
Cyclone dust separator	Flue gas flow rate: 47 m^3/h
Cyclone reactor	Thermal power: 20 kW @ 4.0 kg/h of lignite coal Electrical ceramic heating elements: 6 kW

2.2.1.1 Gas analysis

Continuous sample gas flow extracted from sampling points indicated in Fig. 2.1 of experimental setup (after the combustion cyclone reactor and at bypass oxidizer stream) is conditioned in suitable devices before being supplied to gas analyzer [Sick-Maihak, 2008]. The gas components O_2, CO_2, NO, CO and SO_2 are measured in experimental setup.

The gas analyzer devices installed in the experiment were used in continuous analysis mode. The Hartmann and Braun gas analyzer Magnos 6G for O_2 (paramagnetic measuring principle) was used for the oxidizer stream; the Sick-Maihak gas analyzer S710 for NO, SO_2, CO (non-dispersive infrared absorption measuring principle) and O_2 (paramagnetic) were used for the flue gas stream; and the Asea Brown Boveri (ABB) gas analyzer EL3020 for CO_2 (non-dispersive infrared absorption) was used for the flue gas stream. The amount of water vapor in oxidizer stream was measured with the Bartec humidity device Higrophil H4230-10.

The M&C probes PSP4000-H to collect the gas samples were installed in flue gas and oxidizer streams, assembled with a 0 to 180 ^{o}C regulated electrical heating.

Table 2.2 shows the chemical species measured during the continuous operation of the experiment together with the gas probe position to collect the sample. The measurement principle and its range are also detailed.

Table 2.2 - Measured chemical species under continuous operation

Specie	Probe position	Measurement principle	Range of measurement
O_2	Oxidizer (bypass)	Paramagnetic	0-100 Vol.%
H_2O		Psychrometric gas humidity	2-100 Vol.%
CO_2	Flue gas stream (after the cyclone reactor)	Non-dispersive infrared absorption	0-100 Vol.%
NO		Non-dispersive infrared absorption	0-600 mg/Nm³
SO_2		Non-dispersive infrared absorption	0-1500 mg/Nm³
CO		Non-dispersive infrared absorption	0-300 mg/Nm³
O_2		Paramagnetic	0-100 Vol.%

2.2.1.2 Temperature and pressure measurements

Table 2.3 shows the test facility main instruments and their respective specifications to measure temperature and pressure, as previously depicted in Fig. 2.1. Most of the temperature sensors installed within the cyclone reactor, the electrical heating system, the coal feeding injection and air quench lines and along the oxidizer and flue gas stream lines are type-K thermocouples with mantel isolation, ranging from 0 to 1100 ^{o}C. PT 100 sensors are installed at lower temperatures lines (up to 250 ^{o}C).

Table 2.3 - List of the instruments and its main specifications

Instruments	Range of measurement	Accuracy
Thermocouple type-K	0 - 1100 ^{o}C	±2.2 ^{o}C or ±0.75% (whichever is greater)
	0 - 100 ^{o}C	±2.2 ^{o}C
PT100	0 - 250 ^{o}C	from ± 0.76 to 1.26 ^{o}C
Gauge pressure transmitter	-50 to +50 mbar	up to 0.025%
	-100 to +100 mbar	up to 0.025%

Figure 2.2 shows measurements of pressure and temperature at different points along the experimental setup for a typical continuous operation of the cyclone reactor under air atmosphere conditions set up at 800 ^{o}C. The measured temperatures along the cyclone reactor longitudinal axis are higher than in other positions of the experimental setup and the negative pressure allows the coal injection under continuous operation.

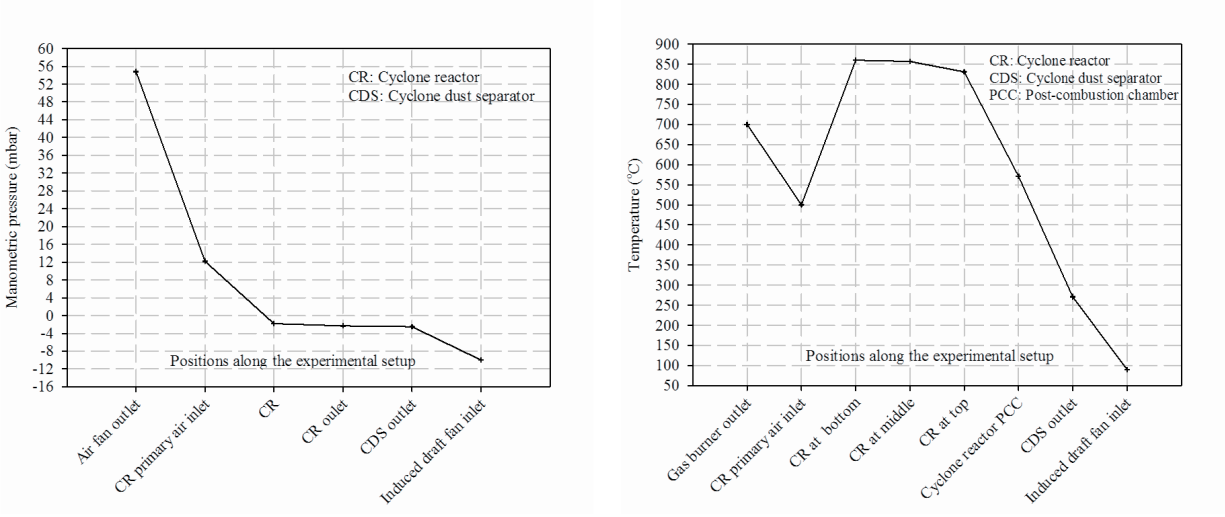

(a) (b)

Figure 2.2 - (a) Pressure and (b) temperature measurements along the experimental setup for the cyclone reactor operating under air atmosphere conditions set up at 800 ^{o}C.

2.2.1.3 Volumetric flow rate measurement

The Brooks variable area flowmeters are used to measure the volumetric flow rate of O_2, CO_2 oxidizer streams to set up the oxy-fuel composition, and the volumetric flow rate in the gas burner, as shown in Table 2.4. The volumetric flow rate of the oxidizer streams (both the air and oxy-fuel ones) streams should be at least of 38 m^3/h, in order to keep the pre-heater minimum volumetric flow rate operation, as detailed previously in Table 2.1.

The composition of the oxy-fuel oxidizer stream at both the variable area flowmeters and the steam generator are checked downstream, by measuring the O_2 volume within the cyclone reactor with the aid of the oxygen potentiometric sensor and by measuring the water vapor volume in bypass oxidizer stream with Bartec humidity device Higrophil H4230-10, as shown in Table 2.2. The CO_2 volume is calculated as the difference of these two measurements.

Table 2.4 - Variable area flowmeters and its main specifications

Stream	Range of measurement	Accuracy
O_2 oxidizer	7.0 - 70.0 m^3/h @ 5 bar, 20 ^oC	± 2% of full scale
CO_2 oxidizer	5.0 - 53.6 m^3/h @ 5 bar, 20 ^oC	± 2% of full scale
Air - gas burner	0.420 - 4.200 m^3/h @ 8 bar, 20 ^oC	± 5% of full scale
Propane - gas burner	0.0180 - 0.180 m^3/h @ 1.020 bar, 20 ^oC	± 5% of full scale
O_2 - gas burner	0.06 - 0.50 m^3/h @ 1.0 bar, 20 ^oC	± 5% of full scale
CO_2 - gas burner	0.13 - 1.38 m^3/h @ 1.0 bar, 20 ^oC	± 5% of full scale

The orifice plates installed along the oxidizer and flue gas lines have their respective mass flow rates calculated according to the ISO 5167 standard, with the measurement of temperature and pressure at each point, as previously detailed.

2.2.1.4 Cyclone combustion reactor

The cyclone reactor drawings are presented, showing its relevant dimensions and sensor positioning, as illustrated in Fig. 2.3.

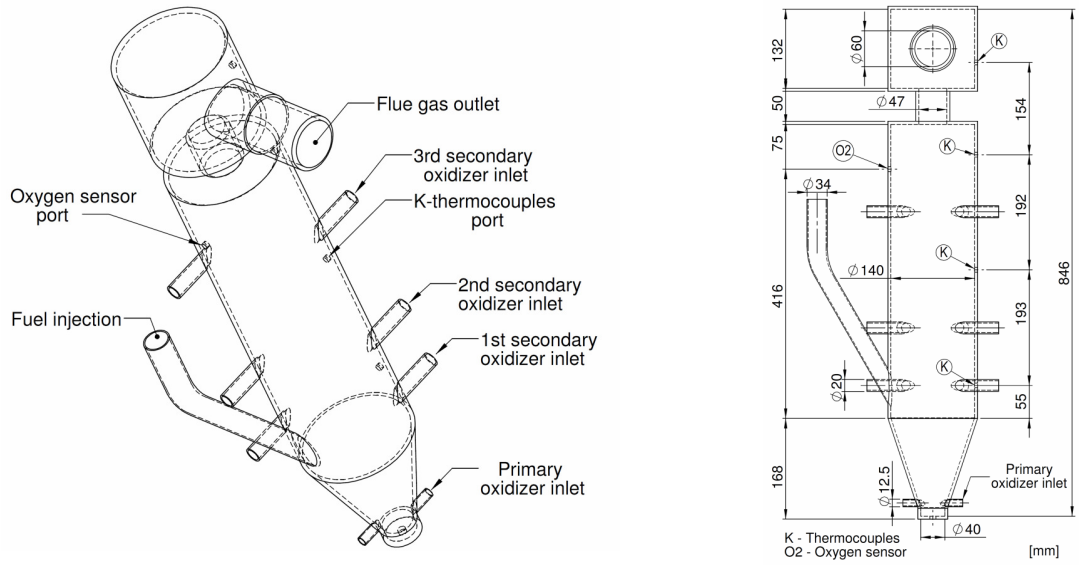

(a) (b)

Figure 2.3 - (a) Perspective and (b) projected views of the cyclone combustion reactor.

The combustion chamber is constructed in stainless steel. The reactor dimensions are 1.0 m height and 0.140 m internal diameter. The oxidizer is injected into the reactor on an average temperature of 900 K, at four tangential positions, whereas the coal particles are

injected downward into an inlet 0.170 m distant from the reactor bottom. Reaction takes place at a 0.0075 m^3 chamber volume. Due to the cyclone reactor geometry and the injection of oxidizer streams tangentially in relation to the reactor wall, swirling flows within the combustion chamber are generated, which contribute to a better recirculation of active chemical species during the combustion. Details of the isothermal swirling flow investigation for the cyclone combustion reactor are shown in Appendix 2.A.1.1.

The combustion reactor surfaces are electrically heated enabling a constant wall temperature up to 1350 K by means of electrical ceramic heating elements installed at outer surface of cyclone reactor. Gas temperatures are measured by three type-K thermocouples installed along the longitudinal axis of cyclone reactor and distant around 10 mm from the inner surface of reactor wall. At the top of the reactor, a video camera registers combustion images. An oxygen-solid electrolyte sensor acquires the oxygen partial pressure within the cyclone reactor, allowing for the investigation of oxygen concentration and global kinetic parameters. In the present work, only the primary oxidizer inlet stream was used.

2.2.1.5 Gas-potentiometric analysis

Several studies in the last decades applied solid electrolyte sensors of stabilized zirconia for *in situ* investigation of combustion processes [Schotte et al. 2010; Hangauer et al., 2009; Shin et al., 2004; Docquier and Candel, 2002; Ivers-Tiffe et al., 2001; Stenberg et al., 1998; Guo et al., 1996; Badwal et al., 1988]. The main advantage of these sensors is their high sensitivity coupled to short response times [Schotte et al. 2010; Shin et al., 2004; Lorentz and Rau, 1998; Lorentz et al., 1996]. In the present research, a Zirox sensor with a temperature range from 923 to 1723 K and able to endure extreme combustion conditions is applied. According to the sensor manufacturer (Zirox), its time response is between 8 and 15 milliseconds and its accuracy for oxygen concentration at normal pressure has a relative error lower than 5%.

Zirox oxygen sensor probe consists of a ceramic tube constructed with an oxygen ion conductor material of yttria stabilized zirconia (YSZ). As depicted in Fig. 2.4a, the oxide ion conductor is covered inner and outer by a platinum electrode layer, which is streamed by the reference and measured gas, respectively. The platinum (Pt) porous electrode adsorbs the oxygen molecules and dissociate them into oxygen atoms, which diffuse into the boundary of the electrode and electrolyte of YSZ (yttria stabilized zirconia) and finally into a triple phase boundary (TPB), where the electron transfer takes place from the electrode to the atomic

oxygen, forming O^{2-} ions. These O^{2-} ions are transported by the movement of ion vacancies created by the doping yttria in zirconia [Docquier and Candel, 2002].

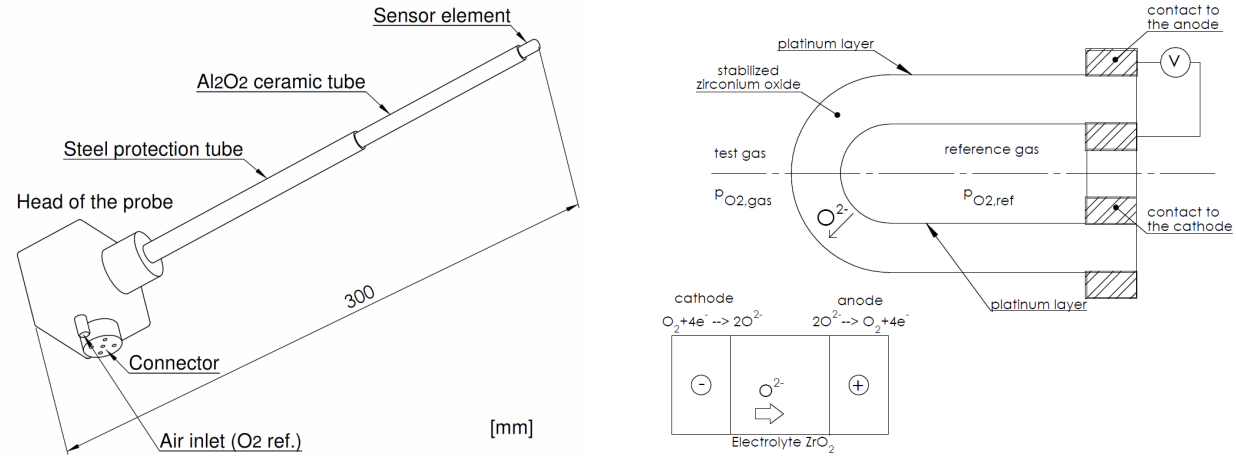

(a) (b)

Figure 2.4 - (a) Perspective view of the solid electrolyte oxygen probe and (b) a schematic drawing of the sensor element.

The overall electrode reactions can be simplified as follow [Ramammorthy et al., 2003]. The set of equations to derive the relationship used by the oxygen sensor to measure the oxygen concentration of the sampled gas is in Appendix 2.A.1.2.

$$O_{2,ads} \rightarrow O_{ads} + O_{ads} \rightarrow O_{tpb}^{2-} \rightarrow O_{ysz}^{X} \tag{2.1}$$

Oxidation and reduction reactions occur at the cathode and anode electrode-electrolyte interfaces, which defines a value of oxygen activity. Assuming fast kinetic rates, the cathode and anode reactions are described as follows, respectively.

$$O_{2,ref} + 4e_{electrode}^{-} \leftrightarrow 2O_{electrolyte}^{2-} \tag{2.2}$$

$$2O_{electrolyte}^{2-} - 4e_{electrode}^{-} \leftrightarrow O_{2,gas} \tag{2.3}$$

The output of this potentiometric sensor is a combined effect of chemical and electrical processes, which can be correlated by using thermodynamic equilibrium and fast kinetic reactions based on Nernst equation [Bhoga and Singh, 2007; Singhal and Kendall, 2003]. The Nernst equation correlates the Gibb's free energy and electromotive force of a chemical system. For a solid electrolyte cell with two oxygen electrodes, the cell reaction is merely the transfer of oxygen from the higher to lower partial pressure, as detailed in Fig.

2.4b. The cell potential and oxygen partial pressures between the two electrodes (the reference electrode immersed in dry air, i.e. 21% O_2 vol., and the electrode immersed in gas combustion reactor) are related by the Nernst Equation 2.4.

$$U = \left(RT/\dot{n}_{el}F\right)\cdot \ln\left(p_{O_2,ref}/p_{O_2,gas}\right) \tag{2.4}$$

Substituting the oxygen partial pressures by molar fractions and molar flow of the electrons of oxygen $\dot{n}_{el} = 4$ in Eq. 2.4, and rearranging it, the oxygen molar fraction of sampled gas can be calculated, knowing the cell potential and gas combustion temperature, according to Eq. 2.5.

$$f_{O_2,gas} = f_{O_2,ref}\exp\left(-4FU/RT\right) \tag{2.5}$$

Substituting the values of Faraday and ideal gas constants, yields the oxygen concentration in vol.% calculated by the sensor.

$$C_{O_2,gas} = 20.64\exp(-46.42(U/T)) \tag{2.6}$$

The oxygen concentration of 20.64% vol. in the reference is calculated with 50% of air relative humidity, according to Zirox manufacturer data [Zirox, 2003]. The sensitivity of the equilibrium potentiometric sensors is given by ($RT/\dot{n}_{el}F$) and depends only on temperature, provided the electrolyte is a pure ionic conductor [Ramammorthy et al., 2003]. On the other hand, the response time is influenced by rate constants involved in the reaction showed in Eq. 2.1. The slowest process will determine the response time of the sensor. The temperature also affects the time response of sensor, i.e. the oxygen ions move faster at high temperatures and the potentiometric cell responds more rapidly to changes in O_2 content of the sampled gases [Badwal et al., 1988].

2.3 Experimental parameter for coal combustion behavior investigation

The test facility was extensively studied by Tappe, 2011, 2009, and Krüger, 2010, in which are described the procedures to obtain the oxygen concentration curves and the calculation of the combustion global kinetic parameters. In order to exemplify how the

experiment is performed, Fig. 2.5 illustrates the oxygen and gas temperature evolution within the combustion chamber during a trial of a 3-g-sample of lignite under air conditions at 1073 K average temperature. Fig. 2.5b is a detailed view of the coal sample combustion showed in Fig. 2.5a in respect to O_2 concentration, and Fig. 2.5c shows the combustion zone with a detailed view of the swirler.

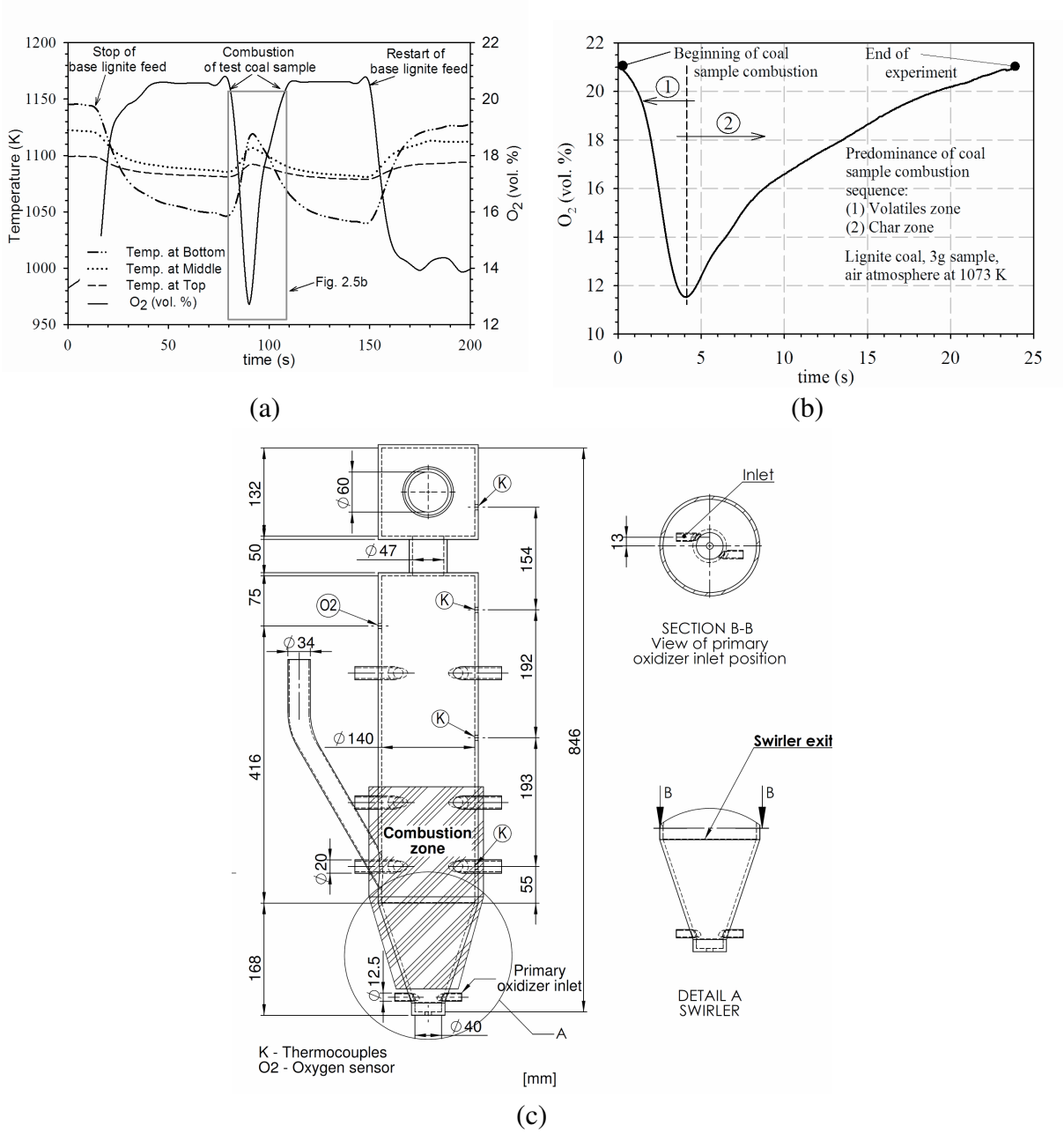

Figure 2.5 - (a) Temperature and oxygen concentration profiles of a typical test and (b) detailed oxygen consumption for a combustion sequence of a coal sample, and (c) the combustion zone with a detailed view of the swirler.

Basically, this test facility is continuously fed with coal in order to reach high temperature levels in the reactor to run the experiments. When the temperature set in the reactor is reached, the continuous fuel feeding is interrupted in order to increase the oxygen concentration within the reactor up to the required level to perform the experiments, as for instance, 21% vol. O_2. The combustion operation in batch mode makes the gas temperature to change, measured on 3 points of the chamber (at bottom, middle and top), indicated previously in Fig. 2.3b. Their average is used to calculate the combustion global kinetic parameters. When new steady conditions are established, i.e. constant gas temperatures and oxygen concentration, the coal sample is injected into the reactor.

As depicted in Fig. 2.5b, the starting point of the combustion sequence is characterized by the sudden drop on the oxygen concentration due to the predominance of volatiles matter combustion right after the injection of the sample. It is followed by char mass combustion until the oxygen concentration reaches initial values. This process can be repeated as a cycle of feeding and combustion.

The determination of the global kinetic parameters is based on the variation of oxygen concentration measured by the oxygen-solid electrolyte sensor and time average temperatures measured by the three thermocouples during the combustion of the sample. Temperature test profiles as shown in Fig. 2.5a allow to identify that highest temperature values are developed at the lowest section of the cyclone reactor or at the swirler exit, where the combustion zone takes place. The swirler or swirl generator is depicted in Detail “C” and Section “D-D” views of Fig. 2.5c.

2.3.1 Experimental parameters for lignite coal

This section summarizes the main experimental parameters used in the test facility to obtain oxygen concentration curves for lignite coal combustion behavior investigation. The experimental parameters are set up for the combustion of 1g of lignite coal and 1625 μm particles mean diameter, and for and air and oxy-fuel atmospheres with water vapor participation at three different gas average temperature levels within the cyclone combustion reactor, as shown in Table 2.5. The volumetric flow rate calculated for the orifice plate (27.3 mm outside diameter and 14 mm inside diameter) installed at the cyclone reactor primary inlet, for air and oxy-fuel stream compositions, taking 873 K as reference oxidizer temperature measured at the upstream flow.

Table 2.5 - Experimental parameters for air and oxy-fuel coal combustion

Experimental condition	Air	Oxy-fuel			
O_2 in oxidizer (vol. %)	21	21	30	30	30	30
H_2O in oxidizer (vol. %)	0	0	0	10	20	30
Oxidizer volumetric flow (m³/h) at 873 K	23	26	25	22	26	27
Oxidizer temperature (K)	873	873				
Reactor temperature (K)	1073, 1173, 1273					
Sample mass (g)	1					
Particle diameter range (μm)	1250-2000					

The proximate and ultimate analyses of the Lusatian pre-dried lignite coal are given in Table 2.6 in dry mass basis and without ash (daf). As observed, the lignite coal has high content of volatile matter and carbon, and it has low content of ash.

Table 2.6 - Proximate and ultimate analysis of the Lusatian pre-dried lignite coal (LTBK)

Proximate Analysis (%)	dry	daf
Volatile Matter	54.1	57.9
Fixed Carbon	39.1	42.1
Ash	6.5	-
Ultimate Analysis (%, daf)		
Carbon	67.05	
Hydrogen	6.95	
Nitrogen	0.70	
Sulfur	0.80	
Oxygen (by difference)	24.50	

2.4 Results and discussion

The behavior of the local O_2 concentration during the combustion of 1 g LTBK samples, particle size of 1625 μm mean diameter, under air and oxy-fuel conditions for three temperature levels is plotted in Figures 2.6, 2.10 and 2.11. For each combination of temperature and atmosphere levels (i.e. at 1073 K, and air atmosphere, for instance), the experiment is repeated or replicated two and three times, resulting an average oxygen concentration curve for each temperature level.

In order to compare the results of oxygen concentration curves between the atmospheres and temperatures, variables are selected from the oxygen concentration curve, as the total elapsed time and the maximum variation of oxygen concentration. The maximum variation of oxygen concentration is calculated by the difference between the inlet oxidizer oxygen concentration (i.e. 21% or 30% in vol.) and the minimum value of oxygen concentration attained in the oxygen concentration curve. The total elapsed time is bounded by time *t=0* and ends up when the O_2 sensor stabilizes, defined for different values of oxidizer atmospheres, as shown in Table 2.7. The value of oxygen concentration at which the O_2 sensor stabilizes is referenced in Zirox, 2003, and it is due to small difference of the oxygen chemical potential between the outer and inner probe electrodes.

Table 2.7 - Oxygen concentration stabilization values for total elapsed time

Oxidizer atmosphere	O_2 (vol. %)
Air	20.6
Oxy-fuel with 21% O_2	20.6
Oxy-fuel with 30% O_2	29.4

The variability within the sample replicates for each set of oxidizer atmospheres is analyzed by means of standard deviation σ calculated for each variable selected in oxygen concentration curve. This is a criteria established in the section of this work to investigate the coal combustion upon the oxygen concentration curves.

Figure 2.6 shows the oxygen concentration curves for air and oxy-fuel atmospheres with 21% O_2 (in vol.) at three gas temperature levels. Differences in oxygen concentration values are observed under oxy-fuel atmosphere at 1173 and 1273 K, if compared with air atmosphere, as discussed by means of variables plotted in Fig. 2.7.

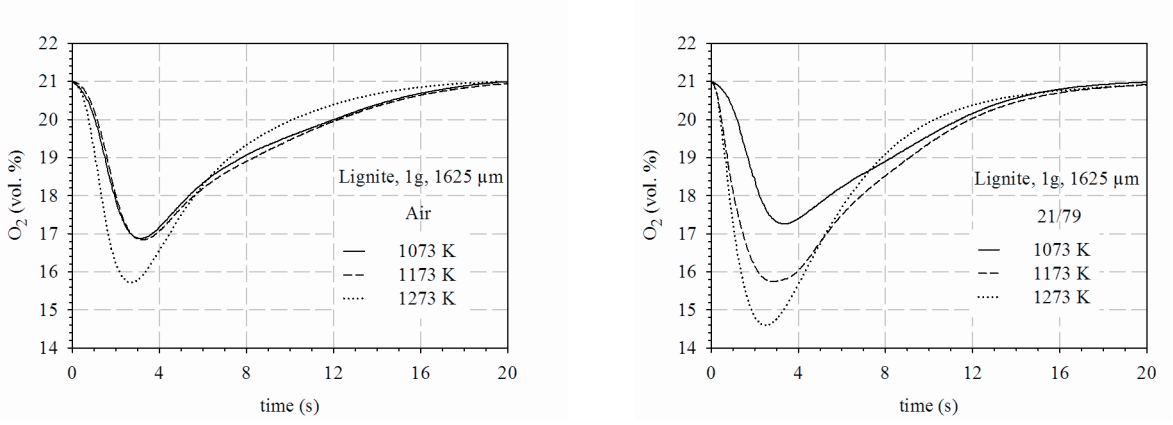

(a) (b)

Figure 2.6 - Oxygen consumption curves (a) under air and (b) oxy-fuel with 21 vol.% O_2.

Figure 2.7a plots the difference of oxygen concentration between air and oxy-fuel atmosphere with 21% O_2 (in vol.) obtained at each gas temperature level and at the time of maximum variation of oxygen concentration during the consumption of sample is achieved. It is noted that that higher values of oxygen concentration difference are attained under oxy-fuel at 1173 and 1273 K than that under air conditions. It shows the influence of CO_2 gasification reaction on coal combustion from temperature values higher than 1073 K, as observed in literature review with TGA and DTF experiments [Rathnam et al., 2009], and with ALVA 20 experiments [Tappe, 2009].

The standard deviation calculated at the time of maximum variation of oxygen concentration is 0.47% of O_2 (in vol.) for all replicates (including all temperature levels: 1073, 1173 and 1273 K, and two atmospheres: air and oxy-fuel); and as the values obtained at 1073 K are within the sample variability or error, there is no influence of oxidizer atmospheres.

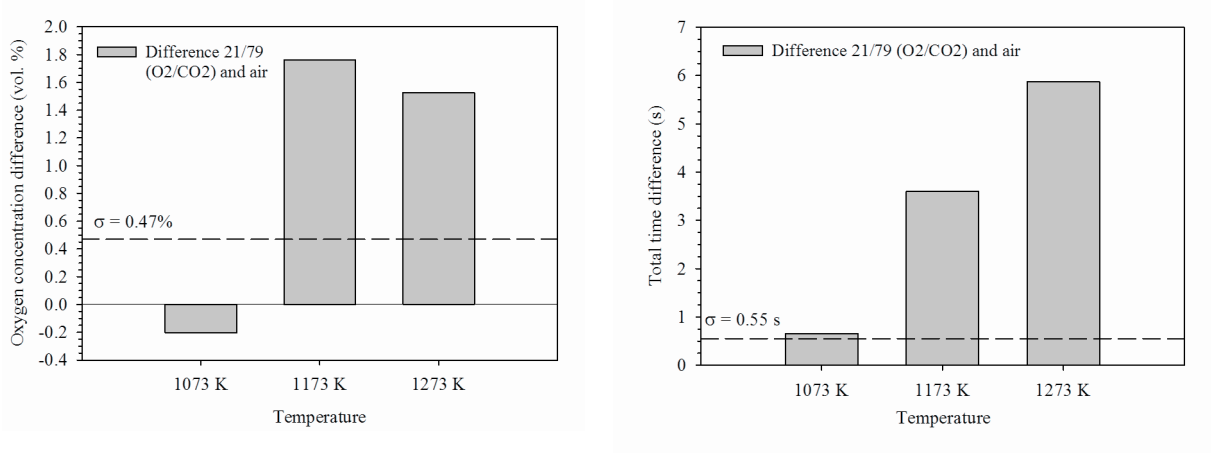

(a) (b)

Figure 2.7 - Bar plots of (a) oxygen concentration and (b) total elapsed time differences between air and oxy-fuel conditions with 21% O_2.

Figure 2.7b plots the difference of total elapsed time between air and oxy-fuel atmosphere with 21% O_2 (in vol.) obtained at each gas temperature level recorded by potentiometric oxygen sensor during the combustion of coal sample.

It is observed that higher values of elapsed time are attained under oxy-fuel at 1173 and 1273 K than that under air conditions. Higher combustion times under oxy-fuel than that in air conditions at high values of temperature (1173 and 1273 K) evidence that the oxy-fuel atmosphere properties influence on the coal sample combustion, i.e. lower mass diffusion coefficients values than that for air atmosphere conditions can be controlling the coal

combustion rate and the increase of temperature has no more influence, as observed also in literature review with DTF experiments [Bejarano and Levendis, 2008].

Further than oxy-fuel atmosphere properties influence, the swirling flow within the cyclone reactor are also influencing the potentiometric oxygen concentration measurements, delaying the stabilization of oxygen concentration measurement at 21% O_2, which requires more investigations. The standard deviation of the total elapsed time recorded by oxygen sensor during the coal sample combustion for all replicates (including all temperature and atmosphere levels) is 0.55 s, and as the values obtained at 1073 K are close to the sample variability, shows that there is no influence of atmosphere levels.

In order to investigate the coal combustion behavior discussed previously, Fig. 2.8 and 2.9 show shots taken from combustion video recording under air and oxy-fuel conditions at 1173 K at the reactor cone section. These pictures are arranged in combustion sequence order, identified by capital letters A, B, C and D, aiming to show the combustion main stages, identified during the experiments, and to complement the oxygen concentration curves analysis.

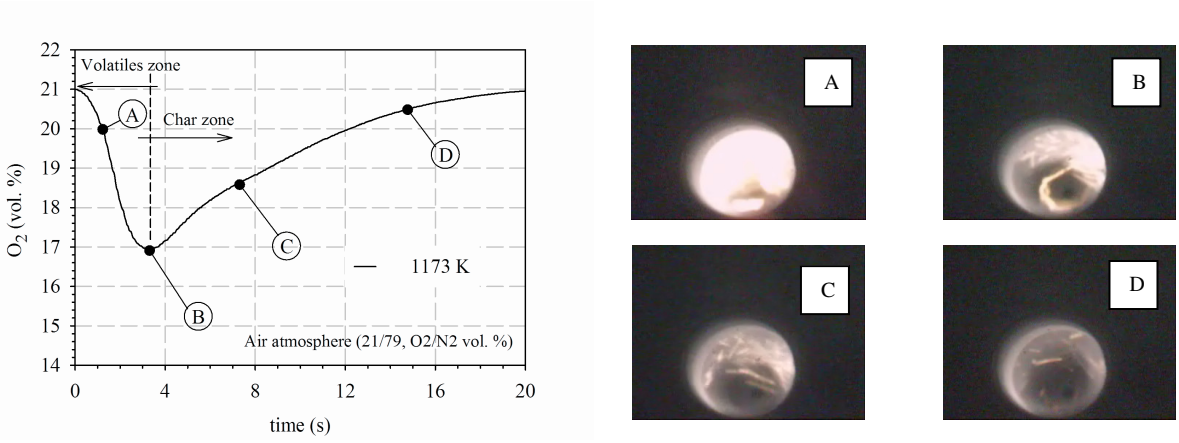

(a) (b)

Figure 2.8 - (a) Oxygen consumption curve under air atmosphere and (b) pictures of the sample combustion sequence.

Picture (A) shows that the volatiles combustion is characterized by high luminosity flame on both atmospheres, followed by char particles combustion, shown in pictures (B), (C) and (D). As observed in pictures (D) at both atmospheres, most of char particles were already burned, and the oxygen sensor concentration profiles of Fig. 2.8 and 2.9 did not reach at 21% of O_2 yet. This behavior can be explained by faster reaction rates at high gas temperature level, burning most of the coal particles; and the remaining time of oxygen concentration

within the cyclone reactor to reach at 21% O_2 (from the time at stage "D" until 21%) is solely due to the rate of the oxygen concentration oxidizer stream recovery governed by the advective and diffusive terms of the swirling flow field.

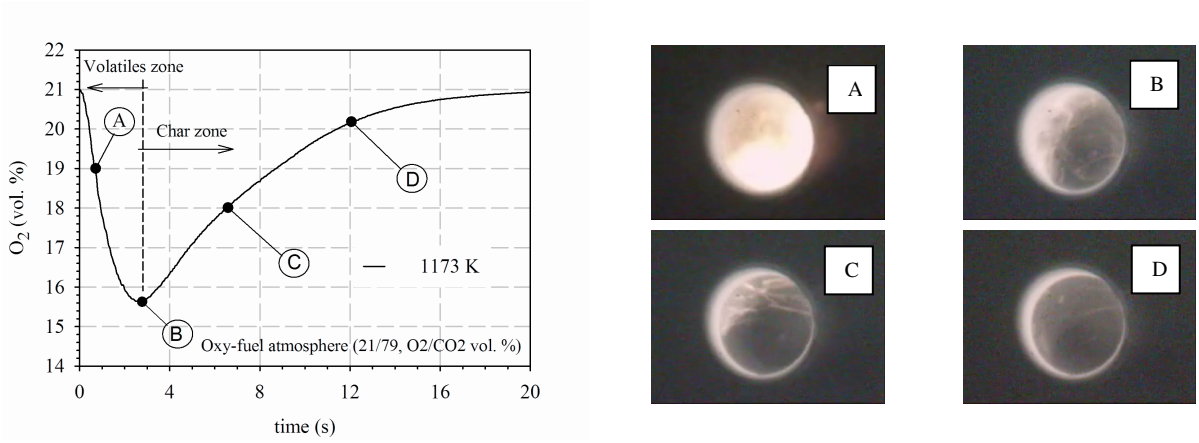

(a) (b)

Figure 2.9 - (a) Oxygen consumption curve under oxy-fuel atmosphere and (b) pictures of the sample combustion sequence.

Oxygen consumption under oxy-fuel conditions, including the participation of water vapor on the oxygen profiles, are plotted in Fig. 2.10 and 2.11. Figure 2.10a shows the oxygen consumption under oxy-fuel atmospheres with 30% vol. O_2 in the oxidizer stream without water vapor and Figure 2.10b includes 10% vol. H_2O.

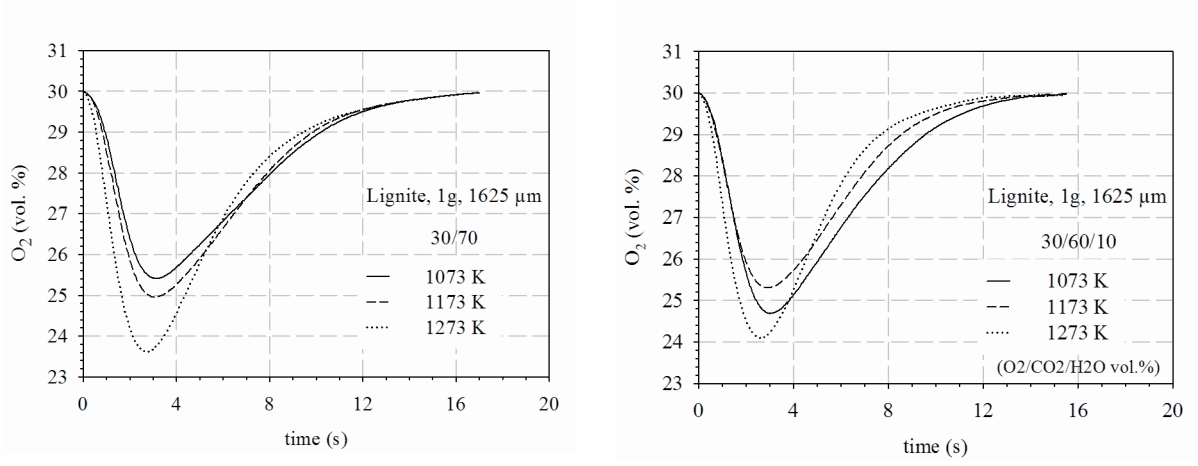

(a) (b)

Figure 2.10 - Oxygen consumption curves under oxy-fuel atmospheres (a) with 30% vol. O_2 without water vapor and (b) with 10% vol. H_2O.

Figures 2.11a and 2.11b show the oxygen consumption curves under oxy-fuel atmospheres with 30% vol. O_2 in oxidizer streams with 20% and 30% vol. H_2O, respectively.

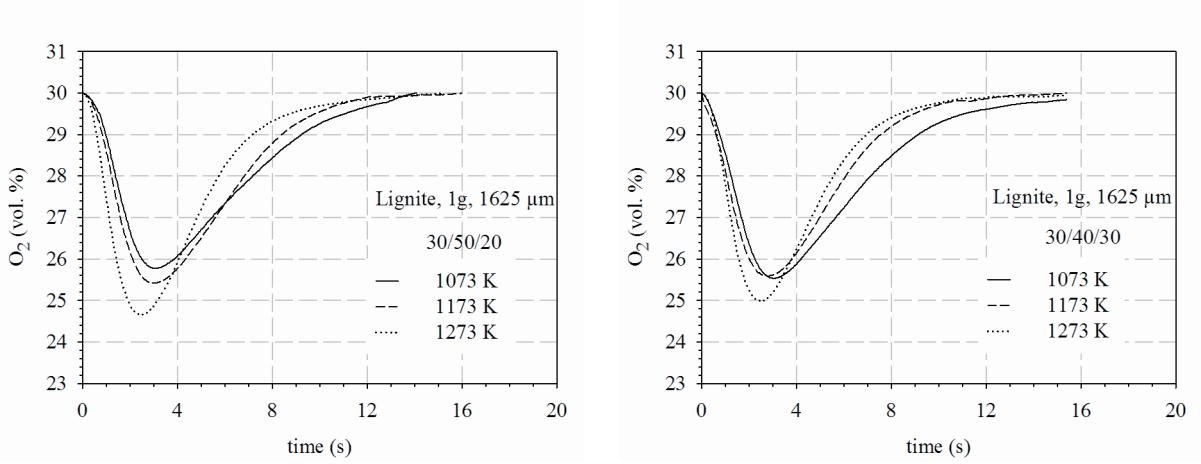

(a) (b)

Figure 2.11 - Oxygen consumption curves under oxy-fuel atmospheres with 30% vol. O_2 and (a) with 20% and (b) 30% vol. H_2O.

The oxygen concentration curves of Fig. 2.10 and 2.11 are discussed with the aid of variables plotted in Fig. 2.12.

Figure 2.12a plots the difference of oxygen concentration between oxy-fuel with 30% O_2 without water vapor, and oxy-fuel with 30% O_2 and water vapor concentrations (10%, 20%, 30% in vol.) atmospheres obtained at each gas temperature level and at the time of maximum variation of oxygen concentration during the consumption of sample is achieved. The increase of water vapor concentration in oxy-fuel atmosphere is followed by the analysis of the difference of oxygen concentration consumption between the atmospheres, taking the basis of comparison the oxy-fuel with 30% O_2 and 70% CO_2 without water vapor (30/70).

It is observed that higher values of oxygen concentration difference or consumption are attained under oxy-fuel 30/70 at 1273 K than that in oxy-fuel atmospheres 30/50/20 and 30/40/30. It shows the influence of CO_2 gasification reaction on coal combustion from temperature values higher than 1173 K and CO_2 concentration higher than 50% (in vol.). Oxygen concentrations higher than 21% (in vol.) in oxy-fuel result in faster reaction rates than that observed at 21%, therefore, the effect of CO_2 gasification reaction takes place only at gas temperature levels higher than 1173 K. At 1073 K, lower values of oxygen concentration difference or consumption are attained under oxy-fuel 30/70 than that in 30/60/10. It indicates that the effect of CO_2 gasification reaction on the coal combustion is not seen for temperatures equal and lower than 1073 K, and the water vapor concentration plays an important role, increasing the oxygen consumption.

The standard deviation attained at the time of maximum variation of oxygen concentration is 0.4% of O_2 (in vol.) for all replicates (including all temperature and

atmosphere levels); and as the values obtained at 1073 K for 30/40/30 and 30/50/20, and at 1173 K for 30/60/10 atmospheres tested are within the sample variability, there is no influence of these oxidizer atmospheres on the maximum variation of oxygen concentration.

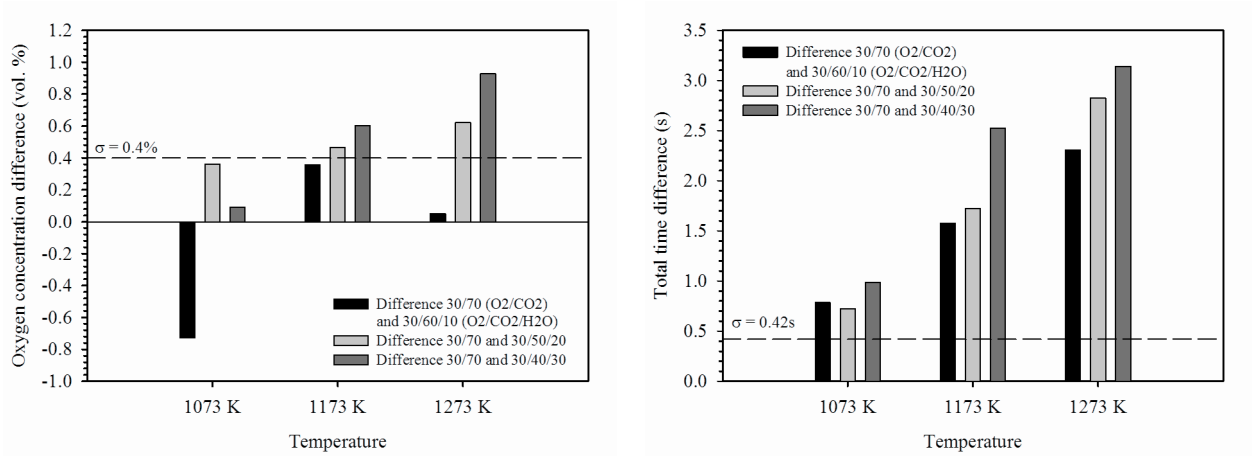

Figure 2.12 - Bar plots of (a) oxygen concentration and total elapsed time (b) differences between oxy-fuel atmospheres with 30% O_2.

In general, through the analysis of these plots, it is possible to conclude that CO_2 gasification reaction takes place at gas temperatures values higher than 1173 K and at CO_2 concentrations higher than 50% (in vol.) for oxy-fuel atmospheres with oxygen concentration values higher than 21% (in vol.). The effect of water vapor concentration is only seen for oxy-fuel atmosphere at 1073 K and with 60% of CO_2 concentration.

Figure 2.12b plots the difference of total elapsed time between oxy-fuel with 30% O_2 without water vapor, and oxy-fuel with 30% O_2 and water vapor concentrations (10%, 20%, 30% in vol.) atmospheres obtained at each gas temperature level recorded by potentiometric oxygen sensor during the combustion of coal sample. Following the same analysis of Fig. 2.12a, the increase of water vapor concentration in oxy-fuel atmosphere is followed by the analysis of the difference of total elapsed time between the atmospheres, taking the basis of comparison the oxy-fuel atmosphere with 30% O_2 and 70% CO_2 without water vapor (30/70).

It is observed that higher values of total elapsed time are attained under oxy-fuel 30/70 at 1173 and 1273 K than that in oxy-fuel atmospheres 30/60/10, 30/50/20 and 30/40/30. It shows that the difference in total elapsed time values recorded by oxygen sensor during the combustion of the coal sample increase with the decrease of CO_2 concentration, showing, at the first moment, that faster reaction rates take place under oxy-fuel atmospheres with lowest CO_2 concentration than that with highest CO_2 concentrations.

However, these results can be affected again by the swirling flow with its advective and diffusive terms within the cyclone reactor, and by the oxidizer atmosphere properties, as also observed previously for oxy-fuel atmosphere with 21% O_2 in Fig. 2.7b. These results show that lower variations of oxygen concentrations observed for atmospheres (30/40/30 and 30/50/20) are more affected by the oxygen concentration gradients of the oxidizer stream than that observed at higher variations of oxygen concentrations (with higher CO_2 and O_2 concentrations, i.e. 30/70 and 30/60/10), therefore, oxy-fuel atmospheres with low CO_2 concentrations have its total elapsed time recorded by the oxygen sensor decreased, resulting in an increase of the difference in total elapsed time between 30/70 and oxy-fuel atmospheres with water vapor. The effect of temperature and oxy-fuel atmosphere properties with water vapor, as mass diffusivity coefficients, can be also contributing to increase this difference, but require further investigations.

The standard deviation of the total elapsed time recorded by oxygen sensor during the coal sample combustion within all replicates (including all temperature and atmosphere levels) is 0.42 s.

Figure 2.13a plots the difference of oxygen concentration between the air and oxy-fuel atmospheres with 21 and 30% O_2 obtained at each gas temperature level and at the time of maximum variation of oxygen concentration during the consumption of sample is achieved.

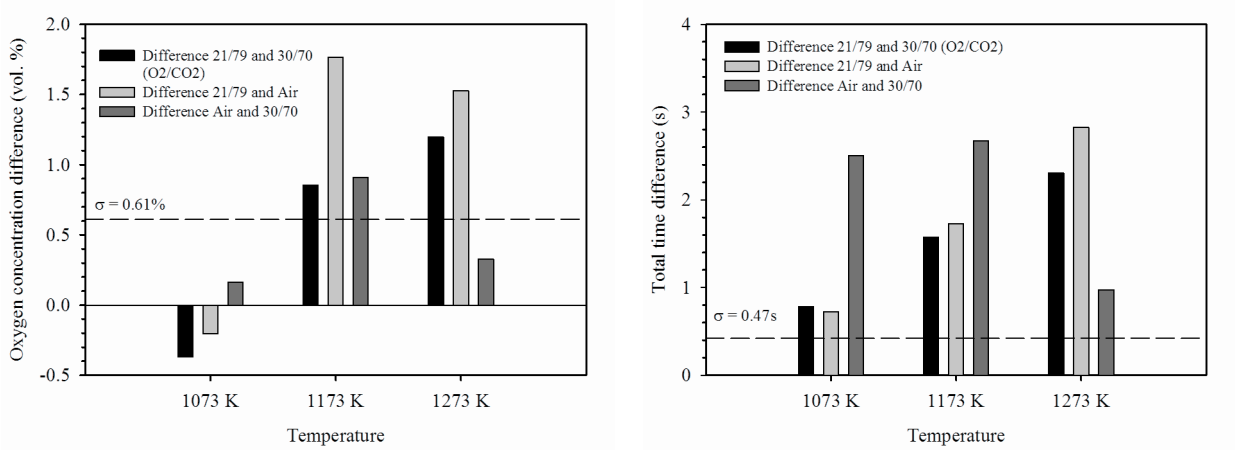

Figure 2.13 - Bar plots of (a) oxygen concentration and (b) total elapsed time differences between air and oxy-fuel atmospheres with 21 and 30% O_2.

At 1073 K, there is no difference of the variation of oxygen concentration between the atmospheres, since the values attained are within the samples variability. At 1173 and 1273 K, the maximum variation of oxygen concentration difference is higher under oxy-fuel 21/79 and

air than that in oxy-fuel 21/79 and 30/70, showing the influence of CO_2 gasification reaction in both oxy-fuel atmospheres with CO_2. At 1273 K, the difference of the maximum variation of oxygen concentration between oxy-fuel atmospheres 21/79 and 30/70 is increased, the difference is decreased between oxy-fuel 21/79 and air in comparison with 1173 K, and there is no significant difference between air atmosphere and oxy-fuel 30/70. These results show the effect of temperature on the coal combustion reactions under kinetic control regime, increasing the variation of oxygen concentration for oxy-fuel 21/79 and 30/70, and air atmosphere.

Figure 2.13b plots the difference of total elapsed time between air and oxy-fuel atmospheres with 21 and 30% O_2 obtained at each gas temperature level. The difference of total elapsed time between oxy-fuel 21/79 and 30/70, and oxy-fuel 21/79 and air, increases with the temperature, showing the effect of CO_2 properties as mass diffusivity coefficients on the elapsed time measured by the potentiometric oxygen sensor, delaying the recovery of the oxidizer oxygen concentration stream at inlet conditions (i.e. 21 or 30% O_2 vol.). The difference of total elapsed time between air and oxy-fuel 30/70 is high at 1073 and 1173 K, and it is low at 1273 K. This can be due to the influence of oxy-fuel atmosphere properties on the oxygen concentration measurements, since there is no significant difference of the oxygen concentration variation at 1073 and 1273 K between both air and 30/70 atmospheres that justifies the difference of the elapsed times. These results indicate that for oxy-fuel atmosphere without water vapor (30/70) and with CO_2 concentration equal to 70% in vol., there is a decrease in oxygen consumption and the elapsed time, compared with oxy-fuel atmosphere with higher CO_2 concentrations. This is due to the influence of CO_2 gasification reaction with carbon of the coal on the maximum variation of oxygen concentration and the effect of oxy-fuel atmosphere properties on the total elapsed time measured by the oxygen sensor.

2.5 Conclusions

This work was aimed to describe a laboratory-size atmospheric cyclone combustion chamber (ALVA 20) test facility developed to study the coal combustion phenomena under air and oxy-fuel atmospheres. Experimental methodology was described and results from 1g of pre-dried lignite coal samples were analyzed. The coal combustion phenomena were investigated by the measurement of O_2 concentration curves with a potentiometric oxygen

sensor and with the aid of images captured from a video camera installed at the top of cyclone reactor. Combustion experiments were performed aiming to investigate the influence of higher partial pressures of CO_2 and H_2O on the conversion of lignite coal under oxy-fuel, comparing to air atmosphere conditions. The major conclusions are:

- Higher values of oxygen concentration variation are attained under oxy-fuel 21/79 at 1173 and 1273 K than that under air conditions. It shows the influence of CO_2 gasification reaction on coal combustion from temperature values higher than 1073 K.
- Higher total elapsed times under oxy-fuel (21/79) than that in air conditions at high values of temperature (1173 and 1273 K) evidence that the oxy-fuel atmosphere properties influence on the coal sample combustion, i.e. lower mass diffusion coefficients values than that for air atmosphere conditions can be controlling the coal combustion rate after the maximum variation of oxygen concentration is reached and the increase of temperature has no more influence on time reduction.
- For oxy-fuel atmospheres with 30% O_2, higher values of oxygen concentration variation or consumption are attained under oxy-fuel without water vapor 30/70 at 1273 K than that in oxy-fuel atmospheres with water vapor 30/50/20 and 30/40/30 ($O_2/CO_2/H_2O$). It shows the influence of CO_2 gasification reaction on coal combustion from temperature values higher than 1173 K and CO_2 concentration higher than 50% (in vol.) in oxy-fuel atmospheres with water vapor.
- For oxy-fuel atmospheres with 30% O_2, higher values of total elapsed time are attained under oxy-fuel 30/70 at 1173 and 1273 K than that in oxy-fuel atmospheres with water vapor 30/60/10, 30/50/20 and 30/40/30. These results can be influenced by the swirling flow with its diffusive and advective terms, and by the oxidizer atmosphere properties, as also observed previously for oxy-fuel atmosphere with 21% O_2 and 79% CO_2 (21/79).
- There is an increase of oxygen concentration variation for oxy-fuel 21/79, 30/70 and air atmospheres with the increase of temperature, evidencing that the coal combustion reactions are under kinetic control regime until the time of maximum variation of oxygen concentration is reached.
- There is no difference of the oxygen concentration variation at 1273 K between air and 30/70 atmospheres, showing that both atmospheres have similar combustion reaction rates.

BIBLIOGRAPHY

Badwal, S.P.S., Bannister, M,J., Chiacci, F.T., 1988. “Response rate techniques for zirconia-based Nernstian oxygen sensors”, Journal of Applied Electrochemistry, v. 18, p. 608-613.

Bhoga, S.S., Singh, K., 2007. “Electrochemical solid state gas sensors: An overview”, Ionics, v. 13, p. 417-427.

Brix, J., Jensen, P.A., Jensen, A.D., 2010. “Coal devolatilization and char conversion under suspension fired conditions in O_2/N_2 and O_2/CO_2 atmospheres”. Fuel, v. 89, p. 3373-3380.

Carotenuto, A.R., Schneider, P.S., Corrêa, R.S., Rech, R.L., Marcilio, N.R., Krautz, J.H., 2011. “Preliminary investigation of the global kinetic parameters of low-rank coals under oxy-fuel conditions”, III Congresso Brasileiro de Carvão Mineral, Gramado, RS, Brasil, 19 pages.

Chigier N.A., Chervinsky A., 1967. “Aerodynamic study of turbulent burning free jets with swirl”, Symposium (International) on Combustion, v. 11, p. 489-499.

Docquier, N., Candel, S., 2002. “Combustion control and sensors - a review”. Progress in Energy and Combustion Science, v. 28, p. 107-150.

Guo, X., Sun, Y., Cui, K., 1996. “Darkening of zirconia - a problem arising from oxygem sensors in practice”, Sensors and Actuators, v. 31, p. 139-145.

Gupta, A.K., Lilley, D.G., Syred, N., 1984. “Swirl flows”, Abacuss Press, London, 475 pages.

Hangauer, A., Spitznas, A., Chen, J., Strzoda, R., Link., H., Fleischer, M., 2009. “Laser Spectroscopic Oxygen Sensor for Real Time Combustion Optimization”, Procedia Chemistry, v. 1, p. 955-958.

ISO 5167-1, 2003. “Measurement of fluid flow by means of pressure differential devices inserted in circular cross-section conduits running full, Parts 1 and 2” , 33 pages.

Ivers-Tiffe, E., Hardtl, K.H., Menesklou, W., Riegel, J., 2001. “Principles of solid state oxygen sensors for lean combustion gas control”, Electrochimica Acta, v. 47, p. 807-814.

Krüger, P., 2010. “Inbetriebnahme einer 20 kWth-atmosphärischen Laborverbrennungsanlage und Durchführung erster experimenteller Arbeiten zum Abbrandverhalten von Lausitzer Trockenbraunkohle”, Dissertation, Brandenburg University of Technology, Cottbus, Germany, 93 pages.

Lilley, D.G., 1985. “Investigation of flow fields found in typical combustor geometries”, NASA Contractor Report Nr.3869, Lewis Research Center, Cleveland, Ohio,USA, 191 pages.

Liu, H., 2009. “Combustion of coal chars in O_2/CO_2 and O_2/N_2 mixtures: a comparative study with non-isothermal thermogravimetric analyzer (TGA) tests”, Energy and Fuels, v. 23, p. 4278-4285.

Lorentz, H., Tittmann, K., Sitzki, L., Trippler, S., Rau, H., 1996. “Gas-potentiometric method with solid electrolyte oxygen sensors for the investigation of combustion”, Fresenius Journal of Analytical and Bioanalytical Chemistry, v. 356, p. 215-220.

Lorentz, H., Rau, H., 1998. “A new method for investigating the combustion behavior of solid fuel in FBC”, Fuel, v. 77, p. 127-134.

Orlu, R., Alfredsson, P.H., 2008. “An experimental study of the near-field mixing characteristics of a swirling jet”, Flow Turbulence Combustion, v. 80, p. 323-350.

Owczarek, C., 2000. “First investigations of the flow field in a cycloidal combustion chamber on the basis of an isothermal model”, Thesis, Brandenburg University of Technology, Cottbus, Germany, 191 pages.

Panda, J., McLaughlin, D.K., 1994 “Experiments on the instabilities of a swirling jet”, Physics of Fluids, v. 6, p. 263-276.

Ramammorthy, R., Dutta, P.K., Akbar, S.A., 2003. “Oxygen sensor: Materials, methods, designs and applications”, Journal of Material Science, v. 38, p. 4271-4282.

Rathnam, R.K., Elliot, L.K., Wall, T., Liu, Y., Moghtaderi, B., 2009. “Differences in reactivity of pulverized coal in air (O_2/N_2) and oxy-fuel (O_2/CO_2) conditions”, Fuel Processing Technology, v. 90, p. 797-802.

Schotte, E., Lorenz, H., Rau, H., 2010. “Gas Potentiometry: Oxygen-Based Redox Process Diagnostics in High-Temperature Environments, Handbook of Combustion”, Wiley-VCH Verlag GmbH, v. 2, p. 89-123.

Shin, W., Izu, N., Matsubara, I., Murayama, N., 2004. “Milisecond-order response measurement for fast oxygen gas sensors”, Sensors and Actuators B, v. 100, p. 395-400.

Sick-Maihak, 2008. “Operating Instructions S700”, v.2.0, Reute, Germany , 276 p.

Singhal, S.C., Kendall, K., 2003. “High Temperature Solid Oxide Fuel Cells: Fundamentals, Design and Applications”, Elsevier Ltda, Oxford, UK, 406 pages.

Sloan, D. G., Smith, P. J., Smoot, L. D., 1986. “Modeling of swirl in turbulent flow systems”, Progress in Energy and Combustion Science, v. 12, p. 163-250.

Steenbergen, W., Voskamp, J., 1998. “The rate of decay of swirl in turbulent pipe flow”, Flow Measurement and Instrumentation, v. 9, p. 67-78.

Stenberg, J., Amand, L.E., Hernberg, R., Leckner, B., 1998. “Measurements of Gas Concentrations in a Fluidized Bed Combustor Using Laser-Induced Photoacoustic Spectroscopy and Zirconia Cell Probes”, Combustion and Flame, v. 113, p. 477-486.

Syred, N., 2006. “A review of oscillation mechanisms and the role of the precessing vortex core (PVC) in swirl combustion systems”, Progress in Energy and Combustion Science, v. 32, p. 93-161.

Syred, N., Beer, J.M., 1974. “Combustion in swirling flows: A review”, Combustion and Flame, v. 23, p. 143-201.

Tappe, S., 2011. “Gaspotentiometrische und thermogravimetrische Abbranduntersuchungen von Braun und Steinkohlen in Luft und O_2/CO_2-Atmosphären”, Thesis, Brandenburg University of Technology, Cottbus, Germany, 145 pages.

Tappe, S., Krautz, H.J., 2009a. “ALVA 20: A 20 kWth Atmospheric Laboratory Test Facility to Investigate the Combustion Behavior under Close-to-Reality Conditions”. Proceedings of the European Combustion Meeting, 6 pages.

Tappe, S., Krautz, H.J., 2009b. “Influence of various O_2/CO_2 concentrations on the burning behavior of different coals”, 34th International Technical Conference on Coal Utilization & Fuel Systems, Clearwater, USA, 7 pages.

Tappe, S., 2007. “ALVA20 Technical Documentation, original from 20kW_{th}-Atmosphärische Laborverbrennungsanlage ALVA 20, Technische Dokumentation”, Cottbus, BTU, Germany, 30 pages.

Toftegaard, M. B., Brix, J., Jensen, P.A., Glarborg, P., Jensen, A.D., 2010. “Oxy-fuel combustion of solids fuels”, Progress in Energy and Combustion Science, v. 36, p. 585-625.
Toh, K., Honnery, D., Soria, J., 2010. “Axial plus tangential entry swirling jet”, Experiments in Fluids, v. 48, p. 309-325.

Wepper, W., 2003. “Engineering of solid state ionic devices”, Ionics, v. 9, p. 444-464.

Zhang, L., Binner, E., Chen, L., Qiao, Y., Li, C., Bhattacharya, S., Ninomiya, Y., 2010a. “Experimental investigation of the combustion of bituminous coal in air and O_2/CO_2 mixtures: 1. Particle imaging of the combustion of coal and char”, Energy Fuels, v. 24, p. 4803-4811.

Zhang, L., Binner, E., Chen, L., Qiao, Y., Li, C., 2010b. “In situ diagnostics of Victorian brown coal combustion in O_2/N_2 and O_2/CO_2 mixtures in drop-tube furnace”, Fuel, v. 89, p. 2703-2712.

Zhuiykov, S., 2006. “Mathematical modelling of YSZ-based potentiometric sensors with oxide sensing electrodes Part I: Model of interactions of measuring gas with sensor”, Sensors and Actuators B, v. 119, p. 456-465.

Zirox, 2003. “Measuring system Oxygen probe KS20 Electronic E2000P Manual”, Zirox Sensoren und Elektronik GmbH, Greifswald, Germany, 28 pages.

APPENDIX 2.A.1 - Swirling flow fundamentals applied to cyclone combustion reactors

2.A.1 Swirling flow fundamentals

The mechanisms and benefits of the swirl stabilized combustion are well known in literature and depend in most of instances on the formation of a central toroidal recirculation zone (CTRZ) which recirculates heat and active chemical species to the root of the flame, allows flame stabilization to occur in regions of relative low velocity where flow and the turbulent flame velocity can be matched, aided by the recirculation of heat and active chemical species [Syred, 2006; Gupta et al., 1984; Syred and Beer, 1974]. The CTRZ is only formed beyond a critical swirl number of 0.6 [Syred, 2006; Syred and Beer, 1974].

Figure 2.A.1.1 shows a schematic diagram of CRZ formation, represented as a function of time mean parameters: pressure $\overline{p}$, axial $\overline{u}$ and tangential $\overline{w}$ velocities.

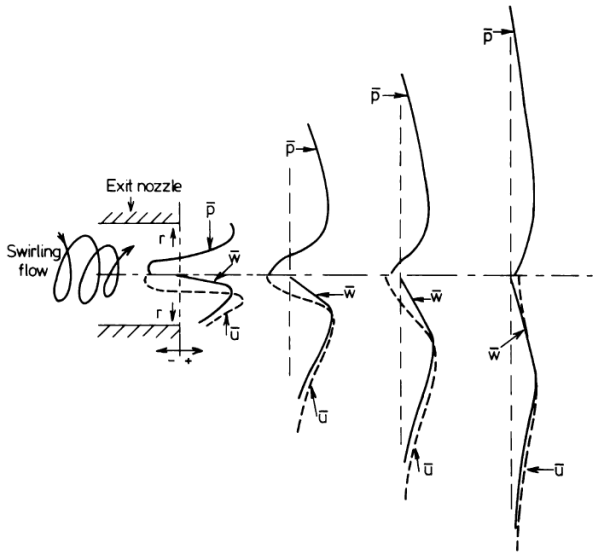

Figure 2.A.1.1 - Schematic diagram of CRZ formation [Syred, 2006].

According to Fig. 2.A.1.1, the process arises as follows:

- Expansion through the nozzle causes axial decay of tangential velocity and hence radial pressure gradient.

- This effect in turn causes a negative axial pressure gradient to be formed in the vicinity of the axis, inducing reverse flow and the formation of a central recirculation zone.

- The radial pressure gradient and central recirculation zone decay along longitudinal axis with the tangential velocity decay.

- The formation of the CRZ is thus dependent on the decay of swirl velocity as swirling flow expands.

Steenbergen and Voskamp, 1998, state that three types of swirl are defined according to the tangential velocity field for flow within straight pipes. Looking at the cross section view of the pipe as depicted in Fig. 2.A.1.2, they distinguish a “concentrated vortex” (CV), with the rotation concentrated near the pipe centre, a “solid body rotation” (SB) with an almost uniform rotation, and a “wall jet” (WJ) with the angular momentum concentrated near the wall.

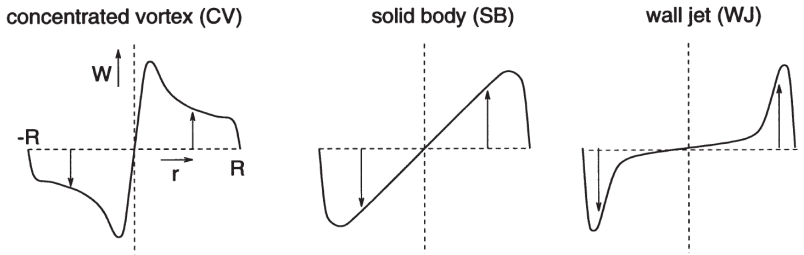

Figure 2.A.1.2 - Classification of swirl types [Steenbergen and Voskamp, 1998].

2.A.1.2 Swirl number

The degree of swirl is usually characterized by the swirl number, which is nondimensional [Gupta, 1984]. There are several definitions for the swirl number, following different assumptions, due to a limited understanding of the underlying physics of swirling jets [Toh et al., 2010]. The swirl number is based on the ratio of the axial flux of azimuthal momentum G_ϕ to the axial flux of axial momentum G_x, multiplied by the equivalent nozzle radius R, given by the following equation.

$$S = \frac{G_\phi}{G_x R} \tag{2.A.1.1}$$

The physical modeling assumptions to derive the flux of axial and azimuthal momentum equations used in swirl number are shown in Fig. 2.A.1.3, which represents a schematic of the cylindrical coordinate system of the free developing swirling jet emanating from a fully developed axially rotating pipe flow [Orlu and Alfredsson, 2008; Chigier and Chervinsky, 1967].

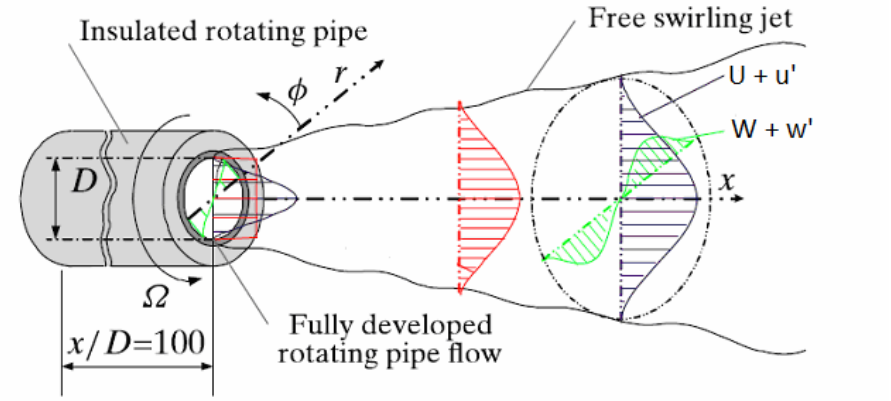

Figure 2.A.1.3 - Schematic of the cylindrical coordinate system of the free developing swirling jet emanating from a fully developed axially rotating pipe flow [adapted from Orlu and Alfredsson, 2008].

The theoretical description of the velocity and pressure field of free swirling jets is based on the incompressible Reynolds-averaged Navier-Stokes (RANS) equations written for a cylindrical inertial frame of reference under the assumptions of a steady and axisymmetric mean flow [Orlu and Alfredsson, 2008].

The axial, radial and azimuthal directions in cylindrical coordinate system is denoted by x, r, ϕ, respectively, and its corresponding velocity components by $w+w', v+v', u+u'$, where w, v, u are the time mean velocities and w', v', u' its turbulent fluctuations.

The continuity and momentum conservation equations for x, r and ϕ directions are as follow [Chigier and Chervinsky, 1967].

Continuity:

$$\left(\frac{\partial}{\partial x}\right)(r\rho u)+\left(\frac{\partial}{\partial r}\right)(r\rho v)=0 \tag{2.A.1.2}$$

Momentum at x:

$$\left(\frac{\partial}{\partial x}\right)\left(\rho u^2\right)+\frac{1}{r}\left(\frac{\partial}{\partial r}\right)(r\rho uv)=-\left(\frac{\partial p}{\partial x}\right)-\left(\frac{\partial}{\partial x}\right)\left[\rho\overline{u'^2}+2u\overline{u'v'}\right]- -\frac{1}{r}\left(\frac{\partial}{\partial r}\right)\left[rv\overline{\rho'u'}+ru\overline{\rho'u'}+r\rho\overline{u'v'}\right] \tag{2.A.1.3}$$

Momentum at r:

$$\frac{\rho w^2}{r} = -\left(\frac{\partial p}{\partial r}\right) - \frac{1}{r}\left(\frac{\partial}{\partial r}\right)\left[r\rho\left(\overline{v'^2}\right) + 2rv\left(\overline{\rho' v'}\right)\right] + \rho\frac{\overline{w'^2}}{r} + 2w\frac{\left(\overline{\rho' w'}\right)}{r} \tag{2.A.1.4}$$

Momentum at ϕ:

$$\left(\frac{\partial}{\partial x}\right)(\rho u w) + \frac{1}{r}\left(\frac{\partial}{\partial r}\right)(r\rho v w) + \frac{(\rho v w)}{r} = -\frac{1}{r}\left(\frac{\partial}{\partial r}\right)r\left[\rho\left(\overline{w' v'}\right) + v\left(\overline{\rho' w'}\right) + w\left(\overline{\rho' v'}\right)\right] - \rho\frac{\left(\overline{v' w'}\right)}{r} - v\frac{\left(\overline{\rho' w'}\right)}{r} - w\frac{\left(\overline{\rho' v'}\right)}{r} \tag{2.A.1.5}$$

The boundary conditions are as follow

At $r = 0$:

$$v = w = \frac{\partial u}{\partial r} = 0 \tag{2.A.1.6}$$

At $r = \infty$:

$$u = w = \frac{\partial u}{\partial r} = \frac{\partial w}{\partial r} = \overline{\rho' u'} = \overline{\rho' v'} = \overline{u' v'} = \overline{u'^2} = 0 \tag{2.A.1.7}$$

Multiplying Eq. 2.A.1.3 by r and integrating with respect to r from $r = 0$ to $r = \infty$, applying the boundary conditions, and rearranging it with $(d/dx)rdr$ in evidence, the momentum equation at x direction yields

$$\frac{d}{dx}\int_{r=0}^{r=\infty} r\left[\rho u^2 + (p - p_\infty) + \rho\left(\overline{u'^2}\right) + 2u\left(\overline{\rho' u'}\right)\right]dr = 0 \tag{2.A.1.8}$$

Multiplying the Eq. 2.A.1.4 by r^2 and integrating with respect to r from $r = 0$ to $r = \infty$, applying the boundary conditions, and rearranging it, the momentum equation at r direction yields

$$\int_{r=0}^{r=\infty} r\left[\rho w^2+\rho\left(\overline{w'^2}+\overline{v'^2}\right)+2\left(w\overline{\rho' w'}+v\overline{\rho' v'}\right)\right]dr=-\int_{r=0}^{r=\infty}2(p-p_\infty)r\,dr \tag{2.A.1.9}$$

Multiplying the Eq. 2.A.1.5 by r^2 and integrating with respect to r from $r=0$ to $r=\infty$, applying the boundary conditions, and rearranging it, the momentum equation at ϕ direction yields

$$\frac{d}{dx}\int_{r=0}^{r=\infty} r^2\rho u w dr=0 \tag{2.A.1.10}$$

Thus, the axial flux of azimuthal momentum conservation equation is given by

$$G_\phi=\int_0^{2\pi}d\phi\int_{r=0}^{r=\infty} r^2\rho u w dr \tag{2.A.1.11}$$

By introducing Eq. 2.A.1.9 into Eq. 2.A.1.8 in order to eliminate the static pressure gradient at momentum conservation equation at x direction, it results in the following equation

$$\left(\frac{d}{dx}\right)\int_{r=0}^{r=\infty} r\left\{\rho\left(u^2-\frac{1}{2}w^2\right)+\rho\left[\left(\overline{u'^2}\right)-\frac{1}{2}\left(\overline{w'^2}+\overline{v'^2}\right)\right]+2u\,\overline{\rho' u'}-v\,\overline{\rho' v'}+w\,\overline{\rho' w'}\right\}dr=0 \tag{2.A.1.12}$$

According to Chigier and Chervinsky, 1967, measurements of turbulent velocities in jets and wakes show that $\overline{u'^2}$, $\overline{v'^2}$ e $\overline{w'^2}$ are of the same magnitude, and measurements in heated jets indicate that $v\overline{\rho' v'}$ are of the same magnitude as $u\overline{\rho' u'}$. Toh, K. et al., 2010, verified that the square of the fluctuations $\overline{u'^2}$ has the magnitudes much lower than the mean velocity component u at x direction. Assuming on the basis of the available experimental evidence that $u\overline{\rho' u'}\sim v\overline{\rho' v'}\sim w\overline{\rho' w'}$ [Chigier and Chervinsky 1967], Eq. 2.A.1.12 reduces to

$$\left(\frac{d}{dx}\right)\int_{r=0}^{r=\infty} r\left[\rho\left(u^2-\frac{1}{2}w^2\right)\right]dr=0 \tag{2.A.1.13}$$

Thus, the conservation equation of axial momentum is

$$G_x = \int_0^{2\pi} d\phi \int_{r=0}^{r=\infty} r\left[\rho\left(u^2 - \frac{1}{2}w^2\right)\right]dr \tag{2.A.1.14}$$

Introducing the equations 2.A.1.11 and 2.A.1.14 into Eq. 2.A.1.1, lead to the expression of the swirl number equation, considering the boundary layer approximation for a turbulent, incompressible and steady flow with appropriate boundary conditions [Orlu and Alfredsson 2008; Gupta et al., 1984; Chigier and Chervinsky, 1967].

$$S = \frac{\int_{r=0}^{r=\infty} r^2 \rho u w dr}{R \cdot \int_{r=0}^{r=\infty} r\left[\rho\left(u^2 - \frac{1}{2}w^2\right)\right]dr} \tag{2.A.1.15}$$

The simplification of pressure and turbulent stress terms results in a certain lack of conservation of the axial and azimuthal momentum downstream the flow. Thus, often, this characterization is difficult to measure with much accuracy [Gupta, 1984].

The swirl number can be estimated with theoretical calculations based on the swirler geometry and on the velocity profiles at the swirler exit. It is noteworthy to mention that velocity profiles developed by different swirlers can result in different flow velocity profiles, even for those with the same swirl number. Therefore, the swirl number provides only a relative indication of swirl magnitude for a swirler when uncoupled of the corresponding velocity profiles [Sloan et al, 1986].

A.1.3 Isothermal flow field investigation applied to ALVA 20 cyclone reactor

The estimation of the swirl number of the flow within the cyclone reactor of the test facility ALVA 20 is based on the study proposed by Owczarek, 2000, for isothermal flow fields. He measured the axial and tangential velocity profiles along the reactor longitudinal and radial axis at six measurement stations, as shown in Fig. 2.A.1.4, with hot wire anemometry instrumentation, using triple-wire probes. Owczarek, 2000, also simulated isothermal flow fields with the commercial CFD software Fluent and compared them with experimental results. He investigated the influence of the primary and secondary oxidizer inlets operating separately and together on the axial and tangential velocity profiles.

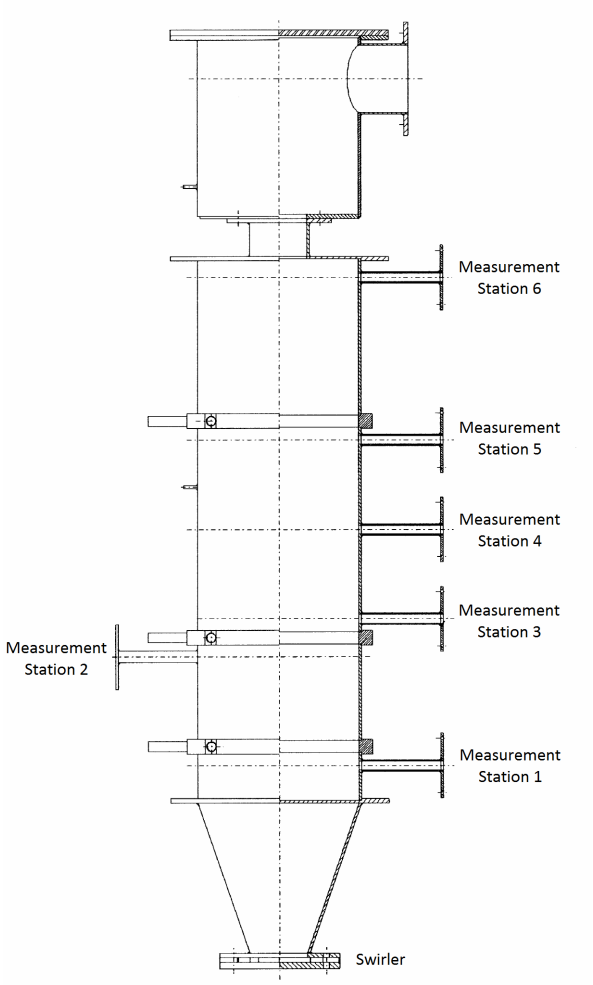

Figure 2.A.1.4 - Cyclone reactor projected view and the measurement stations [adapted from Owczarek, 2000].

Figure 2.A.1.5 shows experimental results for axial and tangential velocity profiles measured at six stations along the longitudinal and radial axis of the reactor with the oxidizer primary air inlet open.

At the swirler exit (station 1), the axial velocity profile shows two regions of reverse flow or central recirculation zones due to the negative axial pressure gradient formed by the tangential velocity and radial pressure decay through the swirler expansion. The axial velocity profile is steady along stations 1, 3 and 5, but the profile changes completely at station 6, becoming flatted with some peaks.

At the station 1, the tangential velocity profile is characterized by a concentrated vortex in the centre region of the reactor with decay along the radius, and this profile is steady along the longitudinal axis of the reactor.

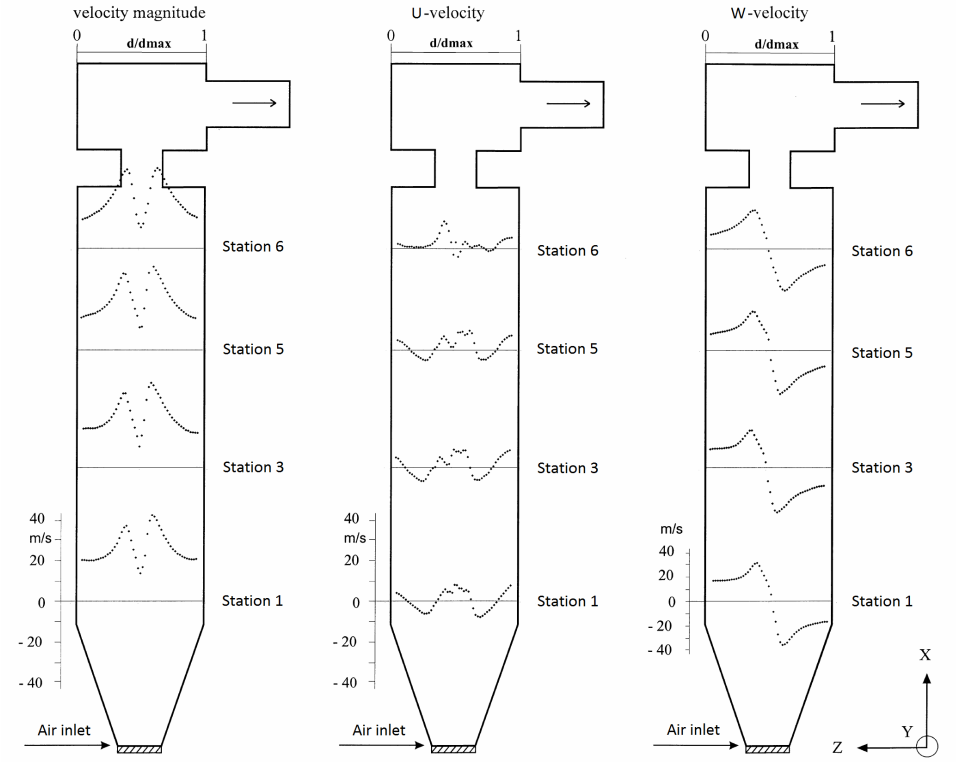

Figure 2.A.1.5 - Axial and tangential velocity profiles measurements [adapted from Owczarek, 2000].

The present work is focused on the velocity profiles obtained only with the primary air inlet open, following the configuration used in the test facility ALVA 20 to study the coal combustion reactivity. Firstly, the axial and velocity tangential profiles near the swirler exit (station 1) were selected from the Fig. 2.A.1.5 as shown in Fig. 2.A.1.6. Usually the swirl numbers are estimated at the swirler exit [Gupta et al., 1984]. The experimental measurements at station 1 are

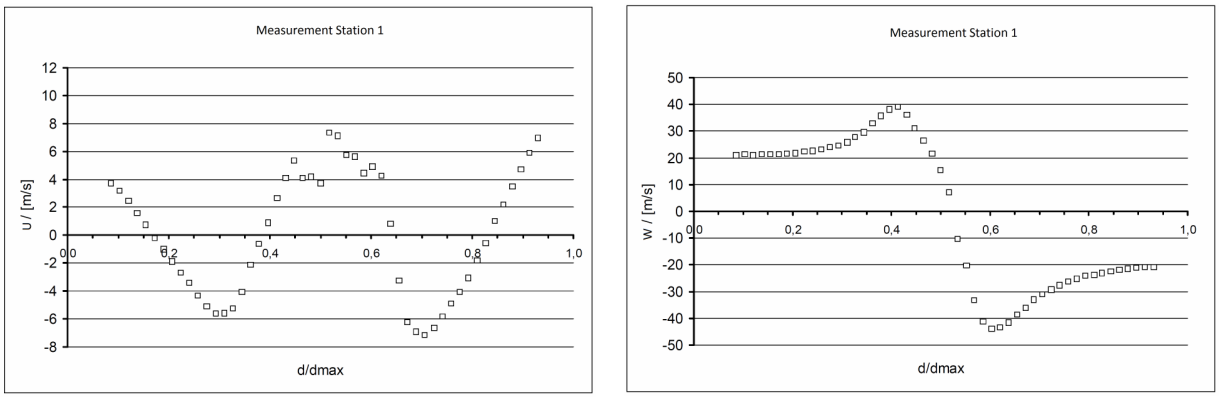

(a) (b)

Figure 2.A.1.6 - (a) Axial and (b) tangential velocity profiles measurements at station 1 [adapted from Owczarek, 2000].

Figure 2.A.1.7 shows the projected views of the cyclone reactors used in ALVA 20 and Owczarek's investigation, depicting the main dimensions (H, D, d).

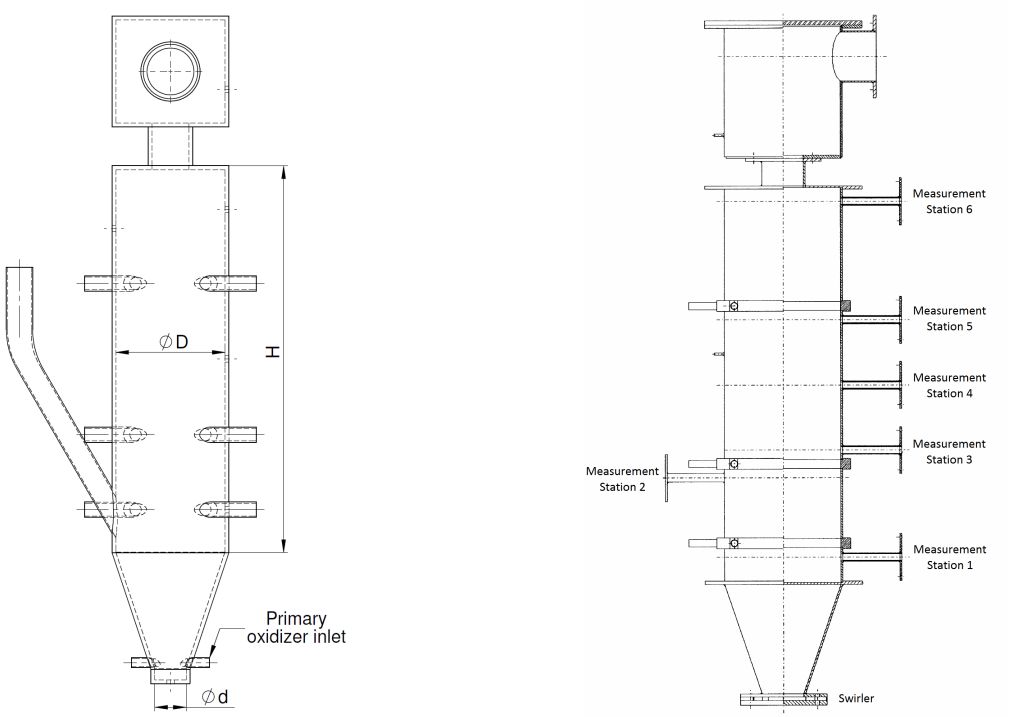

(a) (b)

Figure 2.A.1.7 - Projected views of cyclone reactors used in (a) ALVA 20 and (b) Owczarek's investigation.

Table 2.A.1.1 shows the main parameters used to construct the theoretical velocity magnitudes at swirler exit of ALVA 20 cyclone reactor.

Table 2.A.1.1 - Comparison of the main parameters between the cyclone reactors

Reactor	H (m)	D (m)	d (m)	H/D	D/d	$\dot{m}$ (kg/s)	Nozzles	V_{inlet} (m/s)
ALVA 20	0.496	0.140	0.040	3.5	3.5	0.0027	2	50 @ 800 ^{o}C
Owczarek	0.875	0.250	0.083	3.5	3.0	0.11	8	120 @ 25 ^{o}C

As both cyclone reactors have similar aspect ratios (*H/D* and *D/d*), and the *D/d* parameter has an important influence on the swirl number, the maximum velocity magnitudes at axial and tangential directions at swirler exit are estimated initially for ALVA 20 cyclone reactor, by assuming plug-flow axial and tangential velocity profiles of an incompressible flow passing through sudden expansion in cross-sectional area, as follows [Gupta et al., 1984].

Global continuity equation is given by

$$\dot{m} = 2\pi \int_0^R \rho u r dr = \text{constant} \tag{2.A.1.16}$$

and the global axial flux of swirl momentum equation G_ϕ is given by

$$G_\phi = \int_0^{2\pi} d\phi \int_0^R r^2 \rho u w dr = \text{constant} \tag{2.A.1.17}$$

By applying plug flow/flat swirl profile, where $u = u_1$ and $w = w_1$ (and similar at swirler exit) and hence continuity and swirl momentum give

$$u_1 R_1^2 = u_2 R_2^2 \tag{2.A.1.18}$$

$$u_1 w_1 R_1^3 = u_2 w_2 R_2^3 \tag{2.A.1.19}$$

From the parameters in Table 2.A.1.1, the equations 2.A.1.18 and 2.A.1.19 become

$$u_2 / u_1 \cong 1/9 \tag{2.A.1.20}$$

$$w_2 / w_1 \cong 1/3 \tag{2.A.1.21}$$

These results give an estimation of the reduction of velocity magnitudes through the expansion, but the equations 2.A.1.18 and 2.A.1.19 require the knowledge of the velocity magnitudes at swirler inlet at axial and tangential directions, turning the theoretical calculation of velocity magnitudes in a high uncertainty procedure. However, taking these values as starting points, and aware of these limitations and assumptions, the present work engages the calculation of the velocity magnitudes at swirler exit of ALVA 20 cyclone reactor, using the adjusted velocity profiles to the experimental values obtained in Owczarek's investigation and limiting the maximum velocity magnitude for ALVA 20 cyclone reactor following the relations of equations 2.A.1.20 and 2.A.1.21, taking as reference the inlet tangential velocity value V_{inlet} from Table 2.A.1.1.

The axial and tangential velocity profiles measured at station 1 in Owczarek's work were fitted with mathematical functions, as shown in Fig. 2.A.1.8.

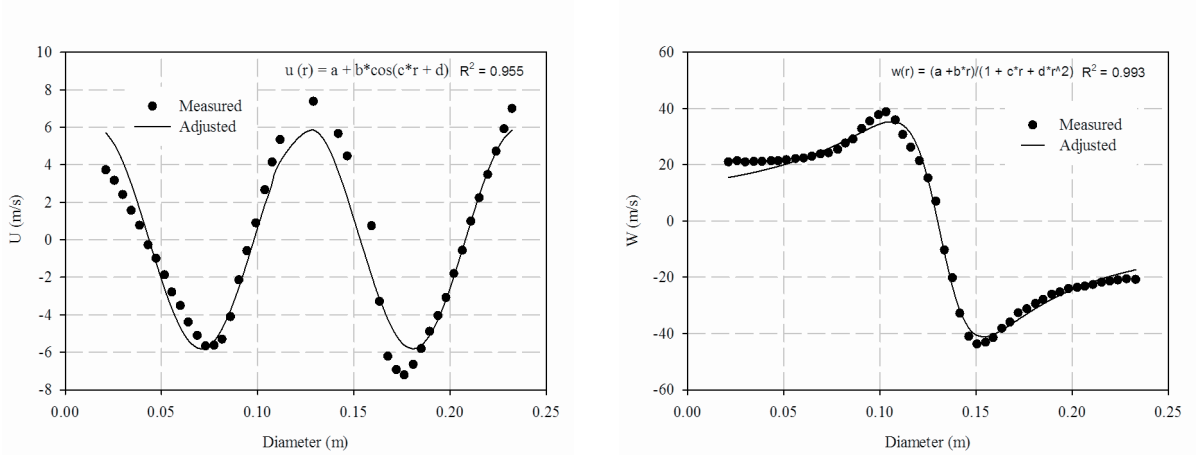

(a) (b)

Figure 2.A.1.8 - Measured (dots) and fitted (lines) velocity profiles for (a) axial and (b) tangential axis at station 1.

By applying these fitted velocity profiles, new coefficients are calculated for the mass flow rate used in ALVA 20 cyclone reactor, resulting in the following velocity profile magnitudes near the swirler exit, as shown in Fig. 2.A.1.9.

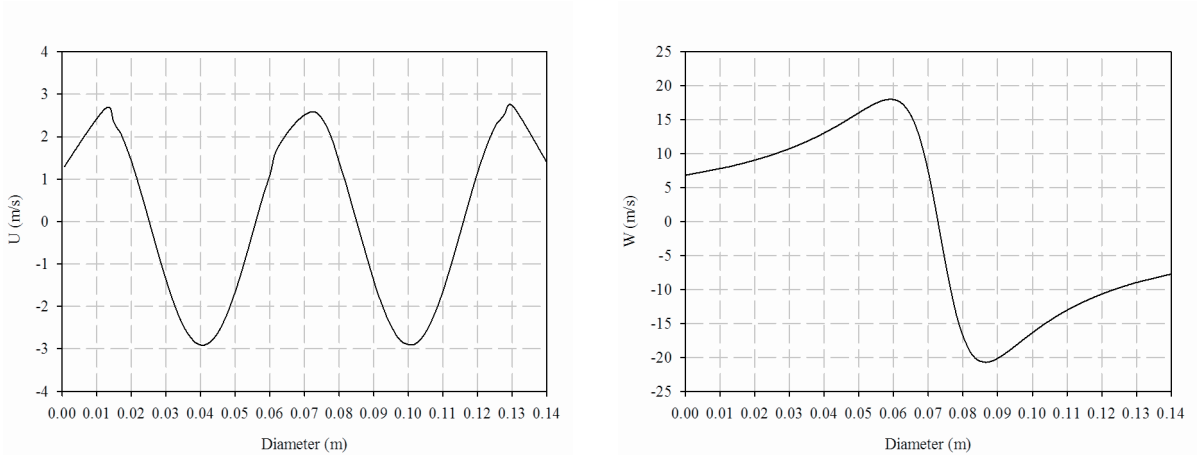

(a) (b)

Figure 2.A.1.9 - Theoretical (a) axial and (b) tangential velocity profiles near the swirler exit of ALVA20 cyclone reactor.

With the theoretical velocity profile magnitudes near the swirler exit of the ALVA 20 cyclone reactor, the swirl number is estimated with the aid of the axial flux of axial momentum G_x modified to include the pressure term of axial momentum, following the swirl number calculations for idealized profiles developed by Lilley, D.G., 1985.

$$G_x = \int_0^{2\pi} d\phi \int_0^R \left[\rho u^2 + (p - p_\infty)\right] r\, dr \qquad (2.A.1.22)$$

$$(p - p_{\infty}) = \int_{d/2}^{R} \left(\frac{\rho w^2}{r} \right) dr \tag{2.A.1.23}$$

The axial flux of azimuthal momentum equation is modified to introduce the integration limits.

$$G_{\phi} = \int_0^{2\pi} d\phi \int_0^{R} r^2 \rho u w dr \tag{2.A.1.24}$$

Table 2.A.1.2 displays values for pressure, axial and swirl momentum calculated by equations 2.A.1.22 to 2.A.1.24 from the integration of velocity profiles, to obtain the swirl number of both cyclone reactors.

Table 2.A.1.2 - Main results used for the swirl number calculation

Reactor	R (m)	$p - p_{\infty}[Pa]$	$G_x[\dot{M}_x]$	$G_x[\dot{M}_x] \cdot R$	$G_{\phi}[\dot{M}_{\phi} m]$	Swirl
ALVA 20	0.070	3.2	0.006	0.00042	0.00064	1.5
Owczarek	0.125	76	2.10	0.2626	0.54	2.0

Results from Table 2.A.1.2 demonstrate that the swirl number is influenced by the magnitude of the axial flux of swirl and axial momentum, and also by the pressure term magnitude of axial momentum. The pressure difference $(p - p_{\infty})$ in cyclone combustion chambers with confined swirling flows contributes to change the axial velocity profile in the centre of the cyclone reactor.

These results show that the swirl number for both cyclone reactors is between 1.5 and 2.0, calculated from the velocity profiles and without the turbulent fluctuating terms. It becomes clear that the swirl number calculation is strongly dependent on the velocity profiles measured at the swirler. These profiles induce the formation of three central toroidal recirculation zones (CTRZ), as the calculated swirl numbers are greater than 0.6 [Syred and Beer, 1974], according to literature.

The swirl number has been used in literature as a parameter for characterizing the cyclone combustion chambers and as well as for comparing them to swirl burners [Syred and Beer, 1974]. For example, swirl numbers of typical burners are assumed to be found in the range from 0.6 to 2.5, whereas the swirl number of cyclone combustion chambers is assumed to range from 2 to 20. In general, cyclone combustion chamber swirl number is appreciably higher than for the swirl generators found in typical burners.

As the knowledge of measured values of velocity and static pressure profiles is rarely available, the swirl number for the cyclone combustion chamber is based solely on the cyclone combustion chamber geometry, and it is less reliable [Sloan et al., 1986]. It is noteworthy to mention that the swirl number is only applicable to isothermal flows and will be subsequently modified for the effects of combustion [Syred and Beer, 1974].

For example, the following relationship provides the swirl number for the cyclone combustion chamber, based on its geometry (i.e. input and exit parameters, total mass flow rate), assuming a uniform axial velocity profile at combustion reactor exit [Owczarek, 2000; Syred and Beer, 1974]. The resulting expression is

$$S \approx \frac{\pi e\, r_o}{2A_T} \tag{2.A.1.25}$$

where r_o is the radius of main section cyclone combustor, e is the distance of the nozzles in relation to cyclone combustor longitudinal axis, and A_T is tangential inlet area.

Substituting the values for the ALVA 20 cyclone reactor, as depicted previously in Fig. 2.5c, i.e. $r_o = 0.070\,\text{m}$, $e = 0.013\,\text{m}$, and $A_T = 1.57x10^{-4}\,\text{m}^2$ with 0.01 m internal diameter and two nozzles, the swirl number attained is 9.0.

The calculation above shows how significant can be the difference between the swirl numbers attained with velocity profiles compared to that obtained with cyclone geometry data. Therefore, the calculation based on the cyclone reactor geometry provides a simple estimation of the swirl number, and the swirl number based on the velocity profiles is preferable.

The analysis of the isothermal swirling flow within a cyclone chamber reactor indicates that the coal reactivity assessment from the potentiometric oxygen sensor measurements is significantly dependent on the flow field within the cyclone reactor, and the modeling assumption of well stirred reactor to estimate the coal global kinetic parameters [Tappe, 2011 and 2009] is investigated with the new oxygen sensor position in Chapter 3 (with DoE) and Chapter 4 (with global kinetic parameters).

APPENDIX 2.A.2 - Fundamentals of potentiometric oxygen sensor

This section summarizes the fundamentals to derive the equation used by the potentiometric oxygen sensor to measure the oxygen concentration of the sampled gas. The overall electrode reactions can be simplified as follow [Ramammorthy et al., 2003]:

$$O_{2,ads} \rightarrow O_{ads} + O_{ads} \rightarrow O_{tpb}^{2-} \rightarrow O_{ysz}^{X} \tag{2.A.2.1}$$

Oxidation and reduction reactions occur at the cathode and anode electrode-electrolyte interfaces, which defines a value of oxygen activity. Assuming fast kinetic rates, the cathode and anode reactions are described according to equations 2.A.2.2 and 2.A.2.3, respectively.

$$O_{2,ref} + 4e_{electrode}^{-} \leftrightarrow 2O_{electrolyte}^{2-} \tag{2.A.2.2}$$

$$2O_{electrolyte}^{2-} - 4e_{electrode}^{-} \leftrightarrow O_{2,gas} \tag{2.A.2.3}$$

The output of this potentiometric sensor is a combined effect of chemical and electrical processes, which can be correlated by using thermodynamic equilibrium and fast kinetic reactions based on Nernst equation [Bhoga and Singh, 2007; Zhuiykov, 2006; Singhal et al., 2003; Wepper, 2003]. The Nernst equation correlates the Gibb's free energy ΔG and electromotive force of a chemical system [Singhal et al., 2003]. For a single component system, the chemical potential μ is equal to the Gibb's free function and defined as:

$$\mu = \mu^{o} + TR\ln\left(p/p_{o}\right) \tag{2.A.2.4}$$

For a solid electrolyte cell with two oxygen electrodes, the cell reaction is merely the transfer of oxygen from the higher to lower partial pressure. Consequently, the chemical work in cell reactions is equal to the difference in chemical potentials, and Eq. 2.A.2.4 becomes:

$$\Delta g = \mu_{O_2,ref} - \mu_{O_2,gas} = TR\ln\left(p_{O_2,ref}/p_{O_2,gas}\right) \tag{2.A.2.5}$$

In order to derive the cell potential, the reversible power of the fuel cell P can be written as a product of the reversible tension U and the electric current I as well as a product of the molar flow of the fuel $\dot{n}_{an,O_2}$ and the free Gibb's energy of the reaction Δg, or a

product of the specific reversible work of fuel cell w and the molar flow of the fuel $\dot{n}_{an,O_2}$ [Singhal et al., 2003], as shown in Eq. 2.A.2.6.

$$P = U\,I = \dot{n}_{an,O_2}\,w = \dot{n}_{an,O_2}\,\Delta g \tag{2.A.2.6}$$

The electrical current due to the molar flow of the electrons of oxygen is given by Eq. 2.A.2.7. It's important to highlight here that $\dot{n}_{el}$ is the molar flow of the electrons of oxygen, which is four times the molar flow of the oxygen molecule $\dot{n}_{an,O_2}$, as previously shown in the reaction 2.A.2.3; and that the Faraday constant is the product of elementary charge $-e$ and Avogadro constant number N_A.

$$I = \dot{n}_{el}(-e)N_A = -\dot{n}_{el}F = -4\dot{n}_{an,O_2}F \tag{2.A.2.7}$$

Combining equations 2.A.2.6 and 2.A.2.7, and the Gibb's function can be written as

$$\Delta g = -\dot{n}_{el}\,F\,U \tag{2.A.2.8}$$

Consequently, the Eq. 2.A.2.5 can be rewritten in terms of the cell potential between the two electrodes and of oxygen partial pressures as:

$$U = (RT/\dot{n}_{el}F)\ln\left(p_{O_2,ref}\,/\,p_{O_2,gas}\right) \tag{2.A.2.9}$$

Substituting the oxygen partial pressures by molar fractions in Eq. 2.A.2.9 and rearranging it, the oxygen molar fraction of sampled gas can be calculated, knowing the cell potential and gas temperature, according to Eq. 2.A.2.10.

$$f_{O_2,gas} = f_{O_2,ref}\exp\left(-\left(\dot{n}_{el}\,FU\right)/(RT)\right) \tag{2.A.2.10}$$

Substituting the values of Faraday and ideal gas constants, and molar flow of the electrons of oxygen $\dot{n}_{el}$, yields the oxygen concentration in vol.% calculated by the sensor.

$$C_{O_2,gas} = 20.64\exp\left(-46.42(U/T)\right) \tag{2.A.2.11}$$

3. Design of experiments applied to a laboratory test facility developed to investigate coal combustion behavior under oxy-fuel and air atmospheres

Abstract

Design of experiments (DoE) analysis was applied in a laboratory test facility developed to investigate the combustion process under turbulent and swirling flows and covering a temperature range similar to those found in practical furnaces. Several experimental studies under air and under oxy-fuel conditions with the aid of gas-potentiometric analysis by using oxide-ion conducting solid electrolytes as stabilized zirconia, installed within the cyclone reactor, were performed with low-rank coals in order to show how the experiments are designed and analyzed with the statistical tools provided by the methodology. All the experiments were carried out at three average gas combustion temperatures: 1073, 1173 and 1273 K. The results show that the analysis of variance (ANOVA) of the experimental data proved to be an important statistical tool to understand the influence of the factors, as temperature and atmosphere compositions, and the interactions between them to study the response variables selected for the coal combustion investigation, as combustion time and oxygen consumption by the coal sample. Results also show that oxidizer oxy-fuel atmosphere with 79% CO_2 (21/79, O_2/CO_2) increases the oxygen consumption for high ash coals, Bonito and Leão, and for pre-dried lignite coal, LTBK, due to the influence of CO_2 gasification reaction on their coal combustion reactions. In addition, results allow to conclude that the oxygen concentration curves measured by the potentiometric oxygen sensor probe depend on its position within the cyclone reactor.

Keywords: DoE, oxy-fuel combustion, low-rank coal, cyclone combustion reactor, potentiometric oxygen sensor.

LIST OF ABREVIATIONS AND SYMBOLS

Abbreviations

ALVA20	20 kW_{th} - Laboratory test facility with cyclone reactor rated capacity of 20 kW_{th} operating under 1 atm.
daf	Dry, ash free
DoE	Design of Experiments
LTBK	Lausitzer Trockenbraunkohle, Lusatian pre-dried brown coal
Vol.	Volume

Symbols

A	Factor
B	Factor
E	Expectation, Error
F	F distribution
H	Hypothesis
p	Pressure, atm
P	Significance level
n	Total of elements of sample, sample size; number of replicates
N	Total of elements of population
S	Sample standard deviation, used as measure of dispersion in second or % (in vol.)
S^2	Sample variance, unbiased estimator of σ^2
SS	Corrected sum of squares
t	Time, s
T	Temperature, K or ºC
$\dot{V}$	Volumetric flow, $m^3\ h^{-1}$
y	Normal random variable
$\bar{y}$	Sample mean, unbiased estimator of μ

Greek symbols

α	Significance level of the test
ß	Effect of the *j*th level of column factor
Δ	Increment, change
ε	Random error
μ	Population mean
σ	Population standard deviation
τ	Effect of the *i*th level of row factor

Subscripts

0	Null
a	Level of factor *A*
b	Level of factor *B*
i	*i*th factor level
j	*j*th factor level
k	*k*th factor level

3.1 Introduction

The need to understand the behavior of coal combustion under oxy-fuel conditions stimulated many experimental works [Brix et al., 2010; Zhang et al., 2010; Liu, 2009; Rathnam et al., 2009; Molina and Shaddix, 2009, 2007; Borrego et al., 2007]. A particular one, developed by Tappe, 2011, 2009, was performed to obtaining the global kinetic parameters of coal combustion under oxy-fuel atmospheres. This test facility aims to simulate coal combustion with the environment conditions found in existing furnaces and calculate the global kinetic parameters of the coal tested by measuring the variation of oxygen concentration of the sample with the aid of a potentiometric oxygen sensor installed within the reactor. The experimental workbench, called ALVA 20, was designed and built at the Chair of Power Plant of Brandenburg University of Technology (Cottbus, Germany).

A new set of experiments performed with test facility searches to identify by means of statistical tools, what are the experimental parameters, as gas temperature, coal type, atmosphere composition, particle diameter, which have significant influences on the oxygen concentration curve results measured by the potentiometric oxygen sensor. In the oxygen concentration curves, specific variables, as combustion times and maximum variation of oxygen concentration are selected in order to infer on the coal combustion phenomenon.

In addition to this investigation, the present analysis requires a previous knowledge of the oxygen concentration curves interpretation, performed in previous works [Tappe, 2009; Carotenuto and Corrêa, 2012, 2011], and the statistical tools are useful to support this analysis when the number of experiments and the combination of its factors are high.

Therefore, the present chapter is focused on the planning of the experimental investigation of the behavior of coal combustion by using the Design of Experiments (DoE) methodology [Montgomery, 2001]. Experiments were performed on the ALVA 20 workbench described in Chapter 2, with a special interest on the behavior of low-rank coals with high content of volatiles (lignite coal) and with high ash content (Brazilian coals), burned under different oxidizer atmospheres and temperatures.

3.2 Low rank coals and experimental parameters

In the present study, the experiments were performed with German pre-dried lignite (LTBK) from the Lusatian region, in Germany, and two high-ash content coals from Leão and

Bonito mining sites located in South Brazil. The coal samples proximate and ultimate analyses in mass base are given in Table 3.1.

Table 3.1 - Proximate and ultimate analysis of the Lusatian pre-dried lignite, Leão and Bonito coals in mass base

	Lignite (LTBK)		Leão		Bonito	
Proximate Analysis (%)	dry	daf	dry	daf	dry	daf
Volatile Matter	54.1	57.9	20.0	40.8	12.6	36.4
Fixed Carbon	39.1	42.1	29.0	59.2	22.0	63.6
Ash	6.5	-	51.1	-	65.4	-
Ultimate Analysis (%, daf)						
Carbon	67.05		73.62		77.61	
Hydrogen	6.95		5.16		5.02	
Nitrogen	0.70		1.31		1.33	
Sulfur	0.80		4.67		10.52	
Oxygen (by difference)	24.50		15.24		5.53	
C/H Ratio	9.65		14.27		15.46	

In addition, char samples from Leão and lignite coals were prepared in order to investigate the combustion behavior of its carbon matrix for different levels of volatile matter. This approach has not been developped in previous works with ALVA 20 [Tappe, 2011, 2009; Carotenuto and Corrêa, 2012, 2011].

Samples were generated in a pyrolysis reactor under N_2 atmosphere flow, heated at temperatures of 535, 545, 730 and 900 ^{o}C. Thus, Table 3.2 summarizes the resulting volatile matter analysis for the coal char samples.

Table 3.2 - Volatile matter content of chars for different levels of devolatilization temperature

Char	Devolatilization temperature	Remaining volatile matter (%, dry)
Leão	545 ^{o}C	7.78
	730 ^{o}C	1.91
	900 ^{o}C	0.63
LTBK	535 ^{o}C	20.03
	900 ^{o}C	3.83

Coal samples were separated in particle ranges of 125-500 μm, and 1250-2000 μm, sieved on a Vibratory Sieve Shaker AS 200 Control equipment from Retsch manufacturer.

The combustion of the sieved samples was carried out under air and oxy-fuel conditions, separated by five CO_2 concentrations levels, with and without water vapor, and at three average gas temperature levels within the cyclone reactor, as detailed in Table 3.3.

Table 3.3 - Experimental parameters for air and oxy-fuel coal and char combustion

Experimental condition	Air	Oxy-fuel				
O_2 in oxidizer (vol. %)	21	21	30	30	30	30
CO_2 in oxidizer (vol. %)	0	79	70	60	50	40
H_2O in oxidizer (vol. %)	0	0	0	10	20	30
Oxidizer volumetric flow (m³/h) at 873 K	23	26	25	22	26	27
Oxidizer temperature (K)	873			873		
Reactor temperature (K)	1073, 1173, 1273					
Sample mass (g)	1 and 3					
Particle diameter range (μm)	125-500, 1250-2000					

3.3 Design of experiments (DoE) for coal and char combustion

The Design of Experiments [Montgomery, 2001] is a broad methodology for planning experimental investigations, with further data analysis, simulation and optimization. The planning of experiments requires the identification of controllable factors and the response variables, as described in the following sections. With the aid of statistical tools provided by DoE, it is aimed to investigate what are the experimental parameters, as gas combustion temperature, coal type, atmosphere composition, particle diameter, which have significant influences on the oxygen concentration curve results measured by the potentiometric oxygen sensor.

3.3.1 Controllable factors and response variables

The identification of the process controllable factors and its respective levels are summarized in Table 3.4, based on the test facility operation as described in Chapter 2, and following the acquired knowledge given by Tappe, 2009. ALVA 20 allows for controlling 5 factors, with different numbers of levels per factor, pointing out the complexity of the analysis of the variable responses. Some controllable factors were not taken into account, like the

oxidizer volumetric flow rate, as it did not bring any influence on the coal reactivity. The particle size ranges are represented by the mean particle diameter of each range. The particle size range from 125 to 500 µm corresponds to 312 µm particle mean diameter and the range from 1250 to 2000 µm corresponds to 1625 µm mean diameter.

Table 3.4 - ALVA 20 controllable factors and experiment levels for DoE

Factor	Level description	Number of levels
Coal and char	Coal: Leão, Bonito and LTBK Char: Leão 545 ^{o}C, 730 ^{o}C and 900 ^{o}C, LTBK 535 ^{o}C and 900 ^{o}C	8
Particles range (µm)	125-500 (312), 1250-2000 (1625)	2
Temperature (K)	1073, 1173 and 1273	3
Oxidizer atmosphere (vol. %)	Air: 21/79 (O_2/N_2) Oxy-fuel without water vapor: 21/79, 30/70 (O_2/CO_2) Oxy-fuel with water vapor: 30/60/10, 30/50/20, 30/40/30 ($O_2/CO_2/H_2O$)	6
Sample mass (g)	1 and 3	2

The combustion of coal and char samples is assessed by O_2 concentration at the oxidizer atmosphere within the cyclone combustion reactor measured by the potentiometric oxygen sensor. The selected response variables are the maximum variation of oxygen concentration ΔO_2, the elapsed times t_1 and t_2, indicated along the oxygen concentration curve, as shown in Fig 3.1. The maximum variation of the oxygen concentration is defined as ΔO_2, which corresponds to the maximum oxygen consumed for the sample from $t=0$ until elapsed time t_1. For raw coals, this interval of time is characterized predominantly by the volatile zone combustion, and this behavior is investigated in the present work.

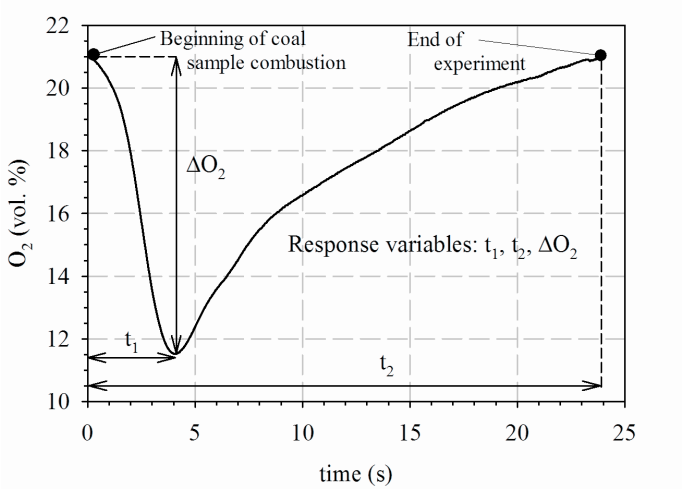

Figure 3.1 - Response variables ΔO_2, t_1 and t_2 from the oxygen concentration curve.

The elapsed time t_2 is bounded by time *t=0* and ends up when the O_2 sensor stabilizes, defined for different values of oxidizer atmospheres, as shown in Table 3.5. The value of oxygen concentration at which the O_2 sensor stabilizes is referenced in Zirox, 2003, and it is due to small difference of the oxygen chemical potential between the outer and inner probe electrodes.

Table 3.5 - Oxygen concentration stabilization values for elapsed time t_2

Oxidizer atmosphere	O_2 (vol. %)
Air	20.6
Oxy-fuel with 21% O_2	20.6
Oxy-fuel with 30% O_2	29.4

In order to complement this analysis, video images recorded by a camera installed at the top of the reactor can give extra information about the behavior of the response variables, and it is defined as t_{video}.

Table 3.6 is a general arrangement for a two-factor factorial design, built with data from Table 3.4. To illustrate the construction of this kind of table, 1g of lignite coal (LTBK) sample with one specific particle range (1250-2000 μm) was selected. The combustion process was performed for 3 temperature levels and 3 oxidizer atmospheres, with 3 replicates.

Table 3.6 - General arrangement for a two-factor factorial design for LTBK

Oxidizer atmosphere oxy-fuel ($O_2/CO_2/H_2O$)	Temperature (K)		
	1073	1173	1273
	Replicate	Replicate	Replicate
	i ii iii	i ii iii	i ii iii
30/60/10	$y_{111}, y_{112}, y_{113}, \ldots, y_{11n}$	Response variable	$y_{131}, y_{132}, y_{133}, \ldots, y_{13n}$
30/50/20	$y_{211}, y_{212}, y_{213}, \ldots, y_{21n}$	y_{ijk}	$y_{231}, y_{232}, y_{233}, \ldots, y_{23n}$
30/40/30	$y_{311}, y_{312}, y_{313}, \ldots, y_{31n}$	…	$y_{331}, y_{332}, y_{133}, \ldots, y_{33n}$

where y_{ijk} is the response variable when factor *A* is at the *i*th level $(i = 1, 2, \ldots, a)$ and factor *B* is at the level *j*th $(j = 1, 2, \ldots, b)$ for *k*th replicate $(k = 1, 2, \ldots, n)$. Replicate means that each combination of temperature and atmosphere levels (i.e. at 1073 K, and 30/60/10 atmosphere, for instance), the experiment is repeated or replicated three times. The fundamentals of DoE

applied for the experiments arranged in Table 3.6 are found in Appendix 3.A.1. The analysis of the results is discussed in the section 3.4.

3.3.2 Overview of the strategy adopted for the design of experiments

This section describes how the experiments in the present work were planned in order to provide an overview of the main tests performed with the laboratory test facility, and the main objectives expected with the experiments. The overview of the experiments is showed in flowchart of Fig. 3.2 and the description for each group of experiments is summarized as follows.

The first preliminary set of experiments was performed with 1g-lignite coal (LTBK) under oxy-fuel atmospheres with the participation of water vapor concentration, as previously shown in Table 3.6, in order to investigate the influence of water vapor in separate on LTBK coal combustion. The design of experiments and analysis of its results with DoE methodology are also used as reference and it is applied for the next experiments.

Thus, the experiments were subdivided in 4 main groups, as shown in Table 3.7, according to the research objectives. Total of 265 experiments, including replicates, have been performed in ALVA 20. The number of replicates for each group of tests is detailed in Tables from 3.A.3.1 to 3.A.3.22 found in Appendix 3.A.3.

Table 3.7 - Groups of experiments performed in ALVA 20

Group	Sample	Mass (g)	Particles mean diameter (μm)	Gas reactor temperature	Oxidizer stream composition	Tests
1st	Coal(Leão + Bonito)	1	312, 1625	1073, 1173, 1273 K	Air, 21/79, 30/70 (O_2/CO_2)	78
2nd	Coal (LTBK)	1	312, 1625	1073, 1173, 1273 K	Air, 21/79, 30/70 (O_2/CO_2), 30/60/10, 30/50/20, 30/40/30 ($O_2/CO_2/H_2O$)	90
3rd	Char (Leão + LTBK) Coal (Leão + LTBK)	3	1625	1073, 1173, 1273 K	Air, 21/79 (O_2/CO_2)	72
*4th	Char (Leão + LTBK) Coal (Leão + LTBK)	3	1625	1073, 1173, 1273 K	Air	25
					Total	265

*New oxygen sensor position within the cyclone combustion reactor

The first and second groups are two set of experiments with 1g low-rank coal samples with particles mean diameters of 312 and 1625 μm. The objective with the 1st group is to investigate the behavior of coals Leão and Bonito burned under air and oxy-fuel atmospheres

with 21 and 30% O_2 (in vol.). The objective with the 2nd group is to investigate the behavior of LTBK coal burned under air and oxy-fuel atmospheres with 21 and 30% O_2 (in vol.) including the participation of water vapor with 10, 20 and 30% in vol. in oxy-fuel with 30% O_2.

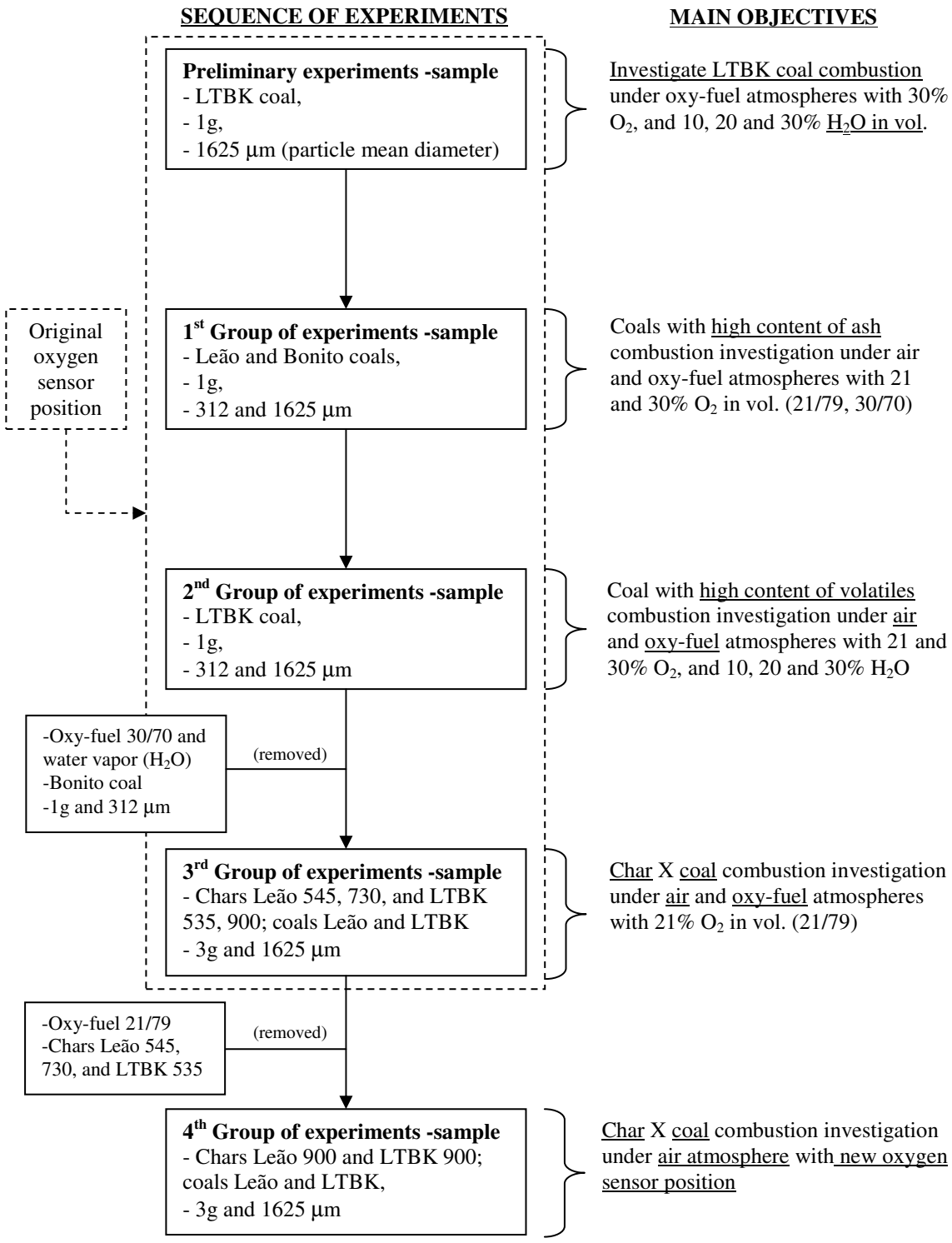

Figure 3.2 - Flowchart of the sequence of experiments with its main objectives.

The third group is a set of experiments with 3g coals and chars samples with particles mean diameter of 1625 μm. The objective is to investigate the behavior of Leão and LTBK coals and chars burned under air and oxy-fuel atmospheres with 21% O_2 (in vol.). As the influence of particle mean diameter and oxy-fuel with 30% O_2 was already verified in first two groups, particles mean diameter of 312 μm and oxy-fuel atmosphere with 30% O_2 were removed in experiments of 3rd and 4th groups.

Samples with 3g mass replace the 1g ones in order to improve the repeatability of the tests and to reduce the number of replicates. The experiments with Bonito coal samples were discontinued in next groups, since they did not burn completely within the cyclone combustion reactor, and the pyrolysis of coal samples were not well succeeded to obtain char samples within the pyrolysis reactor.

The forth group is a set of experiments with 3 g coals and chars samples with particles mean diameter of 1625 μm. The objective is to investigate Leão and lignite coals and chars combustion behavior burned under air atmosphere conditions, with a new potentiometric oxygen sensor position within a cyclone reactor to investigate the influence of swirl flow field on the oxygen sensor measurements. In this group, only char samples of Leão and LTBK coals devolatilized at 900 ^oC were tested in order to compare with the results obtained in 3rd group, and within the 4th group of experiments.

3.4 Results and discussion

The presentation of the results and its analysis are subdivided in sections separated by the groups of experiments following the sequence described in section 3.3.2 (Fig. 3.2). In the end of each section, there is a summary of the major results and conclusions found for the group of experiments investigated.

The analysis of variance (ANOVA) of each group was developed with the aid of Minitab software, and its results analysis follows the DoE methodology found in literature [Montgomery, 2001], with the aid of graphs to show and analyze the main interaction factors on the response variables results. From here and so on the name for maximum variation of oxygen concentration is replaced by the variation of oxygen concentration name. Basically, the statistical analysis is done with the aid of ANOVA tables and the phenomena analysis is inferred with the aid of the main interaction plots between the factors selected from ANOVA analysis, applying the fundamentals of The Theory of Three Zones [Smoot and Smith, 1985]

for air and oxy-fuel atmospheres reviewed in Chapter 1. The plots show the standard deviation σ due to the replications of the samples for each response variable in order to assess how significant is the influence of a factor level and its combination on the response variable results. For instance, if the average variation of a response variable due a level of factor is within the standard deviation, this level of factor is not significant on the result.

The most relevant results are presented and discussed in this section. The Appendix 3.A.2 provides details about a systematic statistical analysis for each group of experiments, used to select the most important factors on the results of response variables.

3.4.1 Analysis for LTBK coal combustion under oxy-fuel with water vapor

The results and the analysis for the set of experiments performed with LTBK coal under oxy-fuel with water vapor is presented and discussed as follow.

A) Phenomena analysis for variation of oxygen concentration ΔO_2 (vol. %)

Figure 3.3 plots the average responses of variation of oxygen concentration for each combination of oxidizer atmosphere and temperature levels.

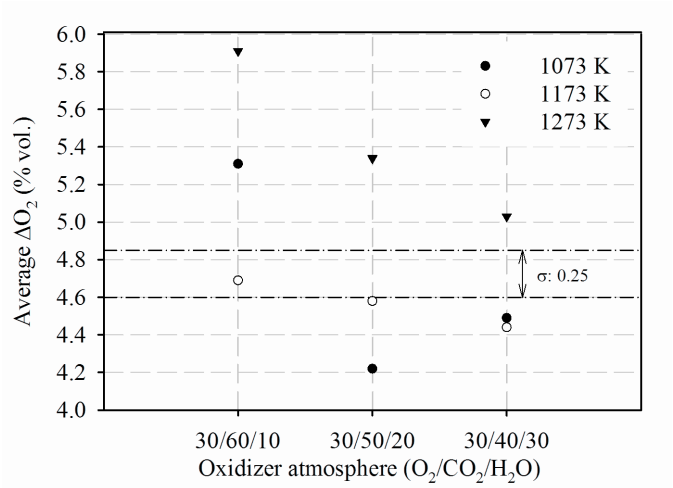

Figure 3.3 - Plot of average variation of oxygen concentration for each combination of oxidizer atmosphere and temperature levels.

High values of variation of the oxygen concentration are attained at 1273 K, regardless of the oxidizer atmosphere. Changing from high to low water vapor concentrations makes the variation of oxygen concentration to increase at 1273 K. The following results are within the samples standard deviation σ, i.e. 0.25% O_2, due to its replications: the difference between the variation of oxygen concentration values at 1073 and 1173 K for atmosphere level 30/40/30;

the influence of temperature level 1173 on the variation of oxygen concentration for all atmosphere levels.

Therefore, observing the results for 1273 K there is a trend, in which the oxidizer atmospheres with low water vapor concentration increase the variation of oxygen concentration. The results allow to conclude that is due to influence of CO_2 gasification reaction on coal combustion reaction rates from temperature higher than 1173 K, which increases the oxygen consumed from CO_2 concentration higher than 50% (in vol.), comparing with that in oxy-fuel with 40% CO_2 (30/40/30). The increase of oxygen concentration variation at 1073 K for atmosphere level 30/60/10 in relation to 1173 K is greater than samples variability, and it is out of the trend observed, requiring new replicates to be performed for these two levels of temperature: 1073 and 1173 K.

B) Phenomena analysis for average time t_1 (s)

Figure 3.4 shows the plot of average responses of time t_1 for each temperature level, including all oxidizer atmospheres. Low values of average time t_1 are attained at high temperature values, regardless of oxidizer atmosphere. This behavior shows that the combustion reaction rates are affected by the increase of gas combustion temperature, resulting in highest reaction rates and oxygen consumptions for all atmosphere levels, in which the kinetic regime controls the coal combustion reaction rates.

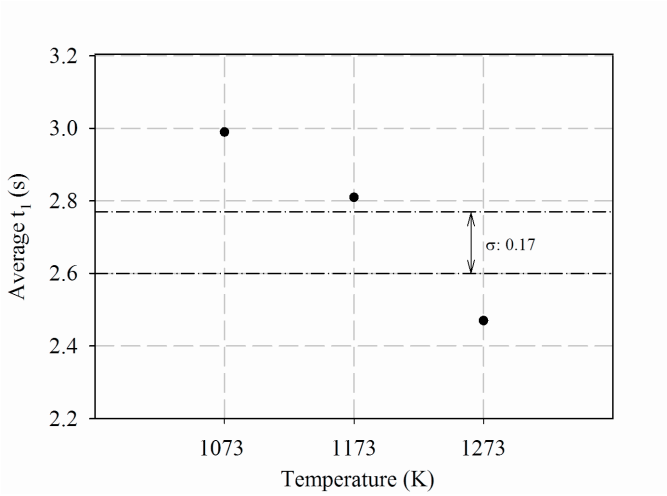

Figure 3.4 - Plot of average time t_1 for each temperature level

C) Phenomena analysis for average time t_2 (s)

Figure 3.5 shows the plot of average responses of elapsed time t_2 for each combination of temperature and oxidizer atmosphere levels. Low values of average time t_2 are attained at

high gas temperature values, regardless of oxidizer atmosphere, showing the effect of temperature on the coal combustion reactions, in which the kinetic regime controls the coal combustion.

Changing from low to high water vapor concentrations decreases the values of average elapsed time t_2. These results allow to conclude that lower variations of oxygen concentrations due to the reduced effect of CO_2 gasification reaction, as observed for atmospheres 30/40/30 and 30/50/20 in Fig. 3.3, are more influenced by oxidizer stream oxygen concentration gradients within the cyclone reactor than that observed at higher variations of oxygen concentrations, as observed for atmosphere with higher CO_2 concentration (30/60/10).

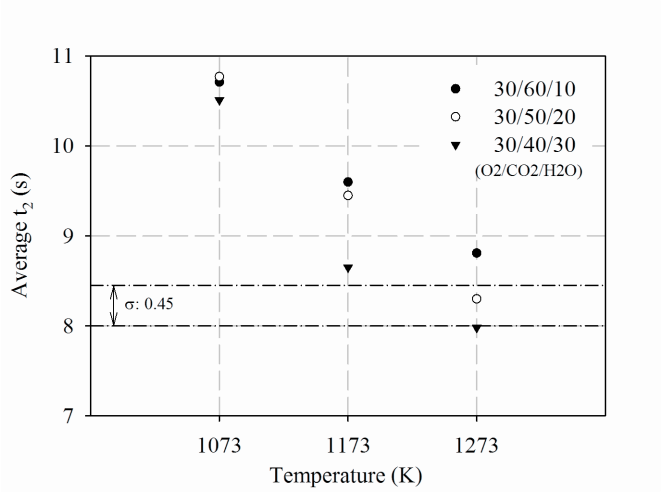

Figure 3.5 - Plot of average elapsed time t_2 for each combination of temperature and oxidizer atmosphere levels.

D) Major findings for LTBK coal combustion under oxy-fuel with water vapor

Low values of average time t_1 and elapsed time t_2, are attained at high values of gas combustion temperature, because the coal combustion reaction rates are under control of kinetic regime, in which the influence of CO_2 gasification reaction ($C + CO_2 \rightarrow 2CO$) is greater than H_2O gasification reaction ($C + H_2O \rightarrow CO + H_2$) for temperatures higher than 1173 K, which increases the oxygen consumption from CO_2 concentrations higher than 50%.

3.4.2 Analysis for 1st group of experiments

The results concern with experiments performed with Bonito and Leão coals, under air and oxy-fuel atmospheres at three levels of combustion gas temperature with two ranges of particle sizes, as described in Table 3.7 and Fig. 3.2.

A) Phenomena analysis for variation of oxygen concentration ΔO_2 (vol. %)

Figure 3.6a shows the average response of variation of oxygen concentration for each combination of particle mean diameter and oxidizer atmospheres, including all temperatures and coals. High variation of oxygen concentration values are attained at small particle mean diameter and depend on the oxidizer atmosphere levels, whereas at large particle mean diameter the influence of oxidizer atmosphere levels on the variation of oxygen concentration is reduced. It is observed that for small particle diameter, the oxy-fuel atmosphere with 30% O_2 (in vol.) has the lowest average variation of oxygen concentration, and the oxy-fuel atmosphere with 21% O_2 (in vol.) has the highest average variation of oxygen concentration.

These results allow to conclude that highest concentrations of CO_2 increase the oxygen consumption due to the influence of gasification reaction of CO_2 with high ash content coals, and lower particle mean diameter has higher variation of oxygen concentration than that attained for large particle mean diameter due to the effect of superficial area.

Figure 3.6b shows the influence of temperature levels on the average response of variation of oxygen concentration. High variation of oxygen concentration is attained at 1273 K for all coals, atmospheres and mean diameters levels. These results allow to conclude that the combustion reactions are controlled by kinetic regime from temperatures higher than 1173 K, in which the gasification reaction of CO_2 plays an important role, as observed for the results attained under oxy-fuel 21/79 in Fig. 3.6a.

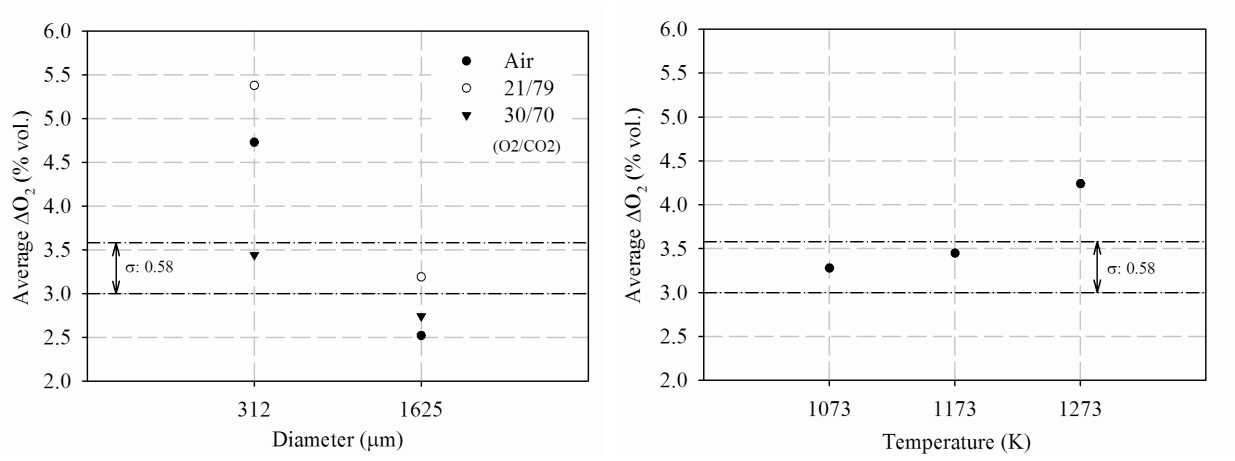

Figure 3.6 - Plots of average variation of oxygen concentration (a) for each combination of mean particle diameter and oxidizer atmosphere and (b) for each combination of temperature levels.

B) Phenomena analysis for average time t_1 (s)

Figure 3.7 shows the average response of t_1 for each combination of particle mean diameter and temperature, including all coals and oxidizer atmospheres. As observed, low values of average time t_1 are attained for small particle mean diameter, and the influence of temperature levels is reduced, and it is within the samples variability due its replications. For large particle mean diameter, the effect of temperature level is seen only at 1273 K, reducing the average time t_1. These results allow to conclude that for large particle mean diameter the kinetic regime influence is greater than that for small particle mean diameter, indicating in the latter a resistance to the diffusion of oxidant into the pores of coal matrix or into the boundary layer, in which the effect of increasing the temperature is reduced on coal combustion rate.

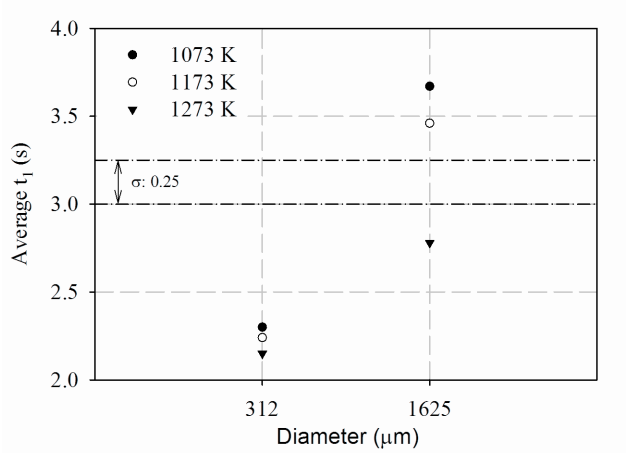

Figure 3.7 - Plot of average time t_1 for each combination of particle mean diameter and temperature.

C) Phenomena analysis for average time t_2 (s)

Figure 3.8a shows the plot of average response of elapsed time t_2 for each combination of particle mean diameter and oxidizer atmosphere, including all coals and temperature levels. As observed, low values of average elapsed time t_2 are attained at small particle mean diameter, and the effect of oxidizer atmosphere on average time t_2 occurs significantly in oxy-fuel with 21% O_2 (in vol.), increasing the average time t_2 for both particle mean diameters.

These results are due to the influence of oxy-fuel atmosphere properties, as low oxygen diffusion coefficient, that brings two effects: (a) increases the resistance of oxidant diffusion through the boundary layer formed around coal particle controlling the coal combustion reaction rate, and (b) delays the recovery of oxygen concentration oxidizer stream at inlet conditions (i.e. 21% O_2 in vol.). The difference of average time t_2 values between air and oxy-fuel 30/70 atmospheres is within the samples variability due its replications, which is

1.16 s, therefore, there is no significant difference and influence on the values of average elapsed time t_2.

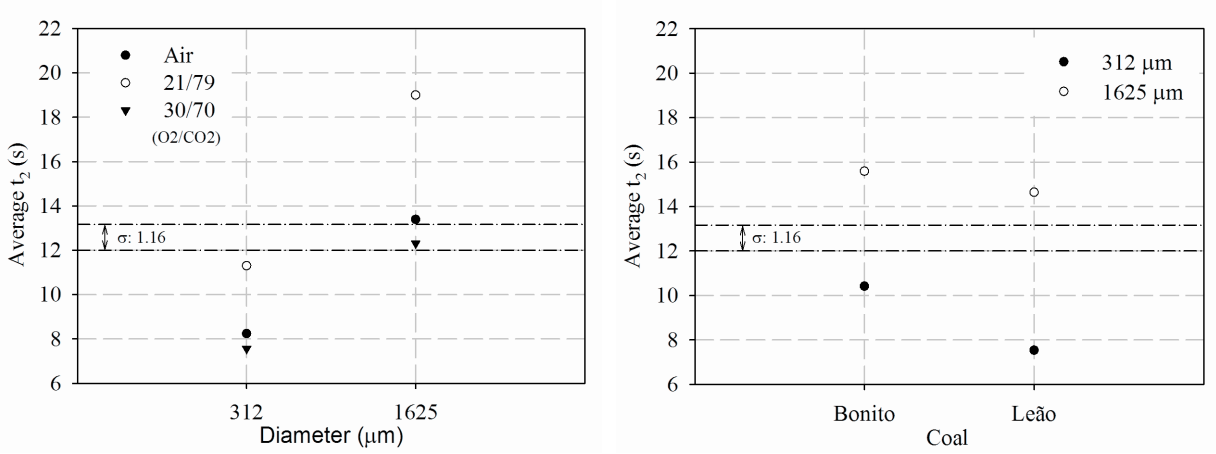

(a) (b)

Figure 3.8 - Plots of average elapsed time t_2 (a) for each combination of particle mean diameter and oxidizer atmosphere and (b) for each combination of diameter and coal.

Figure 3.8b shows the average response of elapsed time t_2 for each combination of coal and particle mean diameter, including all oxidizer atmosphere and temperature levels. As observed, low values of average time t_2 are attained for small particle mean diameter for Leão and Bonito coals, whereas for large particle mean diameter, there is no difference of average time t_2 between the coals. These results allow to conclude that Bonito coal is less reactive than Leão coal, due to its higher content of ash than Leão coal, increasing the average elapsed time t_2. The influence of oxy-fuel atmosphere properties on coal combustion reaction rate increases the average response of t_2 for both coals, decreasing the influence due to the difference of reactivity between them for large particles mean diameter.

D) Major findings for 1st group of experiments

Oxidizer oxy-fuel atmosphere with 79% CO_2 (21/79) has higher oxygen consumption than that in oxy-fuel with 70% CO_2 (30/70) and in air atmospheres for both high ash coals tested (Bonito and Leão), due to the influence of CO_2 gasification reaction ($C + CO_2 \rightarrow 2CO$) on coal combustion, and these findings were not seen in literature review. However, oxy-fuel atmosphere 21/79 increases the average elapsed time t_2, due to the influence of oxy-fuel atmosphere properties, as low oxygen diffusion coefficient, on coal combustion reaction rates and on the recovery of oxygen concentration oxidizer stream at inlet conditions (i.e. 21% O_2 in vol.).

3.4.3 Analysis for 2nd group of experiments

The results concern with the experiments performed with LTBK coal, under air and oxy-fuel atmospheres (with water vapor), at three levels of combustion gas temperature with two ranges of particle size, as described in Table 3.7 and Fig. 3.2.

A) Phenomena analysis for variation of oxygen concentration ΔO_2 (vol. %)

Figure 3.9a shows the average response of variation of oxygen concentration for each combination of oxidizer atmospheres and particle mean diameter, including all temperature levels. As observed, changing from low to high water vapor concentrations in oxidizer atmosphere there is a trend to decrease the variation of oxygen concentration for both particles mean diameters. Within the oxy-fuel atmospheres with water vapor and highest CO_2 concentrations (30/60/10) there is an increase of the variation of oxygen concentration, showing the influence of CO_2 gasification reaction, as discussed in item 3.4.1

The results allow to conclude that the effect of CO_2 gasification reaction is greater in oxy-fuel 21/79 than in other oxidizer atmospheres for large particles mean diameter, whereas for small particles mean diameter, this effect is reduced.

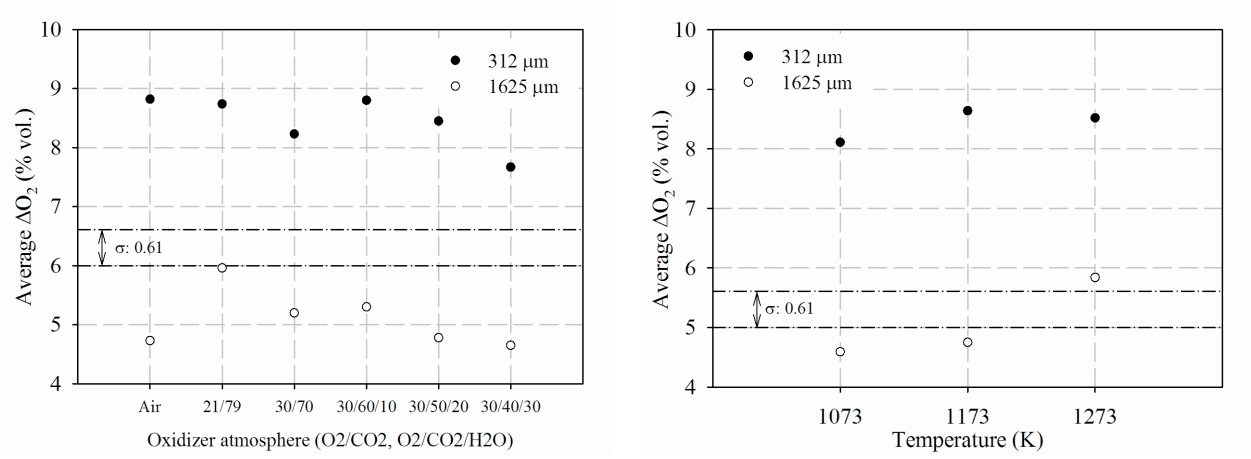

(a) (b)

Figure 3.9 - Plots of average variation of oxygen concentration (a) for each combination of oxidizer atmosphere and particle mean diameter and (b) for each combination of temperature and diameter.

Figure 3.9b shows the average response of variation of oxygen concentration for each combination of temperature and particle mean diameter, including all oxidizer atmospheres. High variation of oxygen concentration is attained for small particles mean diameter, in which the influence of temperature levels is reduced compared with large particle mean diameter.

These results allow to conclude that the coal combustion reaction rate is controlled by the diffusion of oxidant into the particles pores or through the boundary layer for small particles mean diameter. It explains the large effect of high CO_2 concentrations on coal combustion reaction for large particles mean diameter, in which the kinetic regime prevails.

B) Phenomena analysis for average time t_1 (s)

Figure 3.10 shows the plot of average responses of time t_1 for each combination of oxidizer atmosphere and particle mean diameter, including all temperature levels.

As observed in the plot, higher values of average time t_1 are attained in oxy-fuel with 21% O_2 and 30% O_2 (in vol.) and air conditions than in oxy-fuel atmospheres with water vapor for both particle mean diameters. These results are due to the difference in variation of oxygen concentration between the oxidizer atmospheres discussed in Fig. 3.9, in which reactions $C+CO_2 \rightarrow 2CO$ and $C+1/2O_2 \rightarrow CO$ under oxy-fuel and air atmospheres with largest CO_2 and O_2 concentrations increase the oxygen consumption, and consequently increase the average time t_1 recorded by oxygen sensor, i.e. greater is the oxygen consumption greater is average time t_1.

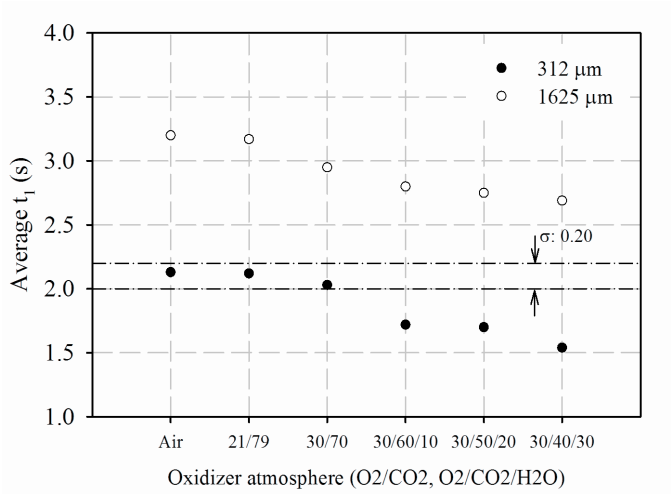

Figure 3.10 - Plot of average time t_1 for each combination of oxidizer atmosphere and particle mean diameter.

C) Phenomena analysis for average time t_2 (s)

Figure 3.11 shows the average responses of elapsed time t_2 for each combination of oxidizer atmosphere and particle mean diameter, including all temperature levels. As verified, particle mean diameter influences significantly on average values of elapsed time t_2, and small particle mean diameter has the lowest average elapsed time t_2 for all oxidizer atmosphere and

temperature levels. Higher average responses of time t_2 are attained under oxy-fuel with 21% O_2 and 30% O_2 (in vol.) and air conditions than in oxy-fuel atmospheres with water vapor for both particle mean diameters. These results allow to conclude that oxy-fuel atmosphere properties influence on the LTBK coal combustion reaction rate, as observed in analysis for the 1st group.

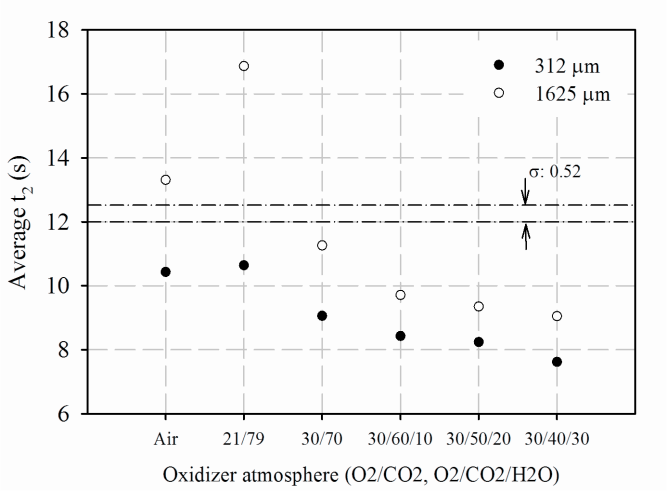

Figure 3.11 - Plot of average elapsed time t_2 for each combination of oxidizer atmosphere and particle mean diameter.

C) Major findings for 2nd group of experiments

Oxidizer oxy-fuel atmosphere with 79% CO_2 (21/79) has higher oxygen consumption than that in oxy-fuel atmospheres with water vapor (30/60/10, 30/50/20, 30/40/30) and in air atmospheres for LTBK coal with large particles mean diameter, due to the greater influence of CO_2 gasification reaction ($C + CO_2 \rightarrow 2CO$) than H_2O gasification reaction ($C + H_2O \rightarrow CO + H_2$), which increases the oxygen consumption with the temperature, when the coal combustion reactions are controlled by kinetic regime. The effect of CO_2 gasification reaction is reduced for small particles mean diameter, when the coal combustion reactions are controlled by the diffusion of oxidant into the particles pores or through the boundary layer, with the reduced influence of gas combustion temperature.

3.4.4 Analysis for 3rd group of experiments

The results concern with the experiments performed with Leão and LTBK coals and chars, under air and oxy-fuel atmospheres only with 21% O_2 (in vol.) at three levels of gas combustion temperature, and with one range of particle size, as described in Table 3.7 and Fig. 3.2.

A) Phenomena analysis for variation of oxygen concentration ΔO_2 (vol. %)

Figure 3.12a shows the plot of average responses of variation of oxygen concentration for each combination of coal and char and oxidizer atmosphere, including all temperatures.

As observed, Leão chars have the lowest variation of oxygen concentration compared with LTBK chars. Low variation of oxygen concentrations are attained at low and high devolatilized temperatures for Leão chars. This occurs due to the low content of volatile matter and high content of ash in Leão char composition, decreasing its reactivity under air and oxy-fuel atmospheres, and consequently, its oxygen consumption.

Plot of Fig. 3.12a also shows that higher variation of oxygen concentration values are found under oxy-fuel than that under air conditions for most of the coals, but for LTBK coal. This last result is due to the samples variability within the replicates, and must be repeated.

The highest variations of oxygen concentrations are attained under oxy-fuel atmosphere for Leão char 545 and LTBK char 900, and it is due to the effect of CO_2 gasification reaction with char, which increases the oxygen consumption in char with low content of volatiles. These results are the extreme importance because show the influence of CO_2 gasification reaction on char combustion for high and low ash coals, separated from the volatiles combustion. The influence of CO_2 gasification reaction is greater in LTBK char than in Leão char, due to the difference between its char carbon content.

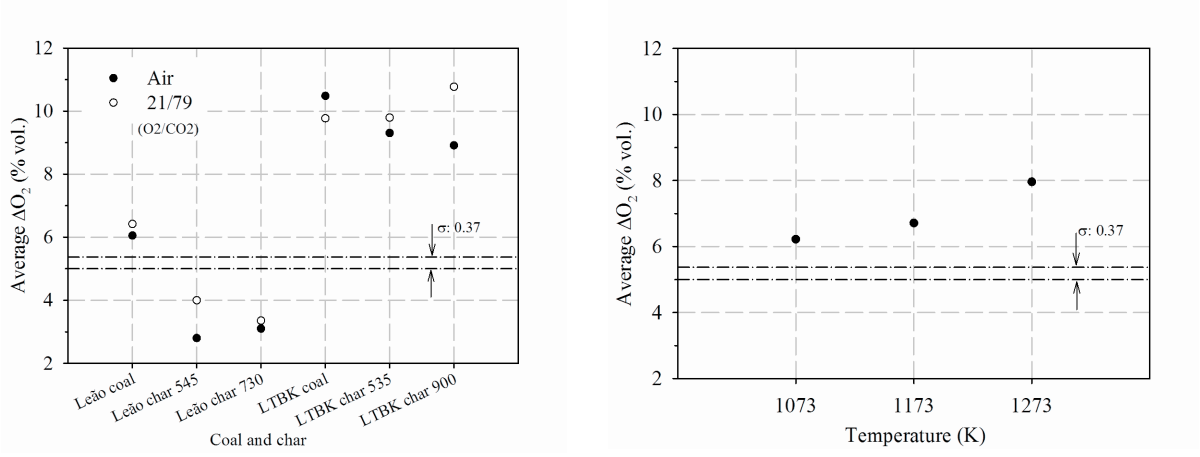

(a) (b)

Figure 3.12 - Plots of average variation of oxygen concentration (a) for each combination of coal and char and oxidizer atmosphere and (b) for each temperature level.

Figure 3.12b shows the plot of average response of oxygen concentration for each temperature level, including all coals and chars and oxidizer atmospheres. As noted, high variation of oxygen concentration value is attained at high temperature level. These results are

due to the influence of gas combustion temperature on the coal combustion reaction rates, influenced by the CO_2 gasification reaction, under kinetic control.

B) Phenomena analysis for average time t_1 (s)

Figure 3.13a shows the plot of average responses of time t_1 for each combination of coal and char and temperature, including all oxidizer atmospheres. High values of average time t_1 are attained at low values of temperature for Leão chars, reaching until 10s at 1073 K for Leão char 730, and 6.8 s for Leão char 545. These results are the extreme importance because show that coal combustion reaction rate for high ash coal is controlled by kinetic regime, in which the increase of gas combustion temperature influence the surface reaction mechanisms, as CO_2 gasification reaction ($C + CO_2 \rightarrow 2CO$).

The impact of temperature levels on average time t_1 is reduced in coals with high content of volatile matter (LTBK coal, LTBK char 535, Leão coal). These results show that diffusion of oxygen trough the film around the char particle is increased with the presence of volatile matter combustion, controlling the combustion reaction rate. There is no influence of temperature on average time t_1 in LTBK char 900. This result indicates that the diffusion of oxygen trough the film around the char particle or through its pores control the rate, in which the increase of combustion gas temperature there is no effect, and require further analysis.

Figure 3.13b shows the influence of temperature on average time t_1 for each combination of temperature, including all coals and chars and oxidizer atmospheres. High values of average time t_1 are attained at low temperature levels, influenced by the lower reaction rates in chars with high content of ash (Leão char 730 and 545), as discussed previously.

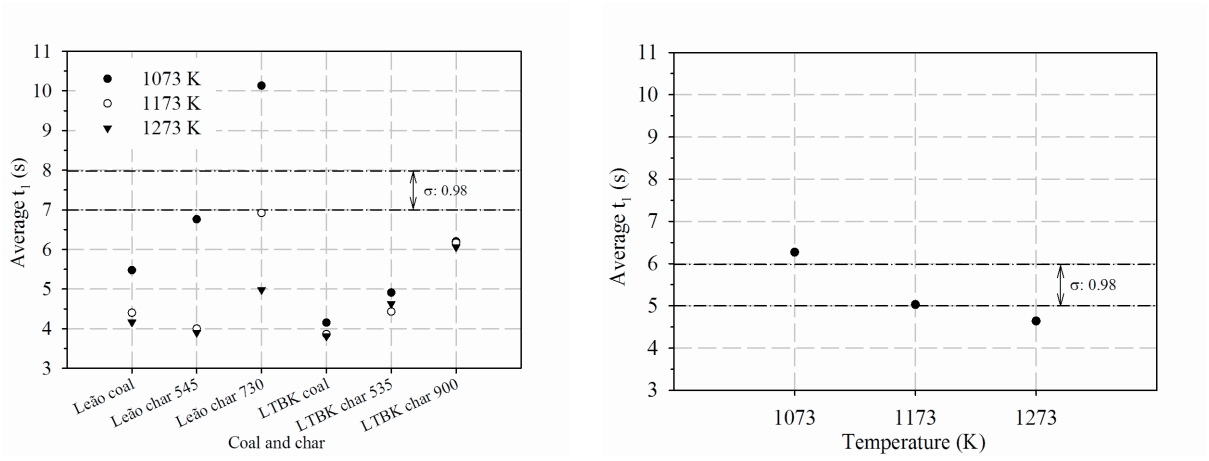

(a) (b)

Figure 3.13 - Plots of average time t_1 (a) for each combination of coal and char and temperature and (b) for each temperature level.

C) Phenomena analysis for average time t_2 (s)

Figure 3.14 shows the average response of elapsed time t_2 for each combination of coal and char and oxidizer atmosphere, including all temperature levels.

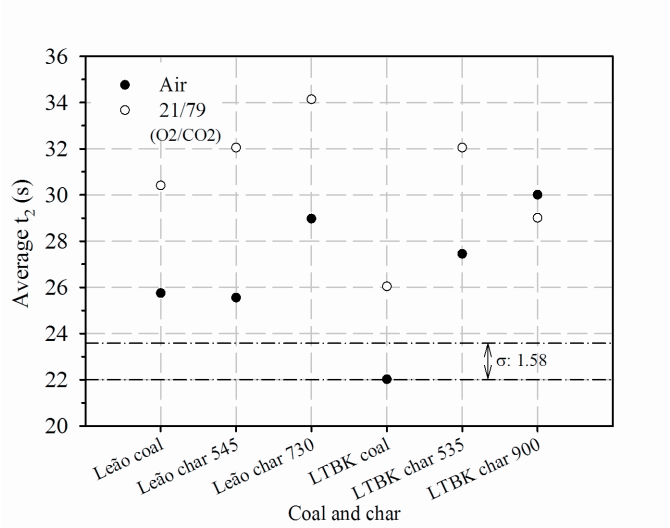

Figure 3.14 - Plot of average elapsed time t_2 for each combination of coal and char and oxidizer atmosphere.

It is observed that higher average elapsed time t_2 values are attained in oxy-fuel than that in air atmospheres, including all coals and temperature levels, but LTBK char 900. These results are due to the influence of oxy-fuel atmosphere properties, as low oxygen diffusion coefficient, that can be increasing the resistance of oxidant diffusion through the boundary layer formed around coal particle, and delays the recovery of oxygen concentration oxidizer stream at inlet conditions (i.e. 21% O_2 in vol.). This last effect is investigated in 4th group of experiments, changing the oxygen sensor position within the cyclone combustion reactor.

High average elapsed time t_2 values are attained in Leão char 730, and in LTBK chars 535 and 900. These results show that higher the content of volatile matter lower is the elapsed average time t_2, even with the effects of oxy-fuel atmosphere properties. The difference of the results attained for LTBK char 900 in comparison with the trend verified for other coals and chars can be associated to the samples variability due its replications.

D) Major findings for 3rd group of experiments

Higher variations of oxygen concentrations are attained under oxy-fuel atmosphere with 79% CO_2 (21/79) than that in air atmosphere for Leão char 545 and LTBK char 900, and it is due to the effect of CO_2 gasification reaction with char, which increases the oxygen consumption. These results are the extreme importance because they allow to conclude that

the CO_2 gasification reaction influences on char combustion for high ash content coals (not seen in literature review), separated from the volatiles combustion effect.

3.4.5 Analysis for 4th group of experiments

The results concerns with the experiments performed with Leão and LTBK coals and chars, under air atmosphere and at three levels of gas combustion temperature, and with one range of particle size, with the oxygen sensor positioned near the centre of cyclone combustion reactor, as described in Table 3.7 and Fig. 3.2.

A) Phenomena analysis for variation of oxygen concentration ΔO_2 (vol. %)

Figure 3.15 shows the plot of average response of variation of oxygen concentration for each combination of coal and char and temperature. As observed, Leão char 900 has lower variation of oxygen concentration than LTBK char 900. These results are influenced by the content of volatile matter and carbon in coals and chars, as discussed in 3rd group, but, now, with the oxygen sensor positioned near the centre of cyclone combustion reactor.

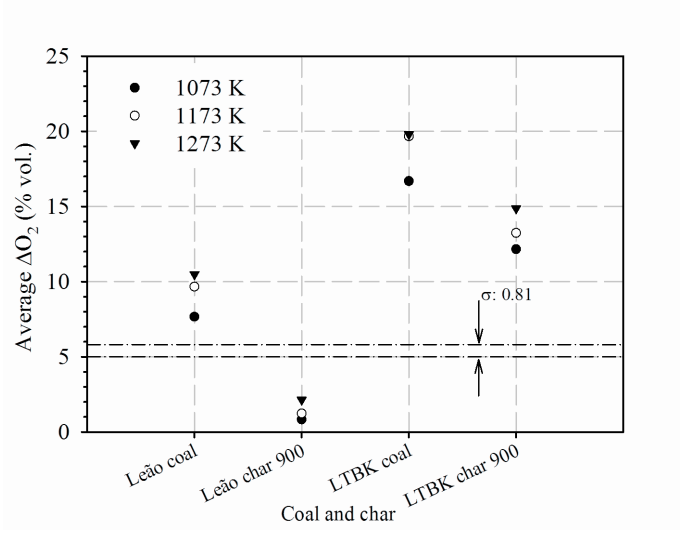

Figure 3.15 - Plot of average variation of oxygen concentration for each combination of coal and char and temperature.

The average response of variation of oxygen concentration is also influenced by the temperature levels for all coals and chars tested. The increase of variation of oxygen concentration is greater in LTBK char 900, Leão coal and LTBK coal than that in Leão char 900. These results are due to the effect of temperature on the coal combustion reactions, which are under the control of kinetic regime. The effect is greater in coals with high content of volatiles (Leão and LTBK) and char with high content of carbon (LTBK char 900) than in

char with high content of ash and low content of carbon (Leão char 900), indicating in latter the effect of char matrix on the coal surface reaction mechanisms, increasing the resistance of the diffusion of oxygen into the pores of particle.

B) Phenomena analysis for average time t_1 (s)

Figure 3.16 shows the plot of average responses of time t_1 for each combination of coal and char and temperature. As noted, the increase of gas combustion temperature reduces the values of average time t_1 for all coals and chars samples tested, in which lowest values of average time t_1 are attained for coals with high content of volatile matter. These results are due to effect of temperature on reaction mechanisms of coal combustion, increased by the volatiles matter combustion, in the case of LTBK coal. For all chars, even with high content of ash, the reaction mechanisms are controlled by the kinetic regime, because the coal combustion reaction responds with the increase of temperature, and the slowest variation of average time t_1 is probably due to the influence of the resistance of oxidant diffusion into particle pores matrix, due to the effect of ash in char matrix, as observed for Leão char 900, and due to the boundary layer in volatiles combustion for LTBK coal.

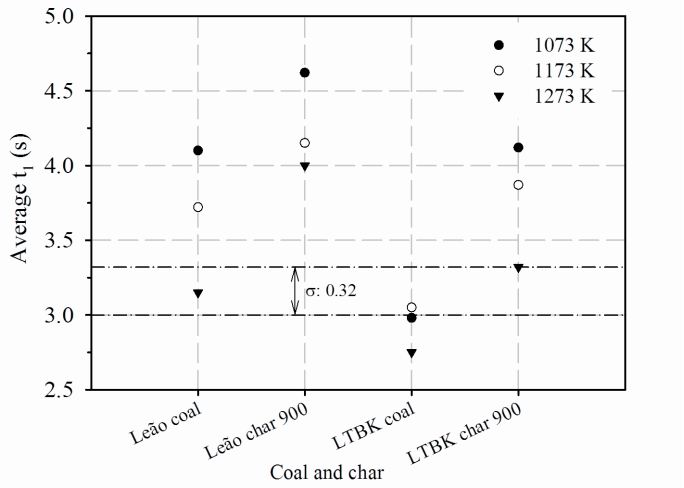

Figure 3.16 - Plot of average time t_1 for each combination of coal and char and temperature.

C) Phenomena analysis for average time t_2 (s)

Figure 3.17 shows the plot of average responses of elapsed time t_2 for each combination of coal and char and temperature. As observed, Leão char 900 has the lowest value of average elapsed time t_2 in the group, and different than the trend observed for the average time t_1 in Fig. 3.16.

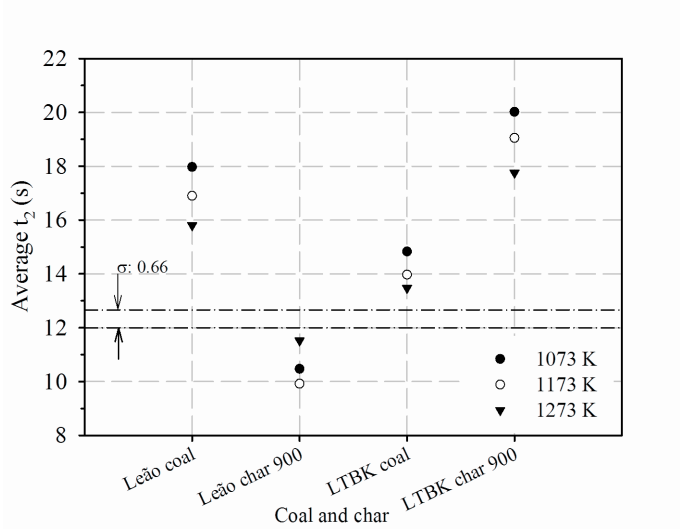

Figure 3.17 - Plot of average elapsed time t_2 for each combination of coal and char and temperature.

Therefore, it indicates that the oxygen sensor did not record all the combustion time of the Leão char 900 samples, because it is expected that coals and chars with low contents of volatile matter and carbon have elapsed times longer than coals and chars with high content of volatile and carbon matter, as also verified in the trend of plot of Figures 3.17 and 3.14 for air.

In order to elucidate this issue, the present work uses the images recorded by a video camera installed at the top of cyclone combustion reactor to make a qualitative and comparative analysis between the elapsed time during the combustion of samples, recorded by oxygen sensor probe and the video camera images, as shown in Fig. 3.18.

Figure 3.18 shows the comparison of the results between the average elapsed time t_2 (recorded by oxygen sensor probe) and the time recorded by the video camera for each coal and char, including all temperature levels.

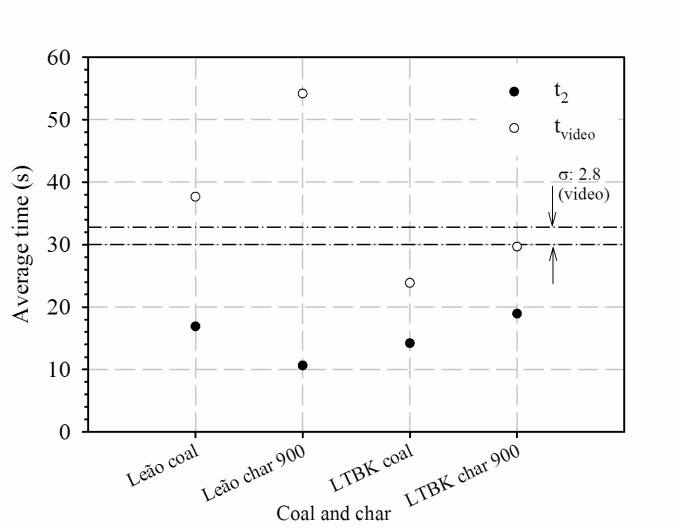

Figure 3.18 - Plot of average elapsed time t_2 and t_{video} for each combination of coal and char.

Investigating the value of average elapsed time t_2 and the time recorded by the video for Leão char 900, it is noted for the average elapsed time t_2, that the oxygen sensor measurement has already stabilized in 21% O_2 (in vol.) and the combustion of sample continues for Leão char 900, comparing with the time computed with the aid of video images. In the case of Leão char 900, the video time is 5.5 times greater than the time recorded by oxygen sensor probe.

The difference of times between the oxygen sensor measurement and video image analysis is low for combustion of LTBK coal. These results show that the oxygen sensor do not measure all the oxygen consumed by the coal and char samples within the cyclone combustion reactor, and the difference between the t_{video} and t_2 is greater for coals and chars with high content of ash than coals and chars with high content of volatiles matter.

3.4.6 Comparison between 3rd and 4th group of experiments

The graphs plotted in Fig. 3.19 and 3.20 show the comparison of average values of variable responses results (variation of oxygen concentration, times t_1 and t_2) between the experiments performed with original oxygen sensor position (3rd group) and with new oxygen sensor position (4th group) for two coals (LTBK, Leão) and one char (LTBK char 900), under air atmosphere conditions and three levels of gas combustion temperature.

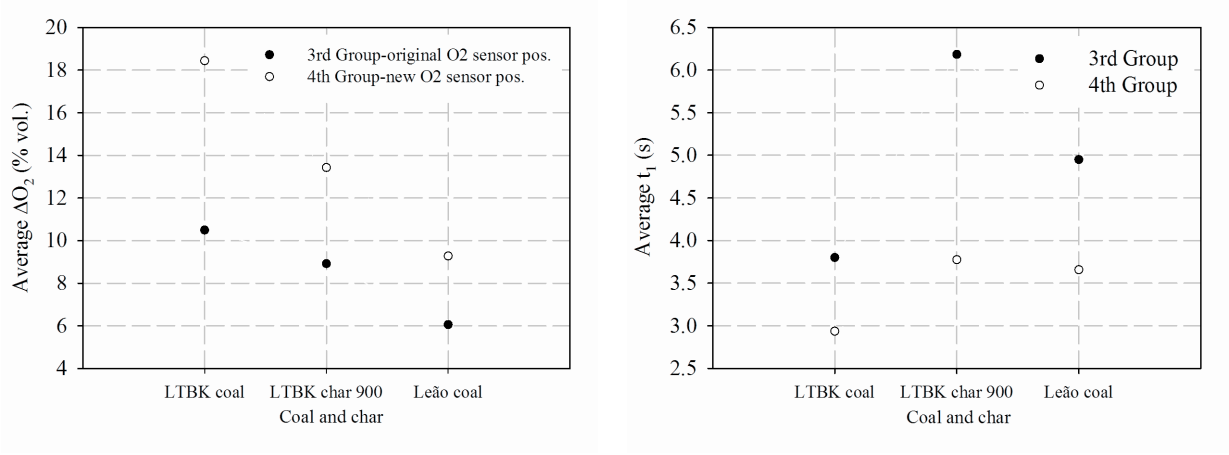

(a) (b)

Figure 3.19 - Plots of average of (a) variation of oxygen concentration ΔO_2 and (b) time t_1 for each combination of coal and char under air atmosphere.

As observed in Fig. 3.19a, high values of variation of oxygen concentration are attained with experiments performed with new oxygen sensor position (4th group), whereas

low values of oxygen concentration are attained with oxygen sensor probe at original position for all coals and chars. As noted in Fig. 3.19b, low values of time t_1 are attained with experiments performed with new oxygen sensor position (4th group), whereas high values of t_1 are attained with oxygen sensor probe at original position for all coals and chars.

As observed in Fig. 3.20, low values of average elapsed time t_2 are attained with experiments performed with new oxygen sensor position (4th group), whereas high values of t_2 are attained with oxygen sensor probe at original position for all coals and chars.

These results shows that the oxygen sensor probe measures the local variation of oxygen concentration and these measurements depend on the swirling flow within the cyclone combustion reactor. As oxygen sensor probe advances into the centre of cyclone reactor high values of variation of oxygen concentration and low values of average time t_1 and t_2 are attained for the combustion of coal and char samples.

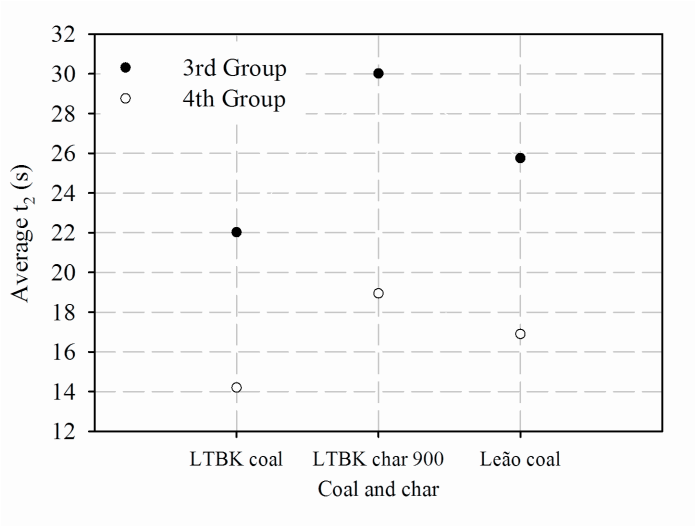

Figure 3.20 - Plot of average elapsed time t_2 for each combination of coal and char under air atmosphere.

3.4.7 Major findings for 4th group of experiments

The oxygen sensor probe do not measure all the oxygen consumed by the coal and char samples with high content of ash, and the oxygen sensor reaches at the oxygen concentration of oxidizer inlet stream (i.e. 21% O_2) before the combustion of char sample ends. The oxygen sensor probe measures the local variation of oxygen concentration and these measurements depend on the position of oxygen sensor within the cyclone reactor due to the swirling flow within the cyclone combustion reactor.

3.5 Conclusions

This work aimed to apply a design of experiments (DoE) methodology in a laboratory test facility developed to study the coal combustion phenomena under air and oxy-fuel atmospheres.

The reactor utilized in the experimental work is a laboratory-size atmospheric cyclone combustion chamber (ALVA 20). Coals and char combustion was investigated by the measurements of O_2 concentration curves with a potentiometric oxygen sensor installed within the cyclone reactor. The DoE methodology was applied to analyze the oxygen concentration curves by means of response variables selected in the curve, replacing the traditional analysis of oxygen concentration curves seen in previous works and in Chapter 2 with ALVA 20.

Different groups of experiments were designed in order to provide a suitable interpretation of the data via analysis of variance.

Combustion experiments were performed aiming to investigate the influence of higher partial pressures of CO_2 and H_2O on the conversion of LTBK coal under oxy-fuel and air atmosphere conditions. The influence of CO_2 concentrations was also investigated for low-rank coals with high content of ash, selected from Leão and Bonito mining sites located in South Brazil.

The major findings and conclusions of the investigation are separated by groups of experiments as follow.

- For LTBK coal combustion under oxy-fuel with water vapor

Low values of average time t_1 and elapsed time t_2, are attained at high values of gas combustion temperature, because the coal combustion reaction rates are under control of kinetic regime, in which the influence of CO_2 gasification reaction ($C + CO_2 \rightarrow 2CO$) is greater than H_2O gasification reaction ($C + H_2O \rightarrow CO + H_2$) for temperatures higher than 1173 K, which increases the oxygen consumption from CO_2 concentrations higher than 50% for LTBK coal combustion.

- For 1st group of experiments

Oxidizer oxy-fuel atmosphere with 79% CO_2 (21/79) has higher oxygen consumption than that in oxy-fuel with 70% CO_2 (30/70) and in air atmospheres for both high ash coals tested (Bonito and Leão), due to the influence of CO_2 gasification reaction ($C + CO_2 \rightarrow 2CO$) on coal combustion, and these findings were not seen in literature review. However, oxy-fuel

atmosphere 21/79 increases the average elapsed time t_2, due to the influence of oxy-fuel atmosphere properties, as low oxygen diffusion coefficient, on coal combustion reaction rates and on the recovery of oxygen concentration oxidizer stream at inlet conditions (i.e. 21% O_2 in vol.).

- For 2nd group of experiments

Oxidizer oxy-fuel atmosphere with 79% CO_2 (21/79) has higher oxygen consumption than that in oxy-fuel atmospheres with water vapor (30/60/10, 30/50/20, 30/40/30) and in air atmospheres for LTBK coal with large particles mean diameter, due to the greater influence of CO_2 gasification reaction ($C + CO_2 \rightarrow 2CO$) than H_2O gasification reaction ($C + H_2O \rightarrow CO + H_2$), which increases the oxygen consumption with the temperature, when the coal combustion reactions are controlled by kinetic regime, and these findings were not seen in literature review. The effect of CO_2 gasification reaction is reduced for small particles mean diameter, when the coal combustion reactions are controlled by the diffusion of oxidant into the particles pores or through the boundary layer, with the reduced influence of gas combustion temperature.

- For 3rd group of experiments

Higher variations of oxygen concentrations are attained under oxy-fuel atmosphere with 79% CO_2 (21/79) than that in air atmosphere for Leão char 545 and LTBK char 900, and it is due to the effect of CO_2 gasification reaction with char, which increases the oxygen consumption. These results are the extreme importance because they allow to conclude that the CO_2 gasification reaction also influences on char combustion for high ash content coals (not seen in literature review), separated from the volatiles combustion effect.

- For 4th group of experiments

The potentiometric oxygen sensor probe do not measure all the oxygen consumed by the coal and char samples with high content of ash, and the oxygen sensor reaches at the oxygen concentration of oxidizer inlet stream (i.e. 21% O_2) before the combustion of char sample ends. The potentiometric oxygen sensor probe measures the local variation of oxygen concentration and these measurements depend on the position of oxygen sensor within the cyclone reactor due to the swirling flow within the cyclone combustion reactor, not seen in literature review for previous works with ALVA 20.

BIBLIOGRAPHY

Borrego, A.G., Alvarez, D., 2007. "Comparison of chars obtained under oxy-fuel and conventional pulverized coal combustion atmospheres", Energy & Fuels, v. 21, p. 3171-3179.

Brix, J., Jensen, P.A., Jensen, A.D., 2010. "Coal devolatilization and char conversion under suspension fired conditions in O_2/N_2 and O_2/CO_2 atmospheres", Fuel, v. 89, p. 3373-3380.

Carotenuto, A.R., Corrêa, R.S., Schneider, P.S., Rech, R.L., Marcilio, N.R., Krautz, J.H., 2012. "Experimental analysis of low-rank coal combustion under air and oxy-fuel conditions", Proceedings of ENCIT 2012, 14th Brazilian Congress of Thermal Sciences and Engineering, ABCM, Rio de Janeiro, Brasil, 08 pages.

Carotenuto, A.R., Schneider, P.S., Corrêa, R.S., Rech, R.L., Marcilio, N.R., Krautz, J.H., 2011. "Preliminary investigation of the global kinetic parameters of low-rank coals under oxy-fuel conditions", III Congresso Brasileiro de Carvão Mineral, Gramado, RS, Brasil, 19 pages.

Liu, H., 2009. "Combustion of coal chars in O_2/CO_2 and O_2/N_2 mixtures: a comparative study with non-isothermal thermogravimetric analyzer (TGA) tests", Energy and Fuels, v. 23, p. 4278-4285.

Molina, A., Shaddix, C.R., 2007. "Ignition and devolatilization of pulverized bituminous coal particles during oxygen/carbon dioxide coal combustion", Proceedings of the Combustion Institute, v. 31, p. 1905-1912.

Molina, A., Shaddix, C.R, 2009. "Particle imaging of ignition and devolatilization of pulverized coal during oxy-fuel combustion", Proceedings of the Combustion Institute, v. 32, p. 2091-2098.

Montgomery, D., 2001. "Design and Analysis of Experiments", John Wiley & Sons. Inc, Printed in USA, 5th edition, p. 684.

Rathnam, R.K., Elliot, L.K., Wall, T., Liu, Y., Moghtaderi, B., 2009. "Differences in reactivity of pulverized coal in air (O_2/N_2) and oxy-fuel (O_2/CO_2) conditions", Fuel Processing Technology, v. 90, p. 797-802.

Smoot, L.D., Smith, P.J., 1985. "Coal Combustion and Gasification", Plenum Press, New York, USA, p. 443.

Tappe, S., Krautz, H.J., 2009a. "ALVA 20: A 20 kWth Atmospheric Laboratory Test Facility to Investigate the Combustion Behavior under Close-to-Reality Conditions", Proceedings of the European Combustion Meeting, 6 pages.

Tappe, S., Krautz, H.J., 2009b. "Influence of various O_2/CO_2 concentrations on the burning behavior of different coals", 34th International Technical Conference on Coal Utilization & Fuel Systems, Clearwater, USA, 07 pages.

Zhang, L., Binner, E., Chen, L., Qiao, Y., Li, C., Bhattacharya, S., Ninomiya, Y., 2010a. "Experimental investigation of the combustion of bituminous coal in air and O_2/CO_2 mixtures: 1. Particle imaging of the combustion of coal and char", Energy & Fuels, v. 24, p. 4803-4811.

Zhang, L., Binner, E., Chen, L., Qiao, Y., Li, C., 2010b. "In situ diagnostics of Victorian brown coal combustion in O_2/N_2 and O_2/CO_2 mixtures in drop-tube furnace", Fuel, v. 89, p. 2703-2712.

Zhang, L., Binner, E., Qiao, Y., Li, C., 2010c. "High-Speed Camera Observation of Coal Combustion in Air and O_2/CO_2 Mixtures and Measurement of Burning Coal Particle Velocity", Energy & Fuel, v. 24, p. 20-37.

Zirox, 2003. "Measuring system Oxygen probe KS20 Electronic E2000P Manual", Zirox Sensoren und Elektronik GmbH, Greifswald, Germany, 28 pages.

APPENDIX 3.A.1 - Fundamentals of DoE applied to ALVA 20 test facility

Here, the factors *A* and *B* are oxidizer atmosphere and reactor gas temperature, respectively. The observations in a factorial experiment can be described by a several types of models. The effect model was chosen in the present work, described by the following relation

$$y_{ijk} = \mu + \tau_i + \beta_j + (\tau\beta)_{ij} + \varepsilon_{ijk} \tag{3.A.1.1}$$

where μ is the overall mean effect, τ_i is the effect of the *i*th level of the row factor *A*, β_j is the effect of the *j*th level of column factor *B*, $(\tau\beta)_{ij}$ is the effect of the interaction between τ_i and β_j, and ε_{ijk} is a random error component. Both factors are assumed to be fixed, and the treatment effects are defined as deviations from the overall mean, so

$$\sum_{i=1}^{a} \tau_i = \sum_{j=1}^{b} \beta_j = 0 \tag{3.A.1.2}$$

Similarly, the interaction effects are fixed and are defined such that

$$\sum_{i=1}^{a} (\tau\beta)_{ij} = \sum_{j=1}^{b} (\tau\beta)_{ij} = 0 \tag{3.A.1.3}$$

Because there are n replicates of the experiment, there are abn total observations. The following testing hypotheses can be considered for a two-factor factorial design, as follows.

The equality of row treatment effects is treated by means of the following hypothesis test

$$\begin{aligned} &H_0 : \tau_1 = \tau_2 = \ldots = \tau_a = 0 \\ &H_1 : \text{at least one } \tau_i \neq 0 \end{aligned} \tag{3.A.1.4}$$

and the equality of column treatment effects by

$$\begin{aligned} &H_0 : \beta_1 = \beta_2 = \ldots = \beta_b = 0 \\ &H_1 : \text{at least one } \beta_j \neq 0 \end{aligned} \tag{3.A.1.5}$$

Row and column treatment interaction is tested as

$$H_0 : (\tau\beta)_{ij} = 0 \quad \text{for all } i,j \qquad (3.A.1.6)$$
$$H_1 : \text{at least one } (\tau\beta)_{ij} \neq 0$$

Let $y_{i..}$ denote the total of all observations under *i*th level of factor *A*; $y_{.j.}$ denote the total of all observations under the *j*th level of factor *B*; $y_{ij.}$ denote the total of all observations in the *ij*th cell; and $y_{...}$ denote the grand total of all observations. The "dot" subscript notation implies summation over the subscript that it replaces. Defining $\bar{y}_{i..}$, $\bar{y}_{.j.}$, $\bar{y}_{ij.}$, and $\bar{y}_{...}$ as the corresponding row, column, cell, and grand (large) averages. Expressed mathematically,

$$y_{i..} = \sum_{j=1}^{b} \sum_{k=1}^{n} y_{ijk} \quad and \quad \bar{y}_{i..} = \frac{y_{i..}}{bn} \quad i = 1,2,\ldots,a \qquad (3.A.1.7)$$

$$y_{.j.} = \sum_{i=1}^{a} \sum_{k=1}^{n} y_{ijk} \quad and \quad \bar{y}_{.j.} = \frac{y_{.j.}}{an} \quad j = 1,2,\ldots,b \qquad (3.A.1.8)$$

$$y_{ij.} = \sum_{k=1}^{n} y_{ijk} \quad and \quad \bar{y}_{ij.} = \frac{y_{ij.}}{n} \quad i = 1,2,\ldots,a \quad j = 1,2,\ldots,b \qquad (3.A.1.9)$$

$$y_{...} = \sum_{i=1}^{a} \sum_{j=1}^{b} \sum_{k=1}^{n} y_{ijk} \quad and \quad \bar{y}_{...} = \frac{y_{...}}{abn} \qquad (3.A.1.10)$$

Equations 3.A.1.7 to 3.A.1.10 represent a typical data for a two-factorial design, as shown in Table 3.A.1.1

Table 3.A.1.1 - Typical data for a two-factor factorial design

	Temperature (K)				
Oxidizer	1073	1173	1273	Totals	Averages
30/60/10	$y_{11.}$	$y_{12.}$	$y_{13.}$	$y_{1..}$	$\bar{y}_{1..}$
30/50/20	$y_{21.}$	$y_{22.}$	$y_{23.}$	$y_{2.}$	$\bar{y}_{2..}$
30/40/30	$y_{31.}$	$y_{32.}$	$y_{33.}$	$y_{3.}$	$\bar{y}_{3..}$
Totals	$y_{.1.}$	$y_{.2.}$	$y_{.3.}$	$y_{...}$	
Averages	$\bar{y}_{.1.}$	$\bar{y}_{.2.}$	$\bar{y}_{.3.}$		$\bar{y}_{...}$

The analysis of variance is built from Table 3.A.1.1, which is derived from a partitioning of the total variability into its component parts. The total corrected sum of squares SS_T is given by

$$SS_T = \sum_{i=1}^{a} \sum_{j=1}^{b} \sum_{k=1}^{n} \left(y_{ijk} - \bar{y}_{...}\right)^2 \tag{3.A.1.11}$$

and is used as a measure of the overall variability in the data. Intuitively, this is a reasonable statement because one can obtain the sample variance of the $y's$ by dividing SS_T by the appropriate number of degrees of freedom (in this case, $abn - 1 = N - 1$). The sample variance is, of course, a standard measure of variability.

Equation 3.A.1.11 may be written symbolically as

$$SS_T = SS_A + SS_B + SS_{AB} + SS_E \tag{3.A.1.12}$$

The total sum of squares SS_T was partitioned into a sum of squares due to "rows", or factor A, (SS_A); a sum of squares due to "columns", or factor B, (SS_B); a sum of squares due to the interaction between A and B, (SS_{AB}); and a sum of squares due to error, (SS_E). These terms are written, as follow

$$SS_A = bn\sum_{i=1}^{a}(\bar{y}_{i..} - \bar{y}_{...})^2 \tag{3.A.1.13}$$

$$SS_B = an\sum_{j=1}^{b}(\bar{y}_{.j.} - \bar{y}_{...})^2 \tag{3.A.1.14}$$

Where SS_A and SS_B represent the sum of squares of the differences between the treatment averages $(\bar{y}_{i..}, \bar{y}_{.j.})$ and the grand average $(\bar{y}_{...})$.

$$SS_{AB} = n\sum_{i=1}^{a}\sum_{j=1}^{b}(\bar{y}_{ij.} - \bar{y}_{i..} - \bar{y}_{.j.} + \bar{y}_{...})^2 \tag{3.A.1.15}$$

SS_{AB} represents a sum of squares of the differences between the cell, row and column treatment averages plus the grand average. SS_A, SS_B and SS_{AB} terms are a measure of the differences between treatment means, whereas the differences of observations within a

treatment y_{ijk} from a treatment cell average $y_{ij.}$ can be due only to random error, and for this reason is called the sum of squares due to error (i.e. within treatments), as written in Equation 3.A.1.16.

$$SS_E = \sum_{i=1}^{a} \sum_{j=1}^{b} \sum_{k=1}^{n} \left(y_{ijk} - \bar{y}_{ij.} \right)^2 \tag{3.A.1.16}$$

The number of degrees of freedom associate with each sum of squares is detailed in Table 3.A.1.2.

Table 3.A.1.2 - Degrees of freedom

Source of variation, effect	Degrees of freedom
A	$a-1$
B	$b-1$
AB interaction	$(a-1)(b-1)$
Error	$ab(n-1)$
Total	$abn-1$

There are $abn = N$ total observations, thus SS_T has $N-1$ degrees of freedom. There are a levels of the factor A (and a treatment means), so SS_A has $a-1$ degrees of freedom and so on for SS_B. The interaction degrees of freedom are simply the number of freedom for cells which is $ab-1$ minus the number of degrees of freedom for the two main effects A and B; that is, $ab-1-(a-1)-(b-1)=(a-1)(b-1)$. Within each of the ab cells, there are $n-1$ degrees of freedom between n replicates; thus, there are $ab(n-1)$ degrees of freedom for error. Note that the number of degrees of freedom on the right-hand of Eq. 3.A.1.12 adds to the total number of degrees of freedom.

Each sum of squares divided by its degrees of freedom is a mean square. The development of the expected values of the mean squares equations are found in Montgomery, 2001. The final equations are presented here as follows.

$E(MS_A)$ is the expected value of the mean square of factor A.

$$E(MS_A) = E\left(\frac{SS_A}{a-1} \right) = \sigma^2 + \frac{bn\sum_{i=1}^{a} \tau_i^2}{a-1} \tag{3.A.1.17}$$

$E(MS_B)$ is the expected value of the mean square of factor *B*.

$$E(MS_B) = E\left(\frac{SS_B}{b-1}\right) = \sigma^2 + \frac{an\sum_{i=1}^{a}\beta_i^2}{b-1} \tag{3.A.1.18}$$

$E(MS_{AB})$ is the expected value of the mean square of the interaction between factors *A* and *B*.

$$E(MS_{AB}) = E\left(\frac{SS_{AB}}{(a-1)(b-1)}\right) = \sigma^2 + \frac{n\sum_{i=1}^{a}\sum_{j=1}^{b}(\tau\beta)_{ij}^2}{(a-1)(b-1)} \tag{3.A.1.19}$$

$E(MS_E)$ is the expected value of the mean square of error.

$$E(MS_E) = E\left(\frac{SS_E}{ab(n-1)}\right) = \sigma^2 \tag{3.A.1.20}$$

Notice that if the null hypothesis are true for no row treatment effects, no column treatment effects and no interaction, it follows that MS_A, MS_B, MS_{AB} and MS_E estimate the variance σ^2. However, lets imagine that there are differences between row treatment effects then MS_A will be greater than MS_E. Similarly, if there are column treatment effects or interaction present, then the corresponding mean squares will be greater than MS_E. Therefore, to test the significance of both main effects and their interaction, it suffices to divide the corresponding mean square by error mean square, according to Eq. 3.A.1.22. Large values of this ratio imply that the data do not support the null hypothesis. Therefore, the null hypothesis H_0 should be rejected and allows to conclude that there are differences in the treatment means if

$$F_0 > F_{\alpha,a-1,N-a} \tag{3.A.1.21}$$

where F_0 is computed with the following relation

$$F_0 = \frac{MS_{Treatmens}}{MS_E} \tag{3.A1.22}$$

Alternatively, the P value approach (called the significance level) can be used, and the decision should be made given the specified value of α set up in the software packages.

In the present investigation, $\alpha = 0.05$, and the resulting P values obtained along the experiments presented in the following sections will be used to analyze the influence of specific factor on the treatment means of the response variables.

Assuming that the model presented on Eq. 3.A.1.1 is adequate and that the error terms ε_{ijk} are normally and independently distributed with constant variance σ^2, then each of the ratios of mean squares $MS_A/\mathrm{MS_E}$, $MS_B/\mathrm{MS_E}$ and $MS_{AB}/\mathrm{MS_E}$ are distributed as F with $a-1$, $b-1$, and $(a-1)(b-1)$ numerator degrees of freedom, respectively, and $ab(n-1)$ denominator degrees of freedom, and the critical region would be the upper tail of the F distribution.

The *F* distribution is very important in the statistical analysis of designed experiments and its values for each test statistic F_0 are tabulated in literature according to the degrees of freedom of each factor and level of significance used in the experiments.

Thus, the test procedure is usually summarized in an analysis of variance table, as shown in Table 3.A.1.3.

Table 3.A.1.3 - The analysis of variance table for the two-factor factorial, fixed effects model

Source of variation	Sum of squares	Degrees of freedom	Mean square	F_0
A treatments	SS_A	$a-1$	MS_A	$F_0 = MS_A/MS_E$
B treatments	SS_B	$b-1$	MS_B	$F_0 = MS_B/MS_E$
Interaction	SS_{AB}	$(a-1)(b-1)$	MS_{AB}	$F_0 = MS_{AB}/MS_E$
Error	SS_E	$ab(n-1)$	MS_E	-
Total	SS_T	$abn-1$	-	-

APPENDIX 3.A.2 -Analysis of variance for the groups of experiments

This section presents the statistical analysis used to select the most relevant factors on the response variables for each group of experiments discussed in section 3.4.

3.A.2.1 Analysis of variance for LTBK coal combustion under oxy-fuel with water vapor

A) Statistical analysis for variation of oxygen concentration ΔO_2 *(vol. %)*

Results from the analysis of variance for the response variable ΔO_2 (vol. %) are summarized in Table 3.A.2.1, obtained with the statistical software (Minitab). The maximum variation of oxygen concentration data are presented in Appendix 3.A.3.

Table 3.A.2.1 - Analysis of variance for variation of oxygen concentration ΔO_2 (vol. %)

Source of variation	Sum of squares	Degrees of freedom	Mean square	F_0	P
Atmosphere A	2.11601	2	1.13295	19.84	< 0.001
Temperature B	3.75162	2	1.93409	33.87	< 0.001
Interaction AB	0.80689	4	0.20172	3.53	0.028
Error	0.97078	17	(0.05710)		
Total	7.64530	25			

Notice that the between-treatment mean square for temperature (factor *B*) is many times greater (1.93) than the within-treatment or error mean square (0.05710), highlighted in Table 3.A.2.1. This indicates that it is unlikely that the treatment means are equal. More formally, the $F_0 = 33.87$ is compared with an appropriate upper-tail percentage point of the $F_{0.05,2,17}$ distribution with the aid of tables in literature [Montgomery, 2001], and yields $F_{0.05,2,17} = 3.59$. Because $F_0 = 33.87 > 3.59$, the null hypothesis is rejected and it's concluded that the temperature level significantly affects the variation of oxygen concentration ΔO_2 (vol. in %). The *P*-value can also be computed for this test. Clearly, the *P*-value is very small in this case, and for *P*-value lower than 0.05, the null hypothesis is rejected. The analysis of variance also shows that the levels of the factor atmosphere *A* influence the treatment means of the variation of oxygen concentration, because $F_0 = 19.84 > 3.59$. However, the interaction between the levels of atmosphere and temperature factors on treatment means of ΔO_2 (vol. %) is small, because $F_0 = 3.53 > F_{0.05,4,17} = 2.96$.

B) Statistical analysis for average time t_1 (s)

The results of the analysis of variance for the response variable t_1 (s) are summarized in Table 3.A.2.2, and its corresponding data are in Appendix 3.A.3.

Table 3.A.2.2 - Analysis of variance for time t_1 (s) data

Source of variation	Sum of squares	Degrees of freedom	Mean square	F_0	P
Atmosphere A	0.05577	2	0.03078	1.01	0.385
Temperature B	1.18253	2	0.58075	19.05	< 0.001
Interaction AB	0.12077	4	0.03019	0.99	0.438
Error	0.51833	17	(0.03049)		
Total	1.87740	25			

The analysis of variance shows that there is a significant influence of temperature on time t_1, because the *P*-value is lower than 0.05, whereas the atmosphere and the interaction between the factors are not significant.

C) Statistical analysis for average time t_2 (s)

The results of the analysis of variance for the response variable t_2 (s) are summarized in Table 3.A.2.3, and its corresponding data are in Appendix 3.A.3. The analysis of variance shows that there is a significant influence of temperature factor *B* on average time t_2, because the *P*-value is lower than 0.001 and between-treatment mean square value 0.58075 is 54 times greater than the error mean square value 0.03049; however, there is no influence of the interaction between the factors atmosphere and temperature on treatment means of time t_2, because P-value is greater than 0.05.

Table 3.A.2.3 - Analysis of variance for elapsed time t_2 (s) data

Source of variation	Sum of squares	Degrees of freedom	Mean square	F_0	P
Atmosphere A	1.9720	2	1.0275	5.04	0.019
Temperature B	22.5444	2	11.1260	54.54	< 0.001
Interaction AB	0.6715	4	0.1679	0.82	0.528
Error	3.4679	17	(0.2040)		
Total	28.6559	25			

3.A.2.2 Analysis of variance for 1st group of experiments

A) Statistical analysis for variation of oxygen concentration ΔO_2 *(vol. %)*

Results of the analysis of variance for the response variable ΔO_2 (vol. %) are summarized in Table 3.A.2.4. The variation of oxygen concentration data is in Appendix 3.A.3.

Table 3.A.2.4 - Analysis of variance for variation of oxygen concentration ΔO_2 (vol. %)

Source of variation	Sum of squares	Degrees of freedom	Mean square	F_0	P
Atmosphere *A*	16.8833	2	6.8503	20.45	< 0.001
Temperature *B*	13.0457	2	9.4763	28.29	< 0.001
Diameter *C*	57.5867	1	54.1281	161.56	< 0.001
Coal *D*	0.0000	1	0.0805	0.24	0.627
Interaction *AB*	8.5459	4	1.6983	5.07	0.002
Interaction *AC*	10.1761	2	5.1525	15.38	< 0.001
Interaction *AD*	7.3477	2	3.4938	10.43	< 0.001
Interaction *BC*	8.7223	2	3.3210	9.91	< 0.001
Interaction *BD*	7.6269	2	2.4632	7.35	0.002
Interaction *CD*	14.3894	1	12.4607	37.19	< 0.001
Interaction *ABC*	12.9012	4	3.0731	9.17	< 0.001
Interaction *ABD*	3.6408	4	0.7348	2.19	0.086
Interaction *ACD*	5.1779	2	2.4851	7.42	0.002
Interaction *BCD*	3.1559	2	1.5571	4.65	0.015
Interaction *ABCD*	0.2867	4	0.0717	0.21	0.929
Error	14.0711	42	(0.3350)		
Total	183.5577	77			

It is observed that for diameter factor *C* the between-treatment mean square (54.12) is many times greater than the within-treatment or error mean square (0.33), indicating that it is unlikely that the treatment means are equal. More formally, the $F_0 = 161.56$ is compared with an appropriate upper-tail percentage point of the $F_{0.05,1,42}$ distribution with aid of tables in literature [Montgomery, 2001] and yields $F_{0.05,1,42} = 4.08$. Because $F_0 = 161.56 > 4.08$, the null hypothesis is rejected and it's concluded that the treatment means differ; that is, the diameter of particle level significantly affects the variation of oxygen concentration ΔO_2 (vol. %). Also, the *P*-value is lower than 0.05, thus, the null hypothesis is also rejected.

The analysis of variance also shows that the levels of factors atmosphere *A* and temperature *B* have a significant influence on the variation of oxygen concentration, because $F_{0.05,2,42} = 3.23$ and $F_0 > F_{0.05,2,42}$. Looking at factor coal *D,* the between-treatment mean

square (0.085) is smaller than within-treatment or error mean square (0.3350), indicating that it is likely that the treatment means are equal. More formally, the $F_0 = 0.24$ is compared with an appropriate upper-tail percentage point of the $F_{0.05,1,42}$ distribution with aid of tables in literature [Montgomery, 2001] and yields $F_{0.05,1,42} = 4.08$. Because $F_0 = 0.24 < 4.08$, the null hypothesis is accepted and it's concluded that the treatment means do not differ; that is, the coal type does not affect the variation of oxygen concentration ΔO_2 (vol. %). The interaction between the factors *AC*, *AD*, *BC*, *CD* and *ABC* also influence the treatment means of variation of oxygen concentration, and they are elucidated with the graphs plotted. The investigation is focused on the main factors *A*, *B* and *C*, and the interaction *AC*, because they have largest F_0 values.

B) Statistical analysis for average time t_1 (s)

The results of the analysis of variance for the response variable t_1 are summarized in Table 3.A.2.5. The t_1 data is in Appendix 3.A.3. According to the data, the diameter factor *C* has the between-treatment mean square (21.96) many times greater than the within-treatment or error mean square (0.059).

Table 3.A.2.5 - Analysis of variance for time t_1 data

Source of variation	Sum of squares	Degrees of freedom	Mean square	F_0	P
Atmosphere *A*	0.09705	2	0.12857	2.15	0.129
Temperature *B*	3.05942	2	1.72214	28.83	< 0.001
Diameter *C*	22.15431	1	21.96798	367.77	< 0.001
Coal *D*	0.00069	1	0.00118	0.02	0.889
Interaction *AB*	0.34170	4	0.09499	1.59	0.195
Interaction *AC*	2.17904	2	1.04386	17.48	< 0.001
Interaction *AD*	0.10130	2	0.06230	1.04	0.361
Interaction *BC*	1.95367	2	0.93802	15.70	< 0.001
Interaction *BD*	0.09380	2	0.04663	0.78	0.465
Interaction *CD*	0.10241	1	0.12226	2.05	0.160
Interaction *ABC*	0.62803	4	0.15033	2.52	0.056
Interaction *ABD*	0.28876	4	0.06957	1.16	0.340
Interaction *ACD*	0.27784	2	0.14478	2.42	0.101
Interaction *BCD*	0.46887	2	0.22062	3.69	0.033
Interaction *ABCD*	0.17528	4	0.04382	0.73	0.574
Error	2.50875	42	(0.05973)		
Total	34.43093	77			

This indicates that it is unlikely that the treatment means are equal, and the particle mean diameter level significantly affects the time t_1. Statistically, it can be verified through F_0 values, as discussed before. As $F_{0.05,1,42} = 4.08$ and $F_0 = 356.77 > 4.08$, the null hypothesis is rejected and it's concluded that the treatment means differ. The analysis of variance also shows that, the levels of factor atmosphere *A* does not influence the time t_1, because $F_{0.05,1,42} < 2.15$, whereas the temperature level significantly affects the time t_1. The analysis of variance also shows that there is a significant interaction between temperature and diameter factors *AC*, because $F_{0.05,2,42} = 3.23$ and $F_0 = 17.48 > 3.28$. The investigation is focused on the main factors *B* and *C*, and the interaction *AC*, because they have largest F_0 values.

C) Statistical analysis for average time t_2 (s)

The results of the analysis of variance for the response variable t_2 are summarized in Table 3.A.2.6, and data is in Appendix 3.A.3.

Table 3.A.2.6 - Analysis of variance for time t_2 data

Source of variation	Sum of squares	Degrees of freedom	Mean square	F_0	P
Atmosphere *A*	473.533	2	189.170	139.78	< 0.001
Temperature *B*	2.604	2	0.116	0.09	0.918
Diameter *C*	674.052	1	680.306	502.70	< 0.001
Coal *D*	62.958	1	56.864	42.02	< 0.001
Interaction *AB*	9.820	4	2.079	1.54	0.209
Interaction *AC*	37.561	2	18.207	13.45	< 0.001
Interaction *AD*	16.878	2	7.600	5.62	0.007
Interaction *BC*	1.376	2	0.425	0.31	0.732
Interaction *BD*	21.407	2	9.133	6.75	0.003
Interaction *CD*	12.889	1	13.576	10.03	0.003
Interaction *ABC*	18.834	4	4.864	3.59	0.013
Interaction *ABD*	9.107	4	2.339	1.73	0.162
Interaction *ACD*	3.156	2	1.426	1.05	0.358
Interaction *BCD*	13.279	2	6.434	4.75	0.014
Interaction *ABCD*	1.990	4	0.498	0.37	0.830
Error	56.839	42	(1.353)		
Total	1416.284	77			

According to the data, the diameter factor *C* has the between-treatment mean square (680.30) many times greater than the within-treatment or error mean square (0.05973). It

indicates that the diameter of particle level significantly affects the time t_2 much more than other factors and interactions. Statistically, it can be verified through F_0 values, as discussed before. The analysis of variance also shows that the atmosphere factor levels also affects significantly the time t_2, whereas temperature factor levels do not influence, because $F_{0.05,2,42} = 3.23$ and $F_0 = 139.17 > 3.23$ and P-value is higher than 0.05. Coal type also influences on the mean-treatments of time t_2, because $F_{0.05,1,42} = 2.15$, i.e., $F_0 = 42.02 > 2.15$.

The interaction between the factors, as *AC* and *CD*, affect the mean-treatments of time t_2, but not as significantly as diameter, atmosphere and coal factors levels. The investigation is focused on the main factors *A*, *C* and *D*, and the interactions *AC* and *CD*, because they have largest F_0 values, as follows.

3.A.2.3 Analysis of variance for 2nd group of experiments

A) Statistical analysis for variation of oxygen concentration ΔO_2 (vol. %)

The results of the analysis of variance for the response variable ΔO_2 (vol. %) are summarized in Table 3.A.2.7. The variation of oxygen concentration data is in Appendix 3.A.3. Coal type and sample mass are not computed as factors as they are of one unique level.

Table 3.A.2.7 - Analysis of variance for variation of oxygen concentration ΔO_2 (vol. %)

Source of variation	Sum of squares	Degrees of freedom	Mean square	F_0	P
Atmosphere *A*	11.0227	5	2.2932	6.11	< 0.001
Temperature *B*	7.7765	2	5.5908	14.90	< 0.001
Diameter *C*	254.7151	1	248.8264	663.29	< 0.001
Interaction *AB*	9.3976	10	0.8700	2.32	0.024
Interaction *AC*	3.7021	5	0.7104	1.89	0.111
Interaction *BC*	5.1080	2	2.4392	6.50	0.003
Interaction *ABC*	5.0457	10	0.5046	1.35	0.231
Error	20.2576	54	(0.3751)		
Total	317.0253	89			

The between-treatment mean square (248.82) for factor diameter *C* is many times greater than the within-treatment or error mean square (0.3751), indicating that the diameter significantly affects the treatment means of variation of oxygen concentration ΔO_2 (vol. %),

because, according to the statistical analysis, $F_{0.05,1,54} \approx 5.5$ and $F_0 = 663.29 > 5.5$, therefore the treatment means of ΔO_2 differ.

The analysis of variance also shows that the levels of temperature and oxidizer atmosphere factor influence also the treatment means of variation of oxygen concentration, because $F_{0.05,2,54} \approx 4.0$ and $F_0 = 14.90 > 4.0$ for temperature; and $F_{0.05,5,54} \approx 2.9$ and $F_0 = 6.11 > 2.9$ for oxidizer atmosphere. There is also an influence on the treatment means of variation of oxygen concentration due to an interaction between the factors temperature and diameter, as seen in *P*-value. The investigation is focused on the factors *A*, *B* and *C*, because they have largest F_0 values; and on the interaction between the factors *AC* and *BC* on the treatment means of variation of oxygen concentration in order to compare with F_0 values of Table 3.A.2.7.

B) Statistical analysis for average time t_1 (s)

The results of the analysis of variance for the response variable t_1 are summarized in Table 3.A.2.8, and data is in Appendix 3.A.3.

Table 3.A.2.8 - Analysis of variance for time t_1 data

Source of variation	Sum of squares	Degrees of freedom	Mean square	F_0	P
Atmosphere *A*	4.42762	5	0.81179	21.23	< 0.001
Temperature *B*	1.56131	2	0.95781	25.05	< 0.001
Diameter *C*	25.67713	1	24.61869	643.78	< 0.001
Interaction *AB*	0.37417	10	0.03580	0.94	0.508
Interaction *AC*	0.10061	5	0.02082	0.54	0.742
Interaction *BC*	0.67026	2	0.31882	8.34	0.001
Interaction *ABC*	0.35790	10	0.03579	0.94	0.508
Error	2.06500	54	(0.03824)		
Total	35.23400	89			

It's possible to see that for factor diameter *C* the between-treatment mean square (24.61) is many times greater than the within-treatment or error mean square (0.038). It indicates that the levels of particle diameter significantly influence the time t_1, consequently, the treatment means of t_1 differ. Factors as oxidizer atmosphere and temperature also affect the treatment means of t_1. The investigation is focused on the main factors A, *B* and *C*,

because they have largest F_0 values; and the analysis of interaction between the factors *BC* is not considered due to small influence on t_1.

C) Statistical analysis for average time t_2 (s)

The results of the analysis of variance for the response variable t_2 are summarized in Table 3.A.2.9 and data is in Appendix 3.A.3. According to Table 3.A.2.9, factor diameter *C* the between-treatment mean square (136.705) is many times greater than the within-treatment or error mean square (0.276). It indicates that the diameter of particle level significantly affects the time t_2 much more than other factors and interactions. The analysis of variance also shows that the levels of atmosphere factor also affects significantly the time t_2, whereas the levels of temperature factor do not influence it; this happens because the temperature factor has $F_{0.05,2,54} \approx 3.2$ and *P*-value higher than 0.05. The interaction between the factors, as *AB*, *AC* and *BC*, affect the mean treatments of time t_2, but not as significantly as levels of diameter and atmosphere factors. Thus, the investigation is focused on the main factors *A* and *C*, and interaction *AC*, due to their largest F_0 values.

Table 3.A.2.9 - Analysis of variance for time t_2 data

Source of variation	Sum of squares	Degrees of freedom	Mean square	F_0	P
Atmosphere *A*	340.353	5	59.795	216.85	< 0.001
Temperature *B*	0.294	2	0.250	0.91	0.409
Diameter *C*	121.718	1	136.705	495.77	< 0.001
Interaction *AB*	30.075	10	2.470	8.96	< 0.001
Interaction *AC*	60.176	5	11.654	42.27	< 0.001
Interaction *BC*	11.461	2	4.911	17.81	< 0.001
Interaction *ABC*	13.025	10	1.302	4.72	< 0.001
Error	14.890	54	(0.276)		
Total	591.992	89			

3.A.2.4 Analysis of variance for 3rd group of experiments

A) Statistical analysis for variation of oxygen concentration ΔO_2 (vol. %)

The results of the analysis of variance for the response variable ΔO_2 (vol. %) are summarized in Table 3.A.2.10. The variation of oxygen concentration data is in Appendix 3.A.3. Coal type and sample mass were not computed as factors.

Table 3.A.2.10 - Analysis of variance for variation of oxygen concentration ΔO_2 (vol. %)

Source of variation	Sum of squares	Degrees of freedom	Mean square	F_0	P
Atmosphere *A*	17.235	1	6.224	45.11	< 0.001
Temperature *B*	38.653	2	15.326	111.09	< 0.001
Coal *C*	617.784	5	120.402	872.71	< 0.001
Interaction *AB*	0.107	2	0.139	1.00	0.376
Interaction *AC*	12.015	5	2.370	17.18	< 0.001
Interaction *BC*	3.369	10	0.336	2.43	0.025
Interaction *ABC*	1.123	10	0.112	0.81	0.617
Error	4.967	36	(0.138)		
Total	695.253	71			

Results presented in Table 3.A.2.10 allow to observe that for factor coal *C* the between-treatment mean square (120.402) is many times greater than the within-treatment or error mean square (0.138). This indicates that the levels of coal, i.e., the types of coal significantly affects the mean treatments of variation of oxygen concentration ΔO_2 (vol. %), because $F_{0.05,5,36} \approx 2.5$ and $F_0 = 872.71 > 2.5$, with the aid of values found in tables from literature [Montgomery, 2001]. The analysis of variance also shows that the levels of temperature and oxidizer atmosphere factors influence the treatment means of maximum variation of oxygen concentration, with $F_{0.05,2,36} \approx 3.3$ and $F_0 = 111.09 > 3.3$ for temperature; and $F_{0.05,1,36} \approx 4.1$ and $F_0 = 45.11 > 4.1$ for oxidizer atmosphere. The investigation is focused on the main factors *A, B,* and *C*, because they have largest F_0 values; and on the interaction between the factors *AC* on the treatment means of variation of oxygen concentration.

B) Statistical analysis for average time t_1 (s)

The results of the analysis of variance for the response variable t_1 are summarized in Table 3.A.2.11. The t_1 data is in Appendix 3.A.3. As observed in Table 3.A.2.11, the factors temperature and coal influence the time t_1, because the between-treatment mean squares (18) of both factors are many times greater than within-treatment or error mean square (0.9640), consequently the treatment means of t_1 differ, as seen, also in *P*-value.

The levels of atmosphere factor do not affect the treatment means of t_1, and most of interactions between the factors have no influence on t_1 too. In order to elucidate this analysis, graphs of the main interactions are plotted. The investigation is focused on the main factors *B* and *C*, and the interaction between them *BC*, because they display largest F_0 values.

Table 3.A.2.11 - Analysis of variance for t_1 data

Source of variation	Sum of squares	Degrees of freedom	Mean square	F_0	P
Atmosphere *A*	1.0537	1	0.6879	0.71	0.404
Temperature *B*	34.6410	2	18.6319	19.33	< 0.001
Coal *C*	94.7613	5	18.5088	19.20	< 0.001
Interaction *AB*	1.5704	2	0.6740	0.70	0.504
Interaction *AC*	14.4933	5	2.7460	2.85	0.029
Interaction *BC*	44.5862	10	4.4093	4.57	< 0.001
Interaction *ABC*	4.4949	10	0.4495	0.47	0.901
Error	34.7033	36	(0.9640)		
Total	230.3041	71			

C) Statistical analysis for average time t_2 (s)

The results of the analysis of variance for the response variable t_2 are summarized in Table 3.A.2.12, and data is in Appendix 3.A.3. As observed through the data, the factor atmosphere significantly influences the time t_2, because the between-treatment mean square (279) is many times greater than within-treatment or error mean square (2.49), consequently the treatment means of t_2 differ, as verified, also in *P*-value. The coal factor affects the time t_2, as shown by F_0 and *P* values.

The interaction between the factors *AB* and *BC* also influence the treatment means of t_2, but not as significantly as the levels of atmosphere factor. The levels of temperature factor do not affect t_2, as checked via *P*-value.

Table 3.A.2.12 - Analysis of variance for t_2 data

Source of variation	Sum of squares	Degrees of freedom	Mean square	F_0	P
Atmosphere *A*	258.454	1	279.001	111.63	< 0.001
Temperature *B*	1.585	2	2.714	1.09	0.348
Coal *C*	372.164	5	71.681	28.68	< 0.001
Interaction *AB*	28.429	2	16.850	6.74	0.003
Interaction *AC*	102.728	5	20.716	8.29	< 0.001
Interaction *BC*	129.741	10	12.941	5.18	< 0.001
Interaction *ABC*	96.838	10	9.684	3.87	0.001
Error	89.974	36	(2.499)		
Total	1079.913	71			

The investigation is focused on the main factors *A* and *C* and the interaction between factors *AC*, due to their largest F_0 values.

3.A.2.5 Analysis of variance for 4th group of experiments

A) Statistical analysis for variation of oxygen concentration ΔO_2 *(vol. %)*

The results of the analysis of variance for the response variable ΔO_2 (vol. %) are summarized in 3.A.2.13. The variation of oxygen concentration data is in Appendix 3.A.3. Note that the oxidizer atmosphere and sample mass were not computed as factors in the software package to analyze the variance, because each factor has one level. Analyzing the results presented in Table 3.A.2.13 it's observed that for factor coal *B* the between-treatment mean square (336.145) is many times greater than the within-treatment or error mean square (0.659).

Table 3.A.2.13 - Analysis of variance for variation of oxygen concentration ΔO_2 (vol. %)

Source of variation	Sum of squares	Degrees of freedom	Mean square	F_0	P
Temperature *A*	11.641	2	13.290	20.16	< 0.001
Coal *B*	1009.468	3	336.145	509.96	< 0.001
Interaction *AB*	4.900	6	0.817	1.24	0.349
Error	8.569	13	(0.659)		
Total	1034.578	24			

This indicates the coal types significantly affect the treatment means of variation of oxygen concentration, because, formally, $F_{0.05,3,13} = 3.41$ and $F_0 = 509.96 > 3.41$, therefore treatment means of ΔO_2 differ.

The analysis of variance also shows that, the levels of temperature factor influence also the treatment means of variation of oxygen concentration, because $F_{0.05,2,13} = 4.67$ and $F_0 = 20.16 > 4.67$ .The investigation is focused on the main factors *A* and *B*, and the interaction between them.

B) Statistical analysis for average time t_1 (s)

The results of the analysis of variance for the response variable t_1 are summarized in Table 3.A.2.14. The t_1 data is in Appendix 3.A.3. As observed in Table 3.A.2.14, the levels of coal influence the treatment means of time t_1, because the between-treatment mean square (19.28) is many times greater than within-treatment or error mean square (0.1007), consequently the treatment means of t_1 differ, as seen, also in *P*-value.

Table 3.A.2.14 - Analysis of variance for t_1 data

Source of variation	Sum of squares	Degrees of freedom	Mean square	F_0	P
Temperature *A*	1.3118	2	0.8948	8.88	0.004
Coal *B*	6.2393	3	1.9425	19.28	< 0.001
Interaction *AB*	0.4346	6	0.0724	0.72	0.642
Error	1.3095	13	(0.1007)		
Total	9.2951	24			

The levels of temperature factor also affect the treatment means of t_1, as verified through F_0 and *P* values. The investigation is focused on the main factors *A* and *B*, and interaction between them.

C) Statistical analysis for average time t_2 (s)

The results of the analysis of variance are for the response variable t_2 summarized in Table 3.A.2.15. The t_2 data is in Appendix 3.A.3.

Table 3.A.2.15 - Analysis of variance for t_2 data

Source of variation	Sum of squares	Degrees of freedom	Mean square	F_0	P
Temperature *A*	5.262	2	3.190	7.39	0.007
Coal *B*	233.970	3	77.965	180.65	< 0.001
Interaction *AB*	8.427	6	1.404	3.25	0.035
Error	5.610	13	(0.432)		
Total	253.270	24			

As observed, the coal factor *B* significantly influence the treatment means of time t_2, because the between-treatment mean square (77.965) is many times greater than within-treatment or error mean square (0.432), consequently the treatment means of t_2 differ, as verified, also in *P*-value.

Also, the levels of temperature factor affect the time t_2, as examined through the F_0 and *P* values, but not as significant as the levels of coal factor. The investigation is focused on the main factors *A* and *B*, and interaction between them.

APPENDIX 3.A.3 - Tables of response variables separated for groups of experiments

The Tables 3.A.3.1 to 3.A.3.3 show the data attained for the preliminary group of experiments: LTBK coal, 1g of sample mass, and 1625 μm particle mean diameter.

Table 3.A.3.1 - Maximum variation of oxygen concentration (vol. %) data

Oxidizer atmosphere oxy-fuel ($O_2/CO_2/H_2O$)	Temperature (K)								
	1073			1173			1273		
	Replicate			Replicate			Replicate		
	i	ii	iii	i	ii	iii	i	ii	iii
30/60/10		5.02			4.96			5.88	
		5.64			4.56			5.70	
		5.28			4.56			6.16	
30/50/20		4.39			4.50			5.45	
		4.06			4.91			5.14	
		-			4.35			5.44	
30/40/30		4.35			4.55			4.99	
		4.89			4.35			4.98	
		4.24			4.44			5.14	

Table 3.A.3.2 - Time t_1 (s) data

Oxidizer atmosphere oxy-fuel ($O_2/CO_2/H_2O$)	Temperature (K)								
	1073			1173			1273		
	Replicate			Replicate			Replicate		
	i	ii	iii	i	ii	iii	i	ii	iii
30/60/10		2.95			2.75			2.55	
		2.95			2.95			2.45	
		3.00			2.95			2.70	
30/50/20		2.95			2.85			2.40	
		3.05			2.95			2.45	
		-			2.95			2.45	
30/40/30		3.05			2.80			2.35	
		2.70			2.85			2.60	
		3.30			2.25			2.35	

Table 3.A.3.3 - Elapsed time t_2 (s) data

Oxidizer atmosphere oxy-fuel ($O_2/CO_2/H_2O$)	Temperature (K)								
	1073			1173			1273		
	Replicate			Replicate			Replicate		
	i	ii	iii	i	ii	iii	i	ii	iii
30/60/10		10.50			10.25			8.70	
		10.85			9.55			8.60	
		10.80			9.00			9.15	
30/50/20		10.10			9.10			8.30	
		11.45			10.00			8.00	
		-			9.25			8.60	
30/40/30		10.40			9.10			8.05	
		10.50			8.85			8.25	
		10.65			8.00			7.65	

The Tables 3.A.3.4 to 3.A.3.9 show the data attained for the 1st group of experiments: Bonito and Leão coals, and 1g of sample mass.

Table 3.A.3.4 - Maximum variation of oxygen concentration (vol. %) data

Bonito coal sample (1g)						
	Particle mean diameter 312 µm			Particle mean diameter 1625 µm		
Atmosphere	Temperature (K)			Temperature (K)		
	1073	1173	1273	1073	1173	1273
Air	3.11	4.06	4.42	1.26	2.18	2.82
	3.49	4.94	5.84	1.20	1.75	2.89
21/79	9.07	5.62	4.62	2.15	2.44	3.56
	7.49	5.06	5.33	2.06	2.07	2.96
	6.55	-	-	-	-	2.99
30/70	3.33	3.46	4.30	1.86	2.19	3.30
	4.60	4.19	4.88	2.15	2.17	2.90
	3.89	-	-	-	-	-

Table 3.A.3.5 - Maximum variation of oxygen concentration (vol. %) data

Leão coal sample (1g)						
	Particle mean diameter 312 µm			Particle mean diameter 1625 µm		
Atmosphere	Temperature (K)			Temperature (K)		
	1073	1173	1273	1073	1173	1273
Air	4.46	5.53	5.73	2.80	2.64	4.12
	3.19	6.14	5.86	2.23	2.73	3.72
21/79	3.88	4.36	3.33	2.18	2.57	5.82
	5.24	4.72	4.74	2.20	2.74	5.43
	-	-	-	-	-	5.50
30/70	1.07	2.65	2.67	1.82	2.18	4.47
	1.20	3.55	3.30	2.82	2.86	4.22
	-	3.67	4.85	-	-	-

Table 3.A.3.6 - Time t_1 (s) data

Bonito coal sample (1g)						
	Particle mean diameter 312 µm			Particle mean diameter 1625 µm		
Atmosphere	Temperature (K)			Temperature (K)		
	1073	1173	1273	1073	1173	1273
Air	2.30	2.25	2.00	3.65	3.60	3.00
	2.35	2.50	2.15	3.50	2.55	3.05
21/79	2.50	2.40	2.35	3.55	3.25	2.65
	2.45	2.55	2.35	3.05	3.10	2.85
	2.40	-	-	-	-	2.85
30/70	2.40	2.20	2.05	3.95	3.60	2.90
	2.25	2.10	1.95	3.85	3.75	3.00
	2.30	-	-	-	-	-

Table 3.A.3.7 - Time t_1 (s) data

Leão coal sample (1g)						
	Particle mean diameter 312 µm			Particle mean diameter 1625 µm		
Atmosphere	Temperature (K)			Temperature (K)		
	1073	1173	1273	1073	1173	1273
Air	2.50	2.25	2.15	2.90	3.05	2.85
	2.00	2.45	2.25	3.35	3.30	2.80
21/79	2.40	2.25	2.30	4.40	3.25	2.35
	2.45	2.35	2.55	3.60	3.85	2.55
	-	-	-	-	-	2.60
30/70	2.00	1.95	2.00	4.05	3.50	2.85
	2.00	1.90	1.90	4.25	4.75	2.75
	-	2.05	1.95	-	-	-

Table 3.A.3.8 - Elapsed time t_2 (s) data

Bonito coal sample (1g)						
	Particle mean diameter 312 µm			Particle mean diameter 1625 µm		
Atmosphere	Temperature (K)			Temperature (K)		
	1073	1173	1273	1073	1173	1273
Air	9.25	8.95	8.25	11.95	14.35	14.45
	9.00	9.85	8.85	12.45	12.60	13.90
21/79	14.10	11.85	7.45	20.15	20.00	22.35
	16.75	13.30	12.90	19.85	19.35	21.30
	14.35	-	-	-	-	18.70
30/70	9.70	7.90	8.55	13.75	11.65	11.40
	10.85	8.20	8.45	14.80	12.00	11.35
	9.95	-	-	-	-	-

Table 3.A.3.9 - Elapsed time t_2 (s) data

Leão coal sample (1g)						
	Particle mean diameter 312 µm			Particle mean diameter 1625 µm		
Atmosphere	Temperature (K)			Temperature (K)		
	1073	1173	1273	1073	1173	1273
Air	6.40	7.70	7.65	12.55	13.70	13.75
	7.10	7.90	8.05	13.15	14.65	13.20
21/79	9.20	7.85	9.10	17.45	15.15	17.60
	8.60	10.65	10.90	17.40	18.80	18.75
	-	-	-	-	-	19.25
30/70	3.80	6.10	6.10	11.25	11.50	12.00
	4.00	6.50	6.50	14.10	12.45	11.50
	-	7.00	-	-	-	-

The Tables 3.A.3.10 to 3.A.3.12 show the data attained for the 2nd group of experiments: lignite raw coal (LTBK), 1g of sample mass.

Table 3.A.3.10 - Maximum variation of oxygen concentration (vol. %) data

	Particle mean diameter (μm)					
	312 μm			1625 μm		
Atmosphere	Temperature (K)			Temperature (K)		
	1073	1173	1273	1073	1173	1273
Air	8.61	8.83	8.25	4.60	4.51	5.79
	8.72	9.55	8.99	4.24	3.77	5.48
21/79	8.05	7.62	9.31	4.35	5.81	8.01
	9.02	8.95	9.54	4.08	6.00	6.76
	-	-	-	-	-	6.72
30/70	7.04	8.51	9.03	4.81	5.15	4.95
	7.95	8.52	8.34	4.36	4.95	6.98
30/60/10	8.49	8.46	8.81	5.02	4.96	5.88
	8.58	8.63	8.78	5.64	4.56	5.70
	9.46	9.02	9.02	5.28	4.56	6.16
30/50/20	7.84	7.59	8.54	4.39	4.50	5.45
	8.22	8.76	8.42	4.06	4.91	5.14
	7.57	9.24	9.91	-	4.35	5.44
30/40/30	6.76	6.81	6.66	4.35	4.55	4.99
	7.15	8.47	7.26	4.89	4.35	4.98
	8.23	10.76	7.00	4.24	4.44	5.14

Table 3.A.3.11 - Time t_1 (s) data

	Particle mean diameter (μm)					
	312 μm			1625 μm		
Atmosphere	Temperature (K)			Temperature (K)		
	1073	1173	1273	1073	1173	1273
Air	2.25	2.20	1.90	4.20	2.95	2.75
	2.20	2.30	1.95	3.20	3.50	2.65
21/79	2.10	2.15	2.10	3.55	3.75	2.85
	2.25	2.05	2.10	3.20	3.20	2.75
	-	-	-	-	-	2.95
30/70	1.85	1.85	2.05	3.00	2.90	3.10
	2.70	1.90	1.85	3.10	3.10	2.50
30/60/10	1.75	1.65	1.70	2.95	2.75	2.55
	1.85	1.75	1.70	2.95	2.95	2.45
	1.75	1.75	1.65	3.00	2.95	2.70
30/50/20	1.70	1.70	1.70	2.95	2.85	2.40
	1.75	1.65	1.60	3.05	2.95	2.45
	1.75	1.80	1.70	-	2.95	2.45
30/40/30	1.55	1.50	1.45	3.05	2.80	2.35
	1.65	1.55	1.50	2.70	2.85	2.60
	1.60	1.60	1.50	3.30	2.25	2.35

Table 3.A.3.12 - Elapsed time t_2 (s) data

Particle mean diameter (μm)						
	312 μm			1625 μm		
Atmosphere	Temperature (K)			Temperature (K)		
	1073	1173	1273	1073	1173	1273
Air	10.30	10.45	10.50	14.30	13.65	12.05
	10.10	10.80	10.45	13.70	14.05	12.15
21/79	9.60	9.75	11.75	14.50	17.55	19.05
	10.70	10.40	11.65	14.80	17.35	17.25
	-	-	-	-	-	17.60
30/70	8.55	8.70	10.35	11.55	11.15	11.20
	8.55	8.75	9.50	11.45	11.20	11.05
30/60/10	7.95	8.65	7.85	10.50	10.25	8.70
	8.45	9.50	8.25	10.85	9.55	8.60
	8.30	8.65	8.30	10.80	9.00	9.15
30/50/20	7.50	8.30	9.25	10.10	9.10	8.30
	7.85	8.50	7.75	11.45	10.00	8.00
	7.80	8.40	8.85	-	9.25	8.60
30/40/30	6.70	6.90	6.80	10.40	9.10	8.05
	8.00	7.00	7.55	10.50	8.85	8.25
	8.10	9.25	8.35	10.65	8.00	7.65

Tables 3.A.3.13 to 3.A.3.18 show the data attained for the 3rd group of experiments: Leão and LTBK chars and coals, 3 g of sample mass, and 1625 μm particle mean diameter.

Table 3.A.3.13 - Maximum variation of oxygen concentration (vol. %) data

Leão coal and char									
	Leão coal			Leão char 545 °C			Leão char 730 °C		
Atmosphere	Temperature (K)			Temperature (K)			Temperature (K)		
	1073	1173	1273	1073	1173	1273	1073	1173	1273
Air	5.28	6.22	6.87	1.96	3.91	3.83	2.59	3.15	3.83
	4.99	6.55	6.43	1.72	2.67	3.10	2.05	3.36	3.55
	-	-	-	-	2.44	-	-	3.22	-
21/79	5.30	6.47	7.44	2.92	4.64	4.90	2.82	3.61	3.98
	5.29	6.96	7.10	3.88	3.69	-	2.46	3.25	4.02

Table 3.A.3.14 - Maximum variation of oxygen concentration (vol. %) data

LTBK coal									
	LTBK coal			LTBK char 535 °C			LTBK char 900 °C		
Atmosphere	Temperature (K)			Temperature (K)			Temperature (K)		
	1073	1173	1273	1073	1173	1273	1073	1173	1273
Air	9.57	10.90	11.78	8.49	9.26	10.31	8.20	8.98	9.70
	9.42	-	10.78	7.92	10.00	9.85	8.52	8.37	9.71
21/79	9.05	10.04	10.35	8.91	9.78	10.54	9.89	9.86	12.08
	9.22	9.91	10.09	8.68	10.45	10.39	10.18	10.10	12.56

Table 3.A.3.15 - Time t_1 (s) data

Leão coal and char									
	Leão coal			Leão char 545 °C			Leão char 730 °C		
Atmosphere	Temperature (K)			Temperature (K)			Temperature (K)		
	1073	1173	1273	1073	1173	1273	1073	1173	1273
Air	5.95	4.35	3.95	8.45	2.50	3.25	11.90	6.85	5.30
	6.45	4.50	4.50	8.25	5.85	4.70	7.90	6.80	5.00
	-	-	-	-	6.25	-	-	7.85	-
21/79	3.95	4.65	4.20	7.75	2.75	3.75	10.20	6.60	4.35
	5.55	4.10	4.00	2.60	2.65	-	10.55	6.50	5.30

Table 3.A.3.16 - Time t_1 (s) data

LTBK coal and char									
	LTBK coal			LTBK char 535 °C			LTBK char 900 °C		
Atmosphere	Temperature (K)			Temperature (K)			Temperature (K)		
	1073	1173	1273	1073	1173	1273	1073	1173	1273
Air	4.10	3.60	3.50	4.30	3.75	4.05	6.45	5.85	6.45
	4.05	-	3.75	4.55	3.90	4.05	6.20	6.20	5.95
21/79	4.15	4.15	4.05	5.45	5.15	5.25	6.10	5.80	5.75
	4.30	3.85	3.95	5.35	4.95	5.20	6.05	6.40	6.55

Table 3.A.3.17 - Elapsed time t_2 (s) data

Leão coal									
	Leão coal			Leão char 545 °C			Leão char 730 °C		
Atmosphere	Temperature (K)			Temperature (K)			Temperature (K)		
	1073	1173	1273	1073	1173	1273	1073	1173	1273
Air	26.85	25.95	25.45	26.90	25.50	26.75	38.35	26.00	28.30
	26.85	25.05	24.35	24.60	26.20	23.95	28.20	29.70	25.40
	-	-	-	-	24.95	-	-	26.90	-
21/79	29.25	30.30	33.05	32.95	30.95	34.75	35.35	33.30	33.95
	28.75	30.65	30.50	30.65	30.95	-	35.65	31.75	34.85

Table 3.A.3.18 - Elapsed time t_2 (s) data

LTBK coal									
	LTBK coal			LTBK char 535 °C			LTBK char 900 °C		
Atmosphere	Temperature (K)			Temperature (K)			Temperature (K)		
	1073	1173	1273	1073	1173	1273	1073	1173	1273
Air	22.65	22.60	21.85	27.50	27.05	27.00	30.05	30.55	31.30
	21.35	-	21.65	26.80	28.70	27.70	28.75	30.20	29.25
21/79	22.50	27.00	29.10	28.30	31.55	37.05	32.35	28.80	23.95
	22.90	25.45	29.30	27.80	31.20	36.40	33.25	29.50	26.25

The Tables 3.A.3.19 to 3.A.3.22 show the data attained for the 4th group of experiments: new position of oxygen sensor, Leão and LTBK coals and chars, 3g of sample mass, 1625 μm particle mean diameter, under air atmosphere conditions.

Table 3.A.3.19 - Maximum variation of oxygen concentration (vol. %) data

	Temperature (K)		
Coal and char (3g)	1073	1173	1273
Leão coal	7.79	10.31	10.14
	7.55	9.04	10.81
LTBK coal	18.01	20.37	19.81
	14.74	18.98	19.78
	17.34	-	-
Leão char 900 °C	0.81	1.43	2.23
	0.86	1.04	2.03
LTBK char 900 °C	11.80	13.09	15.17
	12.52	13.39	14.56

Table 3.A.3.20 - Elapsed time t_1 (s) data

	Temperature (K)		
Coal and char (3g)	1073	1173	1273
Leão coal	4.10	3.89	3.35
	4.10	3.55	2.95
LTBK coal	2.55	3.55	2.75
	3.40	2.55	2.75
	3.00	-	-
Leão char 900 °C	4.90	4.35	4.05
	4.35	3.95	3.95
LTBK char 900 °C	4.20	3.85	3.50
	4.05	3.90	3.15

Table 3.A.3.21 - Elapsed time t_2 (s) data

	Temperature (K)		
Coal and char (3g)	1073	1173	1273
Leão coal	18.05	17.75	15.75
	17.90	16.05	15.85
LTBK coal	14.50	14.00	13.50
	14.80	13.95	13.45
	15.20	-	-
Leão char 900 °C	10.80	10.80	12.25
	10.15	9.05	10.80
LTBK char 900 °C	20.65	19.25	17.40
	19.40	18.85	18.10

Table 3.A.3.22 - Time t_{video} (s) data

	Temperature (K)		
Coal and char (3g)	1073	1173	1273
Leão coal	41	33	37
	35	39	41
LTBK coal	25	23	24
	24	25	22
	24	-	-
Leão char 900 °C	52	58	49
	61	57	48
LTBK char 900 °C	32	30	28
	29	32	27

4. Investigation of global kinetic parameters of low-rank coals combustion within a cyclone reactor under oxy-fuel and air conditions

Abstract

A laboratory test facility developed to burn solid fuels as coal and char within a cyclone combustion reactor is used to assess the reactivity of low rank coals by means of global kinetic parameters and of char combustion reaction coefficients. High ash coals (from Leão and Bonito mining sites located in South Brazil) and pre-dried lignite coal (LTBK, from the Lusatian region, in Germany) were burned under air and oxy-fuel ($O_2/CO_2/H_2O$) atmospheres with 21 and 30% O_2 (in vol.), and with different combinations of CO_2 and H_2O concentrations. Coal and char global kinetic parameters were attained upon the oxygen concentration curves measured by the potentiometric oxygen sensor, installed within the cyclone combustion reactor. Results show that the method used in the present work under a hypothesis of a well stirred reactor to calculate the effective reaction rate constants is not accurate enough to capture the kinetic involved in coal combustion, upon which have several effects, as oxidizer atmosphere compositions and properties, gas combustion temperature, coal and char, sample masses, swirling flow with its advective and diffusive terms, and oxygen sensor position within the cyclone combustion reactor. The oxygen sensor position is an important effect to be taken into account to calculate the global kinetic parameters. The method to calculate the char combustion reaction rate coefficients (diffusive and kinetic) for LTBK char 900 and to determine the control regime of overall coal combustion depends also on the effects observed for the global kinetic parameters. Results show that the kinetic regime of coal combustion under oxy-fuel atmosphere (21/79, O_2/CO_2) is benefited with high velocities of gas, because they reduce the influence of oxy-fuel atmosphere properties on diffusion reaction rate coefficient.

Keywords: Global kinetic parameters, oxy-fuel combustion, low-rank coal, char, cyclone combustion reactor, potentiometric oxygen sensor.

LIST OF ABREVIATIONS AND SYMBOLS

Abbreviations

ALVA20	20 kW_{th} - Laboratory test facility with cyclone reactor rated capacity of 20 kW_{th} operating under 1 atm.
DoE	Design of Experiments
LTBK	Lausitzer Trockenbraunkohle, Lusatian pre-dried brown coal
Pos.	Position
Vol.	Volume

Symbols

Bi	Biot number, -
c	Constant
$c_{p,g}$	Constant-pressure heat specific, J kg^{-1} K^{-1}
C	Concentration, gmol O_2 m^{-3} or % vol
C_g	Oxygen concentration in bulk gas, gO_2 cm^{-3}
C_s	Oxygen concentration on particle's outer surface, gO_2 cm^{-3}
d	Particle or char diameter, µm, cm
D	Binary diffusion coefficient, cm^2 s^{-1}
E	Global activation energy, kJ mol^{-1}
f	Molar fraction, -
h	Mass transfer coefficient (carbon oxide flux), cm s^{-1}
h_g	Gas heat transfer coefficient, W m^{-2} K^{-1}
H	Heat of reaction, cal g^{-1}, J g^{-1}
k_g	Gas thermal conductivity, cal s^{-1} cm^{-1} K^{-1}, W m^{-1} K^{-1}
k_p	Coal thermal conductivity, W m^{-1} K^{-1}
k	Reaction rate constant, (gmol O_2 m^{-3})$^{n-1}$ s^{-1}, cm s^{-1}
L_c	Particle characteristic length, m
M	Molecular mass, g $gmol^{-1}$
$\dot{n}$	Molar flow, mol s^{-1}
N	Moles
p	Pressure, atm
Pr	Prandtl number, -
$\dot{r}_{O_2}$	Reaction rate, gmol O_2 m^{-3} s^{-1}
$\dot{r}_{a,c}$	Actual, observed reaction rate or overall combustion reaction rate, gC cm^{-2} s^{-1}
$\dot{r}_m$	Maximum reaction rate, gC cm^{-2} s^{-1}
r_p	Particle radius, m
R	Ideal gas law constant, 8.314 J K^{-1} mol^{-1}
Re	Reynold's number, -
R_a	Overall reaction rate per external area, gC [cm^{-2} s^{-1} $(atmO_2)^{-1}$]
$R_{a,c}$	Rate coefficient (per unit external area) for chemical rate process, gC [cm^{-2} s^{-1} $(atmO_2)^{-n}$]

$R_{a,d}$	Rate coefficient (per unit external area) for diffusional rate process, gC [cm^{-2} s^{-1} $(atmO_2)^{-1}$]
Sc	Schmidt number, -
Sh	Scherwood number, -
t	Time, s
T	Temperature, K or ºC
u_g	Gas superficial velocity, m s^{-1}
$\dot{V}$	Volumetric flow, m^3 s^{-1}
X_{O2}	Conversion, -

Greek symbols

ε	Particle emissivity, porosity of packed bed, -
Λ	Gravimetric stoichiometric coefficient, gC $(gO_2)^{-1}$
μ	Dynamic viscosity, kg m^-1 s^{-1}
ν	Kinematic viscosity, cm^2 s^{-1}; Stoichiometric coefficient
ρ	Mass density of solution, kg m^{-3}; mass density of solid, g cm^{-3}
σ	Stefan-Boltzmann constant, 5.67E-8 W m^{-2} $(K^4)^-1$ or 1.354 E-12 cal s^{-1} cm^{-2} $(K^4)^{-1}$
ϕ_s	Particle shape factor, -
χ	Ratio of the surface chemical reaction rate to its maximum combustion rate, -

Subscripts

0	Initial or reference conditions
a	Particle external area
atm	Atmospheric
A	Apparent
c	Char, chemical rate, carbon, characteristic
cons	Consumed
CO_2	Carbon dioxide gas
d	Diffusion
eff	Effective
g	Gas
in	Inlet
m	Mass, maximum
N_2	Nitrogen gas
out	Outlet
O_2	Oxygen gas
p	Particle, pressure
ref	Reference
s	Surface
tot	Total
w	Reactor wall

Superscripts

n	Order of reaction; apparent order of reaction
m	True order of reaction

4.1 Introduction

Carbon dioxide capture and storage (CCS) is recognized as a promising option for the mitigation of atmospheric emissions from coal-fired power generation. Among the possible strategies that are under investigation, oxy-fuel technology is pointed as one of the major options in the near-future term [Olajire, 2010; Wall, 2007; Buhre et al., 2005]. In this technology, a combination of almost pure oxygen and recycled flue gas are used as the oxidizer stream instead of air. The recycled flue gas is a heavily concentrated in CO_2 with some water vapor content, ready for sequestration. Additionally, the recycled flue gas controls flame temperature and ensures the similar or equivalent heat transfer patterns found in air-fired atmospheres [Toftegaard et al., 2010; Wall et al., 2009]. Many studies were motivated to understand the impacts on combustibility, pollutant emissions and heat transfer due to the substitution of N_2 by CO_2, with different physical and chemical properties, in combination with its higher partial pressure. Changes on devolatilization and ignition and burnout of coal particles are expected [Wall et al., 2009]. A wide understanding of these effects is an essential requirement for the prediction of coal combustion by mathematical modeling [Cho et al., 2006; Pallarés et al., 2007 and 2009]. To assess the combustion behavior within the furnaces, the basic steps of devolatilization, volatile combustion and char oxidation should be well understood and accurately described [Syred and Beér, 1974].

Many works have been carried out in the last years in order to understand the influence of the presence of CO_2 on devolatilization and ignition [Toftegaard et al., 2010; Molina and Shaddix, 2007, 2009; Murphy and Shaddix, 2006], and volatile and char burnout [Brix et al., 2010; Zhang et al., 2010; Bejarano and Levendis, 2008; Naredi and Pisupati, 2008]. The literature reveals a significant number of works on the impacts of oxy-fuel atmospheres on low-rank coals combustion as Corrêa, R.S., 2013, Tappe and Krautz, 2011, 2009 and Zhang et al., 2010b. Additionally, most of these studies were carried out applying standard techniques of analysis, such as thermogravimetric tests [Qingzhao et al., 2009; Liu, 2009; Milioli and Filho, 2008], drop tube furnaces [Borrego et al., 2007] and entrained-flow reactors [Rathnam et al., 2009]. It is well-known that thermogravimetric tests operate in conditions far from those in industrial furnaces, whereas entrained flow reactors are the unique equipments that can simulate more closely practical combustion environments. Consequently, there is a need of quantitative information obtained by reactors which operate in conditions encountered in existing furnaces. Successful results have been obtained with

fluidized bed reactor to understand the combustion behavior of solid fuels under air conditions with the aid of solid electrolyte oxygen sensor as stabilized zirconia to calculate the global kinetic parameters [Schotte et al., 2010; Lorentz and Rau, 1998; Lorentz et al., 1996].

The literature review performed in this work also identified a lack of information on the impacts of higher partial pressures of water vapor on the oxy-fuel combustion process. Most researches were focused on the impacts of water vapor on adiabatic flame temperature and radiative heat flux [Olajire, 2010; Wall et al., 2009], and further information on coal reactivity is necessary.

In the present work, experiments were performed in a laboratory test facility developed at the Chair of Power Plant Technology of Brandenburg University Technology (Cottbus, Germany). Details of the equipment and the experimental procedures are available in Chapters 2 and 3.

The objective of this chapter is to calculate the global kinetic parameters for coals and chars burned under air and oxy-fuel atmospheres within a cyclone combustion reactor. The coal global kinetic parameters are calculated by measuring the variation on oxygen concentration of samples with the aid of a potentiometric oxygen sensor installed within the reactor. The char combustion reaction rate coefficients are also calculated for LTBK coal devolatilized at 900 ^{o}C in order to investigate which regime can be controlling the global coal combustion reaction rate. The assumptions and limitations of the methodology to evaluate the coal and char combustion reactivity are discussed along the investigation.

The planning of experiments and its subdivision in main groups of coals and chars, as well the main experimental parameters determined for each group of experiments to investigate the coal and char combustion behavior follow the sequence already described in Chapter 3. The next sections concern with fundamentals to calculate the global kinetic parameters and char reaction rate coefficients based on an assumption of a well stirred reactor.

4.2. Global kinetic formulation

The coal combustion reactivity is investigated upon the evolution on oxygen concentration measured by the potentiometric oxygen sensor during the coal sample combustion, assuming that the variation of oxygen concentration is only due to the oxygen consumption by the sample, in accordance to the oxygen balance method [Tappe, 2011, 2009; Lorentz and Rau, 1998], considering a well stirred reactor. These assumptions are to be

verified along the investigation by the global kinetic parameters determination, in which incorporate a combination of complex phenomena, volatiles combustion, the oxygen diffusion into the particle or through the film around particle (mass transfer control), as well as the coal chemical reaction rate at the surface or within the particle.

These behaviors are commonly investigated in details with the drop tube furnace, thermogravimetric analysis or entrained flow reactors. The ALVA 20 test facility was not designed to investigate the phenomena of the coal combustion reaction in separate. However, the global kinetic parameters can indicate the rate-controlling step of the coal combustion, as diffusion or kinetic control regimes [Lorentz and Rau, 1998], provided that the assumptions made in the physical modeling are coherent with the phenomena investigated.

The potentiometric oxygen sensor drawing views and how the Nernst equation (Eq. 4.1) is derived to calculate the oxygen concentration are described in Chapter 2.

The oxygen conservation equation is applied to a control volume drawn in projected view of cyclone combustion reactor, as depicted in Fig. 4.1a.

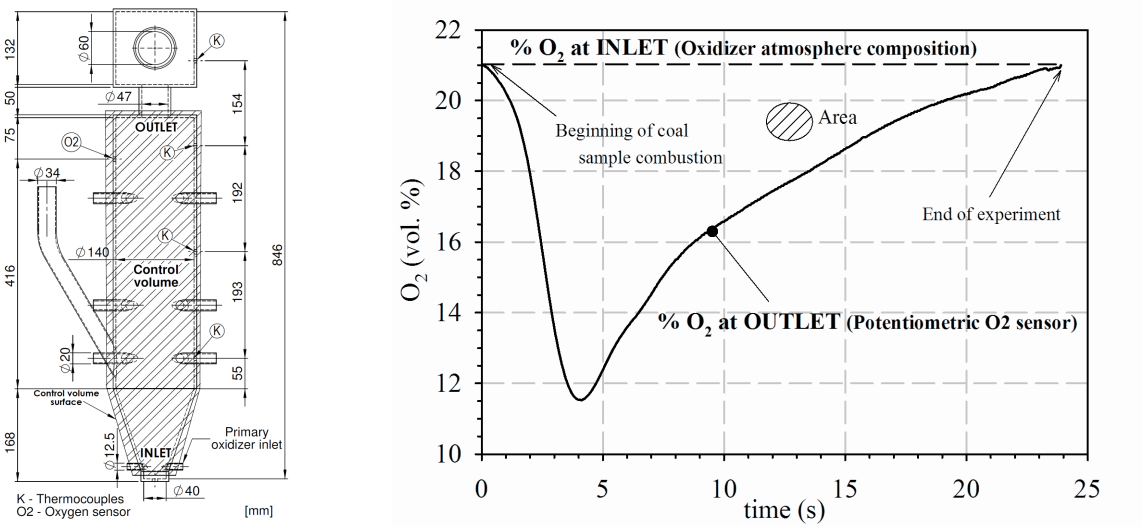

(a) (b)

Figure 4.1 - (a) Control volume for the oxygen conservation equation and (b) the oxygen concentration values at cyclone reactor inlet and outlet.

The inlet and outlet of control volume surface are also indicated in the drawing, and their corresponding positions depend on the measurement of oxygen concentrations. The value of oxygen concentration at the cyclone reactor inlet is provided by the knowledge of oxygen concentration composition in oxidizer atmosphere, whereas the value of oxygen concentration at the cyclone reactor outlet is provided by the measurement of potentiometric oxygen sensor installed at 75 mm of distance from the reactor outlet, assuming that there is no

spatial variation of oxygen concentration during the combustion of coal sample along the whole control volume of cyclone combustion reactor, hatched in the projected view.

Figure 4.1b shows where the values of oxygen concentration at inlet and outlet of cyclone reactors are attained in the oxygen concentration curve of coal sample combustion for the oxygen balance. The formulation developed is based on the variation of oxygen concentration along the combustion reaction registered by the solid electrolyte oxygen sensor.

The oxygen molar flow rate consumed during the combustion of a sample can be expressed in terms of gas combustion average temperature T, oxygen molar fraction f_{O_2} and pressure P, assuming a volumetric flow rate $\dot{V}$ and temperature within the reactor as a reference, applying the ideal gas relations. Thus, the amount of oxygen consumed during the combustion reaction of a sample $N_{O_2,cons}$ is the integral of the area above the oxygen molar fraction curve delimited by the inlet and outlet lines, as shown in Fig. 4.1b, and expressed by the following equation

$$N_{O_2,cons} = \left(P_{atm}\dot{V}/RT\right)\cdot\int_0^t \left(f_{O_2,in} - f_{O_2,out}\right)dt \tag{4.1}$$

The equation to describe the rate of the oxygen consumed during the combustion of a coal sample $\dot{r}_{O_2}$ is derived, assuming a homogeneous irreversible unimolecular reaction $A \xrightarrow{k_{eff}} \text{Products}$ [Levenspiel, 1999], in which the effective reaction rate constant k_{eff} takes into account the volatile and char combustion reaction rate constants. Upon these hypotheses, the global coal combustion reaction rate is derived experimentally based on the oxygen molar conversion rate dX_{O_2}/dt and initial oxygen concentration $C_{O_2,0}$ measurements, as follows

$$\left(-\dot{r}_{O_2}\right) = C_{O_2,0}\, dX_{O_2}/dt \tag{4.2}$$

The oxygen conversion X_{O_2} is the ratio of the amount of oxygen consumed for a given period to the total amount of moles of oxygen consumed on the combustion reaction, in molar basis, as shown in Eq. 4.3.

$$X_{O_2} = N_{O_2,cons}/N_{O_2,tot} \tag{4.3}$$

The coal combustion reaction rate attained experimentally $\dot{r}_{O_2}$ is fitted according to the mathematical relation defined by Eq. 4.4, in which takes into account the temperature and concentration dependent terms in k_{eff} and C_{O_2}, respectively, given by equations 4.5 and 4.6

$$\left(-\dot{r}_{O_2}\right) = k_{eff}\, C_{O_2}^{n} \tag{4.4}$$

where Arrhenius´ law is given by

$$k_{eff} = k_0\, e^{-E_A/RT} \tag{4.5}$$

where k_0 is the frequency or pre-exponential factor and E_A is the global activation energy. Applying the natural logarithmic in both sides of the Eq. 4.5, it is obtained the linearization equation of Arrhenius´ law in order to calculate the angular coefficient E_A/R for each temperature range of experiment work and obtain the global activation energy E_A, as follows

$$\ln k_{eff} = \ln k_0 - \left(E_A/RT\right) \tag{4.6}$$

and

$$C_{O_2} = C_{O_2,0}\left(1 - X_{O_2}\right) \tag{4.7}$$

Substituting the Eq. 4.7 into 4.4, yields the coal combustion reaction rate mathematical function to be fitted

$$\left(-\dot{r}_{O_2}\right) = k_{eff}\, C_{O_2,0}^{n}\left(1 - X_{O_2}\right)^{n} \tag{4.8}$$

The order of reaction n and the effective reaction rate constant k_{eff} are known as global kinetic parameters applied in the present work for coal sample combustion, and they are obtained by the Integral Method [Levenspiel, 1999]. It is important to mention that effective reaction rate constant k_{eff} also takes into account both the mass transfer and chemical reaction kinetic phenomena of the heterogeneous reactions that takes place in the combustion of solids [Lorentz and Rau, 1998]. As the reaction rate constant k is a term dependent of temperature, low variation of k_{eff} values with temperature result in low values of global activation energy, in which the diffusion of oxidant into the pores coal particles and/or through the particle boundary layer can be controlling the global coal combustion rate. This investigating is performed in section 4.3.

By combining the equations 4.4 and 4.8, and reorganizing the terms before integrating them, the following expression is obtained.

$$dX_{O_2} \big/ (1 - X_{O_2})^n = -k_{eff.} C_{O_2,0}^{(n-1)} \, dt \tag{4.9}$$

Integrating Eq. 4.9, assuming first order reaction [Tappe, 2011; Lorentz and Rau, 1998] leads to

$$\ln\left(1 - X_{O_2}\right) = -k_{eff} \, t \tag{4.10}$$

Coal reactivity assessment by means of global kinetic parameters is calculated based on the sequence of curves presented on Fig. 4.2.

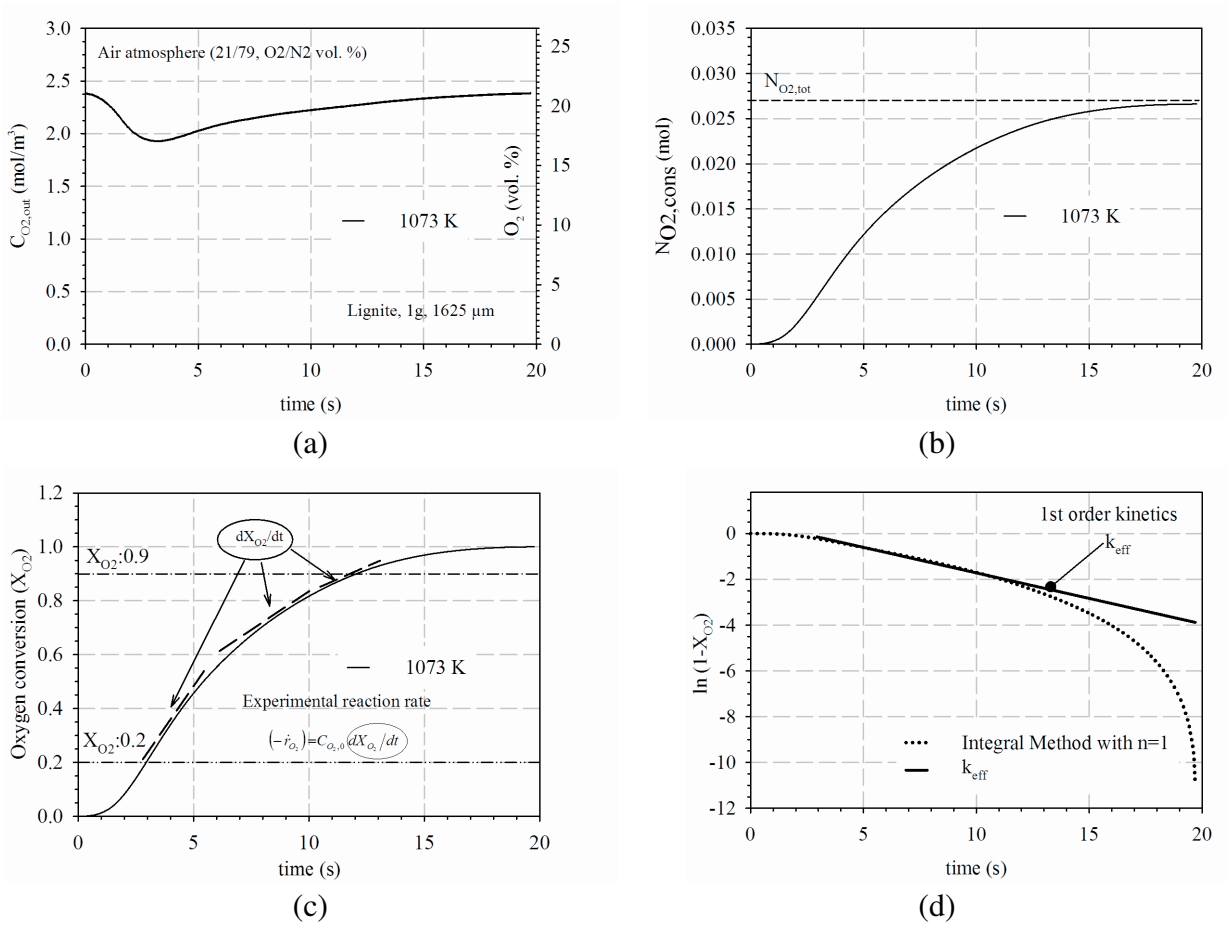

Figure 4.2 - Measured and calculated results for lignite coal air combustion at 1073 K. (a) Evolution of oxygen concentration; (b) oxygen consumption; (c) oxygen conversion; and (d) effective reaction rate constant k_{eff}.

Fig. 4.2a is the starting point, on which the oxygen concentration curve is obtained at 1073 K under air conditions for lignite (LTBK) coal. Other variables are determined and plotted from that curve, as oxygen consumption, oxygen conversion and finally the effective reaction rate constant, showed in Fig. 4.2b, 4.2c and 4.2d respectively. This sequence of plots is applied for all experiments described in Chapter 4 to obtain the coal global kinetic parameters.

Figure 4.3 joins the plots of Fig. 4.2c and 4.2d in the same plot to show the considerations involved in determining the range of fitting to attain the k_{eff} values. The range of oxygen conversion within 0.2 and 0.9 is preferred to avoid the regions of the experimental data near the beginning of conversion in which $\ln(1-X_{O_2}) \to 0$ and the end of conversion in which $\ln(1-X_{O_2}) \to \infty$, influenced also by the stabilization stage of oxygen sensor probe in the latter. After the elapsed time of coal sample conversion defined at $X_{O_2} = 0.9$, the oxygen conversion rates start to be influenced by the behavior of oxygen sensor stabilization towards the initial oxygen concentration of oxidizer stream. Therefore, the best fit attained for all the experiments is achieved for oxygen molar conversion within a range of 0.2 and 0.9 with reaction order of 1.0.

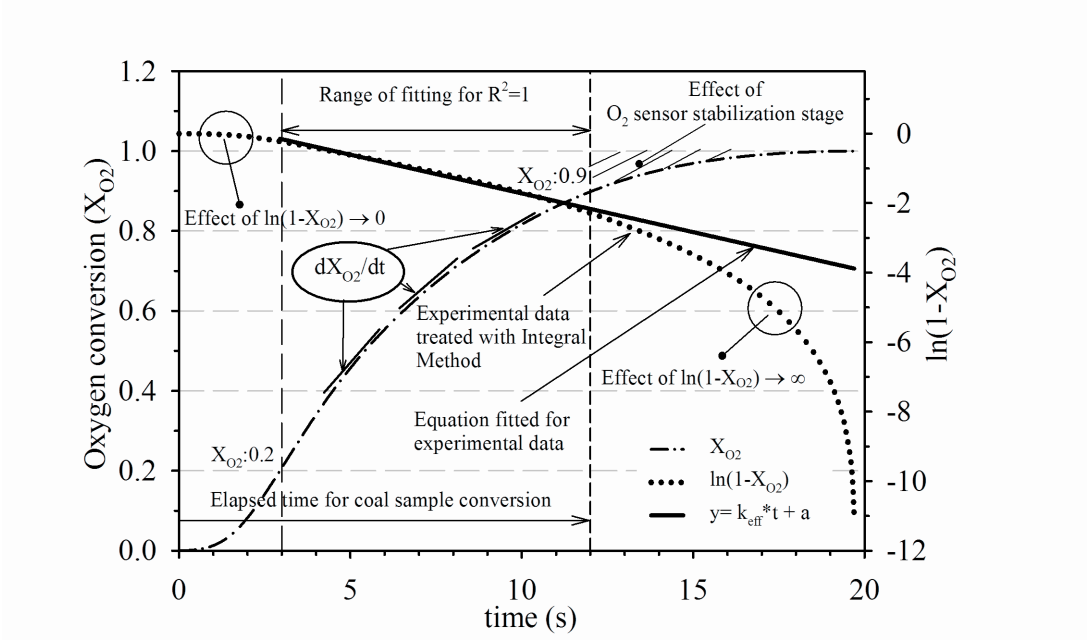

Figure 4.3 - Considerations for the determination of k_{eff} fitting range.

The Fig. 4.3 is an important contribution for Integral Method applied to determine the global kinetic parameters of coal combustion with potentiometric oxygen sensor, because

there is no reference in previous works [Tappe, 2011 and 2010; Krüger, 2010; Lorentz and Rau, 1998] about the effects involved in k_{eff} calculation with oxygen sensor measurement. In literature review [Smith,1982; Young and Smith, 1981; Hamor et al., 1973], the char reaction rate kinetic parameters are also calculated not taking into account the initial and end stages of char conversion and it is discussed in the section of char modeling coefficients.

The hypotheses presented in this section used to calculate the coal global kinetic parameters are summarized as follows

- Well stirred reactor, i.e. there is no spatial variation of oxygen concentration in control volume of the combustion cyclone reactor, depicted in Fig. 4.1a. It is assumed that the measurement of oxygen concentration by the potentiometric oxygen sensor is not dependent of its position within the reactor. This hypothesis is tested along the present work.
- Heterogeneous and homogeneous reactions are modeled by an irreversible unimolecular first order reaction, i.e. $\mathrm{A} \xrightarrow{k_{eff}} \mathrm{Products}$, where the effective reaction rate constant k_{eff} takes into account the volatiles and char combustion reaction rate constants.
- The coefficient reaction rates of main surface mechanisms (k_1, k_2 and k_3) with coal particle under air and oxy-fuel atmospheres, i.e. $C + 1/2\mathrm{O}_2 \xrightarrow{k_1} CO$, $C + CO_2 \xrightarrow{k_2} 2CO$ and $C + H_2O \xrightarrow{k_3} CO + H_2$ can not be determined, because the experimental setup is not equipped with CO sensor measurement within the cyclone combustion reactor. The influence of CO_2 and H_2O concentrations in oxy-fuel atmospheres on the coal combustion reactivity is evaluated by means of k_{eff} results and oxygen concentration curves. The influence of global reaction $C + \mathrm{O}_2 \xrightarrow{k} CO_2$ on coal combustion is investigated in the char modeling, described in section 4.3.
- The oxidizer volumetric flow and global kinetic parameters are calculated for an average gas combustion temperature measured by three thermocouples installed along the cyclone combustion reactor height, as described in Chapter 2. It is noteworthy to mention that the coal particle temperature is recommended to calculate the global kinetic parameters rather than gas combustion temperature, but the cyclone combustion reactor was not designed to allow the measurement of particles temperature.
- The cyclone combustion reactor is an open system operating under constant atmospheric pressure.

4.3 Char combustion reaction rate coefficients

The derivations of the equations presented in this section is based on the work of Smith, 1982, for the combustion modeling of pulverized char particles on polydisperse suspension, submitted to a plug flow. These set of equations are applied for the combustion of LTBK char 900, since its coal matrix after the devolatilization at 900 ^{o}C has 94% in mass of carbon, as described in Chapter 3. Thus, this char is suitable for assessing the char combustion reactivity and for investigating what it is the regime that controls the overall combustion reaction rate, i.e. diffusion and kinetic regimes.

In the present investigation, the focus is on the overall combustion reaction rate looking at the global form of reaction $C + O_2 \rightarrow CO_2$, instead of the intrinsic reaction rate. However, it is noteworthy to mention that the overall reaction rate depends on the diffusion of oxygen and the reactions in the coal matrix pores, and the determination of the intrinsic global rate coefficients for char gasification and combustion depends on the knowledge of pores structure, evolution of specific internal surface area of particle during carbon conversion, as well the surface mechanisms reactions, as carbon-carbon dioxide reaction $C + CO_2 \rightarrow 2CO$, carbon-steam reaction $C + H_2O \rightarrow CO + H_2$, reaction $C + 2H_2 \rightarrow CH_4$, and reaction $C + O_2 \rightarrow CO_2$ [Laurendeau, 1978; Smith, 1977; Batchelder and Busche, 1953].

The assumption of well stirred reactor is maintained to calculate the oxygen conservation rate dX_{O_2}/dt, following the same sequence of plots shown in Fig. 4.2a, 4.2b and 4.2c. The fitting method for calculate the effective reaction rate constant is not applied in this section, since new set of equations are developed to investigate in separate the kinetic $1/k_c$ and diffusion $1/h_m$ resistances on overall combustion reaction rate, as depicted in Fig. 4.4.

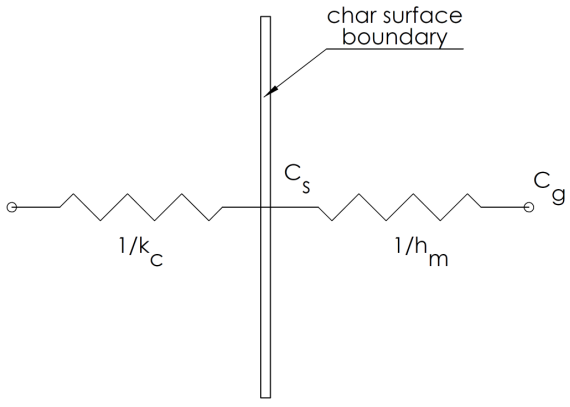

Figure 4.4 - Schematic of the resistances for the overall char combustion rate modeling.

From mass-balance considerations at the char surface boundary, the actual (observed) rate of combustion of carbon $\dot{r}_{a,c}$ per unit external surface area of the particle is given by

$$\dot{r}_{a,c} = \underbrace{h_m\left(C_g - C_s\right)}_{diffusion\ \ rate} = \underbrace{k_c\left(C_s\right)^{\,n}}_{kinetic\ \ rate} \tag{4.11}$$

where C_s is the oxygen concentration at the outer surface of the particle, C_g is the oxygen concentration in the bulk gas, k_c is a chemical rate coefficient of apparent order n in C_s, and h_m is the mass transfer coefficient.

In order to calculate the rate of combustion of carbon $\dot{r}_{a,c}$ for the experimental data, the following expression is required

$$\dot{r}_{a,c} = \frac{dX_{O_2}}{dt}\frac{d_o\rho_o}{6}\frac{1}{(1-0.94X_{O_2})^{2/3}} \tag{4.12}$$

The char diameter *d* equation in terms of oxygen conversion X_{O_2} and initial diameter d_o is given by the following relation, assuming that the particles are modeled as spheres and the char content matter is mostly carbon. The derivation of equations 4.12 and 4.13 is shown in Appendix 4.A.1.

$$d = d_o\left(1-0.94X_{O_2}\right)^{1/3} \tag{4.13}$$

The Eq. 4.13 is applied for particles with a homogeneous structure of pores, considered small if compared with particle dimension [Smith, 1982]. The coefficient applied to the oxygen conversion X_{O_2} is related to the carbon content (in mass fraction) in LTBK char 900, after the devolatilization.

The LTBK char density ρ_o is 0.7 g/cm^3, according to literature [Smith, 1971]. Researches show that the structure of a char is strongly dependent on coal rank and it is certainly associated with thermoplastic properties of coal during heating. For low-rank coal structures such as inertinite, there is a reduction of 10% of particle mean diameter after the devolatilization, generating relatively dense chars [Yu et al., 2007]. For this reason the initial LTBK char particle diameter d_o is 1463 μm for char modeling equations.

In order to eliminate the unknown concentration C_s in Eq. 4.11 and calculate the chemical rate and mass transfer coefficients, the following sequence of equations is derived.

Firstly, as the ratio χ of the surface chemical reaction rate $\dot{r}_{a,c}$ to its maximum combustion rate $\dot{r}_m$ can never be greater than 1, yields

$$\chi = \dot{r}_{a,c} / \dot{r}_m \tag{4.14}$$

where $\dot{r}_m$ is the maximum possible combustion reaction rate, found when chemical reactions are so fast that $C_s \to 0$, and the burning rate is controlled solely by mass transfer of oxygen to the particle, as follows

$$\dot{r}_m = h_m C_g \tag{4.15}$$

Substituting the equations 4.14 and 4.15 into Eq. 4.11 and rearranging the terms, yields the Eq. 4.16 for calculating the overall combustion reaction rate without the need to know the oxygen concentration at char surface. The derivation of this equation is found in Appendix 4.A.1.

$$\dot{r}_{a,c} = C_g^n (1-\chi)^n k_c \tag{4.16}$$

4.3.1 Mass transfer coefficient, h_m

To derive the mass transfer coefficient, the following equations are required [Young and Smith, 1981; Laurendeau, 1978], as follow

The mass transfer coefficient h_m can be obtained from Sherwood Number *Sh* correlations. For a sphere approximation, *Sh* is

$$Sh = \frac{h_m d}{D_{O_2}} = 2\left(1 + c\,\mathrm{Re}^{1/2} Sc^{1/3}\right) \tag{4.17}$$

where *Re* and *Sc* are the Reynolds and Schmidt numbers respectively. Typical values for *c* are $0.30 < c < 0.35$, and Reynolds number is based on particle diameter d, gas velocity u_g and

gas kinematic viscosity v. At high temperatures, a reasonable approximation is $Sc \approx \Pr \approx 1$, thus the Eq. 4.17 becomes

$$Sh = \frac{h_m d}{D_{O_2}} \approx 2c\,\mathrm{Re}^{1/2} \tag{4.18}$$

The binary diffusion coefficient can be calculated by the following correlation

$$D_{O_2}(T,P) = D_{O_2}(T_o,P_o)\left(\frac{T}{T_o}\right)^{1.75}\left(\frac{P}{P_o}\right) \tag{4.19}$$

where the diffusion coefficient for oxygen in nitrogen is $D_{O_2} = 0.207$ cm^2/s, at 300 K and 1 atm [Smith, 1971; Poling et al., 2001]. In order to calculate D_{O_2} is assumed an average boundary layer temperature T, between the particle temperature T_p and the surrounding gas temperature T_g. The diffusion of O_2 into CO_2 gas is $D_{O_2-CO_2} = 0.168$ cm^2/s at 300 K, 1 atm [Yu and Zhang, 2009; Rohling, et al., 2007].

Instead of considering a stagnant atmosphere or pulverized char particles $(d \le 100\,\mu m)$, assumptions generally found in literature, the present work uses relative velocity between gas and particle different than zero $(u_g \neq 0)$, following the reference of magnitudes found in literature for fluidized bed reactor [Adánez and Abánades, 1992], since there is no such data available in literature for this type of cyclone combustor reactor tested in ALVA 20, as verified in Gupta and Lilley, 1984.

Thus, after rearranging Eq. 4.17 and Eq. 4.19, the mass transfer coefficient can be expressed by the following relationship,

$$h_m = 2c\Lambda D_{O_2}(T,P)\left(\frac{u_g}{\nu\, d}\right)^{1/2} \tag{4.20}$$

Λ is defined as the gravimetric stoichiometric coefficient, given by the expression

$$\Lambda = M_c / (v_g M_g) \tag{4.21}$$

where v_g is the molar stoichiometric coefficient for the reactant gas and M_c / M_g is the molecular mass ratio of carbon to reactant gas. For combustion, it is seen that carbon monoxide is the primary product at high temperature. Hence, the surface reaction is usually assumed to be $C + 1/2O_2 \rightarrow CO$ $(\Lambda = 3/4)$ rather than $C + O_2 \rightarrow CO_2$ $(\Lambda = 3/8)$, according to literature review [Young and Smith, 1981; Laurendeau, 1978].

Combining equations 4.15 and 4.20, the following relationship is obtained for the maximum oxygen mass transfer rate, when the chemical reaction is sufficiently fast to consume all the oxygen that reaches the char surface, i.e. $C_s \rightarrow 0$.

$$\dot{r}_m = 2c\Lambda D_{O_2}(T,P)\left(\frac{u_g}{\nu d}\right)^{1/2} C_g \tag{4.22}$$

The diffusion rate coefficient $R_{a,d}$ can be calculated by the following relationship

$$R_{a,d} = \dot{r}_m / p_g \tag{4.23}$$

where p_g is the oxygen partial pressure in the gas remote from the particle (bulk).

4.3.2 Chemical rate coefficient, k_c

The chemical rate coefficient k_c can be calculated by means of $R_{a,c}$, expressed as the rate of carbon combustion per unit external surface area of the particles, in relation to the oxygen partial pressure at the external surface.

$R_{a,c}$ is calculated from the measured rate $\dot{r}_{a,c}$, the oxygen partial pressure in the "bulk" p_g, the global reaction rate coefficient R_a, the diffusion reaction rate coefficient $R_{a,d}$ and the apparent order of reaction *n*, according to the Eq. 4.24, and its derivation is found in Appendix 4.A.1.

$$R_{a,c} = \left(\frac{R_a R_{a,d}}{R_{a,d} - R_a}\right)^n (\dot{r}_{a,c})^{1-n} \tag{4.24}$$

where

$$R_a = \dot{r}_{a,c} / p_g \tag{4.25}$$

The apparent order of surface reaction rate n was taken as 0.5, which gives a true order of intrinsic surface reaction m equal to 0, since the apparent order of reaction is given by the following relationship $n = (m+1)/2$, according to literature [Smoot and Smith, 1985]. The best fit for the relation between $R_{a,c}$ and particle temperature T_p is achieved with $n = 0.5$ [Young and Smith, 1981].

4.3.3 Char particle temperature, T_p

For the reaction of a gas with a solid, the relevant temperature is the one of the solid. It has been shown theoretically [Field, 1969] that the temperature of a burning pulverized-coal-fired particle T_p can be appreciably higher than that of the surrounding gas T_g, i.e. 300 K approximately. Since no means of measuring T_p were available for the experiments described here, values were calculated from the steady-state heat balance for pulverized coal particles [Field, 1969], equating the heat lost by radiation and conduction to the heat released at the surface of the particles. The heat released at the surface may be calculated from the measured reaction rate $\dot{r}_{a,c}$, provided that the mechanism of combustion is known. Thus, for a sphere, the equation to be solved for T_p is

$$\dot{r}_{a,c} H - \frac{2k_g (T_p - T_g)}{d} - \varepsilon\sigma(T_p^4 - T_w^4) = 0 \tag{4.26}$$

where k_g is the gas thermal conductivity, expressed as arithmetic mean of particle and gas temperatures, ε is the particle emissivity, taken as unity, σ is the Stefan-Boltzmann constant, and T_w is the wall reactor temperature. T_w is estimated as an average of the three thermocouples measurements installed at the cyclone reactor heating mantel.

Solution of Eq. 4.26 requires the knowledge of the heat of reaction H, whose bounds are 9797.112 J/g (2340 cal/g) for carbon oxidation into CO, and 3307.572 J/g (7900 cal/g) for carbon oxidation into CO_2. It is assumed that CO is the primary oxidation product [Field, 1969; Smith 1971], and that CO burns to CO_2 in the gas phase, after some distance from the particle and therefore contributes to T_g, but not directly to T_p. According to Field, 1969, values of calculated T_p, assuming *H*=3307.572 J/g, differ from those measured by Smith, 1971 at 700 K.

Also, according to Yang, J.C., 1993, the temperature of the coal particle, T_p, can be estimated by using a lumped-capacitance (i.e., negligible internal thermal resistance within the particle) heat transfer model if the Biot number $\left(Bi = h_g\, L_c / k_p\right) \leq 0.1$, where h_g is the gas heat transfer coefficient in $W.m^{-2}.K^{-1}$, L_c is the characteristic length, defined as the volume/area ratio, (for a sphere of radius r_p, $L_c = r_p / 3$) and k_p is the thermal conductivity of the coal particle in $W.m^{-1}.K^{-1}$. The condition $Bi \leq 0.1$ can be satisfied if the coal particle is very small or if the thermal conductivity of the coal particle is very large.

In the present work, for particle mean diameter of 1625 μm, the Biot number calculated is greater than 0.1, as shown in Appendix 4.A.1, for a specific correlation of convective heat transfer coefficient applied in a packed bed reactor [Rindels at al., 1991]. As verified with the correlation, the great uncertainty for the calculation of the particle temperature in the energy balance equation is the convective heat transfer coefficient, which depends on the gas velocity, the voidage of packed bed, i.e. the relative amount of space left between the particles that are burning together (packed), and the shape factor of the coal particles. Due to these uncertainties, the particle temperature is calculated in steady state for a first approach to investigate the char combustion rate coefficients.

4.3.4 Assumptions for the calculus and analysis of char combustion rate coefficients

Char combustion rate coefficients attained were based on the oxygen concentration measurements, and the calculation was performed with the aid of the EES software, attached in Appendix 4.A.2.

Due the limitation of the number of variables in the software (12000), the time step of oxygen concentration curve was changed from 0.05 to 0.25 s without impact on the result accuracy. The gas properties, as kinematic viscosity, thermal conductivity and density were calculated with the EES database weighted by the respective molar fractions of the mixture. Equations for the viscosity and thermal conductivity of gas mixtures at low pressure were obtained in Poling et al., 2001.

The cyclone reactor wall average temperature T_w values are 1123, 1246 and 1347 K for three 3 of gas temperatures, i.e. 1073, 1173 and 1273 K, respectively.

The temperature values used to calculate the particle temperature with Eq. 4.26 was taken from the temperature curve, measured at the cyclone reactor bottom. As the time step to

measure the gas temperature is 5 s, the gas temperature curve was fitted by a polynomial function. According to literature [Hamor et al., 1973; Smith, 1971; Field, 1969] the analysis is based on the relation $R_a/R_{a,d}$ to check if the char combustion reaction rate is controlled by kinetic or diffusive regimes, following the criteria based on the magnitude of char combustion reaction coefficients, i.e. for ratio values $R_a/R_{a,d} < 0.5$ the control is kinetic, whereas for ratio values $R_a/R_{a,d} > 0.5$ the control is diffusive. The overall combustion reaction rate R_a magnitude determines the influence of chemical reaction in relation to the maximum oxygen mass transfer rate $R_{a,d}$, i.e. the values attained experimentally for R_a that have more than 50% in magnitude of the values calculated for $R_{a,d}$ result in chemical reaction rate coefficients greater than the diffusion reaction rate coefficients (under the same apparent order of surface reaction). The physical sense of this is that it is useless to calculate values of $R_{a,c}$ from any measurement that is predominantly diffusion controlled. This analysis is shown by means of plots in the section 4.4.2.

The superficial gas velocity magnitudes u_g (the flow gas velocity in relation to the particles velocity) used in the present investigation to the calculation of diffusion reaction rate coefficient were attained in literature [Adánez and Abánades, 1992], as a starting point. The u_g values in literature lies between 0.8 and 2.0 m/s for lignite coal with 1.0 mm particle mean diameter, simulated for a fluidized bed reactor.

The determination of the superficial gas velocity depends on the knowledge of the velocity magnitudes within the cyclone reactor and the shape factor of the particle. As the measurement of flow field within the cyclone reactor is out of the scope of this work, and it would require new design of the cyclone combustion reactor and instrumentation, the gas superficial velocity values found in literature are used as reference for the first approach of the calculation of char combustion reaction rate coefficients for particles diameters greater than 100 μm.

The flowchart of Fig. 4.5 summarizes the sequence of calculus presented in this section for attaining the char combustion reaction rate coefficients and assesses what is the regime that controls the combustion reaction rate. As observed through the analysis of flowchart, the variables particle temperature T_p and superficial gas velocity u_g influence the determination of diffusion and chemical reaction rate coefficients, whereas for the overall combustion reaction rate R_a these variables (T_p and u_g) are not taken into account.

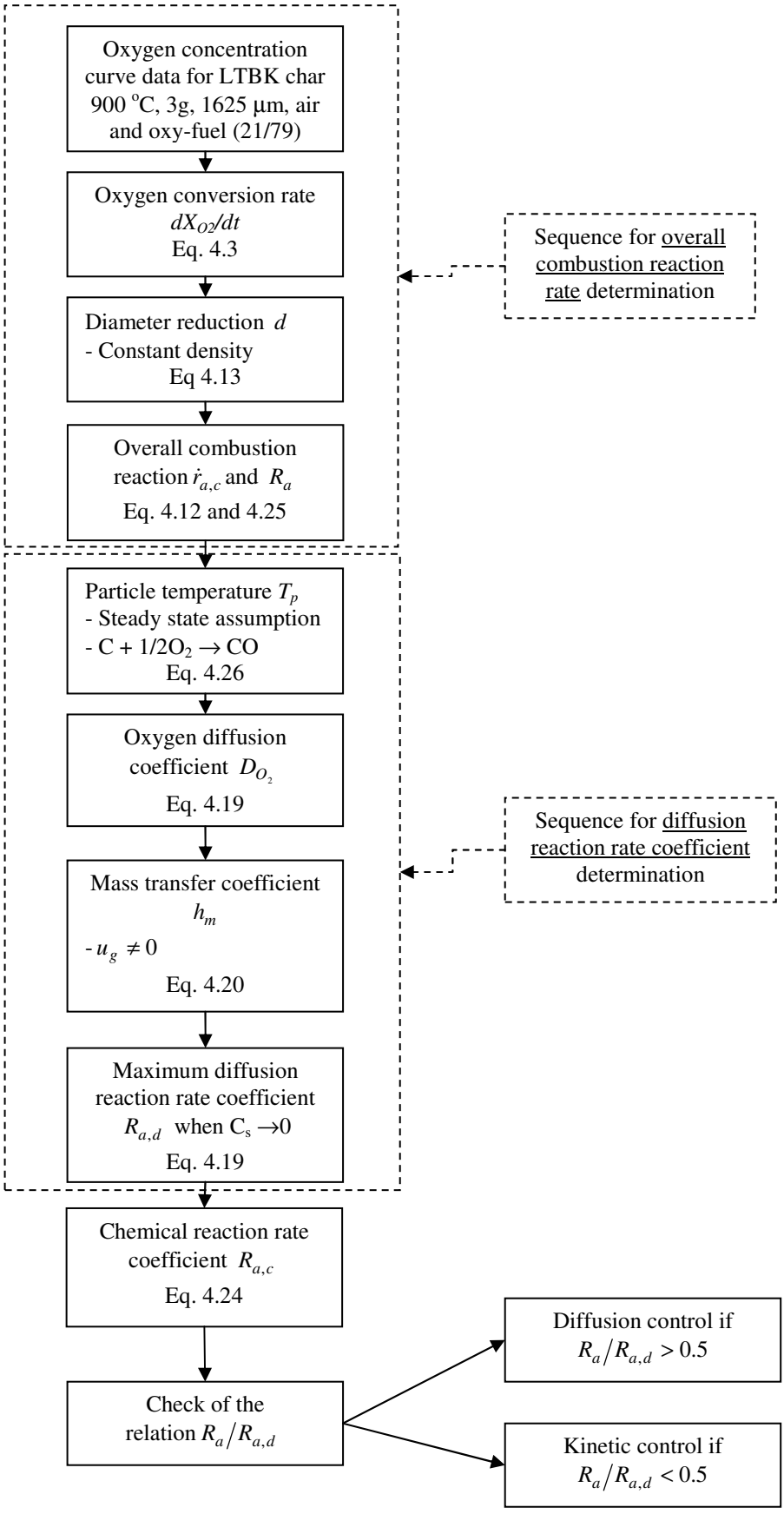

Figure 4.5 - Flowchart of the sequence for the calculation of char combustion reaction rate coefficients.

4.4 Results and discussion

The analysis of the results is separated in two subsections, in which firslty it is discussed the results obtained for effective reaction rate constants, upon which is assessed the coal and char reactivity, and in the sequence it is discussed the char combustion reaction rate coefficients calculated for LTBK char 900.

4.4.1 Assessment of coal and char reactivity with global kinetic parameters

This subsection summarizes the most relevants results of effective reaction rate constants k_{eff} for coals and chars burned under air and oxy-fuel atmospheres. The results are arranged in box plots in order to compare the k_{eff} values between the coal and chars burned under the same and different oxidizer atmospheres. The box plot width shows the difference between the low and high values of k_{eff} and the median value between them, resulting of the increase of gas temperature within the cyclone combustion reactor at three average values (1073, 1173 and 1273 K). When the k_{eff} values decrease with the increase of gas average temperature, the box plot is identified. The graphs of effective reaction rate constants for each coal and char and oxidizer atmosphere summarized in the box plots are found in Appendix 4.A.4. The effective reaction rate constants are calculated from the oxygen concentration curves selected for each coal and char sample and experimental conditions (oxidizer atmosphere, gas combustion temperature, sample mass, particle mean diameter and replicate) found in Appendix 4.A.3, and the analysis and discussion of the oxygen concentration curves are done in Chapter 3 with DoE methodology. The new position of oxygen sensor is tested only for air atmosphere (Fig. 4.6) for reasons explained in Chapter 3.

The plot of Fig. 4.6 shows the values of effective reaction rate constants k_{eff} for coals and chars burned under air atmosphere conditions for two particles mean diameters (312 and 1625 μm). Analyzing the results for coals with 1g mass and particles mean diameter of 1625 μm, it is observed that the median values of effective reaction rate constants of coal with high content of ash (Leão and Bonito) are larger than coal with low content of ash (LTBK) with greater variation of this last one than the other two coals. It allows to conclude that for coal samples with 1g mass under air atmosphere conditions and within this range of gas combustion temperature, the effective reaction rate constants calculated are not coherent with the values expected according to coal composition to evaluate the coal reactivity, due to the influence of swirling flow with its advective and difusive terms on the combustion reaction

rates of coal samples, that are investigated with the new oxygen sensor position to be discussed in the sequence.

Discussing the results for the coal and char with 3g mass with oxygen sensor installed at the original position within the cyclone reactor, it is observed that median values of effective reaction rate constants are greater for coal and char, respectively, with high content of volatiles and carbon (LTBK coal and LTBK char 900) than coal and char with low content of volatiles and carbon (Leão coal and Leão char 730). For Leão char devolatilized at 730 ^{o}C the variation of k_{eff} with gas combustion temperature is greater than other coals and chars, which indicates that the combustion reaction rate is controlled by the kinetic regime for char with high content of ash under air atmosphere conditions.

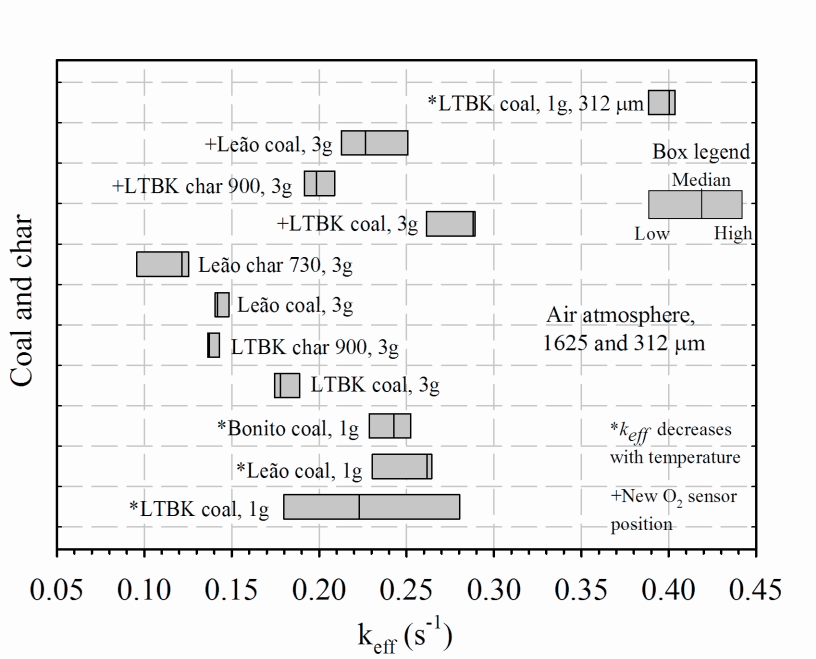

Figure 4.6 - Effective reaction rate constants for coal and char under air atmosphere.

Analyzing the results for coal and char with 3g mass with oxygen sensor installed at new position within the cyclone reactor, i.e. at half radius of cyclone main section, the effective reaction rate constants increase for all coals compared with the values attained for same mass with the oxygen sensor at original position (near the reactor wall). The reactivity of coals with high content of volatiles is greater than LTBK char devolatilized at 900 ^{o}C. However, the influence of the increase of gas combustion temperature is greater in this new position of oxygen sensor for all coals and char than that observed in original position. These results allow to conclude that position of oxygen sensor affects the effective reaction rate constants, due to the influence of the swirling flow (with advective and diffusive terms) on the oxygen concentration measurements which promotes a better recirculation of chemical

species near the centre of cyclone reactor than that near the reactor wall, increasing the effect of gas combustion temperature on the coal reactivity. It is observed that for coals with 1g mass, the k_{eff} results are within the same range for those coals with 3 g mass, which indicate that coal samples with low mass are significantly influenced by the position of oxygen sensor within the cyclone reactor, because same coals with different masses should not have different reactivities.

Analyzing the results for LTBK coal with 1g mass and particles mean diameter of 312 μm, it is observed that the median values of effective reaction rate constants are the highest attained under air atmosphere conditions within this group of coals and chars analyzed for particles with 1625 μm mean diameter. This result allows to conclude that the highest superficial area of sample particles increase the coal reactivity, but the influence of gas combustion temperature is reduced on k_{eff}, if compared with the results attained for LTBK coal with 1g mass and particle diameter of 1625 μm. The small variation of k_{eff} for 312 μm in comparison with that attained for 1625 μm for the same coal and mass is due the influence of the control regime of coal combustion, in which for the coal with small particle mean diameter and high reactivity the predominance can be the diffusion of oxidant through the boundary layer formed around the coal particle. However, the influence of swirling flow on the results of the combustion of coal particles with small mean diameter must be taken into account and investigated with new oxygen sensor position in further experiments.

The plot of Fig. 4.7 shows the values of effective reaction rate constants k_{eff} for coals and chars burned under oxy-fuel atmosphere conditions (21/79, i.e. O_2/CO_2 in % vol.).

Analyzing the results for coals with 1g mass, it is observed that the median values of effective reaction rate constants of coals with high content of carbon and volatiles (LTBK and Leão) are larger than coal with low content of carbon and volatiles (Bonito), showing that under oxy-fuel with 79% CO_2 (in vol.) the coal reactivity is influenced by the coal composition.

This same behavior and analysis can be extended for coals and chars with 3g mass, in which Leão char devolatilized at 730 ^{o}C has the lowest k_{eff} of the group. However, greater variation of effective reaction rate constants are observed for LTBK char 900 which indicates that the char combustion reaction rate is controlled by the kinetic regime, increasing its reactivity with the increase of gas combustion temperature, separated by the volatiles combustion influence.

The difference between the reactivity of the same coals with different masses is probably due to the greater influence of swirling flow on the coal combustion for samples with 1g mass than that observed for samples with 3g mass, as verified under air atmosphere conditions. The new position of oxygen sensor under oxy-fuel atmosphere could not be tested by the reasons explained in Chapter 3. However, there is a trend observed for oxy-fuel atmosphere for both masses, in which the coal reactivity is highest for coal with high content of carbon and volatiles, even with the decrease of effective reaction rate constants with the increase of gas combustion temperature for the char and coals showed in the box plots.

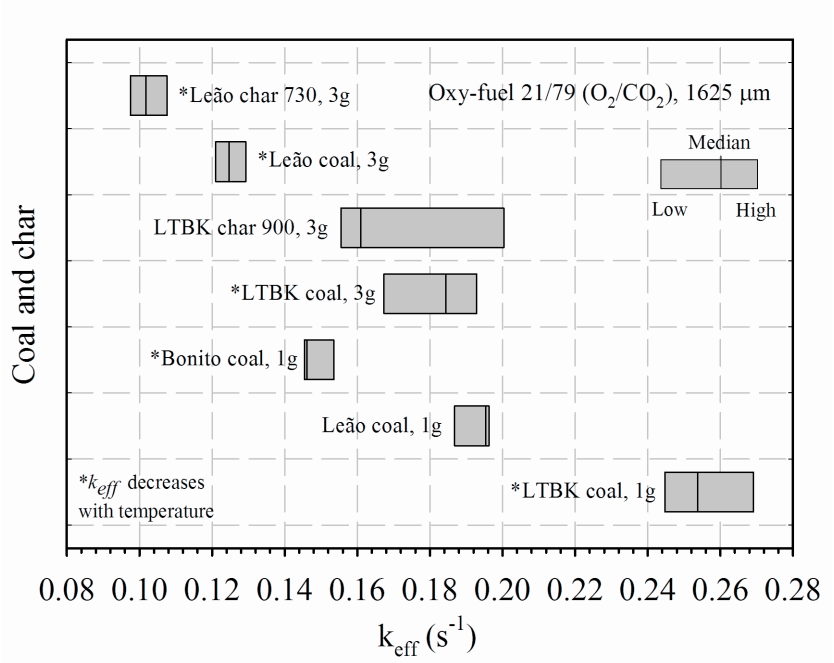

Figure 4.7 - Effective reaction rate constants for coal and char under oxy-fuel atmosphere 21/79 (O_2/CO_2).

The plot of Fig. 4.8 shows the values of effective reaction rate constants k_{eff} for coals Bonito, Leão and LTBK burned under oxy-fuel atmosphere conditions (30/70, i.e. O_2/CO_2 in % vol.), including water vapor concentrations in 10, 20 and 30% only for LTBK coal.

Analyzing the coals Bonito, Leão and LTBK burned under oxy-fuel 30/70, it is observed a trend, in which median values of effective reaction rate constants are larger for coals with high content of carbon and volatiles (LTBK and Leão) than for coals with low content of carbon and volatiles (Bonito). The variation of effective reaction rate constant k_{eff} with the increase of gas temperature for Bonito coal is the largest in the group under oxy-fuel 30/70, indicating that the coal combustion reaction rate is controlled by the kinetic regime. For LTBK coal, the effect of temperature under oxy-fuel 30/70 on coal reactivity is the

smallest in the group and this results can be influencing by the oxygen sensor position within the cyclone reactor, requiring further investigations with the oxygen sensor in new position, as tested for Fig. 4.6, and with the increase of the sample mass.

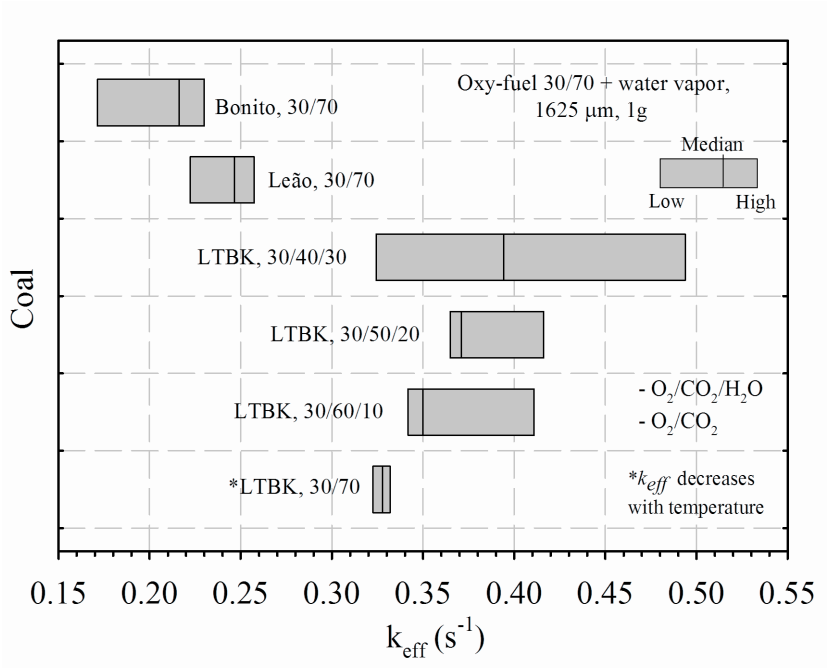

Figure 4.8 - Effective reaction rate constants for coal under oxy-fuel atmospheres 30/70 (O_2/CO_2) and water vapor 30/60/10, 30/50/20, 30/40/30 ($O_2/CO_2/H_2O$).

For oxy-fuel atmospheres with water vapor concentration (30/60/10, 30/50/20 and 30/40/30), it is noted that the median values of effective reaction rate constants of LTBK coal is greater under oxy-fuel with high water vapor concentration than that with low water vapor concentration, and the gas combustion temperature has an important role in increasing the coal reactivity, indicating that the coal combustion is controlled by the kinetic regime. However, the results for LTBK coal under oxy-fuel with water vapor concentration need to be tested with new oxygen sensor position, because the analysis of oxygen concentration curves with DoE in Chapter 3 shows that higher oxygen concentrations are attained under oxy-fuel 30/60/10 than that under 30/50/20 and 30/40/30, indicating greater coal reactivity in the first than in the latter two.

The plot of Fig. 4.9 aims to compare the effective reaction rate constants k_{eff} between oxidizer atmospheres for the same coal and verify what is the most influenced oxidizer atmosphere on the coal reactivity. Analyzing the results for LTBK coal, it is observed through the median values of effective reaction rate constants that coal reactivity increases with the decrease of CO_2 concentration in oxy-fuel atmosphere.

Discussing the results for Leão coal, it is observed through the median values of effective reaction rate constants, that the coal reactivity under air atmosphere is greater than under oxy-fuel 30/70, whereas the coal reactivity under oxy-fuel 21/79 is the lowest of the group. This same behavior verified for Leão coal is also observed for Bonito coal.

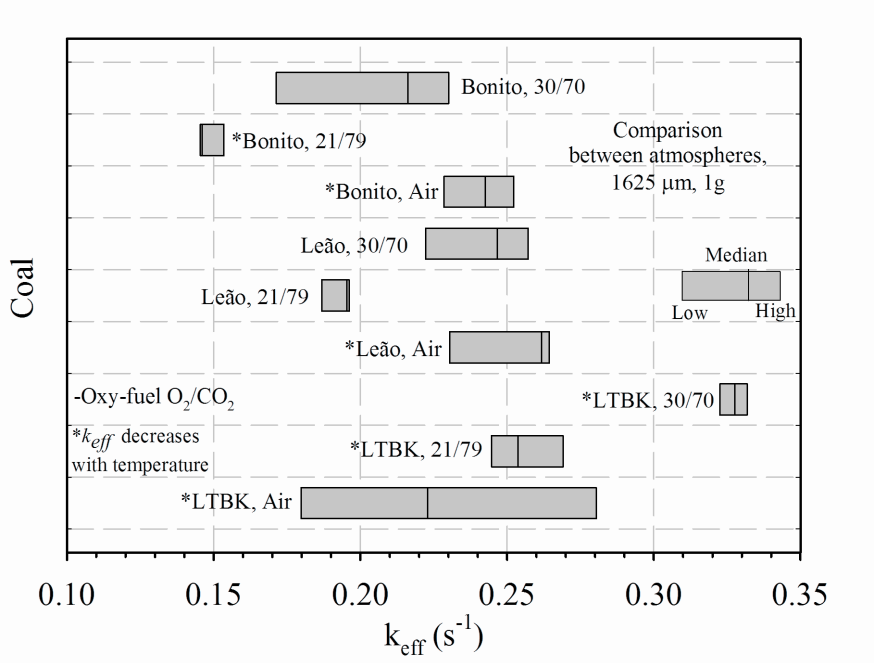

Figure 4.9 - Comparison of effective reaction rate constants for coal between oxy-fuel (21/79, 30/70) and air atmospheres.

From the analysis of effective reaction rate constants calculated under the assumptions for the physical model defined in section 4.2, the results of box plots of Fig. 4.9 allow to conclude that the coal reactivity increases with the decrease of CO_2 concentration in oxy-fuel atmospheres. However, these results are not coherent with the analysis of oxygen concentration curves performed in Chapter 3, in which highest variations of oxygen concentration are attained for oxy-fuel with 79% CO_2. The k_{eff} modeling can be changing the nature of phenomena observed in the oxygen concentration curves.

The plot of Fig. 4.10 compares the effective reaction rate constants k_{eff} only between air and oxy-fuel 21/79 atmospheres for coal and char with 3g mass. Analyzing the results for LTBK coal and char devolatilized at 900 ^{o}C, it is observed through the median values of effective reaction rate constants that coal reactivity increases under oxy-fuel atmosphere with 79% CO_2 (in vol.), and the influence of temperature is higher in LTBK char than that in LTBK coal, which allows to conclude that CO_2 gasification reaction can be controlling the combustion reaction rate of the char without decreasing k_{eff} with temperature, and for this

reason, the effect of oxy-fuel on LTBK char 900 combustion is investigated in the subsection 4.4.2 by means with the char combustion reaction rate coefficients, with views to improve the k_{eff} modeling.

Discussing the results for Leão coal and char devolatilized at 730 ^{o}C, the median values of effective reaction rate constants are lower under oxy-fuel 21/79 than air atmosphre conditions, which allows to conclude that k_{eff} calculated for these fuels do not represent the phenomena observed in oxygen concentration curves analyzed by means of DoE in Chapter 3, in which higher variations of oxygen concentrations are attained under oxy-fuel 21/79 than those under air conditions.

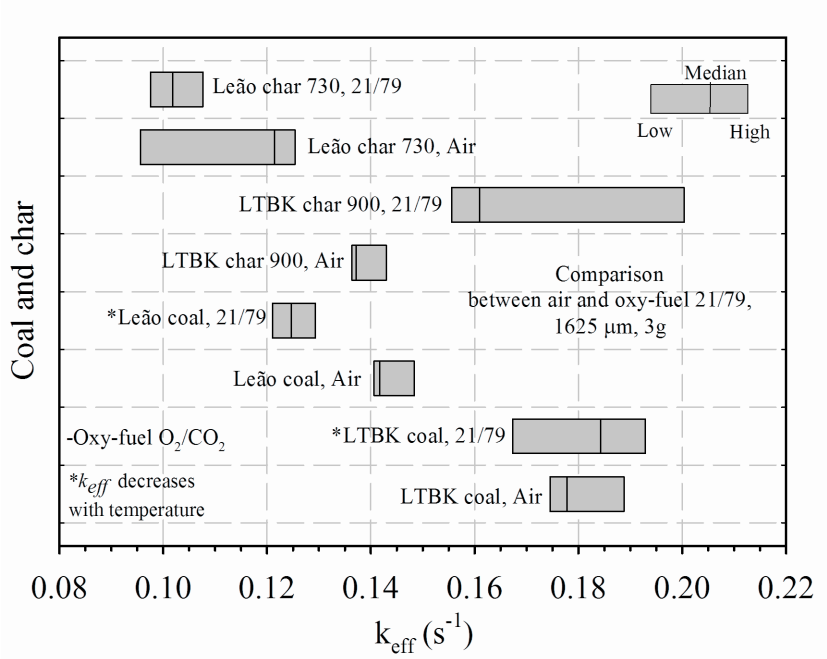

Figure 4.10 - Comparison of effective reaction rate constants for coal and char between oxy-fuel (21/79) and air atmospheres.

Therefore, it is noteworthy to mention and extend these observations for all the results of this section that the method used in the present work, under assumption of a well stirred reactor to calculate the effective reaction rate constants is not accurate enough to capture the kinetic of coal combustion, upon which have several factors as oxidizer atmosphere compositions and properties, gas combustion temperature, coal and char, sample masses, particles mean diameter, swirling flow with its advective and diffusive terms, and oxygen sensor position within the cyclone combustion reactor. The oxygen sensor position is an important effect to be taken into account to calculate the global kinetic parameters.

4.4.2 Assessment of char reactivity with combustion reaction rate coefficients

This subsection summarizes the most relevant results of combustion reaction rate coefficients attained for LTBK char devolatilized at 900 °C, 3g of sample mass and 1625 μm of particles mean diameter. The results showed and analyzed in this subsection aim to deepen the results discussed in Fig. 4.6 and 4.10, investigating the kinetic and diffusive control on the char combustion reaction rate, observed by means of the analysis of effective reaction rate constants for air and oxy-fuel (21/79) atmospheres. The plots of overall combustion reaction rate R_a and chemical reaction rate $R_{a,c}$ coefficients in relation to the oxygen conversion and to the relation $R_a/R_{a,d}$ are aimed to assist in the discussion of the phenomena. The data, used in the plots, are found in Appendix 4.A.5. The plots of Fig. 4.11 shows the results for the evolution of overall combustion reaction rate with the oxygen conversion for air and oxy-fuel (21/79) atmospheres at two average gas combustion temperatures (1073 and 1273 K).

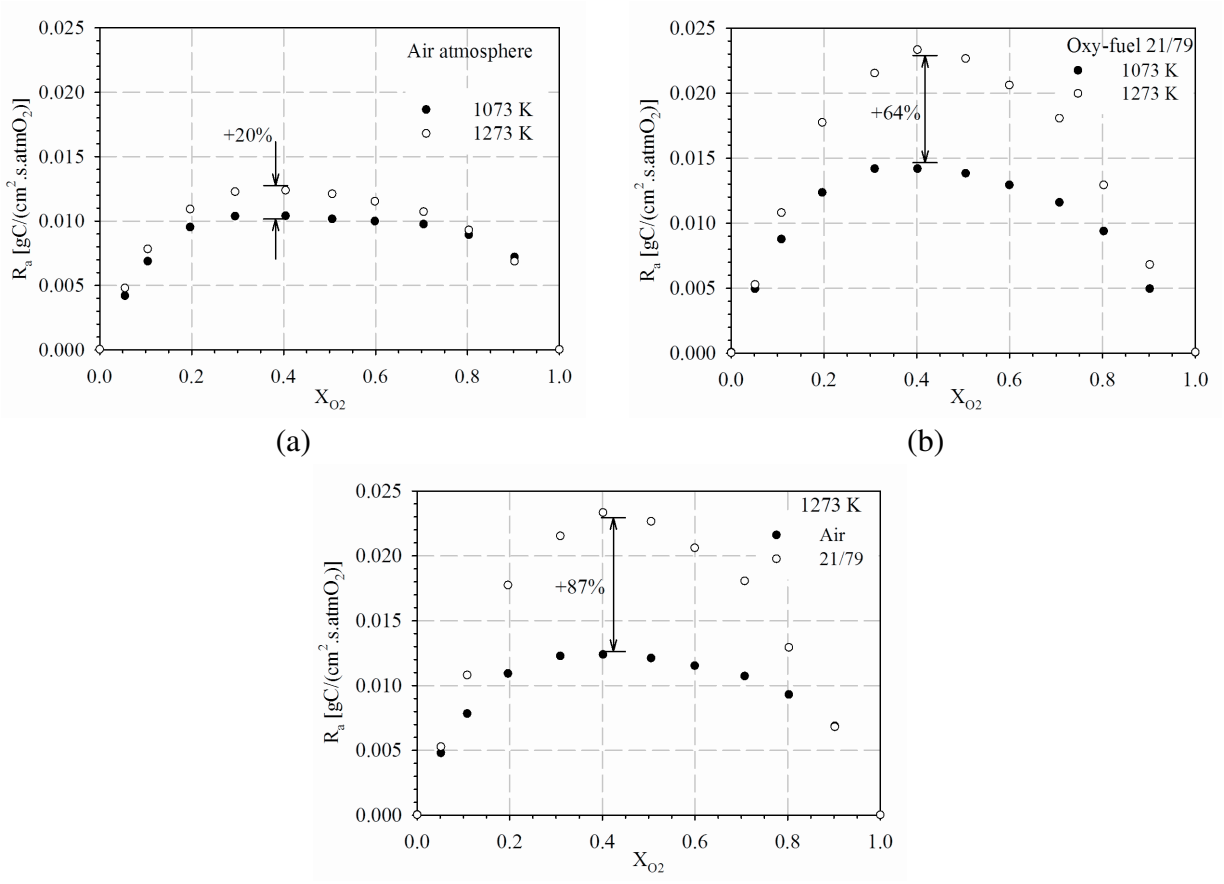

Figure 4.11 - Overall combustion reaction rate for (a) air and (b) oxy-fuel atmospheres, and (c) the comparison between them at 1273 K.

It is observed for Fig. 4.11a, that the maximum increase of overall combustion reaction rate is of 20% with the increase of temperature from 1073 to 1273 K under air atmosphere at oxygen conversion of 0.5, whereas for the oxy-fuel conditions the maximum increase is of 65%, as observed in Fig. 4.11b. These results allow to conclude that the LTBK char combustion in oxy-fuel is under kinetic control regime, as it was observed initially in the analysis of the box plots of Fig. 4.10 through the effective reaction rate constant values, whereas for the char combustion in air conditions the kinetic control regime is not so relevant as that attained for oxy-fuel conditions. Higher gradients of overall combustion reaction rates R_a in relation to oxygen conversion X_{O2} in oxyfuel than those in air conditions at the same temperature are associated with fastest reactions (C + 1/2O_2 → CO and C + CO_2 → 2CO) in oxy-fuel combustion, and the measurement of CO consumption further than O_2 consumption would assist to check this analysis.

The plot of Fig. 4.11c shows the evolution of overall combustion reaction rate at 1273 K under air and oxy-fuel atmospheres. It is observed that maximum char overall combustion reaction rate under oxy-fuel is almost 90% greater than that in air atmosphere at oxygen conversion of 0.4. This result allows to conclude that the oxy-fuel combustion increase the coal combustion reaction in relation to the air, due the effect of gasification reaction of CO_2 with the char, i.e. C + CO_2 → 2CO. The influence of gasification reaction is analyzed by means of chemical reaction rate coefficient $R_{a,c}$ in Fig. 4.13 and 4.14.

The plot of Fig. 4.12 shows the evolution of overall combustion reaction rate at 1073 under air atmosphere for the oxygen sensor positioned near the cyclone reactor wall (original position) and the oxygen sensor positioned in the half radius of cyclone reactor main section (new position).

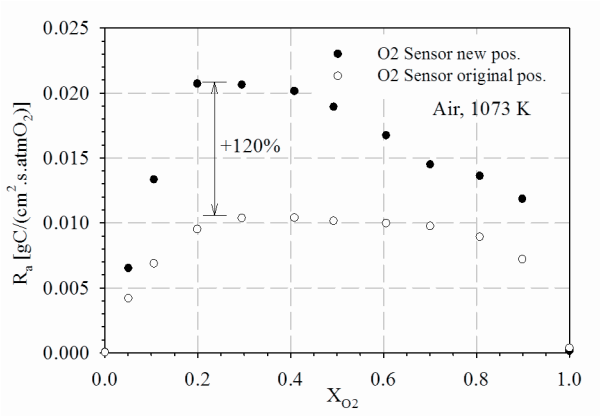

Figure 4.12 - Comparison of overall combustion reaction rate for oxygen sensor original and new positions.

It is observed that results of overall combustion reaction rate for the char is affected by the position of oxygen sensor within the cyclone reactor and the difference of R_a values can reach until 120% between the new and original sensor positions. The influence of the oxygen sensor position on the results was also verified in Fig. 4.6 through the values of effective reaction rate constants. The difference of R_a magnitudes shows that there is a great uncertainty to calculate the reaction rate coefficients within the range of oxygen conversion used in literature (i.e. between 0.2 and 0.9) to fit the char coefficients with the particle temperature [Smith, 1982], and the position of oxygen sensor within the cyclone reactor plays a significant effect on the char combustion reaction rate parameters as also observed for the values of effective reaction rate constants.

The plots of Fig. 4.13 and 4.14 aim to deepen the overall combustion reaction rate discussed in Fig. 4.11 and 4.12 by applying the char combustion reaction rate coefficients to investigate if it is the kinetic or diffusive regime that controls the char combustion. The results are presented with the sensitivity analysis of the gas superficial velocity u_g since there is no measurements of the velocity field for the cyclone combustion reactor installed in ALVA 20 test facility. The regions of kinetic and diffusive control are divided at $R_a/R_{a,d} = 0.5$, where the influence of R_a can be greater than $R_{a,d}$, depending on the velocity field within the cyclone reactor, and this influence is seen with the chemical reaction rate coefficient $R_{a,c}$.

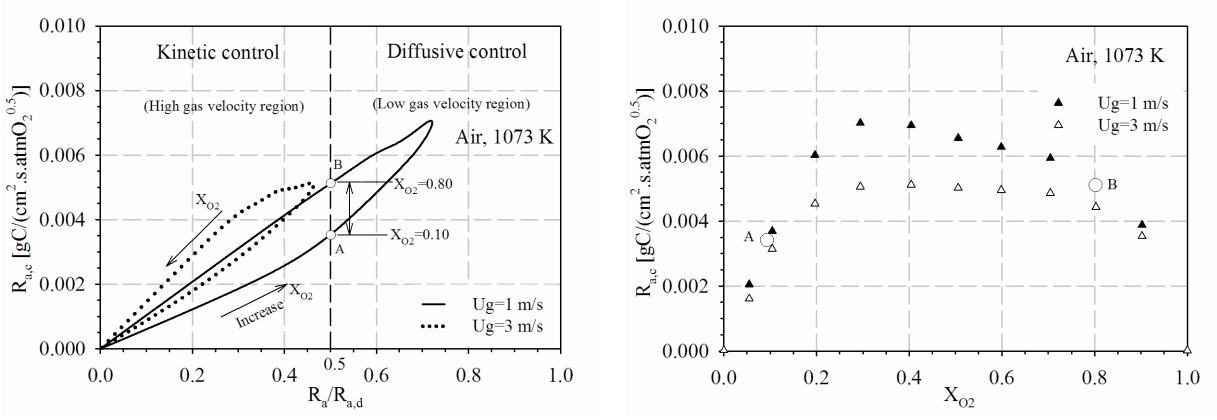

(a) (b)

Figure 4.13 - Plots of chemical reaction rate coefficients (a) with relation $R_a/R_{a,d}$ and (b) with oxygen conversion X_{O2} for air atmosphere conditions at 1073 K.

Fig. 4.13a shows the plot of chemical reaction rate coefficient $R_{a,c}$ with the relation $R_a/R_{a,d}$ for all range of oxygen conversion (0 to 1) under air atmosphere at 1073 K, separated by two values of superficial gas velocity u_g. The values of u_g starts at 1.0 m/s to allow the calculation of $R_{a,c}$ by the Eq. 4.24, since the values attained for R_a are greater than $R_{a,d}$ values calculated for u_g smaller than 1.0 m/s, which indicates initially that the for low velocities of gas under air conditions the char combustion is controlled by diffusion regime, and it is investigated as follow.

Fig. 4.13b shows the plot of chemical reaction rate coefficient $R_{a,c}$ with the oxygen conversion X_{O2} for two values of u_g. This plot aims to support the analysis of phenomena discussed in Fig. 4.13a, observing the evolution of $R_{a,c}$ with oxygen conversion.

Looking at the values of chemical reaction rate coefficient $R_{a,c}$ obtained for $u_g = 1.0$ m/s plotted in Fig. 4.13a, it is observed that the values of $R_{a,c}$ between the range of oxygen conversion of 0.10 to 0.80 is under diffusive control, therefore, the influence of chemical reaction is reduced in this region, allowing to understand the reason by which the increase of R_a with the temperature is low, as verified in the plot of Fig. 4.11a. On the other hand, increasing u_g to 3.0 m/s, changes the control of char combustion from diffusive to kinetic, and all the values of chemical reaction rate coefficient $R_{a,c}$ are within the kinetic control for all oxygen conversion range, in which the effect of temperature on the overall char combustion reaction R_a is increased.

Fig. 4.14a shows the plot of chemical reaction rate coefficient $R_{a,c}$ with the relation $R_a/R_{a,d}$ for all range of oxygen conversion (0 to 1) under oxy-fuel (21/79) atmosphere at 1073 K, separated by two values of superficial gas velocity u_g greater than those simulated for air atmosphere. The values of u_g starts at 3.0 m/s to allow the calculation of $R_{a,c}$ by the Eq. 4.24, since the values attained for R_a are greater than $R_{a,d}$ values calculated for u_g smaller than 3.0 m/s, which indicates initially that the for low velocities of gas under oxy-fuel conditions the char combustion is controlled by diffusion regime, and it is investigated as follow.

Looking at the plot of $R_{a,c}$ for $u_g = 3.0$ m/s in Fig. 4.14a, it is observed that chemical reaction rate coefficient values are within the diffusive control region for oxygen conversion

range between 0.14 and 0.66, which correspond to the highest values of $R_{a,c}$, as seen in Fig. 4.14b, but without influence of the temperature on the overall coal combustion rate.

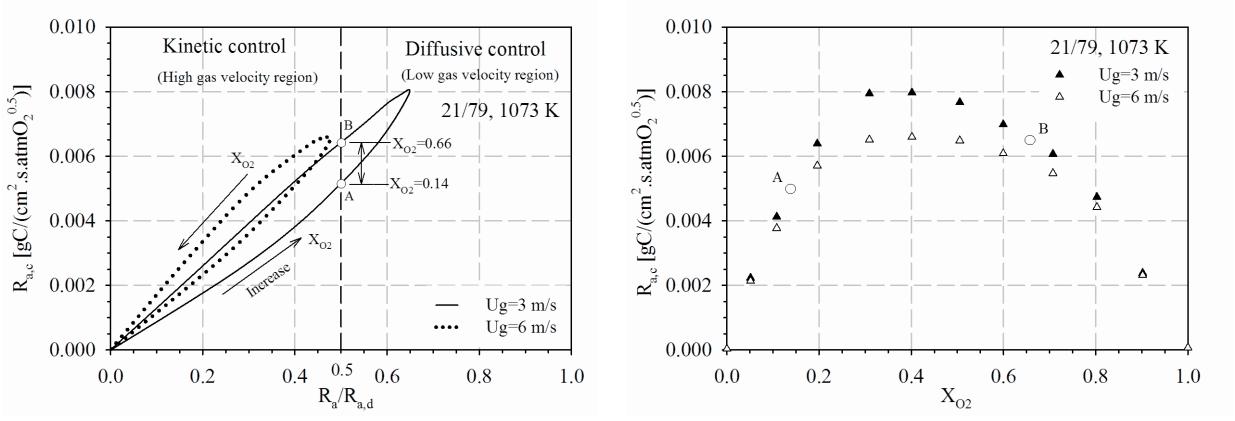

(a) (b)

Figure 4.14 - Plots of chemical reaction rate coefficients (a) with relation $R_a/R_{a,d}$ and (b) with oxygen conversion X_{O2} for oxy-fuel (21/79) atmosphere conditions at 1073 K.

Changing the u_g from 3.0 to 6.0 m/s, the regime control of overall combustion reaction rate changes to kinetic control and the values of $R_{a,c}$ control the overall char combustion, in which the gas combustion temperature and the gasification reaction of CO_2 influence prevail, as observed initially for the results discussed by means of effective reaction rate constants in Fig. 4.10 and latter by means of overall reaction rate in Fig. 4.12 for oxy-fuel atmosphere conditions.

Summarizing the results discussed in plots of Fig. 4.13 and 4.14, it is noteworthy to highlight that the determination of overall coal combustion control regime depends on the knowedge of the velocity field within the cyclone combustion reactor, in which the swirling flow and the oxygen sensor position play an importat role on the oxygen concentration measurements, which influence the magnitude of char overall combustion reaction rate.

According to the sensitivity analysis and within the modeling assumptions to calculate the char combustion reaction rate coefficients, it is observed that for low velocities of gas within the cyclone reactor the diffusive control prevails on the coal combustion, whereas for high velocities of gas the kinetic control prevails. However, higher velocities are required to change the control regime for oxy-fuel in comparison with those for air, which indicate that oxy-fuel atmosphere properties, as oxygen binary diffusion coefficient, can be influencing the overall combustion reaction rate, whereas the gasification reaction of CO_2 with char takes places for gas superficial velocities higher than 6.0 m/s. This analysis allow to conclude that

the kinetic regime of coal combustion under oxy-fuel atmosphere (21/79) within a cyclone combustion reactor is benefited with high velocities of gas, because they reduce the influence of diffusion reaction rate coefficient $R_{a,d}$, giving place for the chemical reaction rate coefficient $R_{a,c}$, in which the temperature and gasification reaction of CO_2 can take place.

The velocities simulated for the analysis of control regime of char combustion provide an indication of the magnitudes of the velocity field within the cyclone combustion reactor where the oxygen sensor is positioned, but must be checked with the measurements of the flow field for this specific reactor in further works with ALVA 20. Higher swirling flow within the cyclone reactor can be attained displacing the oxygen sensor into the centre of cylone reactor than that near the reactor wall, reducing the influence of diffusion regime on the coal combustion, prevailing the kinetic regime. However, for the transition from the diffusion to kinetic regimes succeeds on the control of coal combustion, higher velocities of gas are required, and they are attained in the swirling zones of the combustion chamber.

4.5 Conclusions

This work was aimed to investigate the coal and char global kinetic parameters and char combustion reaction rate coefficients in a laboratory test facility developed to study the coal combustion phenomena under air and oxy-fuel atmospheres. The ALVA 20 reactor was chosen for the experimental work, as it is a laboratory-size atmospheric cyclone combustion reactor able to operate under air and oxy fuel atmospheres. The low-rank coal combustion reactivity was investigated by the measurements of O_2 concentration with a potentiometric oxygen sensor installed within the cyclone reactor, under assumption of a well stirred reactor.

Experiments were performed aiming to investigate the influence of air atmosphere and higher partial pressures of CO_2 and H_2O in oxy-fuel atmosphere on the LTBK coal reactivity, and also investigate the influence of air atmosphere and higher partial pressures of CO_2 concentrations in oxy-fuel atmosphere on low-rank coals reactivity with high content of ash, derived from Leão and Bonito mines located in South Brazil.

Two different oxygen sensor positions within the cyclone combustion reactor (one near the reactor wall and other at the half radius of main reactor section) were tested in order to see the influence of swirling flow on the coal and char combustion global kinetic parameters, as well on the char combustion reaction rate coefficients.

The results allow to conclude that the method used in the present work to calculate the effective reaction rate constant is not accurate enough to capture the kinetic involved in coal combustion, upon which comprehends several effects, as oxidizer atmosphere compositions and properties, gas combustion temperature, coal and char, sample masses, swirling flow with its advective and diffusive terms, and oxygen sensor position within the cyclone combustion reactor. The oxygen sensor position is an important effect to be taken into account to calculate the global kinetic parameters. Therefore, the effective reaction rate constants calculated for the coals and chars tested under oxidizer atmosphere conditions investigated are specific for this type of cyclone combustion reactor installed in ALVA 20 test facility and they are useful to compare the reactivity of different coals and chars for air and oxy-fuel atmospheres under such considerations:

- Potentiometric oxygen sensor must be positioned at the centre of the cyclone combustion reactor main section in order to reach in the recirculation zones of the swirling flow, and attain the maximum variation of oxygen concentration during the coal combustion reaction, as tested for air atmosphere conditions.
- Coal sample mass tested should be 3g instead of 1g for all atmospheres to avoid the adverse effect verified for coals of 1g mass burned under air atmosphere.
- The comparison of effective reaction rate constants between the oxidizer atmospheres for the same coal and char should be taken with care and with the aid of oxygen concentration curves following the methodology developed in Chapter 3, in which the phenomena can be directly investigated without the interference of effective reaction rate constant modelling assumptions, because the effective reaction rate constants modeling equations and fitting can be changing the nature of phenomena observed directly in the oxygen concentration curves. For example, the reactivity of Leão and Bonito coals samples of 1g was reduced under oxy-fuel 21/79 in relation to air atmosphere with the analysis of effective reaction rate constants in comparison with the analysis of oxygen concentration curves in Chapter 3.

The method to calculate the char combustion reaction rate coefficients for LTBK char 900 and to determine the overall coal combustion control regime depends on the knowedge of the velocity field within the cyclone combustion reactor, in which the swirling flow and the oxygen sensor position play an importat role on the magnitude of char overall combustion reaction rate too.

According to the sensitivity analysis to determine the char combustion reaction rate coefficients, higher velocities are required to change the control regime for oxy-fuel in

comparison with those for air, which indicate that oxy-fuel atmosphere properties, as oxygen binary diffusion coefficient, influence the overall combustion reaction rate. Therefore, the kinetic regime of coal combustion under oxy-fuel atmosphere (21/79) within a cyclone combustion reactor is benefited with high velocities of gas, because they reduce the influence of oxy-fuel atmosphere properties on diffusion reaction rate coefficient $R_{a,d}$, giving place for the chemical reaction rate coefficient $R_{a,c}$, in which the temperature and gasification reaction of CO_2 can occur.

BIBLIOGRAPHY

Adánez , J., Abánades, J. C., 1992. "Modeling of Lignite Combustion in Atmospheric Fluidized Bed Combustors. 1. Selection of Submodels and Sensitivity Analysis", Industrial & Engineering Chemical Research, v. 31, p. 2286-2296.

Batchelder, H. R., Busche, R. M., 1953. "Kinectics of coal gasification - Proposed mechanism of gasification", Indrustrial and Engineering Chemistry, v. 45, p. 1856-1878.

Bejarano, P.A., Levendis, Y.A., 2008**.** "Single-coal-particle combustion in O_2/N_2 and O_2/CO_2 environments", Combustion and Flame, v. 153, p. 270-287.

Borrego, A.G., Alvarez, D., 2007. "Comparison of chars obtained under oxy-fuel and conventional pulverized coal combustion atmospheres", Energy & Fuels, v. 21, p. 3171-3179.

Brix, J., Jensen, P.A., Jensen, A.D., 2010. "Coal devolatilization and char conversion under suspension fired conditions in O_2/N_2 and O_2/CO_2 atmospheres". Fuel, v. 89, p. 3373-3380.

Buhre, B.J.P., Elliott, L.K., Sheng, C.D., Gupta, R.P., Wall, T., 2005. "Oxy-fuel combustion technology for coal-fired power generation", Progress in Energy and Combustion Science, v. 31, p. 283-307.

Cho, C.P., Jo, S., Kim, H.Y., Yoon, S.S., Kim, Y., 2006. "Effects of oxygen concentration on the combustion characteristics of interacting coal particles", 8th Asia-Pacific International Symposium on Combustion and Energy Utilization, Sochi, Russia Federation, 06 pages.

Corrêa, R. S., 2013. "Investigation of Pulverized, Pre-Dried Lignite Combustion under Oxy-Fired Conditions in a Large-Scale Laboratory Furnace", Thesis, Brandenburg University of Technology, Cottbus, Germany, p. 249.

Field, M. A., 1969. "Rate of combustion of size-graded fractions of char from a low-rank coal between 1200 and 2000 ^{o}K", British Coal Utilization Research Association, Randalls Road, Leatherland, Surrey, p. 237-252.

Gupta A.K., Lilley D.G., Syred N., 1984. “Swirl flows”, Abacuss Press, London, p. 475.

Hamor, R. J., Smith, I. W., Tyler, R. J., 1973. “Kinetics of combustion of a pulverized brown coal char between 630 and 2200 ^{o}K”, Combustion and Flame, v. 21, p. 153-162.

Laurendeau, N. M., 1978. “Heterogeneous kinetics of coal char gasification and combustion”, Progress in Energy and Combustion Science, v. 4, p. 221-270.

Levenspiel, O., 1999. “Chemical Reaction Engineering”, 3rd Edition, John Wiley & Sons, New York, USA, p. 668.

Liu, H., 2009. “Combustion of coal chars in O_2/CO_2 and O_2/N_2 mixtures: a comparative study with non-isothermal thermogravimetric analyzer (TGA) tests”, Energy and Fuels, v. 23, p. 4278-4285.

Lorentz, H., Rau, H., 1998. “A new method for investigating the combustion behavior of solid fuel in FBC”, Fuel, v. 77, p. 127-134.

Lorentz, H., Tittmann, K., Sitzki, L., Trippler, S., and Rau, H., 1996. “Gas-potentiometric method with solid electrolyte oxygen sensors for the investigation of combustion”, Fresenius Journal of Analytical and Bioanalytical Chemistry, v. 356, p. 215-220.

Milioli, F.E., Silva Filho, C.G., 2008. “A thermogravimetric analysis of the combustion of a brazilian mineral coal”, Quim. Nova, v. 31, p. 98-103.

Molina A., Shaddix C.R., 2007. “Ignition and devolatilization of pulverized bituminous coal particles during oxygen/carbon dioxide coal combustion”, Proceedings of the Combustion Institute, v. 31, p. 1905-1912.

Molina A., Shaddix C.R, 2009. “Particle imaging of ignition and devolatilization of pulverized coal during oxy-fuel combustion”, Proceedings of the Combustion Institute, v. 32, p. 2091-2098.

Murphy, J.J, Shaddix, C.R., 2006. "Combustion kinetics of coals chars in oxygen-enriched environments", Combustion and Flame, v. 144, p. 710-729.

Naredi, P., Pisupati, S., 2008. "Interpretation of char reactivity profiles obtained using a thermogravimetric analyser", Energy & Fuels, v. 22, p. 317-320.

Olajire A.A., 2010. "CO_2 capture and separation technologies for end-of-pipe applications - A review", Energy, v. 35, p. 2610-2628.

Pallarés, J., Arauzo, I., Williams, A., 2007. "Integration of CFD codes and advanced combustion models for quantitative burnout determination", Fuel, v. 86, p. 2283-2290.

Pallarés, J., Gil, A., Cortés, C., Herce, C., 2009. "Numerical study of co-firing coal and Cynara cardunculus in a 350 MWe utility boiler", Fuel Processing Technology, v. 90, p. 1207-1213.

Qingzhao, L., Changsui, Z., Xiaoping, C., Weifang, W., Yingjie, L., 2009. "Comparison of pulverized coal combustion in air and in O_2/CO_2 mixtures by thermogravimetric analysis", Journal of Analytical and Applied Pyrolysis, v. 85, p. 521-528.

Poling, B.E., Prausnitz, J.M., O'Connell, J.P., 2001. **"**The properties of gases and liquids", The McGraw-Hill Companies, 5th Edition, New York, USA, p. 803.

Rathnam, R.K., Elliot, L.K., Wall, T., Liu, Y., Moghtaderi, B., 2009. "Differences in reactivity of pulverized coal in air (O_2/N_2) and oxy-fuel (O_2/CO_2) conditions", Fuel Processing Technology, v. 90, p. 797-802.

Rindels, A.J, Gulliver, J.S., Wetzel, J.M., Voller, V., 1990. "Analysis of the ELFUEL coal drying facility", Project Report No. 308, University of Minesotta, St. Anthony Falls Hydraulic Laboratory, 21 pages.

Rohling, J. H., Shen, J., Wang, C., Zhou, J., Gu, C. E., 2007. "Determination of binary diffusion coefficients of gases using photothermal deflection technique", Applied Physics B, v. 87, p. 355-362.

Schotte, E., Lorenz, H., Rau, H., 2010. “Gas Potentiometry: Oxygen-Based Redox Process Diagnostics in High-Temperature Environments, Handbook of Combustion”, Wiley-VCH Verlag GmbH, v. 2, p. 89-123.

Smith, I.W., 1982. “The combustion rates of coal chars: a review”, 19th Symposium (International) on Combustion/ The Combustion Institute, p1045-1065.

Smith, I.W., 1977. “The intrinsic reactivity of carbons to oxygen”, Fuel, v. 57, p. 409-414.

Smith, I.W., 1971. “Kinetics of combustion of size-graded pulverized fuels in the temperature range 1200-2270 K”, Combustion and Flame, v. 17, p. 303-314.

Smoot, L.D., Smith, P.J., 1985. “Coal Combustion and Gasification”, Plenum Press, New York, USA, p. 443.

Syred N., Beer J.M., 1974. “Combustion in swirling flows: A review”, Combustion and Flame, v. 23, p. 143-201.

Tappe,S., 2011. “Gaspotentiometrische und thermogravimetrische Abbranduntersuchungen von Braun und Steinkohlen in Luft und O_2/CO_2-Atmosphären”, Thesis, Brandenburg University of Technology, Cottbus, Germany, 145 pages.

Tappe, S., Krautz, H.J., 2009a. “ALVA 20: A 20 kWth Atmospheric Laboratory Test Facility to Investigate the Combustion Behavior under Close-to-Reality Conditions”. Proceedings of the European Combustion Meeting, 6 pages.

Tappe, S., Krautz, H.J., 2009b. “Influence of various O_2/CO_2 concentrations on the burning behavior of different coals”, 34th International Technical Conference on Coal Utilization & Fuel Systems, Clearwater, USA, 07 pages.

Toftegaard, M. B., Brix, J., Jensen, P.A., Glarborg, P., Jensen, A.D., 2010. “Oxy-fuel combustion of solids fuels”, Progress in Energy and Combustion Science, v. 36, p. 585-625.

Wall, T., 2007. “Combustion Processes for Carbon Capture”, Proceedings of the Combustion Institute, v. 31, p. 31-47.

Wall, T., Liu, Y., Spero, C., Elliot, L., Khare, S., Rathman, R., Zeenathal, F., Moghtaderi, B., Buhre, B., Sheng, C., Gupta, R., Yamada, T., Makino, K., Yu, J., 2009. “An overview on oxy-fuel coal combustion - State of the art research and technology development”, Chemical Engineering Research and Design, v. 87, p. 1003-1016.

Yang, J.C., 1993. “Environmental Implications of Combustion Processes”. Chapter 4, CRC Press, Boca Raton, FL, Puri, I. K., Editor, p. 97-137.

Young, B. C, Smith, I. W., 1981. “The kinetics of combustion of petroleum coke particles at 1000 to 1800 K: the reaction order”, Eighteenth Symposium (International) on Combustion, The Combustion Institute, p. 1249-1255.

Yu, J., Lucas, J. A., Wall, T. F., 2007. “Formation of the structure of chars during devolatilization of pulverized coal and its thermoproperties: A review”, Progress in Energy and Combustion Science, v. 33, p. 135-170.

Yu, J., Zhang, M.C., 2009. “Mass transfer coefficients for the combustion of a char particle in O2/CO2”, Energy & Fuels, v. 23, p. 5717-5724.

Zhang, L., Binner, E., Chen, L., Qiao, Y., Li, C., Bhattacharya, S., Ninomiya, Y., 2010a. “Experimental investigation of the combustion of bituminous coal in air and O_2/CO_2 mixtures: 1. Particle imaging of the combustion of coal and char”, Energy & Fuels, v. 24, p. 4803-4811.

Zhang, L., Binner, E., Chen, L., Qiao, Y., Li, C., 2010b. “In situ diagnostics of Victorian brown coal combustion in O_2/N_2 and O_2/CO_2 mixtures in drop-tube furnace”, Fuel, v. 89, p. 2703-2712.

APPENDIX 4.A.1 - Derivations of equations used in char combustion reaction rate coefficients

a) The derivation of Eq. 4.13

The Eq. 4.13 provides the calculus of the char diameter d for one particle in terms of oxygen conversion X_{O2} and this relationship is derived, assuming that the char density ρ_o is constant [Hamor et al., 1973]. From the relation for the determination of the volume of one spheric particle, yields

$$d = \left(\frac{6\, m_{char}}{\pi \rho_o} \right)^{1/3} \qquad 4.A.1.1$$

where the mass of char particle m_{char} is expressed according to the following relation

$$m_{char} = \left\{ \left[\underbrace{\frac{90.2}{96.1}}_{\%\ Carbon} \left(1 - X_{O_2}\right) \right] + \underbrace{\frac{5.9}{96.1}}_{\%\ Ash} \right\} m_o \qquad 4.A.1.2$$

where the content of carbon and ash in mass basis is obtained from the proximate analysis for LTBK without volatiles mass (3.9%). The initial mass of char m_o in grams is calculated for a constant densitiy ρ_o of 0.7 g/cm^3 e initial particle diameter d_o of 0.1463 cm.

Substituting the Eq. 4.A.1.2 into the Eq. 4.A.1.1 and rearranging the terms, yields

$$d = d_o \left(1 - 0.94\, X_{O_2}\right)^{1/3} \qquad 4.A.1.3$$

b) The derivation of Eq. 4.12

The Eq. 4.12 provides the calculus of char overall reaction rate from the experimental data, and it is obtained as follows. The molar rate of carbon consumption at surface of the particle $\dot{n}_{carbon}$ is given by the relation

$$\dot{n}_{carbon} = \frac{1}{M_{carbon}} \frac{dm_{char}}{dt} \qquad 4.A.1.4$$

where M_{carbon} is the molar mass of carbon.

The mass rate of carbon consumption at the outer surface of the char particle $\dot{m}_c$ in terms of oxygen conversion is given by the expression

$$\dot{m}_{char} = -m_o \frac{dX_{O_2}}{dt} \qquad 4.A.1.5$$

Substituting the Eq. 4.A.1.5 into Eq. 4.A.1.4, and the expression of the initial mass of char in terms of d_o and ρ_o , i.e. $m_o = \left(d_o^3 \pi \rho_o / 6\right)$ yields

$$\dot{n}_{carbon} = \frac{1}{M_{carbon}} \left(- \frac{d_o^3 \pi \rho_o}{6} \frac{dX_{O_2}}{dt} \right) \qquad 4.A.1.6$$

Dividing both sides of Eq. 4.A.1.6 by the outer surface area of char particle $A_s = \pi d_c^2$, and rearranging the terms yields the overall combustion reaction rate yet to be simplified

$$\left(- \dot{r}_{area,chemical}\right) = \frac{1}{M_{carbon}} \left(\frac{d_o^3}{d_c^3} \frac{\rho_o}{6} \frac{dX_{O_2}}{dt} \right) \qquad 4.A.1.7$$

Substituting the Eq. 4.A.1.3 into Eq. 4.A.1.7 and rearranging the terms, the following expression is attained for the overall combustion reaction rate in mass basis (eliminating M_c).

$$\left(- \dot{r}_{a,c}\right) = \frac{dX_{O_2}}{dt} \frac{d_o \rho_o}{6} \frac{1}{(1 - 0.94 X_{O_2})^{2/3}} \qquad 4.A.1.8$$

For convention, the negative signal due to the consumption of carbon given by the char combustion reaction rate by the expression 4.A.1.8 is not shown in the section 4.3.

c) The derivation of Eq. 4.16

The derivation of Eq. 4.16 to calculate the char overall combustion reaction rate without the knowledge of oxygen concentration at the particle surface is obtained as follows. The relation for the overall combustion reaction rate $\dot{r}_{a,c}$ in terms of mass transfer coefficient h_m is given by the relationship

$$\dot{r}_{a,c} = h_m\left(C_g - C_s\right) \qquad 4.A.1.9$$

Isolating the oxygen concentration at the outer surface of char particle C_s yields

$$C_s = C_g - \frac{\dot{r}_{a,c}}{h_m} \qquad 4.A.1.10$$

The relation for the overall combustion reaction rate $\dot{r}_{a,c}$ in terms of chemical rate coefficient k_c is given by the relationship

$$\dot{r}_{a,c} = k_c C_s^n \qquad 4.A.1.11$$

Substituting the Eq. 4.A.1.10 and the relationship $\chi = \dot{r}_{a,c}/\dot{r}_m$ into Eq. 4.A.1.11 yields

$$\dot{r}_{a,c} = k_c\left(C_g - \frac{\chi\,\dot{r}_m}{h_m}\right)^n \qquad 4.A.1.12$$

Substituting the relationship $\dot{r}_m = h_m C_g$, in which the $C_s \to 0$, into the Eq. 4.A.1.12 and rearranging the terms yields

$$\dot{r}_{a,c} = C_g^n\left(1-\chi\right)^n k_c \qquad 4.A.1.13$$

d) The derivation of Eq. 4.24

The derivation of Eq. 4.24 to calculate the chemical reaction rate coefficient $R_{a,c}$ is obtained as follows. Rearranging the Eq. 4.A.1.13 yields

$$\frac{\dot{r}_{a,c}}{\left(1-\chi\right)^n} = C_g^n\,k_c \qquad 4.A.1.14$$

Substituting the relationship $\chi = \dot{r}_{a,c}/\dot{r}_m$ into Eq. 4.A.1.14 and rearranging the terms, yields

$$\frac{\chi}{(1-\chi)^n} = \frac{C_g^n k_c}{C_g h_m} \qquad 4.A.1.15$$

Substituting the oxygen concentration terms C_g by the oxygen partial pressure terms p_g and rearranging them, the following expression is obtained in function of chemical $R_{a,c}$ and diffusion $R_{a,d}$ reaction rate coefficients

$$\frac{\chi}{(1-\chi)^n} = \frac{R_{a,c}}{R_{a,d}}\left(p_g\right)^{n-1} \qquad 4.A.1.16$$

To eliminate χ and derive the expression to calculate $R_{a,c}$ from the Eq. 4.A.1.16, the following manipulations are required. The variable χ is substituted by the relationship $\chi = \dot{r}_{a,c}/\dot{r}_m$ as follows

$$\frac{\dot{r}_{a,c}/\dot{r}_m}{\left(1-\dot{r}_{a,c}/\dot{r}_m\right)^n} = \frac{R_{a,c}}{R_{a,d}}\left(p_g\right)^{n-1} \qquad 4.A.1.17$$

The maximum possible combustion reaction rate $\dot{r}_m$ is replaced by the relationship $\dot{r}_m = R_{a,d}\, p_g$ and it is introduced into the Eq. 4.A.1.17. After some manipulation, the following expression is obtained

$$\frac{\dot{r}_{a,c}}{\left(R_{a,d}\, p_g - \dot{r}_{a,c}\right)^n}\left(R_{a,d}\, p_g\right)^{n-1} = \frac{R_{a,c}}{R_{a,d}}\left(p_g\right)^{n-1} \qquad 4.A.1.18$$

Substistuting the $\dot{r}_{a,c}$ by the relationship $\dot{r}_{a,c} = R_a\, p_g$ and rearranging the terms yields the first expression for $R_{a,c}$

$$R_{a,c} = \frac{R_a}{\left(p_g\right)^{n-1}}\frac{R_{a,d}^n}{\left(R_{a,d} - R_a\right)^n} \qquad 4.A.1.19$$

Eliminating the oxygen partial pressure by the relationship $p_g = \dot{r}_{a,c}/R_a$ yields the relationship used to calculate the char chemical reaction rate coefficient $R_{a,c}$

$$R_{a,c} = \left(\frac{R_a R_{a,d}}{R_{a,d} - R_a} \right)^n \left(\dot{r}_{a,c} \right)^{1-n} \quad \text{4.A.1.20}$$

e) The Biot number

The determination of the Biot number is based on the following relationship [Rindels et al., 1990] to calculate the convective heat transfer coefficient

$$h_g = 2.06 \rho_g u_g c_{p,g} \frac{\phi_s}{\varepsilon} (\mathrm{Re})^{-0.58} (\mathrm{Pr})^{-0.67} \quad \text{4.A.1.21}$$

where Prandtl and Reynolds numbers are given by the expressions

$$\mathrm{Re} = \frac{\rho_g u_g d_o}{\mu_g} \quad \text{4.A.1.22}$$

$$\mathrm{Pr} = \frac{c_{p,g} \mu_g}{k_g} \quad \text{4.A.1.23}$$

The Biot number is given by the following relationship

$$Bi = \frac{h L_c}{k_p} \quad \text{4.A.1.24}$$

where the fluid properties are calculated following the ideal gas law for air atmosphere at 1173 K, as follow.

- ρ_g is the density, 0.308 kg/m3
- μ_g is the viscosity, 0.00046 kg/(m.s)
- $c_{p,g}$ is the constant-pressure specific heat, 1170 J/(kg.K)
- d_o is the initial particle diameter, 0.001625 m
- k_p is the char thermal conductivity, 0.22 W/(m.K) [Rindels et al., 1990]
- ϕ_s is shape factor for lignite particles, 0.8 [Rindels et al., 1990]
- L_c is the ratio between the volume and the surface of particle, 0.000278 m
- u_g is the superficial gas velocity, 1.5 and 2.0 m/s (Fluidized Bed Reactor)

- ε is the relative amount of space between the particles that are burning together, 0.5

The calculus for convective heat transfer coefficient and Biot number are summarized in Table 4.A.1.1. The great uncertainty in calculating the convective heat transfer coefficient h is the velocity of the flow in relation to the particles velocity u_g and the amount of space between the particles ε while they are burning together. The calculus of particle temperature depends also on the knowledge of these parameters for the energy balance equation determination.

Table 4.A.1.1 - Heat transfer coefficient and Biot number

u_g (m/s)	ε	Re	Pr	h (W/m^2.K)	Biot
1.5	0.5	16	0.25	672.9	0.82
2.0	0.5	21	0.25	760	0.93

APPENDIX 4.A.2 - Program developed in EES (Engineering Equation Solver) to calculate the char combustion reaction rate coefficients

```
"Program to calculate the char combustion reaction rate coefficients for LTBK char (devolatized at 900 oC), with 3g mass,
1625 micronmeters of particles mean diameter, in OXY-FUEL 21/79 (O2/CO2)"

"NOTE: System units in kPa, mass (kg), Kelvin, Degrees, kJ

the system units must be in mass basis, due to oxidizer density (kg/m3)"

"Gas properties at 1073 K"

T1=1073

"The sequence of equations below uses the viscosity by WILKE's Method (1950), page 487 of the book:
[The properties of gases and liquids, fifth edition] using the EES library for the chemical components"
"For this calculation, the molar fractions and temperature are fixed,
and they are used to compare the values attained with molar fractions f[i] and gas temperature Tg[i] variables, calculated in the sub-routine"


f_1 = 0.21                                          "molar fraction of O2 in the mixture"
f_2 = 0.79                                          "molar fraction of CO2 in the mixture"

eta_m = (f_1*Viscosity(O2,T=T1))/(f_1+f_2*phi_12) + (f_2*Viscosity(CO2,T=T1))/(f_2+f_1*phi_21)
"dynamic viscosity of the mixture, kg/(m.s), WILKE's Method"

phi_12 = ((1 + ((Viscosity(O2,T=T1)/Viscosity(CO2,T=T1))^0.5
)*((Molarmass(CO2)/molarmass(O2))^0.25))^2)/((8*(1+ (molarmass(O2)/molarmass(CO2))))^0.5)

phi_21 = phi_12*((Viscosity(CO2,T=T1)*molarmass(O2)/(Viscosity(O2,T=T1)*molarmass(CO2))))


"Determination of thermal conductivity of the mixture (Wassiljewa, same method used for the calculus of the viscosity of the mixture)
For this calculation, the molar fractions and gas temperature are fixed,
and they are used to compare the values attained with molar fractions f[i] and gas temperature Tg[i] variables, calculated in the sub-routine"
"f_1 = 0.21                                          molar fraction of O2 in the mixture"
"f_2 = 0.79                                          molar fraction of CO2 in the mixture"

kond_m = ((f_1*Conductivity(O2,T=T1))/(f_1+f_2*kond_12) +
(f_2*Conductivity(CO2,T=T1))/(f_2+f_1*kond_21))* (1/4.1868)*(1/100)
"thermal conductivity of the mixture, [cal/(s.cm.K)]"

kond_12 = ((1 + ((Conductivity(O2,T=T1)/Conductivity(CO2,T=T1))^0.5
)*((Molarmass(CO2)/molarmass(O2))^0.25))^2)/((8*(1+ (molarmass(O2)/molarmass(CO2))))^0.5)

kond_21 =
kond_12*((Conductivity(CO2,T=T1)*molarmass(O2)/(Conductivity(O2,T=T1)*molarmass(CO2))))


kond_air = Conductivity(Air,T=T1)                   "EES library W/(mK)"


kond_air_1 = Conductivity(Air,T=T1)* (1/4.1868)*(1/100)
```

"thermal conductivity of the mixture, [cal/(s.cm.K)]"

"calculus of the density of the mixture oxy-fuel 21/79 for molar fractions and gas temperature fixed"

rho_oxy = f_1*Density(O2,T=T1,P=P) + f_2*Density(CO2,T=T1,P=P) "kg/m3"
"Determination of kinematic viscosity of the mixture oxy-fuel 21/79 for molar fractions and gas temperature fixed"

mu_oxy=(eta_m/rho_oxy)*1E4 "kinematic viscosity in oxy-fuel 21/79, cm2/s"

"**********"
veloc = 2.0E2 "gas superficial velocity, cm/s"
"Ref. paper: Modeling of lignite combustion in atmospheric fluidized bed, Table 2; u= 0.8 a 2.0 m/s for particles mean diameter of 1.0 mm"
"Parameter used for the sensitivity analysis and it is different than zero for particles greater than 100 micronmeters"

Sch =1 "Schmidt number is 1 for gases, according to Levenspiel - page 660 - Dimensionless groups"

ccc = 0.35 "the value of this constant comes from the Sherwood number"

{DO2 = 0.207} "O2/N2 in cm2/s; paper Kinetics of combustion of size-graded pulverized fuels in the temperature range 1200-2270 K"

DO2 = 0.168 "According to the literature, the binary diffusivity of O2 in CO2 is between 75 to 80% of the diffusivity of O2 in N2; paper: Oxy-fuel combustion of Solids, Toftegaard et al., 2010; Table 9, em cm2/s; or paper: Determination of binary diffusion coefficients of gases usung photothermal deflection technique, Applied Physics, 2007"

"Proximate analysis for pre-dried lignite coal in mass basis %"

y_h2o = 8/100 "wet"

y_ash = 5.9/100 "ash"

y_mv = 51/100 "volatile"

y_cf = 35.1/100 "fixed carbon"

y_total = y_h2o + y_ash + y_mv + y_cf

y_char = y_total - (y_mv + y_h2o) "char"

"Proximate analysis for LTBK char (after the devolatilization at 900 oC) in mass basis %"

y_h2oc = 0.06/100 "wet"

y_mvc = 3.83/100 "volatile"

y_cfc = 1 - (y_h2oc + y_mvc + y_ash) "fixed carbon"

y_charc = 1 - (y_mvc + y_h2oc) "char"

"Data of the lignite coal before the devolatilization"

rho = 1.2 "Lignite density, g/cm3"

```
do=0.1625                                   "initial mean diameter of coal particle, cm"

ro=do/2                                     "cm"
vo=(4/3)*pi#*((ro)^3)                       "initial volume of one coal particle, cm3"


"Data for one particle of lignite char"

dco=0.9*do                                  "Paper Yu et al., 2007; reduction of 10% of
coal diameter after the devolatilization with proportional reduction of particle volume. Formation of the
structure of chars during devolatilization of pulverized coal and its thermoproperties: A review"

rco=dco/2                                   "cm"

aco = 4*pi#*((rco)^2)                       "char external surface area, cm2"

vco=(4/3)*pi#*((rco)^3)                     "char volume, cm3"

rhoco = rho*y_char*(vo/vco)                 "initial density of char, g/cm3"

mco=(pi#*rhoco*((dco)^3))/6                 "initial mass of char, gC"

mcc = (y_cfc/y_charc)*mco                   "initial mass of carbon contained in the char,
gram"

mac = (y_ash/y_charc)*mco                   "initial mass of ash contained in the char,
gram"

ycc = y_cfc/y_charc                         "mass fraction of fixed carbon contained in
the char"

yac = y_ash/y_charc                         "mass fraction of ash contained in the char"

{gama = 9.5e-3*1e-1}                        "dimensional characteristic of a particle
(volume/external area), cm"
                                            "Table 1 of the paper: The intrinsic reactivity
of carbons to oxygen. Ref. 2 - brown-coal char. 4e-3 to 1.5e-2 mm; mean values for the range; applied
only for pulverized coal particles."

gama = dco/6                                "cm; relation from the paper: The intrinsic
combustion reactivity of pulverized coal chars: the use of experimental pore diffusion coefficients"

"Note: xx[i], efetiv[i] e phi[i] are rather sensitives to the gama relation and to specific superficial area of
the particle Ag"

"Correlations coefficients for the gas profile temperature measured with thermocouple T3"
"(thermocouple installed at the cyclone reactor exit) with the average gas temperature at 1073 K within
the cyclone reactor"
"7th Degree Polynomial Fit:  y=a+bx+cx^2+dx^3 correlation coefficients for gas combustion
temperatureTg[i]
Coefficient Data: R2=0.99"
a =9.96581857651E+2
b =-1.74651182784
c =5.24005524964
d =-6.97874013348E-1
e =3.85655026986E-2
f = -1.08093026975E-3
g =1.52253276140E-5
hhh =-8.57695580840E-8
```

"Data used for the calculation of particle temperature (Tp)"

Tw = 1123.15 "wall cyclone reactor temperature, K"
epsilon = 1 "emissivity"

H = 2300 "cal/g; reaction C + 1/2O2 --> CO"

"Conversion factor for the constants for the calculation of Tp[i]"

J = sigma# "STEFAN-BOLTZMANN CONSTANT, (W)*(1/m2)*(1/K4)"

J1 = (J/4.1868)*1E-4 "STEFAN-BOLTZMANN CONSTANT, (cal/s)*(1/cm2)*(1/K4)"

"Data for the calculation of the mass transfer coefficient, kd[i]"

P = 101.325 "absolute pressure of reference, kPa"

To = 300 "temperature of reference, K"

"Data for the calculation of oxygen (O2) consumption in the reaction, assuming a well stirred reactor"

RR# = 0.082 "universal constant of ideal gas law, (atm.L/gmol.K)"

vol_O2_e = 21 "molar fraction of O2 or volume of O2 in the cyclone reactor inlet stream, % V/V"

{m_oxi = 9.3} "air mass flow rate, kgar/h"
m_oxi = 15 "oxy-fuel 21/79 mass flow rate, kg/h"

"Data used in the sub-routine of the program"

N=141 "number of time steps along the oxygen concentration curve in the combustion of sample, measured by the oxygen sensor"

NO2A[0]=0 "accumulated moles of O2 consumed in initial time t=0 or i=0"

X[0]=0 "oxygen conversion in initial time t=0"

ACO2s[0]=0 "accumulated area of oxygen concentration in initial time (gmolO2/m3).(s)"

t[0]=0

"Real order of the reaction rate per external surface of char particle pores, with the oxygen parcial pressure applied in particle surface pores"
mm=0.0 "affects the curve for the determination of effectiveness factor; paper The intrinsic reactivity of carbons to oxygen; Table 1 - Brown coal char"

"Apparent order of the reaction rate per external surface of char particle, with the oxygen partial pressure applied in particle surface"
nn=(mm + 1)/2 "order of reaction in the oxygen partial pressure in the external surface of char particle" "range from 0.1 to 1. nn=0.5 due to the best fitting; Fig. 5 of the paper: Combustion rates of coal chars: review"

"Determination of the effective diffusion coefficient in the particle (De)"

```
{Ag = 250}                                          "specific area (total) of surface particle,
[m2/g]"
"Table 1 of paper: The intrinsic reactivity of carbons to oxygen. Ref. 2 - brown-coal char 337 - 1346
m2/g; mean value for the 1st simulation. Sensitivity parameter for the intrinsic reaction rate

Ag = 130                                            "129 m2/g; Ref. Table 2, char EBC 900
(coke) no activated, of the paper: Activation of brown coal chars with oxygen. It is better to use the
initial area, because it is unknown the evolution of Ag with the burn-off, except if it is known the
conversion curve, use the maximum 130, otherwise the calculation does not converge - under
investigation"

tort = 2                                            "particle tortuosity, dimensionaless"
"Ref. from Eq. 10 of paper: Internal burning of pulverized semi-anthracite"

rhog = 1.8                                          "helium gas density, g/cm3"


"**for constant density of char**"

teta = 1 -(rhoco/rhog)                              "particle porosity"
                                                    "rhog = 1,8; helium density from Table 3 of
paper: Internal burning of pulverized semi-anthracite; adimensional"

rp = (2*teta*((tort)^0.5))/(Ag*1e4*rhoco)           "mean radius of particle pores, cm"

rp_ang = rp*(1e8)                                   "mean radius of particle pores, Angstrom"


Dp = 9.7e3*(rp)*((1073/molarmass(O2))^0.5)          " Knudsen coefficient, cm2/s"

De = (Dp*teta)/tort                                 "effective diffusion coefficient, cm2/s"


"7th Degree Polynomial Fit:  y=a+bx+cx^2+dx^3...    Coefficient Data: for mm=0.5; determination
of effectiveness factor, when the relationship [(kd[i].dc[i])/De] is large"
"1st approach for the calculation of effectiveness factor; paper: Aris e Mehta, 1971 - Communications
on the theory of diffusions and reaction - VII - The isothermal pth order reaction"

aa =1.05976988528
bb =-2.14926815335e-1
cc =2.48430187118e-1
dd =-1.28660981531e-1
ee =3.36218593604e-2
ff =-4.59512155784e-3
gg =3.09943131263e-4
hh =-8.16462488835e-6

"Gravimetric stoichiometric coefficient, eq. 57 of paper: Heterogeneous kinetics of coal char
gasification and combustion"

"reaction C + 1/2O2 --> CO"

LL = 0.75                                           "gram of C/gram de O2"

"Beginning of the sub-routine - without constants"

"*************************************************************************************"

DUPLICATE i=1,N
```

```
    "Experimental data of the oxygen sensor"
    t[i] =lookup('Lookup 1', i,'tempo')                    "Experimental data: time, s"

    volO2s[i] =lookup('Lookup 1', i,'fracaoO2')            "Experimental data: molar fraction of O2 or
volume of O2 within the reactor, measured at the reactor outlet, % V/V"

    "Combustion gas temperature within the cyclone reactor"

    Tg[i] = a + b*t[i] + c*t[i]^2 + d*t[i]^3 + e*t[i]^4 + f*t[i]^5 + g*t[i]^6  + hhh*t[i]^7 "Polynomial fitting of 7th
degree for the gas combustion temperature, K"

    "Moles of O2 consumed in the char combustion reaction"

    CO2e[i] = ((P/101.325)*vol_O2_e*1e-2*1000)/(RR#*Tg[i])"gmolO2/m3; absolute pressure of the
system (reactor), 1 atm"

    CO2s[i]= ((P/101.325)*volO2s[i]*1e-2*1000)/(RR#*Tg[i])"O2 concentration at the reactor outlet,
gmolO2/m3"

    rho_oxi[i] =f_1[i]*Density(O2,T=Tg[i],P=P) + f_2[i]*Density(CO2,T=Tg[i],P=P) "density of oxydizer
atmosphere (Air or OXY-FUEL 21/79), kg/m3"

    v_oxi[i] = m_oxi/rho_oxi[i]                            "volumetric flow rate of oxidizer atmosphere
(Air or oxy-fuel 21/79), m3ar/h or m3oxy-fuel/h"

    nO2e[i]=CO2e[i]*v_oxi[i]*(1/3600)                      "molar flow rate of O2 at reactor inlet,
gmolO2/s"

    nO2s[i] =CO2s[i]*v_oxi[i]*(1/3600)                     "molar flow rate of O2 at reactor outlet,
gmolO2/s"

    nO2c[i]=(CO2e[i] - CO2s[i])*v_oxi[i]*(1/3600)          "molar flow rate of O2 consumed in the
reaction, gmolO2/s"

"Oxygen conversion"

    NDO2C[i]=(nO2c[i] - 0)*0.25                            "moles of O2 consumed, gmol O2"

    NO2A[i]=NDO2C[i] + NO2A[i-1]                           "moles of O2 consumed accumulated, gmol
O2"

    MO2A[i]=NO2A[i]*MOLARMASS(O2)                          "mass of O2 consumed accumulated, gO2"

    X[i]=NO2A[i]/NO2A[141]                                 "O2 conversion"


    "Particle diameter"

    mcc[i]=mco*(ycc*(1-X[i]) + yac)                        "mass of char (carbon + ash), gC"

    dc[i]=dco*((1- ycc*X[i])^(1/3))                        "particle diameter [cm], assuming density
constant of char"

    "O2 binary mass diffusivity"

    DO2[i] = DO2*(((Tp[i] + Tg[i])/(2*To))^1.75)*(P/P)     "cm2/s; eq. 64 of paper Heterogeneous
kinetics of coal char gasification and combustion"

    "Overall reaction rate per external surface of char"
    DXDT[i]=(X[i] -X[i-1])/0.25                            "DX/DT"
```

```
    ra[i]=DXDT[i]*(dco*rhoco)*(1/6)*(1/((1- ycc*X[i])^(2/3)))"Overall reaction rate per external surface
(a) of char, [gC/(cm2.s)], for constant density and variable diameter"

    "Particle temperature Tp[i]"

    K[i]=Conductivity(Air,T=Tg[i])*(1/4.1868)*(1/100)        "thermal conductivity of oxidizer atmosphere
(Air) for comparison, [cal/(s.cm.K)]"

    kond_m[i] = ((f_1[i]*Conductivity(O2,T=Tg[i]))/(f_1[i]+f_2[i]*kond_12[i]) +
(f_2[i]*Conductivity(CO2,T=Tg[i]))/(f_2[i]+f_1[i]*kond_21[i]))* (1/4.1868)*(1/100) "thermal conductivity
of the mixture, [cal/(s.cm.K)]"

    kond_12[i] = ((1 + ((Conductivity(O2,T=Tg[i])/Conductivity(CO2,T=Tg[i]))^0.5
)*((Molarmass(CO2)/molarmass(O2))^0.25))^2)/((8*(1+ (molarmass(O2)/molarmass(CO2))))^0.5)

    kond_21[i] =
kond_12[i]*((Conductivity(CO2,T=Tg[i])*molarmass(O2)/(Conductivity(O2,T=Tg[i])*molarmass(CO2))))

    ra[i]*H - (2*Kond_m[i]*(Tp[i] - Tg[i]))/dc[i] - epsilon*J1*(Tp[i]^4 - Tw^4) = 0" Eq. for the calculation of
particle temperature with thermal conductivity of OXY-FUEL in 21/79; steady state assumption"

    "***Calculation of kinematic viscosity****"
    f_1[i] = volO2s[i]*1e-2                                  "molar fraction of O2"
    f_2[i] = 1 - f_1[i]                                      "molar fraction of CO2"

    eta_m[i] = (f_1[i]*Viscosity(O2,T=Tg[i]))/(f_1[i]+f_2*phi_12[i]) +
(f_2[i]*Viscosity(CO2,T=Tg[i]))/(f_2[i]+f_1[i]*phi_21[i]) "dynamic viscosity of the mixture, kg/(m.s), by
WILKE's Method"

    phi_12[i] = ((1 + ((Viscosity(O2,T=Tg[i])/Viscosity(CO2,T=Tg[i]))^0.5
)*((Molarmass(CO2)/molarmass(O2))^0.25))^2)/((8*(1+ (molarmass(O2)/molarmass(CO2))))^0.5)

    phi_21[i] =
phi_12[i]*((Viscosity(CO2,T=Tg[i])*molarmass(O2)/(Viscosity(O2,T=Tg[i])*molarmass(CO2))))
    mu_oxi[i]=(eta_m[i]/rho_oxi[i])*1E4                      "kinematic viscosity in oxy-fuel 21/79, cm2/s"
    "Mass transfer coefficient, assuming the reaction C + 0.5O2 --> CO; flux of CO; with DO2 variable"

    Kd[i] = 2*ccc*LL*DO2[i]*((veloc/(mu_oxi[i]*dc[i]))^0.5)*((Sch)^(1/3)) + (2*ccc*LL*DO2[i])/(dc[i])
"cm/s; mass transfer coefficient of paper Heterogeneous kinetics of coal char gasification and
combustion"

    rad[i]=Kd[i]*CO2s[i]*32E-6                               "rate of mass transfer due to the diffusion of
O2 through the film, [gC/cm2.s]"

    "Chemical and diffusion reaction rate coefficients"

    PO2[i] = CO2s[i]*RR#*Tg[i]*1E-3                          "oxygen partial pressure in the mixture, atm"

    Ka[i] = ra[i]/PO2[i]                                     "Overall reaction rate per external surface of
char in terms of O2 partial pressure in the mixture, [gC/(cm2.s.atmO2)]"

    Kad[i] = rad[i]/PO2[i]                                   "Diffusion reaction rate coefficient,
[gC/(cm2.s.atmO2)]"


    Kac[i] = ((ra[i])^(1- nn))*(((Ka[i]*Kad[i])/(Kad[i] - Ka[i]))^nn)"Chemical reaction rate coefficient,
[gC/(cm2.s.((atmO2)^nn))]"

    KKa[i] = Kac[i]/(Kad[i])                                 "ratio between the coefficients"
```

```
    chi[i] = ra[i]/rad[i]                                   "Variable Chi of the paper: The combustion
rates of chars: a review, eq. 10"


    KK[i] = Ka[i]/(Kad[i])                                  "ratio between the coefficients; maximum
allowed is 0.5 for the chemical reaction rate coefficient be used, according to papers of Field, 1969
and Smith, 1982."

    "Oxygen concentration in particle surface"

    CO2ss[i] = CO2s[i]*32e-6 - (ra[i]/(LL*Kd[i]))           "Oxygen concentration in particle surface,
[gO2/cm3]"

    CO2ssv[i] = CO2s[i] - (ra[i]/(LL*Kd[i]))*(1e6/32)       "Oxygen concentration in particle surface,
[gmolO2/m3]"

    "Calculation of Sherwood number"

    Sher[i] = (Kd[i]*dc[i])/(DO2[i])                        "dimensionless: total mass transfer/molecular
mass transfer"

    "Calculation of intrinsic reaction rate - Further works with ALVA 20"
    "Fundamentals found in papers: Smith, 1977 - The intrinsic reactivity of carbons to oxygen; Smith,
1982 - The combustion rates of coal chars: a review
    Aris e Metha, 1971. Communications on the theory of diffusion and reaction  - VII, The isothermal
pth order reaction
    Smith and Tyler, 1972 - Internal burning of pulverized anthracite: the reaction between particle
structure and reactivity
    Laurendeau, 1978 - Heterogeneous kinetics of coal char gasification and combustion
    Smoot e Smith. 1985 - Coal combustion and gasification"
    "Determination of the effectiveness factor"
    gama[i] = dc[i]/6                                       "cm; with variable diameter"

    xx[i] = ((gama[i]*ra[i]*(mm + 1))/(8*De*CO2ss[i]))      "with variable gama and De constant"
    "value in the abscissa of Fig. 12 from paper: Communications on the theory of diffusion and
reaction  - VII The isothermal pth order reaction; when the relation [(kd[i].dc[i])/De] is large"

    efetiv[i] = aa + bb*xx[i] + cc*(xx[i]^2) + dd*(xx[i]^3) + ee*(xx[i]^4) + ff*(xx[i]^5) + gg*(xx[i]^6) +
hh*(xx[i]^7)                                                "Eta; effectiveness factor; dimensionless;
fitted according to the value of reaction order, mm"       "xx[i] --> large, Effetiv --> 0, diffusive control
by the film in the particle, with reaction rate at surface particle"

    "Thiele Modulus (phi)"
    phi[i] = ((2*abs(xx[i]))/(ABS(efetiv[i])*(mm+1)))^0.5   "Thiele modulus; dimensionaless"
    "phi[i] --> large, restriction of the diffusion of oxidant into particle pores"

    "Chemical reaction rate coefficient per external surface of particle pores"
    {Ki[i] = ra[i]/(ABS(efetiv[i])*gama*rhoco*Ag*1E4*(PO2[i]^mm)*((1-(ra[i]/(rad[i]+1E-
10)))^mm))}"gC/(cm2.s.atmO2^mm); variable diameter and constant density of char"

    Ki[i] = ra[i]/(ABS(efetiv[i])*gama[i]*rhoco*Ag*1E4*(PO2[i]^mm)*((1-
chi[i])^mm))"gC/(cm2.s.atmO2^mm); variable diameter and constant density of char in terms of chi[i]"
    "magnitude order of E-7"

    "Chemical reaction rate per external surface of particle pores"
    PO2s[i] = CO2ssv[i]*RR#*Tg[i]*1E-3                      "oxygen partial pressure at char surface, atm"
    ri[i] = Ki[i]*((PO2s[i])^mm)                            "gC/(cm2.s)"
    rri[i] = ri[i]*10                                       "kgC/(m2.s)"

END
```

APPENDIX 4.A.3 - Oxygen concentration curves

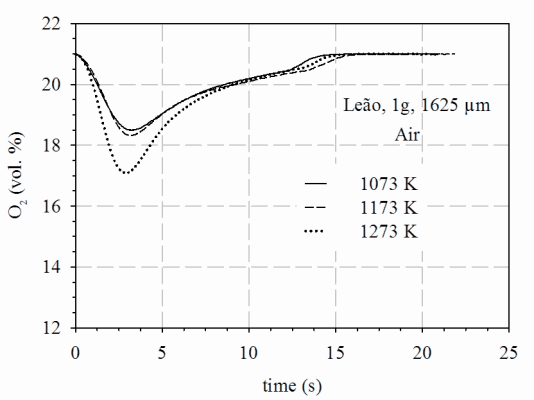

(a)

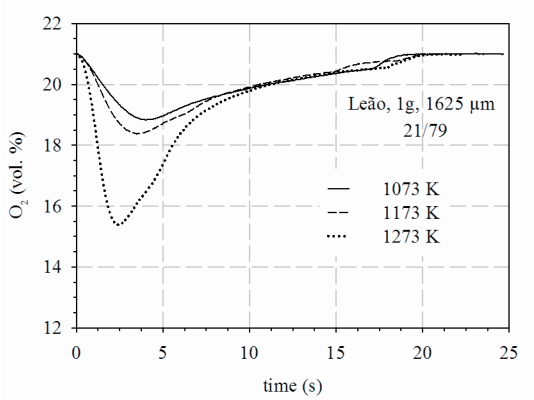

(b)

Figure 4.A.3.1 - Oxygen concentration curves under (a) air atmosphere and (b) oxy-fuel with 21% O_2 for Leão coal.

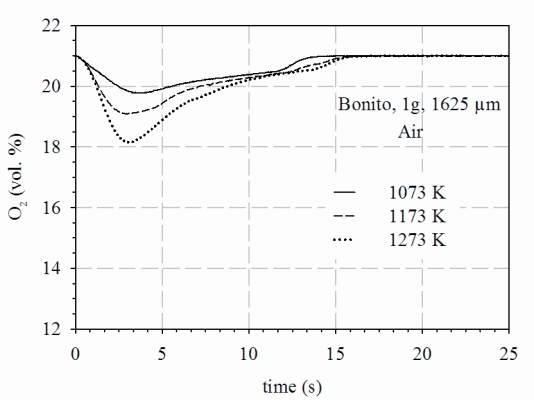

(a)

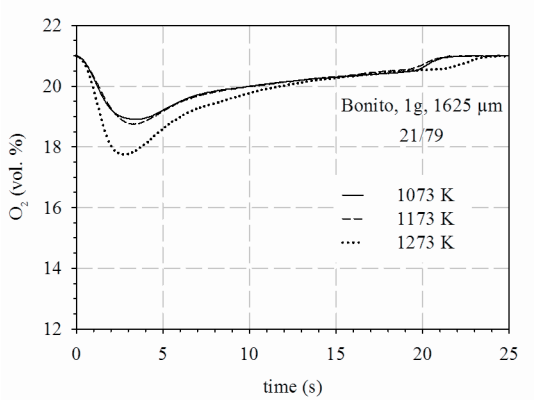

(b)

Figure 4.A.3.2 - Oxygen concentration curves under (a) air atmosphere and (b) oxy-fuel with 21% vol. O_2 for Bonito coal.

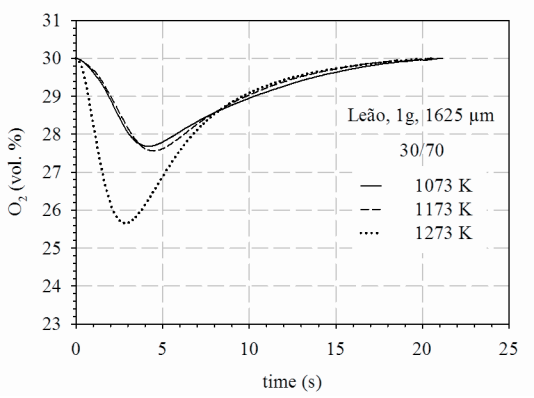

(a)

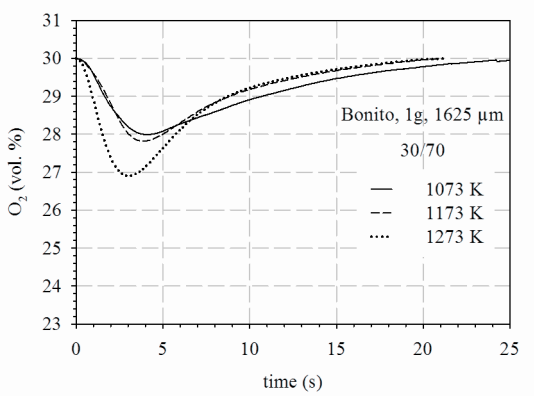

(b)

Figure 4.A.3.3 - Oxygen concentration curves under oxy-fuel atmosphere with 30% vol. O_2 for (a) Leão and Bonito (b) coals.

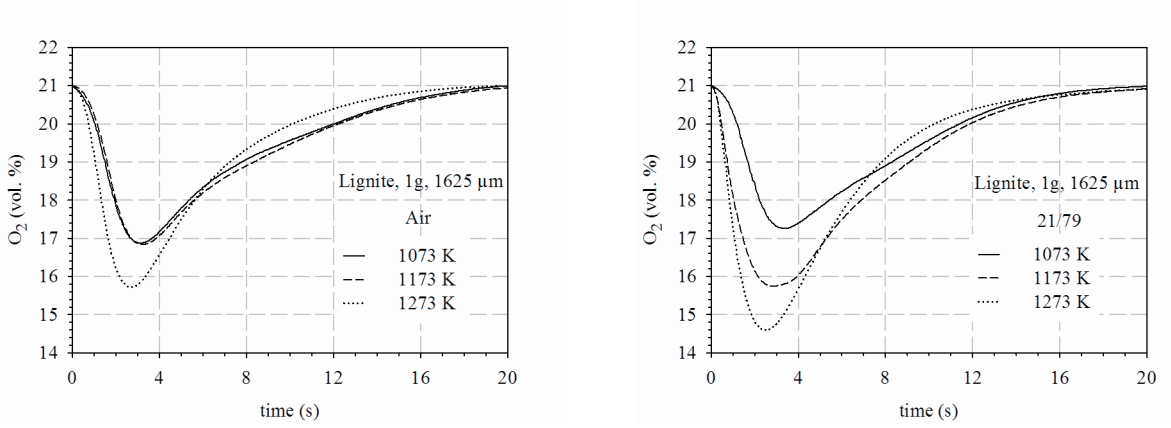

(a) (b)

Figure 4.A.3.4 - Oxygen concentration curves under (a) air atmosphere and (b) oxy-fuel with 21% vol. O_2 for lignite coal (LTBK).

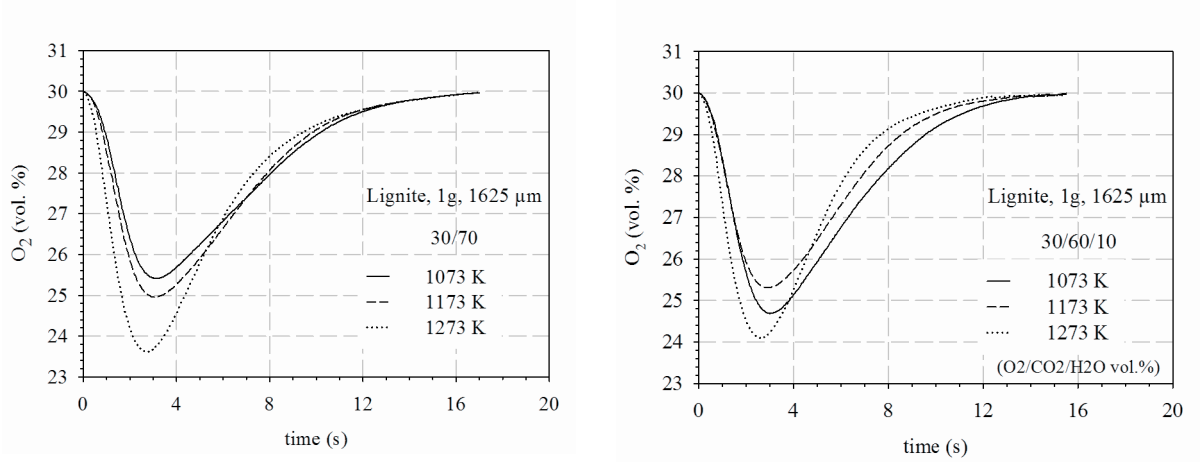

(a) (b)

Figure 4.A.3.5 - Oxygen concentration curves under oxy-fuel atmospheres with 30% vol. O_2 (a) without water vapor and (b) with 10% vol. H_2O for lignite coal (LTBK).

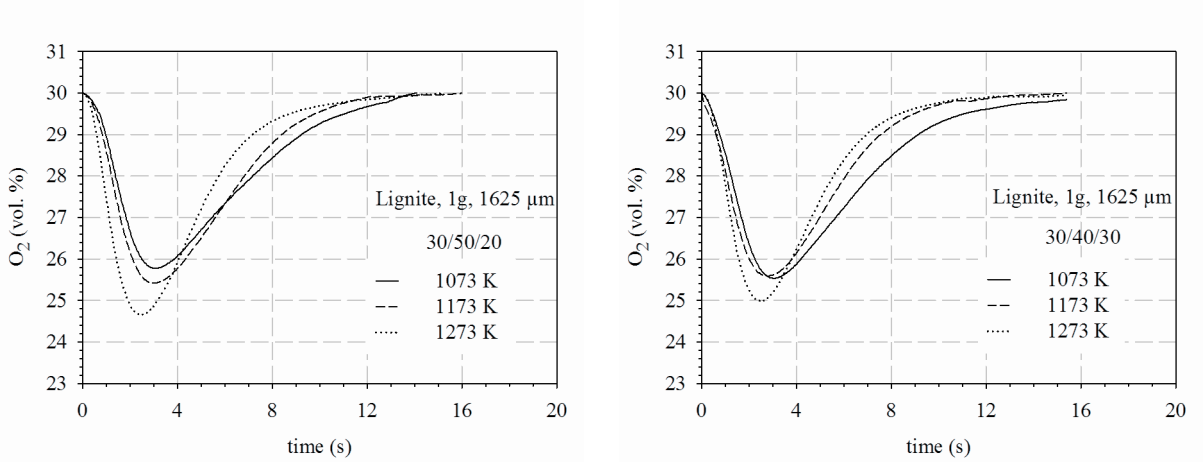

(a) (b)

Figure 4.A.3.6 - Oxygen consumption curves under oxy-fuel atmospheres with 30% vol. O_2 and (a) with 20% and (b) 30% vol. H_2O for lignite coal (LTBK).

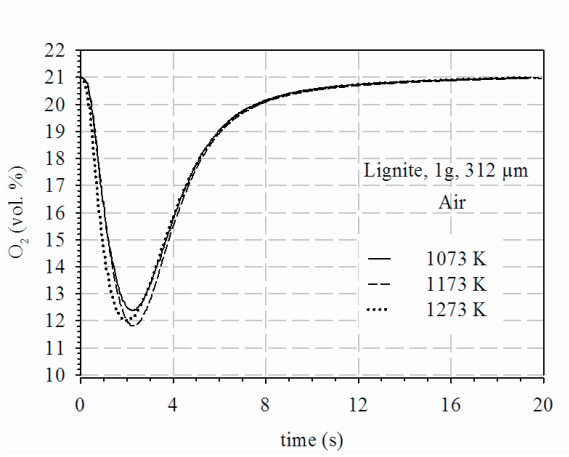

Figure 4.A.3.7- Oxygen concentration curves under air atmosphere for lignite coal (LTBK), 312 µm mean diameter.

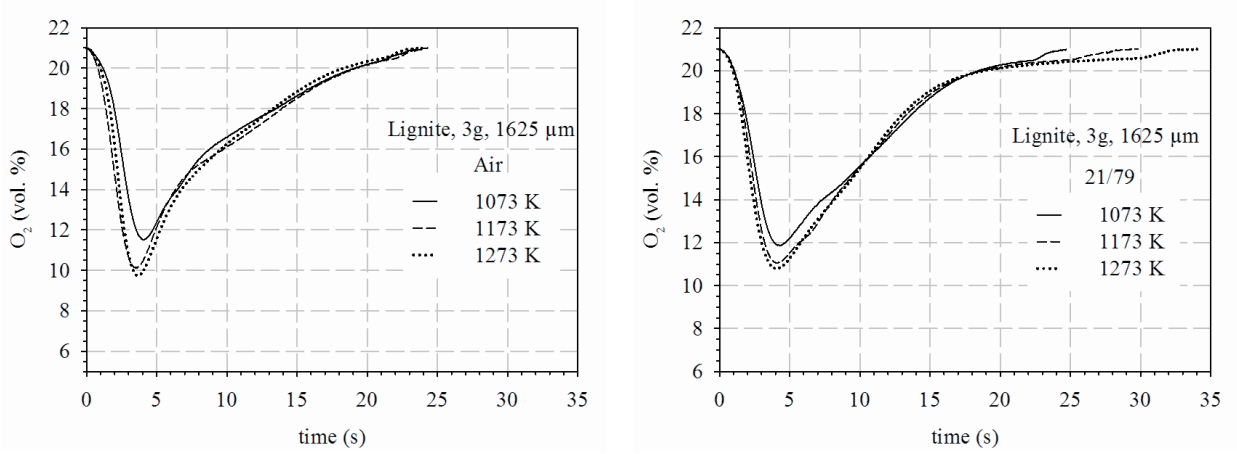

(a) (b)

Figure 4.A.3.8 - Oxygen concentration curves under (a) air atmosphere and (b) oxy-fuel with 21% vol. O_2 for lignite coal (LTBK).

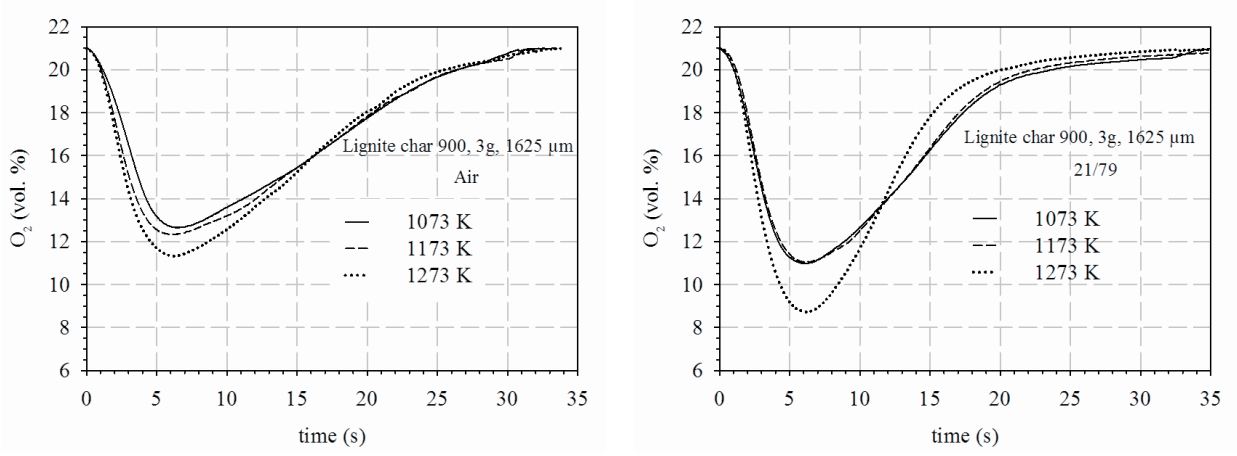

(a) (b)

Figure 4.A.3.9 - Oxygen concentration curves under (a) air atmosphere and (b) oxy-fuel with 21% vol. O_2 for LTBK char 900.

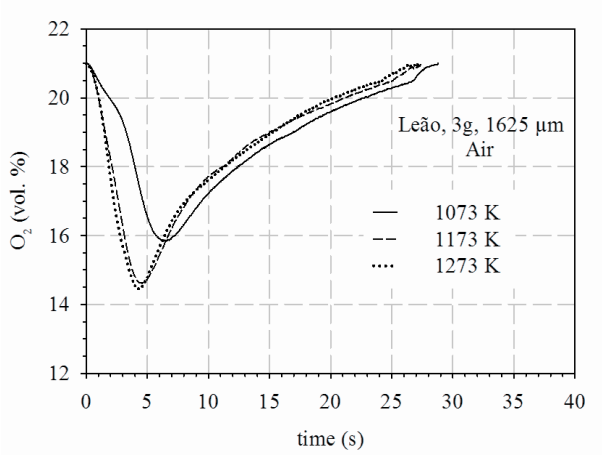

(a)

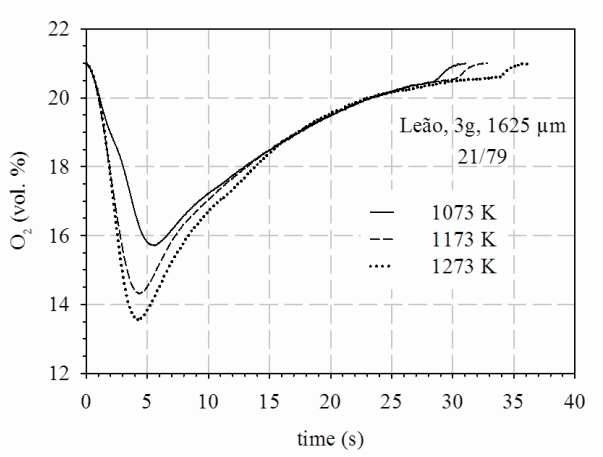

(b)

Figure 4.A.3.10 - Oxygen concentration curves under (a) air atmosphere and (b) oxy-fuel with 21% vol. O_2 for Leão coal.

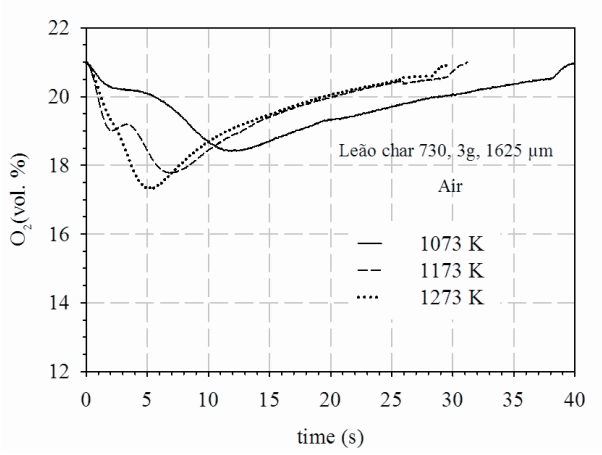

(a)

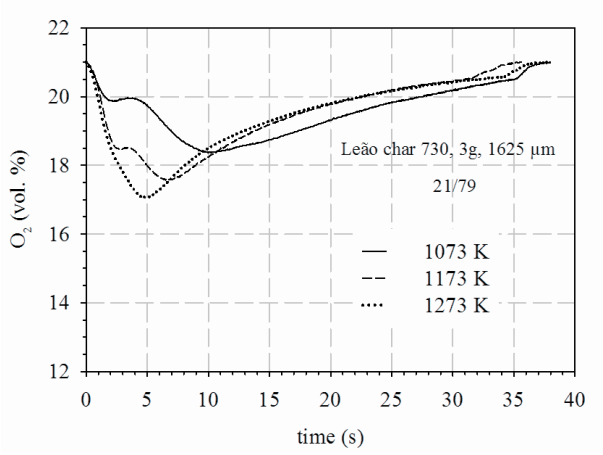

(b)

Figure 4.A.3.11 - Oxygen concentration curves under (a) air atmosphere and (b) oxy-fuel with 21% vol. O_2 for Leão char 730.

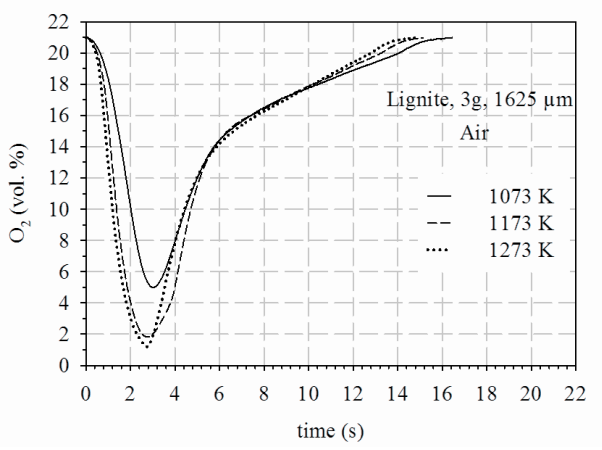

(a)

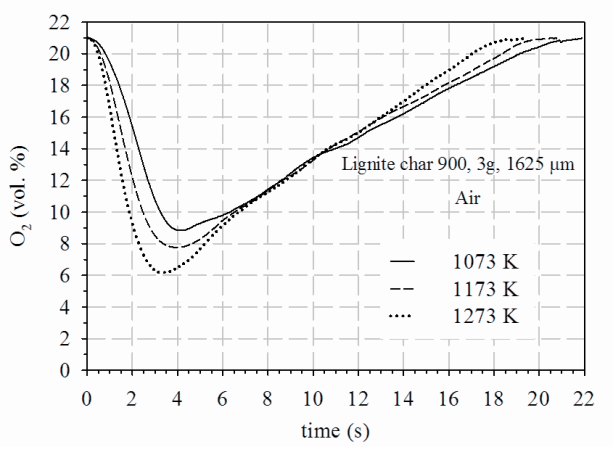

(b)

Figure 4.A.3.12 - Oxygen concentration curves for (a) lignite (LTBK) and (b) LTBK char 900 under air atmosphere for oxygen sensor at new position.

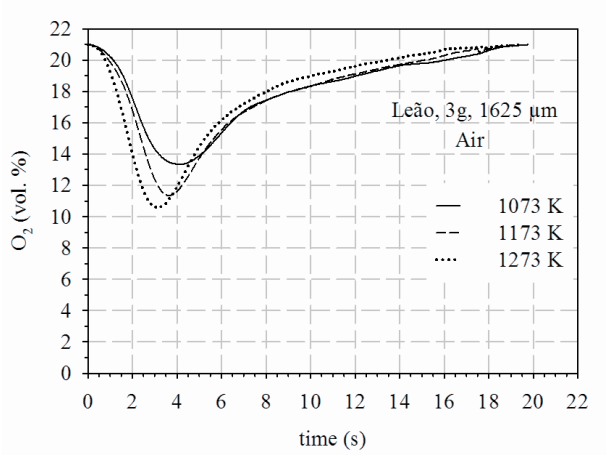

Figure 4.A.3.13 - Oxygen concentration curves for Leão coal under air atmosphere with the oxygen sensor at new position.

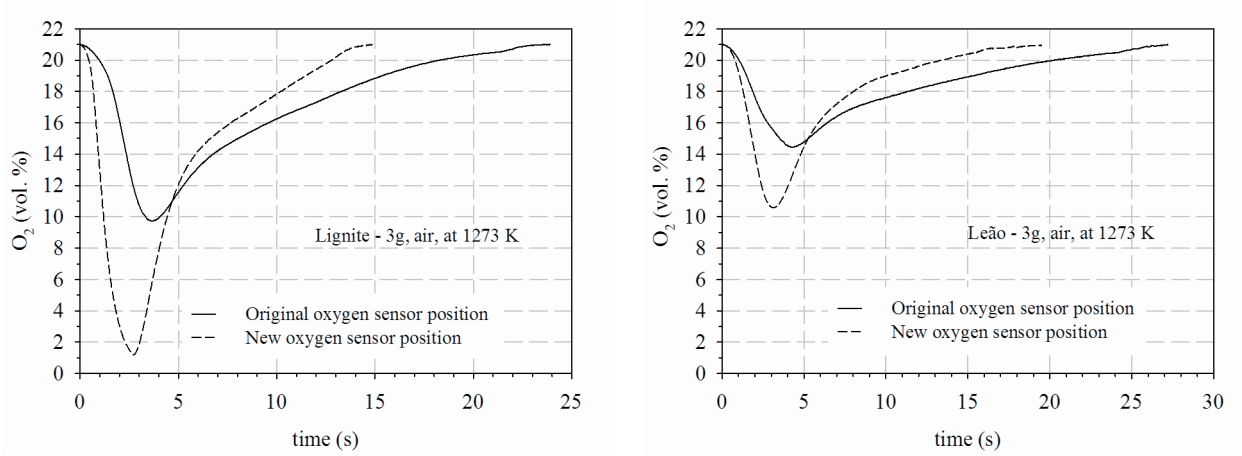

Figure 4.A.3.14 - Oxygen concentration curves for (a) lignite coal (LTBK) and (b) Leão coal under air atmosphere at original and new oxygen sensor positions.

APPENDIX 4.A.4 - Graphs of effective reaction rate constants k_{eff}

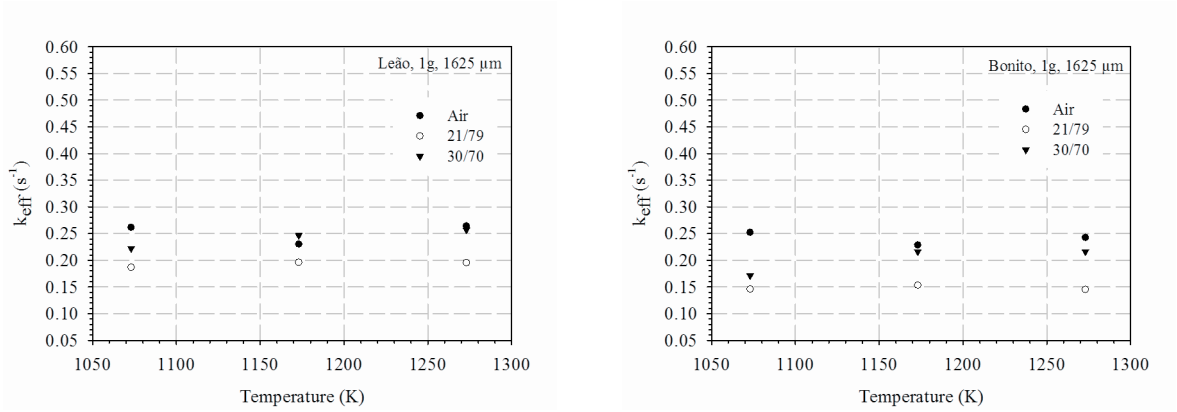

Figure 4.A.4.1 - Effective reaction rate constant values under air and oxy-fuel atmospheres (21/79 and 30/70, O_2/CO_2 em % vol.) for (a) Leão and (b) Bonito coals.

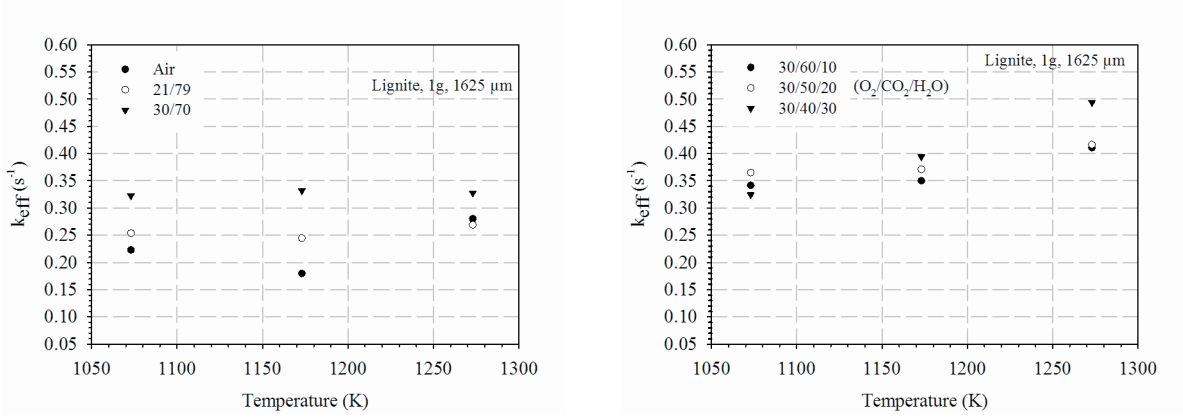

Figure 4.A.4.2 - Effective reaction rate constant values (a) under air and oxy-fuel atmospheres without water vapor (21/79, 30/70) and (b) oxy-fuel (30% vol. O_2) with water vapor in 10, 20 and 30% in vol for lignite coal (LTBK), 1625 µm particle mean diameter.

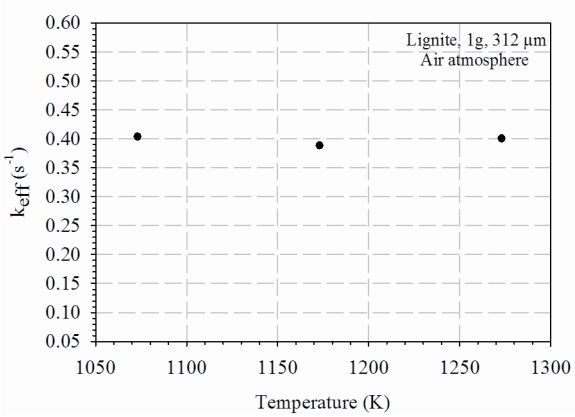

Figure 4.A.4.3 - Effective reaction rate constant values under air atmosphere for lignite coal (LTBK), 312 µm particle mean diameter.

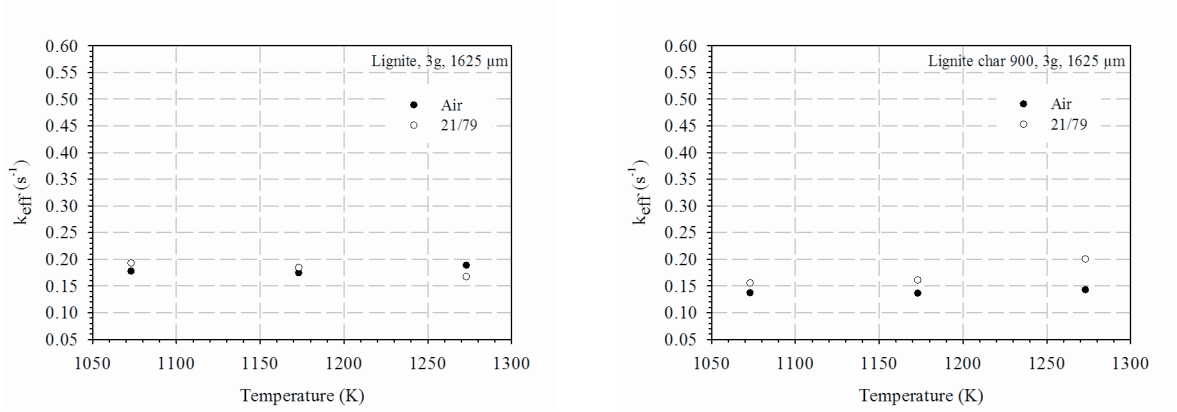

(a) (b)

Figure 4.A.4.4 - Effective reaction rate constant values under air and oxy-fuel atmosphere (21/79) for (a) lignite coal (LTBK) and (b) lignite char 900.

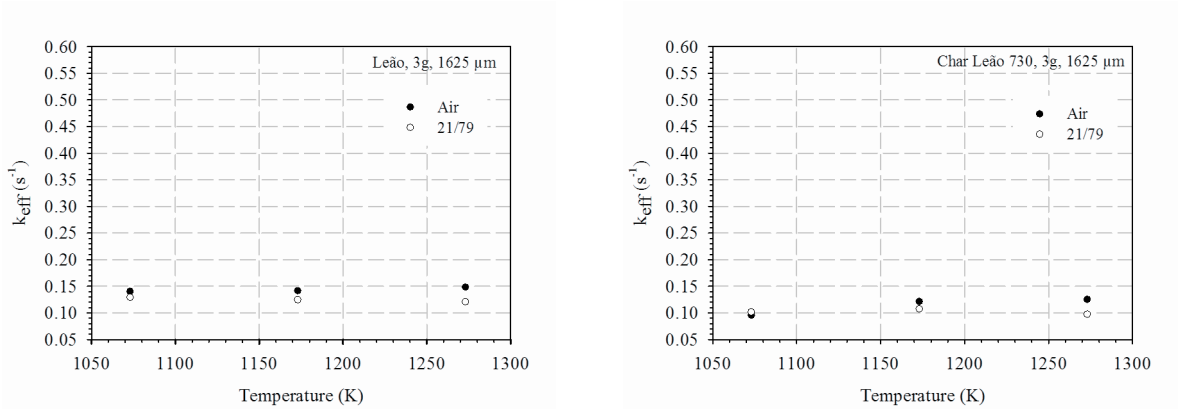

(a) (b)

Figure 4.A.4.5 - Effective reaction rate constant values under air and oxy-fuel atmosphere (21/79) for (a) Leão coal and (b) Leão char 730.

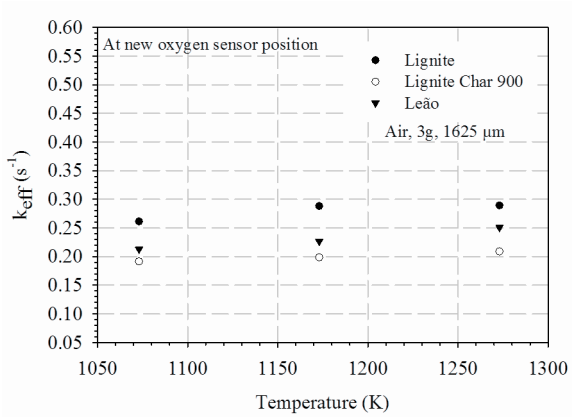

Figure 4.A.4.6 - Effective reaction rate constant values under air atmosphere for Leão and lignite (LTBK) coals and LTBK char 900 at new oxygem sensor position.

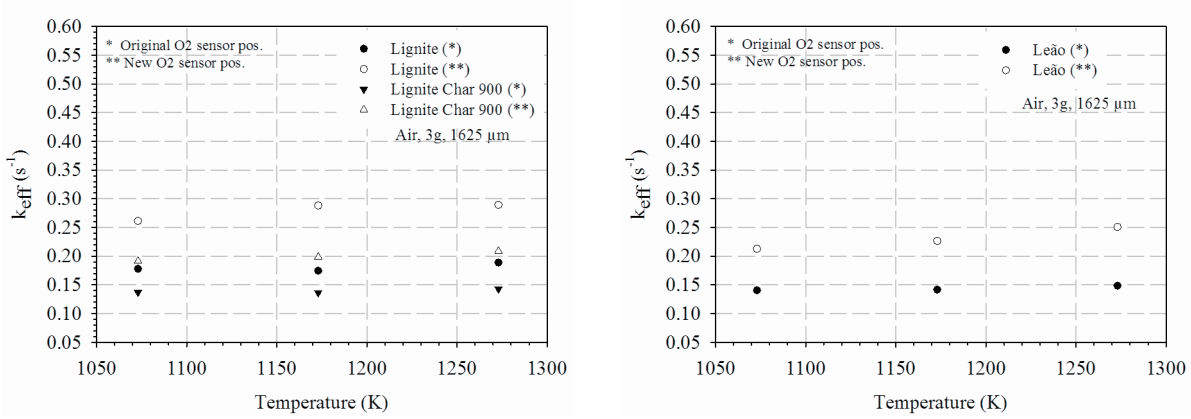

(a) (b)

Figure 4.A.4.7 - Comparison of effective reaction rate constant values between original and new oxygen sensor positions for (a) lignite coal (LTBK) and LTBK char 900 and (b) Leão coal.

APPENDIX 4.A.5 - Tables for the determination of char combustion reaction rate coefficients of LTBK char 900, 3g, 1625 μm

Table 4.A.5.1 - Measured reaction rates and derived reaction rate coefficients under air atmosphere at 1073 K

u_g (m/s)	Time (s)	T_g (K)	X_{O_2}	R_a [gC/(cm^2 s atmO_2)]	$R_{a,d}$ [gC/(cm^2 s atmO_2)]	Ratio $R_a/R_{a,d}$	$R_{a,c}$ [gC/(cm^2 s atm$O_2^{0.5}$)]	T_p (K)
1.0	3.25	1028	0.05	0.00421	0.01280	0.329	0.00205	1240
	4.25	1035	0.10	0.00689	0.01339	0.514	(0.00370)	1291
	5.75	1046	0.20	0.00953	0.01399	0.681	(0.00603)	1331
	7.25	1055	0.29	0.01038	0.01439	0.722	(0.00702)	1346
	9.00	1064	0.40	0.01041	0.01481	0.703	(0.00694)	1353
	10.75	1071	0.51	0.01017	0.01527	0.666	(0.00656)	1355
	12.50	1076	0.60	0.01000	0.01583	0.632	(0.00628)	1358
	14.75	1079	0.70	0.00977	0.01669	0.585	(0.00594)	1361
	17.25	1078	0.80	0.00894	0.01773	0.504	(0.00515)	1351
	20.75	1068	0.90	0.00721	0.01925	0.375	0.00388	1316
2.0	3.25	1026	0.05	0.00359	0.01668	0.215	0.00165	1225
	4.25	1035	0.10	0.00689	0.01766	0.390	0.00330	1291
	5.75	1046	0.20	0.00953	0.01841	0.518	(0.00490)	1331
	7.25	1055	0.29	0.01038	0.01891	0.549	(0.00551)	1346
	9.00	1064	0.40	0.01041	0.01943	0.536	(0.00556)	1353
	10.75	1071	0.51	0.01017	0.01999	0.509	(0.00540)	1355
	12.50	1076	0.60	0.01000	0.02068	0.484	0.00530	1358
	14.75	1079	0.70	0.00977	0.02174	0.449	0.00515	1361
	17.25	1078	0.80	0.00894	0.02302	0.388	0.00464	1351
	20.50	1069	0.90	0.00734	0.02474	0.297	0.00371	1318
3.0	3.00	1026	0.05	0.00359	0.01977	0.181	0.00161	1225
	4.25	1035	0.10	0.00689	0.02093	0.329	0.00315	1291
	5.75	1046	0.20	0.00953	0.02181	0.437	0.00454	1331
	7.25	1055	0.29	0.01038	0.02238	0.464	0.00506	1346
	9.00	1064	0.40	0.01041	0.02297	0.453	0.00512	1353
	10.75	1071	0.51	0.01017	0.02362	0.431	0.00502	1355
	12.5	1076	0.60	0.01000	0.02440	0.410	0.00496	1358
	14.75	1079	0.70	0.00977	0.02562	0.381	0.00486	1361
	17.25	1078	0.80	0.00894	0.02708	0.330	0.00443	1351
	20.75	1068	0.90	0.00721	0.02919	0.247	0.00354	1316

Table 4.A.5.2 - Measured reaction rates and derived reaction rate coefficients under air atmosphere at 1273 K

u_g (m/s)	Time (s)	T_g (K)	X_{O_2}	R_a [gC/(cm^2 s atmO_2)]	$R_{a,d}$ [gC/(cm^2 s atmO_2)]	Ratio $R_a/R_{a,d}$	$R_{a,c}$ [gC/(cm^2 s atm$O_2^{0.5}$)]	T_p (K)
1.0	2.75	1256	0.05	0.00481	0.01236	0.389	0.00238	1412
	3.75	1263	0.10	0.00784	0.01276	0.614	(0.00453)	1448
	5.25	1273	0.20	0.01093	0.01324	0.825	(0.00889)	1478
	6.75	1280	0.30	0.01228	0.01366	0.899	(0.01302)	1493
	8.25	1285	0.40	0.01240	0.01408	0.880	(0.01233)	1499
	9.75	1287	0.49	0.01212	0.01455	0.833	(0.01048)	1502
	11.5	1288	0.59	0.01153	0.01515	0.761	(0.00861)	1503
	13.75	1284	0.71	0.01073	0.01605	0.669	(0.00710)	1501
	16	1278	0.80	0.00931	0.01700	0.548	(0.00552)	1488
	19.75	1262	0.90	0.00688	0.01864	0.369	0.00367	1452
3.0	2.75	1256	0.05	0.00481	0.01907	0.252	0.00215	1412
	3.75	1263	0.10	0.00784	0.01967	0.398	0.00363	1448
	5.25	1273	0.20	0.01093	0.02037	0.537	(0.00546)	1478
	6.75	1280	0.30	0.01228	0.02097	0.586	(0.00644)	1493
	8.25	1285	0.40	0.01240	0.02156	0.575	(0.00654)	1499
	10.00	1288	0.51	0.01207	0.02232	0.541	(0.00631)	1503
	11.75	1288	0.61	0.01139	0.02317	0.492	0.00587	1502
	13.75	1284	0.71	0.01073	0.02431	0.441	0.00547	1501
	16.25	1277	0.81	0.00913	0.02578	0.354	0.00455	1486
	19.75	1262	0.90	0.00688	0.02789	0.247	0.00336	1452
5.0	2.75	1256	0.05	0.00481	0.02368	0.203	0.00209	1412
	3.75	1263	0.10	0.00784	0.02443	0.321	0.00342	1448
	5.25	1273	0.20	0.01093	0.02527	0.432	0.00493	1478
	6.75	1280	0.30	0.01228	0.02600	0.472	0.00571	1493
	8.25	1285	0.40	0.01240	0.02671	0.464	0.00583	1499
	9.75	1287	0.49	0.01212	0.02748	0.441	0.00572	1502
	11.75	1288	0.61	0.01139	0.02864	0.398	0.00539	1502
	13.75	1284	0.71	0.01073	0.03000	0.358	0.00510	1501
	16.25	1277	0.81	0.00913	0.03176	0.287	0.00433	1486
	19.75	1262	0.90	0.00688	0.03425	0.201	0.00326	1452

Table 4.A.5.3 - Measured reaction rates and derived reaction rate coefficients under oxy-fuel (21/79) at 1073 K

u_g (m/s)	Time (s)	T_g (K)	X_{O_2}	R_a [gC/(cm^2 s atmO_2)]	$R_{a,d}$ [gC/(cm^2 s atmO_2)]	Ratio $R_a/R_{a,d}$	$R_{a,c}$ [gC/(cm^2 s atm$O_2^{0.5}$)]	T_p (K)
2.0	2.75	1019	0.05	0.00496	0.01655	0.299	0.00231	1254
	3.75	1034	0.11	0.00878	0.01733	0.506	(0.00445)	1315
	5.00	1053	0.20	0.01236	0.01793	0.690	(0.00744)	1357
	6.50	1072	0.31	0.01419	0.01841	0.771	(0.00984)	1381
	7.75	1085	0.40	0.01419	0.01877	0.756	(0.00973)	1389
	9.25	1095	0.51	0.01383	0.01930	0.716	(0.00907)	1395
	10.75	1098	0.60	0.01294	0.01992	0.650	(0.00793)	1395
	12.75	1095	0.71	0.01160	0.02089	0.556	(0.00663)	1387
	15.00	1084	0.80	0.00939	0.02192	0.428	0.00500	1359
	19.00	1057	0.90	0.00496	0.02289	0.217	0.00244	1261
3.0	2.75	1019	0.05	0.00496	0.01973	0.251	0.00223	1254
	3.75	1034	0.11	0.00878	0.02065	0.425	0.00413	1315
	5.00	1053	0.20	0.01236	0.02134	0.579	(0.00639)	1357
	6.50	1072	0.31	0.01419	0.02190	0.648	(0.00794)	1381
	7.75	1085	0.40	0.01419	0.02231	0.636	(0.00797)	1389
	9.25	1095	0.51	0.01383	0.02292	0.603	(0.00767)	1395
	10.75	1098	0.60	0.01294	0.02363	0.548	(0.00698)	1395
	12.75	1095	0.71	0.01160	0.02475	0.469	0.00607	1387
	15.00	1084	0.80	0.00939	0.02594	0.362	0.00474	1359
	19.00	1057	0.90	0.00496	0.02704	0.183	0.00239	1261
6.0	2.75	1019	0.05	0.00496	0.02690	0.184	0.00214	1254
	3.75	1034	0.11	0.00878	0.02814	0.312	0.00377	1315
	5.25	1056	0.21	0.01280	0.02918	0.439	0.00570	1362
	6.50	1072	0.31	0.01419	0.02977	0.477	0.00651	1381
	7.75	1085	0.40	0.01419	0.03029	0.469	0.00659	1389
	9.25	1095	0.51	0.01383	0.03108	0.445	0.00648	1395
	10.75	1098	0.60	0.01294	0.03200	0.405	0.00608	1395
	12.75	1095	0.71	0.01160	0.03346	0.347	0.00547	1387
	15.00	1084	0.80	0.00939	0.03502	0.268	0.00442	1359
	19.00	1057	0.90	0.00496	0.03640	0.136	0.00232	1261

Table 4.A.5.4 - Measured reaction rates and derived reaction rate coefficients under oxy-fuel (21/79) at 1273 K

u_g (m/s)	Time (s)	T_g (K)	X_{O_2}	R_a [gC/(cm^2 s atmO_2)]	$R_{a,d}$ [gC/(cm^2 s atmO_2)]	Ratio $R_a/R_{a,d}$	$R_{a,c}$ [gC/(cm^2 s atm$O_2^{0.5}$)]	T_p (K)
4.0	2.50	1277	0.05	0.00529	0.02044	0.259	0.00237	1439
	3.50	1287	0.11	0.01081	0.02137	0.506	(0.00525)	1494
	4.75	1295	0.21	0.01775	0.02240	0.792	(0.01195)	1537
	5.75	1297	0.30	0.02154	0.02316	0.930	(0.02412)	1559
	6.75	1298	0.39	0.02334	0.02394	0.975	(0.04380)	1573
	8.00	1295	0.51	0.02266	0.02491	0.909	(0.02334)	1581
	9.25	1290	0.61	0.02062	0.02594	0.795	(0.01498)	1583
	10.50	1284	0.70	0.01807	0.02701	0.669	(0.01101)	1577
	12.50	1271	0.81	0.01294	0.02847	0.454	0.00679	1544
	15.50	1251	0.90	0.00682	0.02986	0.228	0.00331	1464
6.0	2.50	1277	0.05	0.00529	0.02444	0.216	0.00231	1439
	3.50	1287	0.11	0.01081	0.02555	0.423	0.00486	1494
	4.75	1295	0.21	0.01775	0.02677	0.663	(0.00938)	1537
	5.75	1297	0.30	0.02154	0.02767	0.778	(0.01357)	1559
	6.75	1298	0.39	0.02334	0.02858	0.817	(0.01619)	1573
	8.00	1295	0.51	0.02266	0.02973	0.762	(0.01441)	1581
	9.25	1290	0.61	0.02062	0.03093	0.667	(0.01175)	1583
	10.50	1284	0.70	0.01807	0.03217	0.562	(0.00957)	1577
	12.50	1271	0.81	0.01294	0.03387	0.382	0.00638	1544
	15.50	1251	0.90	0.00682	0.03546	0.192	0.00324	1464

Table 4.A.5.5 - Measured reaction rates and derived reaction rate coefficients under air atmosphere at 1073 K at new oxygen sensor position

u_g (m/s)	Time (s)	T_g (K)	X_{O_2}	R_a [gC/(cm^2 s atmO_2)]	$R_{a,d}$ [gC/(cm^2 s atmO_2)]	Ratio $R_a/R_{a,d}$	$R_{a,c}$ [gC/(cm^2 s atm$O_2^{0.5}$)]	T_p (K)
3.0	2.25	1089	0.05	0.00653	0.02008	0.325	0.00299	1294
	3.00	1094	0.11	0.01336	0.02140	0.624	(0.00716)	1372
	4.00	1102	0.20	0.02073	0.02252	0.921	(0.02192)	1425
	5.00	1110	0.29	0.02065	0.02303	0.897	(0.01957)	1434
	6.25	1119	0.41	0.02017	0.02372	0.850	(0.01643)	1443
	7.25	1125	0.49	0.01895	0.02426	0.781	(0.01328)	1445
	8.75	1134	0.61	0.01676	0.02509	0.668	(0.01014)	1442
	10.25	1141	0.70	0.01452	0.02593	0.560	(0.00807)	1432
	12.25	1146	0.81	0.01363	0.02766	0.493	0.00740	1434
	14.50	1148	0.90	0.01187	0.02980	0.398	0.00623	1418
5.0	2.25	1089	0.05	0.00653	0.02505	0.261	0.00286	1294
	3.00	1094	0.11	0.01336	0.02668	0.501	(0.00621)	1372
	4.00	1102	0.20	0.02073	0.02805	0.739	(0.01208)	1425
	5.00	1110	0.29	0.02065	0.02866	0.720	(0.01189)	1434
	6.25	1119	0.41	0.02017	0.02950	0.684	(0.01131)	1443
	7.50	1127	0.51	0.01868	0.03032	0.616	(0.00997)	1446
	8.75	1134	0.61	0.01676	0.03114	0.538	(0.00860)	1442
	10.25	1141	0.70	0.01452	0.03212	0.452	0.00724	1432
	12.25	1146	0.81	0.01363	0.03419	0.399	0.00680	1434
	14.50	1148	0.90	0.01187	0.03674	0.323	0.00588	1418

5. RESUMO DOS RESULTADOS E CONCLUSÕES

A presente tese teve como objetivo principal investigar a reatividade dos carvões de baixo *rank* quando submetidos à combustão em atmosferas de ar e de oxicombustão, utilizando a bancada experimental ALVA 20, desenvolvida na Universidade Técnica de Brandemburgo, em Cottbus, na Alemanha. A investigação foi dividida em três Capítulos (2, 3 e 4) apresentados em forma de artigos escritos na língua inglesa.

O Capítulo 2 trata da descrição da bancada experimental e como os experimentos são realizados para a investigação da combustão do carvão em atmosferas de ar e de oxicombustão, cujos procedimentos são utilizados nos Capítulos 3 e 4. No Capítulo 2, foram investigadas amostras de carvão linhito (LTBK) de 1g, submetidas à oxicombustão composta com duas atmosferas de O_2/CO_2 sem vapor d'água (21/79 e 30/70) e três atmosferas de $O_2/CO_2/H_2O$ (30/60/10, 30/50/20 e 30/40/30) em base molar, incluindo, também, a participação da atmosfera de ar. A investigação da combustão do LTBK foi realizada diretamente através das curvas de concentração de oxigênio medidas pelo sensor potenciométrico de oxigênio instalado no interior do reator ciclônico. Os principais resultados e conclusões são:

- Para as atmosferas de oxicombustão (O_2/CO_2) com 30% O_2, valores mais elevados da variação de concentração de oxigênio são obtidos na atmosfera de oxicombustão sem vapor d'água 30/70 (O_2/CO_2) em 1273 K do que as obtidas nas atmosferas de oxicombustão com vapor d'água 30/50/20 e 30/40/30 ($O_2/CO_2/H_2O$). Estes resultados mostram a influência da reação de gaseificação do CO_2 na combustão do carvão para temperaturas mais altas do que 1173 K e concentrações de CO_2 maiores do que 50% (em vol.) em atmosferas de oxicombustão com vapor d'água e 30% de O_2.
- Para as atmosferas de oxicombustão (O_2/CO_2) com 30% O_2, valores mais elevados de tempo de combustão são obtidos na atmosfera de oxicombustão 30/70 em 1173 e 1273 K do que os obtidos nas atmosferas de oxicombustão com vapor d'água 30/60/10, 30/50/20 e 30/40/30. Estes resultados podem estar sendo influenciados pelo escoamento no interior do reator ciclônico (com seus termos difusivos e advectivos) e pelas propriedades da atmosfera oxidante, como os coeficientes de difusão de massa do O_2 no CO_2, conforme observado para a atmosfera de oxicombustão com 21% de O_2 e 79% de CO_2 (21/79).
- Há um aumento na variação da concentração de oxigênio nas atmosferas de oxicombustão (21/79, 30/70) e de ar com o aumento da temperatura, evidenciando que as reacões de

combustão até o tempo em que a máxima variação de concentração de oxigênio é atingida, é controlada pelo regime cinético.

- Não há diferença da variação da concentração de oxigênio em 1273 K entre as atmosferas de ar e de oxicombustão 30/70, indicando que ambas atmosferas têm taxas de combustão similares.

O Capítulo 3 é referente ao planejamento e análise de experimentos, utilizando a metodologia do DoE, motivado pelo grande número de experimentos realizados e da necessidade de entender a influência dos fatores, como temperatura e as composições das atmosferas oxidantes, e as interações entre esses fatores na combustão do carvão. A investigação da combustão dos carvões testados é realizada através das curvas de concentração de oxigênio com a ferramenta estatística ANOVA (Análise de Variância).

Os experimentos foram divididos em quatro principais grupos. Foram testados os carvões brasileiros de alto teor de cinzas (Leão e Bonito) e o carvão linhito de alto teor de voláteis em atmosferas de ar e de oxicombustão. Para as amostras do carvão LTBK, a oxicombustão foi composta com duas atmosferas de O_2/CO_2 sem vapor d'água (21/79 e 30/70) e três atmosferas de $O_2/CO_2/H_2O$ (30/60/10, 30/50/20 e 30/40/30) em base molar, enquanto para as amostras dos carvões Leão e Bonito, a oxicombustão foi composta com duas atmosferas de O_2/CO_2 (21/79 e 30/70). As amostras de carvão foram peneiradas para uma faixa de tamanho de partículas de 1250 a 2000 μm e 125 a 500 μm, e com massas de 1g e 3g. Em adição aos testes, amostras de char dos carvões Leão e LTBK foram preparadas para investigar o comportamento da combustão de suas matrizes carbonosas com diferentes níveis de matéria volátil. Os principais resultados e conclusões são

- Para o primeiro grupo de experimentos

A atmosfera de oxicombustão com 79% CO_2 (21/79, O_2/CO_2) tem consumo maior de oxigênio do que as atmosferas de ar e de oxicombustão com 70% CO_2 (30/70, O_2/CO_2) para carvões com alto teor de cinzas (Bonito e Leão), devido à influência da reação de gaseificação ($C + CO_2 \rightarrow 2CO$) na combustão desses carvões em concentrações maiores de CO_2. Entretanto, a atmosfera de oxicombustão 21/79 aumenta o tempo de combustão, devido à influência das propriedades da atmosfera com CO_2, como baixo coeficiente de difusão do oxigênio, nas taxas de reação de combustão e na recuperação da concentração de oxigênio na corrente de entrada do oxidante (i.e. 21% O_2 em vol.).

- Para o segundo grupo de experimentos

Atmosferas de oxicombustão com maior concentração de CO_2, i.e. 21/79 (O_2/CO_2) tem consumo maior de oxigênio do que as atmosferas de ar e de oxicombustão com vapor d'água e menor concentração de CO_2, i.e. 30/60/10, 30/50/20, 30/40/30 ($O_2/CO_2/H_2O$), para o carvão LTBK com partículas de diâmetro médio de 1625 μm, devido a maior influência da reação de gaseificação do CO_2 ($C + CO_2 \rightarrow 2CO$) do que a reação de gaseificação do H_2O ($C + H_2O \rightarrow CO + H_2$), que aumenta o consumo de oxigênio com a temperatura, quando as reações de combustão são controladas pelo regime cinético. O efeito da reação de gaseificação do CO_2 é reduzido para partículas de diâmetro médio de 312 μm, quando as reações de combustão são controladas pela difusão do oxidante no interior dos poros das partículas ou pelo filme que se forma entorno delas, condição na qual a influência da temperatura do gás de combustão é reduzida.

- Para o terceiro grupo de experimentos

Consumos mais elevados de oxigênio são obtidos em atmosferas de oxicombustão com 79% CO_2 (21/79, O_2/CO_2) em relação às obtidas em atmosfera de ar para o char do carvão Leão devolatilizado em 545 ^oC e para o char do carvão LTBK devolatilizado a 900 ^oC, devido ao efeito da reação de gaseificação do CO_2, que aumenta o consumo de oxigênio na combustão. Estes resultados são de extrema relevância porque permitem concluir que a reação de gaseificação também influencia a combustão de char obtidos de carvões com alto teor de cinzas, separada do efeito da combustão dos voláteis nestes carvões.

- Para o quarto grupo de experimentos

O sensor potenciométrico de oxigênio mede a variação local da concentração de oxigênio e essas medidas dependem da posição do sensor de oxigênio dentro do reator devido à influência do escoamento com *swirl* dentro deste reator, conforme verificado através de medidas de consumo de oxigênio em atmosfera de ar com nova posição do sensor de oxigênio próxima ao centro da secção principal do reator.

O Capítulo 4 trata da investigação da reatividade dos carvões de baixo *rank* por meio do cálculo dos parâmetros cinéticos globais e dos coeficientes da taxa de reação de combustão do char, considerando a hipótese de um reator bem misturado. Os resultados mostram que a hipótese do reator bem misturado não é o suficiente para capturar a cinética da combustão do carvão por batelada no interior do reator ciclônico. A investigação da reatividade dos carvões através da composição da atmosfera oxidante e temperaturas do gás de combustão, massas da amostra, diâmetro das partículas, posição do sensor de oxigênio, tem influência do

escoamento com *swirl* e seus termos advectivos e difusivos, sendo que os resultados dos parâmetros cinéticos são fortemente influenciados pela posição do sensor de oxigênio no interior do reator ciclônico.

Portanto, as constantes efetivas da taxa de reação calculadas para o carvão e char submetidos à combustão em atmosferas de ar e de oxicombustão são específicas para este tipo de reator de combustão ciclônco instalado na bancada experimental ALVA 20 e estes parâmetros são úteis para comparar a reatividade de diferentes carvões e char para as atmosferas de ar e de oxicombustão sob determinadas condições:

- O sensor potenciométrico de oxigênio precisa estar posicionado no centro da secção principal do reator ciclônico para alcançar as zonas de recirculação do escoamento com *swirl*, e conseguir a máxima variação de concentração de oxigênio ou de consumo durante a reação de combustão, conforme verificado para a atmosfera de ar.
- A massa de amostra de carvão testado deve ser de 3g em vez de 1g para todas as atmosferas para evitar o efeito adverso observado para as amostras de 1g submetidas à combustão em ar atmosférico, no qual a reatividade do carvão com alto teor de cinzas é maior do que o do carvão com alto teor de carbono e voláteis.
- A comparação das constantes efetivas da taxas de reação entre as atmosferas oxidantes para o mesmo carvão e char devem ser realizadas com precaução e com o auxílio das curvas de concentração de oxigênio seguindo a metodologia desenvolvida no Capítulo 3 sem a interferência das hipóteses de modelagem para o cálculo das constantes efetivas da taxa de reação, porque esta modelagem pode estar mudando a natureza do fenômeno investigado diretamente nas curvas de concentração de oxigênio. Esta observação é constatada, por exemplo, pela redução da reatividade da combustão das amostras de 1g do carvão Bonito na atmosfera de oxicombustão 21/79 em compararação ao ar pela constante efetiva da taxa de reação, diferentemente do que é observado diretamente pela análise da curva de concetração de oxigênio realizada no Capítulo 3 pelo DoE.

O método para calcular os coeficientes das taxas de reação de combustão do char LTBK 900 e para determinar o regime de controle da reação global de combustão depende do conhecimento do campo de velocidades no interior do reator ciclônico, no qual o escoamento com *swirl* e a posição do sensor de oxigênio têm um papel imporante na magnitude da taxa de reação global de combustão do char.

De acordo com a análise de sensibilidade para determinar os coeficientes das taxas de reação de combustão do char, velocidades mais elevadas são necessárias para mudar o regime

de controle para oxicombustão em comparação às obtidas para a combustão em ar, o que indica que as propriedades da atmosfera de oxicombustão, como o coeficiente binário de difusão do oxigênio no CO_2, influenciam a reação global de combustão do carvão. Portanto, o regime cinético da combustão do carvão em atmosfera de oxicombustão (21/79) dentro do reator de combustão ciclônico é favorecido com velocidade elevadas de escoamento, porque elas reduzem a influência das propriedades da atmosfera de oxicombustão no coeficiente da taxa de reação por difusão, dando lugar ao coeficiente da taxa de reação por cinética, no qual a temperatura e a reação de gaseificação do CO_2 podem influenciar.

6. SUGESTÕES DE TRABALHOS FUTUROS

- Investigar os parâmetros cinéticos globais com o reator em regime de operação contínua de combustão de carvão em atmosferas de oxicombustão e de ar com o sensor de oxigênio posicionado no centro do reator e próximo da zona de combustão. Para isso, é necessário modificar o reator ciclônico para permitir o deslocamento do sensor de oxigênio no interior do reator e modificar o sistema de dosagem contínua de alimentação de carvão para operar com faixas de tamanhos de partículas menores.
- Adaptar o reator de combustão ciclônico para a medição da temperatura da partícula e da emissão de CO a fim de explorar modelos cinéticos das reações de gaseificação do CO_2 nas atmosferas de oxicombustão, tendo em vista que a reação de Boudouard ou de gaseificação do CO_2 com a partícula de carvão, i.e. $C + CO_2 \rightarrow 2CO$ é endotérmica, e o monitoramento da temperatura da partícula além do CO contribuiria para a investigação mais aprofundada do fenômeno analisado pelas curvas de concentração de oxigênio medidas pelo sensor potenciométrico.